# PERTURBATION OF ASTROCYTIC KEAP1-NRF2-ARE PATHWAY AND GLUTAMATE TRANSPORTER EXPRESSION IN SPINAL ASTROCYTIC DEGENERATION

By

Duanghathai Wiwatratana

### A DISSERTATION

Submitted to Michigan State University in partial fulfillment of the requirements for the degree of

Comparative Medicine and Integrative Biology – Doctor of Philosophy

2021

#### **ABSTRACT**

# PERTURBATION OF ASTROCYTIC KEAP1-NRF2-ARE PATHWAY AND GLUTAMATE TRANSPORTER EXPRESSION IN SPINAL ASTROCYTIC DEGENERATION

By

## Duanghathai Wiwatratana

Several cellular mechanisms are known to be involved in methylmercury (MeHg) induced central nervous system (CNS) toxicity, including the dysregulation of intracellular Ca<sup>2+</sup>, redox, and glutamate homeostasis. However, the factors that make particular neurons susceptible to MeHg toxicity, and the latency period of neurological signs and symptoms, have not yet been clearly delineated. For example, the spinal dorsal root ganglia (DRG) is the primary target of MeHg. Mercury (Hg) granules are first detected in spinal cord motor neurons (SMNs) in the non-symptomatic phase, whereas Hg granules are detected in glia later, following with neurological symptoms (Møller-Madsen, 1991). This finding suggested that the latent period (non-symptomatic phase) is associated with Hg accumulation in neurons, while the symptomatic phase occurs following Hg accumulation in glia, and the susceptibility is not associated with Hg granule accumulation in cells (Møller-Madsen, 1991). Astrocytes generally provide glutathione (GSH) for neurons to detoxify toxic insult. In the spinal cord, MeHg might perturb the antioxidant pathway, Keap1-Nrf2-ARE pathway in the spinal cord astrocytes (SCAs) consequently contribute to DRG or SMN susceptibility to MeHg toxicity. In this study, the comparative responses of different SCAs maturity to a non-toxic MeHg concentration (0.1 µM) suggested that the fully mature SCAs (Day in vitro 30; DIV30), were more susceptible to MeHg than SCAs on DIV14. The perturbation of the Keap1-Nrf2-ARE pathway in SCAs (DIV 30) during exposure to sub-toxic MeHg concentration (0.50 µM) caused a biphasic increase in

antioxidant genes such as Keap1, Nrf2, Gclc, Abcc1 mRNAs expression. The concomitant increase of glutamate transporter Slc7a11 encoded for the system Xc-, and Slc1a3 encoded for EAAT1, and Slc1a2 encoded for EAAT2 expression during MeHg exposure might suggest the cooperative expression or function of these glutamate transporters. This concomitant expression was further demonstrated in studies using Nrf2-knockout (Nrf2-KO) derived SCAs. The increase of basal Slc7a11 mRNA, was concurrent to the increase of basal Slc1a3 and Slc1a2 mRNA expressions in Nrf2-KO derived SCA. The function of time of MeHg exposure indicated that Nrf2-KO derived SCAs were more susceptible to MeHg than the wild-type (WT)-derived SCAs. The pronounced susceptibility of Nrf2-KO derived SCAs was mainly due to the loss of GSH) metabolism and transport genes Gclc, GPx1, GPx4, and Abcc1 mRNAs in this genotype. MeHg significantly reduced these mRNA expressions in both genotypes. However, not all Nrf2-ARE regulated genes were affected by MeHg in similar ways in these genotypes. For example, MeHg induced the increase of Slc7a11 mRNA expression in WT-derived SCAs, but it appears to cause the reduction of this mRNA expression in Nrf2 KO-derived SCAs. Administration of antioxidant N-acetyl-L-cystine (NAC) in pretreatment (NP), co-treatment (CO), and post-treatment of MeHg (MP) prevented the reduction of SCAs metabolic functions for over 160h. The mechanism of NAC action in preventing MeHg induced SCAs degeneration is primarily due to its thiol antioxidant property.

In conclusion, this study suggests that age and genetic predisposition contribute to SCAs susceptibility to MeHg toxicity. The dysregulation of the antioxidant pathways and glutamate homeostasis in SCAs potentially contributes to SMNs or DRG susceptible to MeHg.

Copyright by DUANGHATHAI WIWATRATANA 2021

In dedication to my family:
My father, my mother, husband David, and my brother: Your long patience, endless support, and unending love encourage me to accomplish this significant part of the journey.

#### **ACKNOWLEDGEMENTS**

It has been my great fortune to pursue my Ph.D. under the supervision of Dr. William D. Atchison, an opportunity for which I am very grateful. Your patience and kind support have been and still are always appreciated. Your mentoring enriched not only my educational background in neurosciences and pharmacology, but also enhanced my research skills and my own mentoring skills. This has been very valuable for helping other students. These experiences ultimately prepared me to be well equipped in my professional career. Your instruction and encouragement of proper English speech from our earliest association helped me tremendously and continues to be very much appreciated. Your guidance in working and learning has left a significant imprint in my mind. Some actual examples are crawling before running, one thing at a time, be realistic, all data are good data and always keep them, every question is valid (no such this as a stupid question), and don't reinvent the wheel. After working in academia for a little while, I have come to realize that your guidance has always been practical and true!! Hopefully, the tardiness of my realization doesn't detract from my heartfelt appreciation of your guidance. I have been applying your words in several aspects of my professional life. Your enrichment of my research thinking skills has made me confident in working as an independent researcher in any field. I could not have been successful in my current position that works in a new culture and environment and requires integrative multiple disciplines. You are always appreciated, Dr. Atchsion!!! Thank you for being so patient and allowing me to be one of your students. You are loved and respected!!! I am also very pleased to have Drs. Patricia Ganey, Colleen Hegg, and Kyle Miller as my

research committee. They always provide time and unlimited mental and educational

support. Thank you so much, Dr. Ganey for spending your time discussing my research designs, data interpretation, and presentation. Dr. Hegg, the time you devoted to correcting my drafts and the guidance you provided in my writing of results and discussions is priceless. Thank you so much for being so kind and supporting me, Dr. Hegg. Dr. Miller, you always came up with the new perspectives that challenged me. Your mentoring in conducting good research and data interpretation are superb and touching!!! Thank you so much for challenging me and providing a different perspective on things!!! Drs. Ganey, Hegg, and Miller, you are my heroes!!!

I could not have learned in the CMIB program while struggling to pursue my Ph.D. without a warm welcome and kind support from Dr. Vilma Yuzbasiyan-Gurkan. Your warm welcome even before I entered the program made me feel like I was in good hands. You encouraged me to expand my knowledge, which has helped me discover some exciting and inspiring areas that I would love to carry on in my research. You were always kind and dedicated your time to all CMIB students without conditions. Even after you were no longer the CMIB director, you kept supporting and encouraging me to finish my writing and defend my dissertation periodically. Your care and love are always touching and appreciated, Dr. Vilma.

I would like to thank Dr. Atchison's lab members, Drs. Ravindra Hajela, Sara Ciotti, Brenda Marredo-Rossado, and Aaron Bradford, for their guidance at the beginning of my research. You all helped me with techniques in the lab, including cell culture and calcium fluorometry. Thank you Dr. Yukun Yuan, for knowledge enrichment and Chinese language lessons. Thank you Dr. Michael Sceniak for being a good role model as an effective researcher and for our several discussions of science and plants. My best friend in Atchison's lab is Dr. Rosa Jaiman. Thank you so much, Rosa, for unconditional training

for the astrocyte cell culture and sharing all techniques and knowledge without reservation. You are an excellent mentor and friend!!! I also would like to thank Dr. Heidi Hannon for guiding me in establishing the animal colony and some research techniques. Thank you Melissa Jaiman for all your support and for encouraging me to take the MSU Confocal class with Dr. Frame. It was a very useful class and helped me to obtain beautiful pictures and perform data analysis in a timely manner. I also value the great opportunity I received to mentor several undergraduate students. You all enhanced my role as a graduate student and have influenced future career. Each of you are diligent and dedicated to research. Thank you for being part of my professional training. I am proud of all of you and honored to be part of your professional and academic development. Thank you, Lizabeth, Garret, Kimberly, Sarangelica, Nicole, Ashley, and Glorain, to name a few, for your part in making mentoring such a wonderful and enjoyable experience. I could have not been finished my research without assistance from my best friends in Dr. Kaminski's and Dr. Galligan's labs. Bob Crawford, Roxanne Fernades, and Dr. Ryan Mui were all very helpful to me. Bob, I greatly appreciate your patient guidance as I established my Flow Cytometry techniques and qPCR data analysis. Rox, you are my rock!! Thank you so much for being a part of every aspect of my research technique establishments such as RNA isolation, qPCR, western blotting, etc. Without you, I could not have started my qPCR techniques!!!! Thank you, Ryan, for your unwavering support and help, especially when I had difficulty writing my research proposal. Your input nailed it down for me! Otherwise, it was going to be 100 pages for the proposal!!! I appreciate all the advice and kind offers for the Nrf2 knockout mice from Dr. Cheryl Rockwell and Nrf2 activator compounds from Dr. Karen Liby from Pharmacology and Toxicology department.

I could not have pursued my PhD without my boyfriend's encouragement and support back then, and now my husband David Lockhart. I remember that when I wanted to give up on pursuing the Ph.D. because of the cost of the investment, and you advised that "Lack of education is more expensive than education". Thank you for being very patient and cooperative with me in all aspects. Your kind patience in training (mentoring) me to be accepted and understand the cultural differences have been valued and paid off. Congratulations, sweetheart, for your hard work!!

My family has been infinitely supportive of me to accomplish my education. Thank you my father, who believes in and allowed me to continue my advanced education in the US. Papa, your encouragement and emphasis on the importance of learning mathematics and sciences made a big impact on me and shaped who I am today. Papa, I really appreciate your support without hesitation and your offers to help in all aspects. Thank you, Mommy, my sweet lady, who stays beside me even when I was doing my research. Your sacrifice, kindness, and support including cooking, cleaning, helping with some PDL coating for my cell culture are worth far more than my simple thank you. I love you, Papa and Mommy. Thank you, my younger brother, Nat, who has been taking care of our family in Thailand while I was studying in the US. Without your assistance and caring of Papa and Mommy, I would not have had the peace of mind to continue my education. Thank you for being a good brother and son, Nat.

# TABLE OF CONTENTS

LIST OF TABLES.	xiv
LIST OF FIGURES	xv
KEY TO ABBREVIATIONS	xix
CHAPTER ONE: INTRODUCTION	2
1.1.3 Antioxidant genes: a role in selective neuronal vulnerability	4 8 10
a. Astrocytic heterogeneityb. Astrocytic roles in the central nervous system	13
iii. Supply neuronal glutathione	19
iv. Regulation of neuronal glutamate receptor subunit expression	27
exposure (Minamata Bay and Agano River, Japan) and acute high dose exposure (Iraq)	
Chronic low dose exposure (the Faroe and the Seychelles Islands)  1.1.9 Pharmacokinetics and pharmacodynamics of methylmercury	
toxicitya. Disruption of intracellular calcium homeostasis	51 54
antioxidant pathway  1.2 Research Objectives, rationale, and techniques:	78 78
the cellular mechanisms involving the redox and glutamate homeostasis	87
	87
cysteine (NAC) during MeHg exposure in SCAs	87

1.2.2 Research model system: Primary spinal cord astrocyte cell culture	88
a. Primary astrocyte cell culture as an experimental model	
system for understanding astrocytes in health and diseases	
b. The astrocyte cell culture protocol factors	89
1.2.3 Research Techniques:	90
a. The principle of real-time cell viability assay	90
b. Real-time quantitative polymerase-chain-reaction (qPCR)	93
CHAPTER TWO: THE MECHANISM BY WHICH METHYLMERCURY-INDUCEI	
SPINAL CORD ASTROCYTE CELL CULTURE DEGENERATION THROUGH THI	E
DYSREGULATIONS OF THE KEAP1-NRF2-ARE PATHWAY AND GLUTAMATE	
	97
	98
	100
	108
O Company of the comp	108
	108
	109
	110
	110
	111
2.3.7 Cell morphology and structure determination with coomassie brilliant	Ē
	112
	112
2.3.9 Real-Time Quantitative Reverse Transcription-PCR	
	114
2.4.1 Aged-related SCA degeneration by MeHg induced toxicity	114
2.4.2 The concentration and time-dependent MeHg-toxicity to the	
pathologic morphology of SCAs	116
2.4.3 Sub-micromolar MeHg (0.5µM) dysregulated the expression of <i>Keap1</i>	
and Nrf2 mRNA in SCAs	
2.4.4 Sub-micromolar MeHg (0.5µM) affected the expression of <i>Gclc</i> mRNA	,
	.7.
encoding to a rate-limiting enzyme for GSH synthesis in a bi-phasic	
	117
2.4.5 MeHg induced a time-dependent increase of the detoxification	
transporter Mrp1 and antioxidant precursor transporter system Xc- mRNA	
expressions	118
2.4.6. MeHg induced the increase of EAAT1/GLAST and EAAT2/GLT-1 mR	
	119
2.4.7 MeHg induced <i>Vegfa</i> mRNA expression in SCAs in a bi-phasic fashion	
	120
2.4.8 Immunocytochemistry indicated a reduction of Mrp1, system Xc- and	
EAAT2/GLT-1 expression following 5μM MeHg exposure in SCAs	120
	137

CHAPTER THREE: CHARACTERIZATION OF AN NRF2 ROLE IN THE REGULATION
OF METHYLMERCURY- INDUCED TOXICITY IN PRIMARY SPINAL CORD
ASTROCYTES DERIVED FROM C57BL/6J MICE AND NRF2 KNOCKOUT MIC149
3.1 Abstract
3.2 Introduction 153
3.3 Materials and methods 159
3.4 Results
3.4.1 The susceptibility of SCAs derived from neonatal wild type C57BL/6J
and Nrf2 knockout mice to MeHg
3.4.2. MeHg exposure reduces Nrf2 mRNA expression in both WT and Nrf2
KO derived SCAs but has differential effects on Keap1 mRNA in these
genotypes 160
3.4.3 MeHg reduces Gclc, GPx1, and GPx4 mRNA expression in both WT and
Nrf2 KO derived SCAs 161
3.4.4 Nrf2 KO derived SCAs express Abcc1 mRNA to a greater extent than
the WT derived SCAs; however, a greater Abcc1 mRNA expression did not
provide greater resistance to MeHg than the WT 163
3.4.5 Nrf2 KO derived SCAs expressed Slc7a11 mRNA greater than the WT
derived SCAs, and MeHg affected Slc7a11 mRNA expression in these
genotypes differently 163
3.4.6 Nrf2 KO derived SCAs exhibit higher basal levels of Slc1a3 and Slc1a2
mRNAs relative to WT derived SCAs and MeHg reduces the mRNA
expression in both WT and Nrf2 KO derived SCAs 165
3.4.7 MeHg induced the reduction of transporter proteins, Mrp1, system Xc-
and EAAT2/GLT-1 expression in both WT and Nrf2 KO derived SCAs 176
3.4.8 MeHg differential regulated Vegfa mRNA expression in WT and Nrf2
KO derived SCAs 181
3.5 Discussion
CHAPTER FOUR: MECHANISMS BY WHICH AN N-ACETYL CYSTEINE IN THE
PROTECTION OF THE SPINAL CORD ASTROCYTE CELL CULTURE FROM
METHYLMERCURY INDUCED TOXICITY 207
4.1 Abstract
4.2 Introduction
4.3 Materials and methods
4.3.1 Chemicals
4.3.2 MeHg exposure and NAC treatment regimens
4.3.3 Cell viability assay with ethidium homodimer 217
4.4 Results
4.4.1 NAC protected SCAs from MeHg in a concentration-dependent
fashion
4.4.2 Pretreatment, cotreatment, and posttreatment with 1.0mM NAC and
5μM MeHg maintained <i>Keap1</i> mRNA levels at similar levels to <i>Keap1</i> mRNA
levels in vehicle treatment
4.4.3 NAC protected and reversed the reduction of GSH metabolic pathways
and transporters such as Gclc, GPx1, GPx4, and Abcc1 mRNA levels in SCAs
treated with MeHg221

4.4.4 NAC protected and reversed the dysregulation of glutamate transport	Ī
	223
4.4.5 Pretreatment with NAC 2h and subsequently removal before exposure	e
to MeHg was not protective	224
4.5 Discussion	240
CHAPTER FIVE: CONCLUSION AND DISCUSSION	254
5.1 The comparative concentration-response curves and function of time of susceptibility between the early developmental stage (DIV14) and the fully	
developmental stage (DIV30) of SCAs exhibited aged related susceptibility 5.2 The primary antioxidant pathway Keap1-Nrf2-ARE pathways were	. 255
dysregulated during MeHg exposure in SCAs	256
5.3 The regulation of redox and glutamate homeostasis are intertwined in SCAs	257
5.4 The biphasic elevation of <i>Vegfa</i> mRNA expression during MeHg exposure in	
SCAs would contribute to the blood spinal cord barrier (BSCB) permeability 5.5 Genetic disruption of Nrf2, a master regulator of the Keap1-Nrf2-ARE	259
pathway, rendered SCAs are more susceptible to MeHg	261
5.6 The loss of Nrf2 in Nrf2 KO derived SCAs contributed to the significant	
reduction of GSH synthesis and metabolism pathways	263
5.7 Other signaling pathways involved in the regulation of some of the genes	06.4
underlying the Nrf2 and ARE pathway	264
5.8 Genetic predisposition exhibited differential mechanisms by which MeHg induced neurotoxicity in SCAs	266
5.9 The antioxidant NAC could protect and rescue SCAs from MeHg induced	200
degeneration in a concentration-dependent manner	267
5.10 The primary NAC mechanism in protecting SCAs during MeHg exposure	- /
in the NAC pretreatment paradigm was its direct antioxidant property	
or GSH-independent antioxidant mechanism	269
APPENDIX	272
DEEEDENCES	- 0
	$\Omega Q_{7}$

# LIST OF TABLES

Table 1 The physicochemical properties and toxicokinetics of Hg species: sources, potential exposure, toxicity, and reference value and regulation limits	29
Table A1 Primers lists for this research	276
Table A2 Primary antibodies used in this research	277
Table A3 Secondary antibodies used in this research	278

# LIST OF FIGURES

Figure 1.1. The regulation of cellular ROS and RNS	3
Figure 1.2 Keap1-Nrf2-ARE pathway	7
Figure 1.3 The extracellular glutamate uptake is regulated by EAATs	18
Figure 1.4 The glutamate-glutamine cycle and GSH metabolism	21
Figure 1.5 Global cycle of Hg	39
Figure 1.6 Proposed cellular mechanisms by which MeHg induced toxicity in the CNS: the interaction between astrocytes and neurons	85
Figure 1.7 Working hypothesis.	86
Figure 1.8 The principle of the Real-Time Cell Viability Assay	91
Figure 2. 1 Research aims 1: Determination of SCAs sensitivity during MeHg exposure and the cellular mechanisms involving the redox and glutamate homeostasis.	107
Figure 2.2 SCA Cell Culture (DIV14) exposed to 0, 0.1, 0.5, 1, 2, and 5 $\mu$ M MeHg from 30 min to 27 h	122
Figure 2.3 SCA cell culture (DIV30) exposed to 0, 0.1, 0.5, 1, 2 and 5 $\mu$ M MeHg from 30 min to 27 h	123
Figure 2.4 Comparison of the susceptibility to MeHg between SCAs DIV14 (early developmental stage) and DIV 30 (fully developed stage)	124
Figure 2.5 Pathological and morphological features of SCAs at DIV 14 exposed to different MeHg concentrations for 3h and 24h	125
Figure 2.6 The expression profile of <i>Keap1</i> mRNA during 0.5µM MeHg exposure to SCAs for 18 h	126
Figure 2.7 The expression profile of <i>Nrf2</i> mRNA during 0.5μM MeHg exposure to SCAs for 18 h	127
Figure 2.8 The biphasic expression profile of <i>Gclc</i> mRNA during 0.5µM MeHg exposure to SCAs for 24 h	128
Figure 2.9 The expression profile of <i>Abcc1</i> (Mrp1) mRNA during 0.5µM MeHg exposure to SCAs for 18 h	129
Figure 2.10 The expression profile of <i>Slc7a11</i> (systemXc-) mRNA during 0.5µM MeHg exposure to SCAs for 24 h	130

Figure 2.11 The expression profile of $Slc1a3$ (GLAST in murine or EAAT1 in human) mRNA during 0.5 $\mu$ M MeHg exposure to SCAs for 12 h
Figure 2.12 The expression profile of <i>Slc1a2</i> (GLT-1 in murine or EAAT2 in human) mRNA during 0.5µM MeHg exposure to SCAs for 12 h
Figure 2.13 Comparison of the expression profiles of $Slc1a3$ and $Slc1a2$ during 0.5µM MeHg exposure to SCAs for 12 h and their control
Figure 2.14 The biphasic expression profile of <i>Vegf</i> mRNA during 0.5µM MeHg exposure for 24 h
Figure 2.15 Comparision of morphological features and transporter protein expressions of SCAs following $5\mu M$ MeHg exposure for $18h$
Figure 2.16 The reduction of Mrp1, system Xc- and GLT-1 proteins in SCAs following 5µM MeHg for 18h
Figure 3.1 Comparison of the susceptibility of DIV 30 SCAs to MeHg between SCAs derived from wild type C57BL/6J mice pups and Nrf2 knockout mice pups 166
Figure 3.2 Relative mRNA expression of $Nrf2$ mRNA derived from wild type SCAs (WT) and Nrf2-KO SCAs (KO) when exposed to 5 $\mu$ M MeHg for 18h
Figure 3.3 Relative mRNA expression of <i>Keap1</i> mRNA derived from wild type SCAs (WT) and Nrf2-KO SCAs (KO) when exposed to 5µM MeHg for 18h 168
Figure 3.4 Relative mRNA expression of $Gclc$ mRNA derived from wild type SCAs (WT) and Nrf2-KO SCAs (KO) when exposed to 5 $\mu$ M MeHg for 18h
Figure 3.5 Relative mRNA expression of $GPx1$ mRNA derived from wild type SCAs (WT) and Nrf2-KO SCAs (KO) when exposed to 5 $\mu$ M MeHg for 18h
Figure 3.6 Relative mRNA expression of $GPx4$ mRNA derived from wild type SCAs (WT) and Nrf2-KO SCAs (KO) when exposed to 5 $\mu$ M MeHg for 18h
Figure 3.7 Relative mRNA expression of $Abcc1$ mRNA derived from wild type SCAs (WT) and Nrf2-KO SCAs (KO) when exposed to $5\mu$ M MeHg for $18h$
Figure 3.8 Relative mRNA expression of $Slc7a11$ mRNA derived from wild type SCAs (WT) and Nrf2-KO SCAs (KO) when exposed to 5 $\mu$ M MeHg for 18h 173
Figure 3.9 Relative mRNA expression of $Slc1a3$ mRNA derived from wild type SCAs (WT) and Nrf2-KO SCAs (KO) when exposed to $5\mu M$ MeHg for $18h$
Figure 3.10 Relative mRNA expression of $Slc1a2$ mRNA derived from wild type SCAs (WT) and Nrf2-KO SCAs (KO) when exposed to 5 $\mu$ M MeHg for 18h 175
Figure 3.11 Comparative morphologies and transporter protein expressions of SCAs derived from WT following $5\mu M$ MeHg exposure for $18h$

Figure 3.12 Comparative morphologies and transporter protein expressions of SCAs derived from Nrf2 KO following $5\mu M$ MeHg exposure for $18h$	s 178
Figure 3.13 Comparative effect of 5µM MeHg to SCAs from WT and Nrf2 KO follow 18h exposure	ing 179
Figure 3.14 Comparative effect of $5\mu M$ MeHg to the expression of transporter proteins in SCAs derived from WT and Nrf2 KO following 18h exposure	180
Figure 3.15 Relative mRNA expression of $Vegfa$ mRNA derived from wild type SCA (WT) and Nrf2-KO SCAs (KO) when exposed to $5\mu$ M MeHg for 18h	
Figure 3.16 Proposed mechanisms involved in the regulation of <i>Slc7a11</i> in Nrf2 KO derived SCAs	
Figure 3.17 Proposed mechanism of MeHg in the induction of <i>Abcc1</i> (Mrp1) expression in Nrf2 KO-derived SCAs	197
Figure 3.18 Proposed mechanism of MeHg induced <i>Vegf</i> mRNA expression in SCAs.	202
Figure 4.1 Research aim 3: Working hypothesis of NAC actions in SCAs during MeHg exposure	215
Figure 4.2 MeHg exposure and NAC treatment regimens	216
Figure 4.3 Cell metabolic activity as a function of time when SCAs were treated with 0.1, 1.0, and 10mM NAC for 2h prior to exposure with $5\mu$ M MeHg	226
Figure 4.4 Cell metabolic activity as a function of time when SCAs were cotreated with 0.1, 1.0, and 10mM NAC and $5\mu M$ MeHg or vehicle	227
Figure 4.5 Cell metabolic activity as a function of time when SCAs were exposed to $5\mu M$ MeHg for 3h and 0.1 or 1.0 mM NAC was subsequently administered	228
Figure 4.6 The effect of NAC on regulation of <i>Keap1</i> mRNA during MeHg exposure SCAs.	in 229
Figure 4.7 The effects of NAC on regulation of <i>Nrf2</i> mRNA during SCAs exposure to MeHg	0 230
Figure 4.8 The effect of NAC on regulation of <i>Gclc</i> mRNA during SCAs exposure to MeHg.	231
Figure 4.9 The effect of NAC on regulation of <i>GPx1</i> mRNA during SCAs exposure to MeHg	
Figure 4.10 The effect of NAC on regulation of <i>GPx4</i> mRNA during SCAs exposure to MeHg.	
Figure 4.11 The effect of NAC on regulation of <i>Abcc1</i> mRNA during SCAs exposure to MeHg	

Figure 4.12 The effect of NAC on regulation of <i>Slc7a11</i> mRNA during SCAs exposu MeHg	
Figure 4.13 The effect of NAC on regulation of <i>Slc1a3</i> mRNA during SCAs exposur MeHg.	
Figure 4.14 The effect of NAC on regulation of <i>Slc1a2</i> mRNA during SCAs exposur MeHg.	
Figure 4.15 Cell metabolic activity as a function of time when SCAs were treated w. 1.0 or 10mM NAC or vehicle (DMSO+ $H_2O$ ) for 2h, subsequently removed before administration of 5 $\mu$ M MeHg.	ith 238
Figure 4.16 Morphology of SCAs when treated with 1.0mM NAC or vehicle (DMSC for 2h, subsequently removed before 5µM MeHg administration	
Figure A.1 Representative diagram of immunological positive to GFAP in SCAs DIV30	273
Figure A.2 Pathological and morphological features of SCAs DIV14 as a function of time of 0.5µM MeHg exposure, from 1h to 4h	
Figure A.3 Pathological and morphology features of SCAs DIV14 as a function of time of 0.5µM MeHg exposure, from 6h to 24h	275
Figure A.4 SCAs were treated with 10μM edaravone (EDAVA) 1h prior to exposure with 5μM MeHg	
Figure A.5 SCAs were treated with 100μM edaravone (EDAVA) 1h prior to exposur with 5μM MeHg	
Figure A.6 SCAs were treated with 1µM edaravone (EDAVA) 1h prior to exposure with 5µM MeHg	281
Figure A.7 SCAs were treated with 10mM edaravone (EDAVA) 1h prior to exposure with 5µM MeHg	
Figure A.8 SCAs were treated with 1µM CDDO-IM for 1h prior to exposure with 5µM MeHg	283
Figure A.9 SCAs were treated with 10μM CDDO-IM for 1h prior to exposure with 5μM MeHg	284
Figure A.10 SCAs were treated with 1µM CDDO-ME for 1h prior to exposure with 5µM MeHg	285
Figure A.11 SCAs were treated with 10µM CDDO-ME for 1h prior to exposure with 5µM MeHg	

#### **KEY TO ABBREVIATIONS**

ABC - ATP-binding cassette

Abcc1- ATP-binding cassette subfamily C member 1

ACh - Acetylcholine

ACM - Astrocyte condition media

AIF - Apoptosis-inducing factor

Akt – (referred to as) protein kinase B

ALS - Amyotrophic lateral sclerosis

AMPA - α-amino-3-hydroxy-5-methyl-4-isoxazolepropionic acid

AMPARs - α-amino-3-hydroxy-5-methyl-4-isoxazole propionic-acid/ kainate receptors

ANOVA - Analysis of variance

ADP+ – Adenosine diphosphate

APN - aminopeptidase

ATP - Adenosine 5'-triphosphate

ATPase – Adenylpyrophosphatase

ARE - Antioxidant-response element

BAPTA-AM - 1,2-Bis(2-aminophenoxy)ethane-N,N,N',N'-tetraacetic acid

tetrakis(acetoxymethyl ester)

BBB - Blood-brain barrier

BSA - Bovine serum albumin

BSCB -Blood spinal cord barrier

BSO - L-buthionine-S,R-sulfoximine

bZip - Basic-region leucine zipper

Ca2+ - Calcium

[Ca<sup>2+</sup>]<sub>in</sub> - Intracellular calcium concentration

 $Ca^{2+}$ -AMPARs -  $Ca^{2+}$ -permeable- $\alpha$ -amino-3-hydroxy-5-methyl-4-isoxazole propionicacid/ kainate receptors

CAC - Cortical astrocyte cell culture

CaCl2 - Calcium chloride

CaMK - Ca<sup>2+</sup>/calmodulin kinase

cAMP - Cyclic adenosine monophosphate

CCCP - Carbonyl cyanide m-chlorophenyl hydrazone

CDDO - 2-cyano-3,12-dioxooleana-1,9-dien-28-oic acid

CDDO – IM - 1-[2-cyano-3-,12dioxooleana-1,9(11)-dien-28-oyl]imidazole (CDDO-imidazole)

CDDO-Me - CDDO-ethyl amide (C-28 methyl ester of CDDO)

CHO - Chinese hamster ovary cells

CGCs - Cerebellar granule cells

CMEC - Cardiac microvascular endothelial cells

CNC - Cap "n" collar

CNS - Central nervous system

CO – Cotreatment (Methylmercury and NAC)

CO<sub>2</sub> - Carbon dioxide

CPN-9 - N-(4-(2-pyridyl)(1,3-thiazol-2-yl))-2-(2,4,6-trimethylphenoxy) acetamide

CsA - cyclosporin A

Ct - Cycle threshold

Cul3- Cullin bases E3 ubiquitin ligase

Cu<sup>2+</sup>/Zn<sup>2+</sup> SOD- Copper/Zinc superoxide dismutase

Cyss - Cystine

Cys -Cysteine

DA - Dopamine

DAPI - 4',6-diamidino-2-phenylindole

dBcAMP - dibutyryl cyclic adenosine monophosphate

DCF - 2',7'-dichlorofluorescein

DEM - Diethylmaleate

DIV - Day in vitro

DMEM - Dulbecco's modified eagle medium

DMPS - 2,3-dimercapto-1-propane sulfonate

DMSA - meso 2,3-dimercaptosuccinic acid

DMSO - Dimethyl sulfoxide

DNase I - Deoxyribonuclease I

DRG - Dorsal root ganglia

DTNB - 5,5'-dithiol-bis(2-nitrobenzoic) acid

DTT - Dithiothreitol

EAA - Excitatory amino acid

EAAC1 - Excitatory amino acid carrier 1

EAATs - Excitatory amino acid transporters

EC-SOD -Extracellualr superoxide dismutase

EGL - External granule layer

EGTA - Ethylene glycol-bis(2-aminoethylether)-N,N,N',N'-tetraacetic acid

EPPs - End-plate potentials

EpRE - Electrophile response element

**EPSCs** - Excitatory postsynaptic currents

EPSPs - Excitatory postsynaptic potentials

EthD-2 - Ethidium homodimer-2

fALS – Famililar amyotropic lateral sclerosis

FBS - Fetal bovine serum

Fe2+- Iron

g - gram

GABA - Gamma-aminobutyric acid

GABA<sub>A</sub>Rs- γ-aminobutyric acid type-A receptors

Gapdh - Glyceraldehyde-3-phosphate dehydrogenase

GCL - Glutamate-cysteine ligase

GCLC -Glutamate-cysteine ligase catalytic subunit

GCLM - Glutamate-cysteine ligase modifier subunit

GD - Gestation day

GFP - Green fluorescent protein

GFAP - Glial fibrillary acidic protein

GLAST – Glutamate/aspartate transporter

Gln - Glutamine

GLT1 - Glutamate transporter 1

Glu - Glutamate

[Glu]<sub>ex</sub> - Extracellular glutamate concentration

[Glu]<sub>in</sub> - Intracellular glutamate concentration

GluR – Glutamate receptors

Gly - Glycine

GPx-Glutathione peroxidase

Gpx 1 - Glutathione peroxidase 1

Gpx 4 - Glutathione peroxidase 4

GR - Glutathione reductase

GSH - Glutathione

GS - Glutamine synthetase

GSK-3β - Glycogen synthase kinase- 3 beta

Gst - Glutathione transferase

 $\gamma$ -GT -  $\gamma$ -glutamyltranspeptidase

GVIA - ω - Conotoxin GVIA

GSK- $3\beta$  - Glycogen synthase kinase- $3\beta$ 

IGL - Internal granule layer

h – hours

HBSS - Hanks' Balanced Salt Solution

HEPES - 4-(2-hydroxyethyl)-1-piperazineethanesulfonic acid

HepG2 - Human hepatoma cells

Hg – Mercury, referred to as elemental mercury

Hg+ - Mercurous

Hg<sup>2+</sup> - Mercuric mercury, represented as an example of inorganic mercury

Ho-1 – Heme oxygenase 1

HgS - Mercury sulfide

5-HIAA - 5-hydroxy-indole-3-acetic acid

HIF - Hypoxia inducing factor

HIF-1α - Hypoxia inducing factor-1α

HNE - Hydroxynonenal

Ho-1 - Heme oxygenase

H<sub>2</sub>O<sub>2</sub>-Hydrogen peroxide

HRE - Hypoxia response element

hTg SOD G93A – Human transgenic superoxide dismutase glycine 93 alanine

IC50 - Half-maximal inhibitory concentration

I-GABA<sub>A</sub> - γ-aminobutyric acid type-A receptors current

IL-1β - Interleukin-1β

iPSC - Induced pluripotent stem cell

IPSCs - Inhibitory postsynaptic currents

IPSPs - Inhibitory postsynaptic potentials

K+ - Potassium

KCl - Potassium chloride

Keap1- Kelch-like ECH-associated protein 1

KH<sub>2</sub>PO<sub>4</sub> - Monopotassium phosphate

L - Litre

LDH - Lactate dehydrogenase

LPS - Lipopolysaccharide

LTD - Long term depression

LTP - Long term potentiation

LVA - Low voltage-activated

Ψm – Mitochondrail membrane potential

µm – Micrometer

μg – Microgram

μg/g – microgram(s) per gram(s)

μL - Microliter

μM - Micromolar

M - Molar

mAChRs - Muscarinic acetylcholine receptors

MAO-B - Monoamine oxidase B

MeHg – Methylmercury

MEPP - Miniature end-plate potential

MEPSPs - Miniature excitatory postsynaptic potentials

MgSO<sub>4</sub> - Magnesium sulfate

min - Minute

miRNA - MicroRNA

mL - Milliliter

ML - molecular layer

MLNs - cerebellar Molecular layer neurons

mm - Milimeter

mM - Millimolar

MN - Motor neurons

MNDs - Motor neuron disease

Mn<sup>2+</sup> - Manganese

MnSOD – Maganese superoxide dismutase

MP - MeHg posttreatment

MPTP - 1-methyl-4-phenyl-1,2,5,6-tetrahydropyridine

mPTP - Mitochondrial transition pore

MRLs+- positive Minimal Risk Levels

Mrp – Multidrug resistance proteins

MTT - Methylthiazolyldiphenyl-tetrazolium bromide

NAC – N-acetyl-L-cysteine or N-acetylcysteine

NaCl - Sodium chloride

Na+ - Sodium

Na<sub>2</sub>HPO<sub>4</sub> - Disodium phosphate

NASPM - 1-naphthyl acetyl spermine

ng - Nanogram

NGS - Normal goat serum

nm - Nanometer

nM – Nanomolar

NMDARs - N-methyl-D-aspartate receptors

NMJ Neuromuscular junctions

NP - NAC 2 h pretreatment

NO - Nitric oxide

NOS - Nitric oxide synthase

NOX - NADPH oxidase

Nqo-1 - NAD(P)H: quinone oxidoreductase 1

Nrf<sub>2</sub> - Nuclear factor erythroid 2-related factor 2

Nrf2 KO- Nuclear factor erythroid 2-related factor 2 knockout

NSC34- Neuroblastoma spinal cord cell 34 (motor neuron like cells)

NSPCs - Neuronal stem progenitor cells

O2 - Oxygen

OCLN - Occludin

OH -- Hydroxyl radicals

**OXPHOS** - Oxidative phosphorylation

PBS - Phosphate-buffered saline

PC12 cells- Pheochromocytoma cells

PCBs – Polychlorinated biphenyls

PD - Parkinson's disease

PKA - Protein kinase A

PKC - Protein kinase C

PKCs- cerebellar Purkinje cells

PND – Postnatal day

ppm – part per million

Prx - Peroxiredoxins

qPCR - Real-time quantitative polymerase-chain-reaction

Rbx1- RING-box protein 1

RfC - Reference Concentration and

RfD - Reference Dose

RNS - Reactive nitrogen species

**ROI** - Regions of interest

ROS - Reactive oxygen species

sALS - Sporadic amyotrophic lateral sclerosis

SDS-PAGE – Sodium dodecyl sulfate-polyacrylamide gel electrophoresis

sEPSCs - Spontaneous excitatory postsynaptic potentials

sIPSCs - Spontaneous inhibitory postsynaptic potentials

Slc - Solute carrier

Slc1a3 - Solute carrier family 1 member 3

Slc1a2 - Solute carrier family 1 member 2

*Slc7a11* - Solute carrier family 7 member 11

SEM - Standard error of the mean

SER - Smooth endoplasmic reticulum

SERCA - Sarco/endoplasmic reticulum Ca<sup>2+</sup> ATPase

sMaf - Small musculoaponeurotic fibrosarcoma

SNAP-23 - Synaptosome-associated protein of 23 kDa

SNAT - Sodium-coupled neutral amino acid transporter

SOD - Superoxide dismutase

O<sub>2</sub>--Superoxide anion

OXPHOS - Oxidative phosphorylation

TBI - Traumatic brain injury

tBHQ - tert-butylhydroquinone

TCA - Tricarboxylic acid

TPEN - N,N,N',N'-tetrakis (2-pyridylmethyl)ethylenediamine

Txnrd-Thioredoxin reductase

USEPA - the US Environmental Protection Agency

USNRC - the US National Research Council

VDCCs - Voltage-dependent calcium channels

VEGF - Vascular endothelial growth factor

VGCCs - Voltage-gated calcium channels

VGLUTs - Vesicular glutamate transporters

v/v – Volume by volume

WHO – the World Health Organization

WT – Wild-type

w/v – Weight by volume

XO - Xanthine oxidase

Zn<sup>2+</sup>- Zinc

 $[Zn^{\scriptscriptstyle 2+}]_{in}$  - intracellular zinc

CHAPTER ONE INTRODUCTION

### 1.1 Background

## 1.1.1 Oxidative stress: the role in physiology and pathophysiology

Under normal physiology, reactive oxygen species (ROS) are produced in many cellular compartments throughout the activity of several enzymatic pathways (Wallace, 2005; Frazzini et al., 2006). ROS include the superoxide anion (O2-), hydrogen peroxide (H<sub>2</sub>O<sub>2</sub>), and hydroxyl radicals (OH<sup>-</sup>) (Schieber and Navdeep, 2014). Besides, the NADPH oxidases, nitric oxide synthase (NOS), peroxisomes, and cyclooxygenases are all participating in the cellular oxidative burden. Mitochondria produce the majority of cellular ROS as a toxic by-product of oxidative phosphorylation (OXPHOS) during the ATP formation (Wallace, 2005; Frazzini et al., 2006). Therefore, mitochondrial possess a critical role as an active organelle for both generating of ROS and the recycling of these free radicals. Approximately 2-4% of the oxygen consumed by mitochondrial is diverted to form O<sub>2</sub>-. The supper oxide is converted to H<sub>2</sub>O<sub>2</sub> by superoxide dismutase (SOD). H<sub>2</sub>O<sub>2</sub> is later transformed into water (H<sub>2</sub>O) by glutathione peroxidase (Gpx) or converted to O<sub>2</sub> and H<sub>2</sub>O by catalase (**Figure 1.1**) (Fukai and Ushio-Fukai, 2011; Lubos et al., 2011). In mammalian cells, SOD consists of three isoforms: the cytoplasmic Cu<sup>2+</sup>/Zn<sup>2+</sup> homodimer SOD (Cu<sup>2+</sup>/Zn<sup>2+</sup> SOD a.k.a. SOD1), the mitochondrial manganese SOD (MnSOD a.k.a. SOD2), and the extracellular Cu<sup>2+</sup>/Zn<sup>2+</sup> tetrameric SOD (EC-SOD a.k.a. SOD3), all of which require catalytic metal (Cu<sup>2+</sup> or Mn<sup>2+</sup>) for their activation (Fukai and Ushio-Fukai, 2011; Yan and Spaulding, 2020).

The OXPHOS in the brain is the potential process to generate a high quantity of ROS relative to other parts of the body since the brain cells utilize about 20% of the oxygen consumed by the body, while it accounts for only 2% of the bodyweight (Dringen and Hirrlinger, 2003). In addition, the brain is especially vulnerable to oxidative stress due to

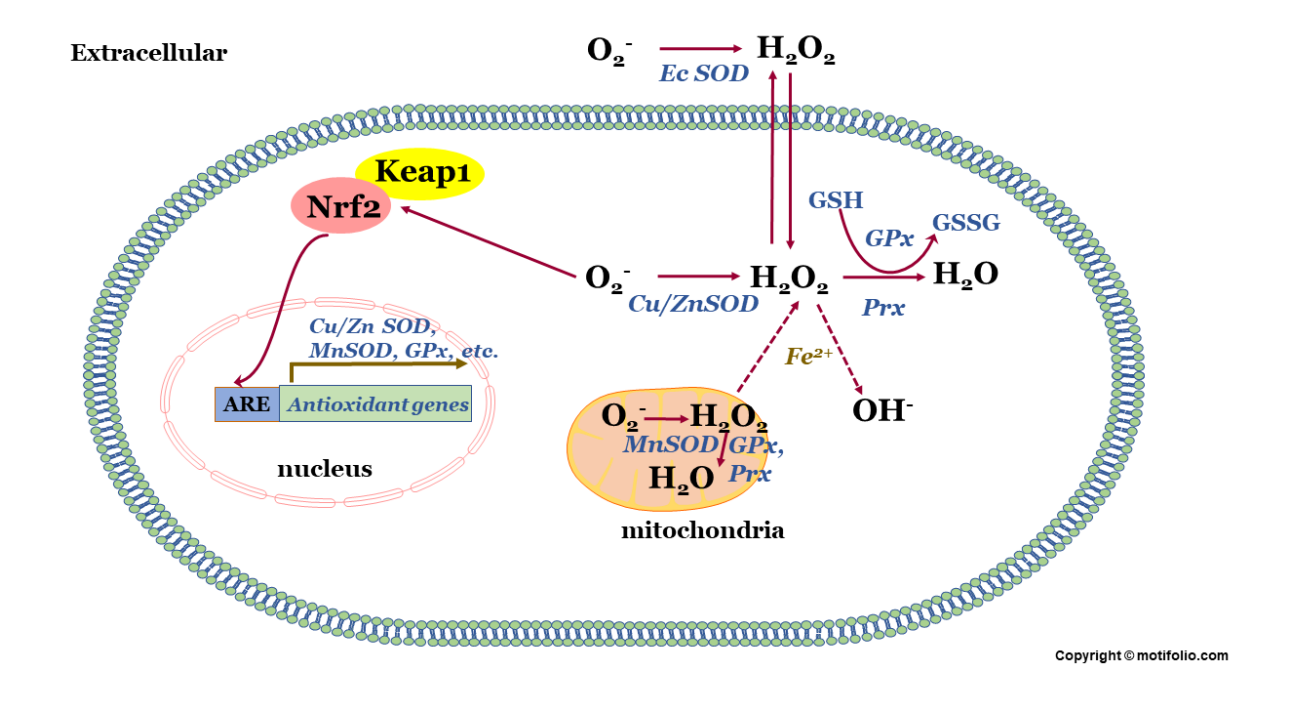


**Figure 1.1 The regulation of cellular ROS and RNS.** ROS and RNS are byproducts form normal physiological activities, particularly during OXPHOS for ATP generation. Extracellular superoxide dismutase (EcSOD or SOD3), cytosolic copper, zinc SOD ( $Cu^{2+}/Zn^{2+}$  SOD or SOD1), and mitochondrially located manganese SOD (MnSOD or SOD2) play a major role in the diversion of superoxide ( $O_2$ -) into hydrogen peroxide ( $O_2$ -) into hydrogen peroxide ( $O_2$ -).  $O_2$ - is subsequently enzymatically reduced by glutathione peroxidases ( $O_2$ -), catalase, and peroxiredoxins ( $O_2$ -) into non-reactive compounds; oxygen ( $O_2$ -) and water ( $O_2$ -).  $O_2$ - could further react with free Fe<sup>2+</sup> resulting in a highly reactive molecule, hydroxyl radical ( $O_2$ -) in "Fenton reaction." Therefore, removal  $O_2$ - is essentially protected against oxidative damage (Lubos et al., 2011). The ROS/RNS formation is tightly regulated with the stress response pathway Keap1-Nrf2-ARE pathway (the antioxidant pathway) to maintain the cellular redox.

the relatively lower antioxidant enzymatic activities such as SOD, glutathione peroxidase (GPx), glutathione reductase (GR) and catalase, compared to those in other tissues. Besides, the brain contains an abundance of lipids with unsaturated fatty acids that are the targets for lipid peroxidation. In normal physiology, superoxide and nitric oxide (NO)

produced by NOS activation are not toxic unless they react non-enzymatically with each other to form peroxynitrite, a potent reactive nitrogen species (RNS) in the brain (Aoyama and Nakaki, 2013). ROS and RNS are essential molecules for maintenance of normal thiol-redox homeostasis, mitochondrial function, and signal transductions, including long term potentiation (LTP) and long term depression (LTD) in synaptic plasticity (Massaad and Klann, 2011). The generation of ROS and RNS is counter balanced by an appropriate antioxidative system to control redox homeostasis. The imbalance of the redox homeostasis is investigated by antioxidative defend systems i.e., Keap1-Nrf2-ARE pathway (see more detail in the next section). When the antioxidative defense fails to defend against the oxidative stress, the common pathophysiology will occur, including the mitochondrial dysfunction, oxidative nucleic acid and protein damage, and membrane lipid peroxidation (Lubos et al., 2011) as a common pathophysiology in neurodegenerative disease and brain aging.

1.1.2 Stress response or antioxidant pathway: the Keap1-Nrf2-ARE pathway
The Keap1-Nrf2-ARE pathway is the primary regulator of cytoprotective response to
endogenous and exogenous stress caused by ROS/RNS and electrophiles (Kansanen et
al., 2013). A master regulator in the induction of cytoprotective and antioxidant genes in
this pathway is the nuclear factor-erythroid 2-related factor 2 (Nrf2, encoded by *Nfe2l2*gene (Tonelli et al., 2018)) (Hayes and Dinkova-Kostova, 2014). Nrf2 is a transcription
factor that regulates several cellular detoxification and antioxidant genes (see genes listed
in Table 1 review by Hayes and Dinkova-Kostova (2014). Nrf2 as well as Nrf1 belongs to
the Cap "n" collar (CNC) family of transcription factors that possess the conserved basicregion leucine zipper (bZip) motif (Tonelli et al., 2018). This motif is responsible for Nrf2

heterodimerization with the small musculoaponeurotic fibrosarcoma (sMaf) proteins (Motohashi and Yamamoto, 2004)under unbalance of redox homeostasis. The Nrf2-sMaf heterodimerization subsequently binds to the antioxidant-response element (ARE) or electrophile response element (EpRE) in the promoter region of a vast array of cytoprotective/antioxidant genes (Zhu and Fahl, 2001).

The high turn overexpression property of Nrf2 is regulated by its partner Kelch-like-ECHassociated protein (Keap1). Under the homeostatic conditions, Nrf2 is negatively regulated by Keap1 to maintain Nrf2 basal level under the low level (Motohashi and Yamamoto, 2004) to prevent the constitutive activation of the oxidative stress response (Bryan et al., 2013). Keap1 functions as a ubiquitin adaptor for cullin bases E3 ubiquitin ligase (Cul<sub>3</sub>), and RING-box protein 1 (Rbx1) (Cul<sub>3</sub>/Rbx1) that results in a continuous degradation of Nrf2 through a ubiquitin-proteasome degradation (Niture et al., 2014; Tonelli et al., 2018). The Keap1 facilitating proteasomal degradation of high turn over Nrf2 results in a half-life of approximately 10–20 min (Bryan et al., 2013). Keap1 is a cysteine-rich protein containing 25 cysteines in mice and 27 cysteines in human (Kansanen et al., 2013). Most of these cysteines can be modified in vitro by different oxidants and electrophiles (Kansanen et al., 2013). Therefore Keap1 acts as a primary sensor for electrophiles and oxidants (Shah et al., 2018). Under the loss of redox homeostasis in which ROS/NOS is overproduction, the thiol (or "sulfhydryl") group on Keap1 cysteines is oxidized, resulting in a disruption of the interaction with Nrf2, and Nrf2 translocation into the nucleus where it dimerizes with the sMaf proteins (Tonelli et al., 2018). The Nrf2 and sMaf heterodimerization binds to the ARE region and initiates expressions of a multitude of antioxidant proteins, detoxification enzymes, and xenobiotic transporters (Ma, 2013; Hayes and Dinkova-Kostova, 2014). Nrf2 activation through the Keap1-dependent pathway extends its half-life by approximately 7.5 to 15 min (Bryan et al., 2013). Nevertheless, the changes in Nrf2 half-life associated with oxidative stress and specific electrophiles vary immensely between cell lines due to the dramatic differences in the protein's detectable basal levels (Kwak et al., 2002; Bryan et al., 2013). Alternative pathways that regulate Nrf2 for the cytoprotective effects include 1. phosphorylation of Nrf2 by various protein kinases, PKC, PI3K/Akt, GSK-3b, JNK, 2. interaction with other protein partners such as p21, caveolin-1, and 3. epigenetic factors such as micro-RNAs -144, -28 and -200a, and promoter methylation (Bryan et al., 2013). Besides primary negative regulation Keap1 complexing with Cul3/Rbx1, additional Nrf2 negative regulators are presented in the nucleus, including Src subfamily A members Fyn, Src, Yes, and Fgr. These transcription factors phosphorylate the nuclear Nrf2 at tyrosine 568 (Nrf2 Tyr 568), leading to nuclear export and the degradation of Nrf2 Tyr 568 (Jain and Jaiswal, 2007). The glycogen synthase kinase-3β (GSK-3β) is an effector of Src family members. GSK-  $3\beta$  is activated by the  $H_2O_2$ , which phosphorylates the Tyr 216 of GSK-3β. Activated GSK-3β later phosphorylates Fyn kinase at the threonine residue(s) (Jain and Jaiswal, 2007). The regulation of Nrf2 by GSK- 3β-Fyn is considered a Keap1independent pathway and was suggested to be an alternative pathway in the

therapeutic target (Culbreth and Aschner, 2018).

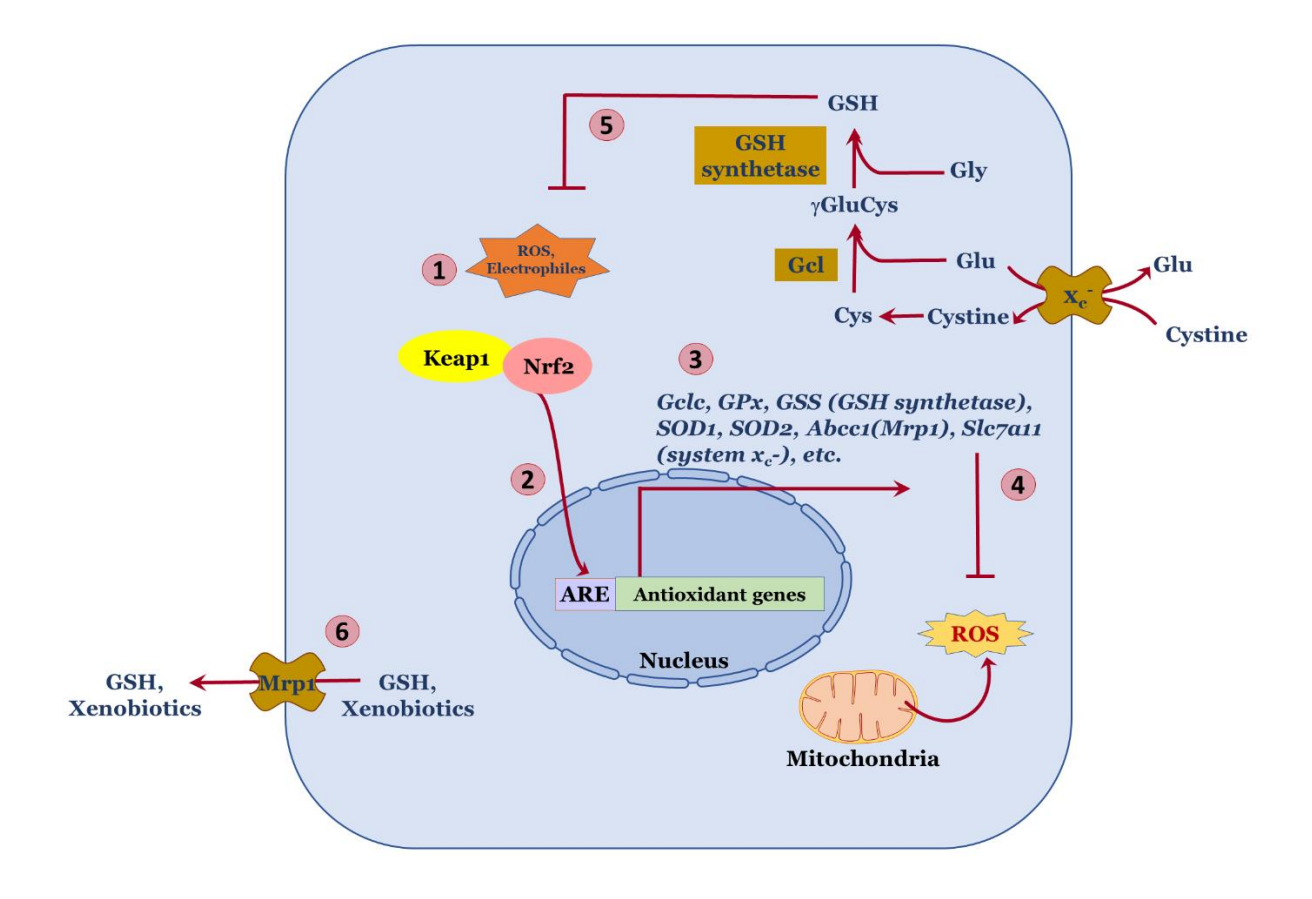


**Figure 1.2 Keap1-Nrf2-ARE pathway.** This major antioxidant pathway is activated when the oxidative stress or electrophiles occur intracellularly. In normal physiology, when the redox homeostasis is maintained, Keap1 constitutively regulates the expression of Nrf2 by which it binds Nrf2 to undergo proteosome degradation. When ROS or electrophiles occur, the redox sensor Keap1 dissociates from Nrf2 due to their bond breaking by electrophiles or ROS (1). Nrf2 later translocates into the nucleus, where it binds to the ARE region (2). Subsequently, several antioxidant genes, including the GSH synthesis enzymes (Gcl, GSS), GSH precursor transporter (systemXc-), GSH transporter (Mrp1) are expressed (3). These antioxidant genes are later translated to function as ROS detoxifiers (4). For example, the system Xc- imports cystine as a substrate precursor for cysteine (Cys), Gcl as a rate-limiting enzyme for GSH synthesis, and GSS as GSH synthesis for GSH synthesis. GSH has a significant role in the detoxification of ROS and electrophiles in cells (5) and exports xenobiotics and electrohples through the GSH transporter Mrp1 (6).

Another pathway to suppress Nrf2 activity is regulated by Bach1, a competitive Nrf2 protein for binding to the ARE (Dhakshinamoorthy et al., 2005). The transcriptional repressor Bach1(Reichard et al., 2007) inhibits the expression of antioxidant genes by it dimerizes with sMaf at the ARE region, thereby the transcriptional silencing (Dhakshinamoorthy et al., 2005). When the cells are exposed to antioxidants within 0.5-1h, these Nrf2 negative regulators are phosphorylated by unknow tyrosine kinase in the nucleus. Subsequently, they are exported from the nucleus to the cytoplasm, where they are ubiquitinated and degraded (Niture et al., 2014). The nuclear export and later ubiquitin degradation of these Nrf2 negative regulators permits to nuclear import of Nrf2 and increases efficiency for the induction of antioxidant genes (Niture et al., 2014).

#### 1.1.3 Antioxidant genes: a role in selective neuronal vulnerability

The most interesting and intriguing in aged related and neurodegenerative diseases and MeHg toxicity is the selective vulnerability of certain neurons. Several lines of evidence suggested that different neurons have different levels of vulnerability to oxidative stress (Wang, 2010). For example, hippocampus CA1 neurons and cerebellar granule cells (CGCs) have been reported as the most susceptible to oxidative stress (Wang and Michaelis, 2010), and consequently are purported to be the first to undergo functional decline (Wang, 2010; Salim, 2016). In MeHg exposure, CGCs are the most susceptible neurons in the cerebellum (Edwards et al., 2005; Kaur et al., 2007; Fujimura and Usuki, 2014) and observed their massive degeneration in Minamata Disease brain autopsy (Eto, 1997).

Transcriptomic studies suggested that those neurons' selective vulnerability to oxidative stress is related to these neurons expressing the oxidative restress response gene higher

than those resistant neurons (Wang et al., 2009b; Wang, 2010). In the CA1 region, the Nrf2 regulated antioxidant genes Nqo1 (NAD(P)H: quinone oxidoreductase 1), Mtla1 ( Metallothionein 1), and Nrf2 expressions were 1.5 -fold higher than that in CA3 region (Wang et al., 2005). Other Nrf2 regulated genes such as Gst (glutathione transferase), Txnrd1 (Thioredoxin reductase1), Ho-1 (Heme oxygenase), and all three SOD isoform genes expressed relative higher in CA1 region (Wang et al., 2005). In the cerebellar granule cells, while the protein expression of SOD1 and Gpx1 levels were similar, the SOD2 level was higher in cerebellar granule cells than that in the cortical neuron (Wang et al., 2009b). These findings speculated the high intrinsic oxidative stress status in vulnerable neurons could be due to their high level of ROS/RNS formation (Wang et al., 2005; Wang et al., 2007; Wang et al., 2009b; Wang, 2010) thus render them more susceptible to toxic insults including oxidative stress. In contrast, the basal SOD2 level in CGCs is lower than that in the cerebellar Purkinje cells (PKCs) and cerebellar molecular layer neurons (interneurons) (MLNs). While no different SOD1 and catalase expressions in these three types of cerebellar neurons, the Gpx1 and Txnrd1 basal mRNA levels are significantly lower in CGCs than the PKCs and MLNs (Fujimura and Usuki, 2014). Thus, the antioxidant expression particularly, SOD2, Gpx1, and Txnrd1, might contribute to the intrinsic vulnerability of CGCs to MeHg compared to their neighboring PKCs and MLNs, which are resistant to MeHg (Fujimura and Usuki, 2014). The differential antioxidant gene expressions may possess a critical role in intrinsic neuronal selective vulnerability to oxidative stress and toxic insults.

#### 1.1.4 Astrocytes

Astrocytes, also known as astroglia, received their name from their characteristic star-like appearance (Pekny and Pekna, 2014). Astrocytes comprise the amplest and diverse type of glial cells found in both white matter and gray matter in the CNS. Not only as neuronal supporters, but astrocytes also possess functionally diverse and directly contribute to a myriad of cellular processes essential for normal CNS physiology, including synaptogenesis, neurotransmission, trophic regulation, and blood-brain barrier formation, to name a few (Allaman et al., 2011; Chaboub and Deneen, 2012; Fernandez-Fernandez et al., 2012; Bolaños, 2016).

## a. Astrocytic heterogeneity

Astrocytes are heterogeneous in several aspects, not only their morphology, for example, development, morphology, location, protein expression, and function. Astrocytes have been classified into 2 general morphologies based on cellular morphology (Vaughn and Pease, 1967) and the intermediate filament immunoreactivity(Raff et al., 1983; Miller and Raff, 1984). Type 1 astrocytes (or protoplasmic astrocytes) possess highly branched bushy processes and are widely distributed in the gray matter. Type-2 astrocytes (or fibrous astrocytes) possess straight lengthy processes and are mainly located in the white matter (Chaboub and Deneen, 2012; Tabata, 2015). The protoplasmic astrocytes are immunoreactive negatively to a cell surface ganglioside epitope A2B5 antibody (Raff et al., 1983; Miller and Raff, 1984), and sporadic and relatively lower react to glial fibrillary acidic protein (GFAP) (Ludwin et al., 1976; Hewett, 2009), while the fibrous astrocytes react to both GFAP and A2B5 antibody (Raff et al., 1983; Miller and Raff, 1984). Functionally, protoplasmic astrocytes are associated with both synapses and

endothelial cells; their processes contact blood vessels forming perivascular endfeet. Therefore, they are directly participating in the neurovascular unit and blood-brain barrier (BBB). The function of fibrous astrocytes likely participate in myelination (Chaboub and Deneen, 2012) since they are predominantly located in the white matter, and their somas are often evenly spaced and ranked in rows between the axon bundles, and their processes terminate at nodes of Ranvier (Li et al., 2016).

Regional populations of astrocytes appear to exhibit local heterogeneity as well as in the spinal cord. Due to the limitation of astrocyte-specific makers, and GFAP reacts to a different degree in the different developmental stage (Kerstetter and Miller, 2012), the classification of SCAs into fibrous and protoplasmic astrocytes significantly understates the complex nature of glial cells in the mammalian CNS (Miller and Raff, 1984). For example, those antibodies using for classification into type-1 and type -2 astrocytes had a limitation in the classification of SCAs. Five types of SCAs were found according to morphology, immunoreactivity, and serum response classification (Fok-Seang and Miller, 1992; Miller et al., 1994). Many phenotypic traits of the astrocyte lineage are responsive to local environmental cues (i.e., are adaptable), suggesting that plasticity contributes to this diversity (Hewett, 2009). Additionally, astrocytes arise from multiple distinct progenitor pools in the developing CNS, therefore raising the possibility is that some astrocyte heterogeneity may result from intrinsic differences between these progenitors (Hewett, 2009).

The environmental cues, including the serum types, possibly participate in astrocyte diversity and functions not only *in vivo* but also *in vitro*. The culture conditions, as well as cell culture media compositions, affect astrocyte cell culture's characteristics and

functions. For example, both primary astrocyte cell culture and the explant astrocyte culture accumulated Glu and GABA. However, the explant astrocyte culture did not take up noradrenaline and serotonin, while the primary astrocyte cell culture indicated the massive uptake of these neurotransmitters (Hösli and Hösli, 1995). The discrepancy in neurotransmitter uptaken by astrocytes is also affected by cell culture medium composition, including serum type. Despite the Glu uptake, the serotonin uptake was decreased when astrocytes were grown in horse serum (HS) compared to fetal bovine serum (FBS), and this uptake was abolished in chemical define medium (Kimelberg et al., 1992).

The variation of sera lot has indicated its effect on the expression of T-type voltage-dependent (gated) calcium channels (VDCCs or VGCCs) (Barres et al., 1989). Besides, the expression of L-type VGCCs in primary cortical astrocyte cell culture has suggested being induced by the cAMP inducing compounds such as dibutyryl cyclic adenosine monophosphate (dBcAMP) (L., 1990), 8-bromo-cAMP (Paco et al., 2016), forskolin, isoproterenol and vasoactive intestinal peptide (Barres et al., 1989). Not only its effect to VGCC expressions, only 1h forskolin incubation, but the primary cortical astrocyte cell culture also transformed their morphology from flat polygonal type 1 astrocytes to the mature astrocytes characteristics with the round-up of a cell body, cytoplasmic retraction and multipolar processes formation (Barres et al., 1989). The addition of the epidermal growth factor in the defined medium supplement for primary astrocyte cell culture compared to the medium supplement with 10% FBS increased astrocyte survival, and induced astrocytes differentiation resembled the morphology of fibrous astrocytes (type 2) in vivo (J.E., 1985). The addition of dBcAMP or prostaglandin on primary astrocyte

cell culture in the absence of FBS facilitated astrocyte maturation with process formation, an increase of aspartate aminotransferase (Tardy, 1981), antioxidant genes and transporters (Paco et al., 2016), and increase of Glu uptake and glutamine synthetase (GS) activity (Stanimirovic et al., 1999). These enzyme activities and gene expressions are highly expressed in mature astrocytes (Paco et al., 2016). The expression of glutamate transporter (GLT-1 or EAAT2) has been particularly concerned in primary astrocyte cell culture without neuronal coculture. Due to purify astrocyte cell culture with serumcontaining media exhibited the undifferentiated astrocytes, which expressed only glutamate/aspartate transporter (GLAST or EAAT1) (Swanson et al., 1997). The expression pattern of these glutamate transporter confers astrocyte maturity that GLAST expression is predominating at an early stage, while GLT-1 expression was undetectable at birth, but they were progressively observed with maturity (Sutherland et al., 1996; Ullensvang et al., 1997). The treatment of astrocyte cell culture with dBcAMP induced the GLT-1 expression and increased GLAST expression that resembled the neuronal astrocyte coculture (Swanson et al., 1997). Indeed, using astrocyte cell culture as a model to study their role in CNS has some limitations in their authentic functions to translation in their roles in the *in vivo*, unless the conditional treatments that facilitate the cell culture *in* vitro system to maintain or continue to develop as in vivo system.

### b. Astrocytic roles in the central nervous system

Astrocytes are heterogeneous, and they fill multiples roles in the CNS. Here will discuss some of the astrocytic roles in the interaction with neurons. For example, their interaction in the regulation of glutamate homeostasis, glutamate-glutamine cycle, and antioxidant GSH supply.

#### i. Glutamate homeostasis and synaptic transmission

In normal physiology, the intracellular glutamate ([Glu]in) concentration in neurons is approximately 10mM, while extracellular glutamate ([Glu]ex) concentration has been estimated to be 0.6mM. The substantial excitotoxic damage to neurons in intact tissue is expected to occur when the [Glu]<sub>ex</sub> reaches 2-5mM (Emerit et al., 2004). To avoid excitotoxicity during glutamatergic transmission, [Glu]<sub>ex</sub> and compartmentalization are exquisitely controlled, particularly by astrocytes. The astrocytic role in regulating glutamate homeostasis is tight with their role in the glutamate-glutamine (Glu-Gln) cycle (explanation in the next session). Upon neuronal activation and glutamate release, astrocytes control [Glu]ex by uptaking extracellular synaptic glutamate through glutamate transporters or excitatory amino acid transporters (EAATs). This process purposes of terminating postsynaptic neuronal activity to prevent glutamate-mediate excitotoxicity. The "high- affinity" glutamate transporter, EAATs are Na+-dependent transporters (Danbolt, 2001). Their transport of Glu is driven by the electrochemical gradient of both Na<sup>+</sup> and K<sup>+</sup> with the stoichiometry for each glutamate uptake is the co-transport of three Na+, one H+ and one K+ efflux (Figure 1.2) (Zerangue and Kavanaugh, 1996a; Levy et al., 1998; Chen and Swanson, 2003; Danbolt et al., 2016). This mechanism allows the translocation of synaptic Glu, [Glu]<sub>ex</sub> crossing the cellular membrane against its [Glu]<sub>in</sub> concentration gradient which is several thousand-fold concentration (Murphy et al., 1990) and keeps the [Glu]<sub>ex</sub> in the synaptic cleft below the level of Glu receptor being activated (< 1µM) (Gegelashvili and Schousboe, 1997), thereby, protection from neuronal excitotoxicity to occur.

EAATs are classified into five subtypes according to their isoforms (EAAT1-5) (Danbolt, 2001). The first two isoforms which are highly expressed in astrocytes, EAAT1 and EAAT2 in human are known in murine animals as glutamate aspartate transporter (GLAST) and glutamate transporter-1 (GLT-1), respectively. The EAAT1/GLAST and EAAT2/GLT-1 represent a majority of EAATs and play a prominent role in synaptic glutamate clearance due to their high affinity to Glu. Owning to their amino acid 65% homology, EAAT1 and EAAT2 posse the affinity to Glu with Km value ranging from 10 to 77 µM and 36-97 µM, respectively (Gegelashvili and Schousboe, 1997). The EAAT2 was accounted for over 90% of total adult CNS Glu uptake (Haugeto et al., 1996; Suchak et al., 2003). This is because of the differences in their expression profile. During embryonic (E) and early developing CNS stages, EAAT1/GLAST is prominently expressed in radial glial cells and immature astrocytes in the forebrain, cerebellum, and spinal cord (Shibata et al., 1997), while the intense expression is decreased by age (Sutherland et al., 1996; Shibata et al., 1997). In the mouse spinal cord, GLAST immunoreactivity starts to be appeared on the ventral spinal cord on radial glia at E11 when a small ventral horn begins to be formed. It became intense by embryonic 13 (E13) when the ventral horn had become enlarged and contained several neuronal cell bodies. In the dorsal spinal cord, GLAST immunoreactivity appeared at E13 and became intense at E15, during which period cells in the dorsal horn increased in number (Shibata et al., 1997). Therefore, the GLAST appears on preexisting radial glial cells at stages when spinal cord neurons migrate from the ventricular zone to the mantle zone (Shibata et al., 1997). Conversely, the expression of EAAT2/GLT-1 gradually prominent concomitant with the developmental stages of the CNS. EAAT2/GLT-1 is not detectable in rat brain early after birth (Sutherland et al., 1996), but their expression is detectable in the forebrain and cerebellum in the second and third weeks, respectively (Ullensvang et al., 1997). Their expression reached the maximum by postnatal week 5 (Sutherland et al., 1996; Ullensvang et al., 1997). After CNS maturation, EAAT2/GLT-1 represents the major EAATs in mature astrocytes (Haugeto et al., 1996; Sutherland et al., 1996; Ullensvang et al., 1997). In the brain, GLT-1 is widely distributed in the entire forebrain (Torp et al., 1994; Camacho and Massieu, 2006) where their predominant expression in the hippocampus, cerebral cortex, caudate-putamen, and lateral septum (Rothstein et al., 1994; Torp et al., 1994) while GLAST is greater enriched in cerebellum than other brain regions (Rothstein et al., 1994; Torp et al., 1994; Sutherland et al., 1996). The intensity of GLAST expression in cerebellum is further different in a subcellular distribution which its expression is predominant in Bergman glia cells of the Purkinje cell layer (Sutherland et al., 1996) but is almost absent in cerebellar granule cell layer or deep white matter (Rothstein et al., 1994; Shibata et al., 1997). While the two transporters differe considerably in regard to their regional distribution, their cellular distribution are similar in which their appear to be expressed primarily in glia cells (Torp et al., 1994). The differential pattern of GLAST and GLT-1 expression from early developing to developed CNS suggests their roles that are not only involved in the regulation of synaptic transmission but also their critical role in neuronal migration and differentiation (Shibata et al., 1997). EAAT1 and EAAT2 take up about 80-90% of extracellular glutamate (Murphy et al., 1990; Danbolt, 2001; Aoyama et al., 2008; Mahmoud et al., 2019). The EAAT3 (or excitatory amino acid carrier (EAAC1 in murine animals) are restricted in neurons, particularly large pyramidal cortical neurons and Purkinje cells (Rothstein et al., 1994). EAAT3/EAAC1 expression is throughout the brain with higher expression in the cerebral cortex, hippocampus, cerebellum, and basal ganglia (Rothstein et al., 1994; Bjørn-Yoshimoto and Underhill, 2016). EAAT3/EAAC1 expression is not restricted to

glutamatergic neurons. Their expressions were also exhibited in GABAergic neurons and dopaminergic neurons, which is highly sensitive to EAAT3 dysfunction (Nafia et al., 2008). EAAC1 is highly expressed in soma and dendrites, particularly the neck of the dendritic spines, but not in the spine head or synaptic axon terminal (Rothstein et al., 1994). The EAAC1 is highly enriched in newborns, and the distribution of Glu transporters in rat spinal cord also possesses differential patterns, which a strong immune reactivity to EAAC1 in the dorsal horn, specifically the Rexed layer 2. In contrast, the ventral horn where the spinal cord motor neurons (SMN) located exhibited moderated EAAC1 immune reactivity (Rothstein et al., 1994). This SMN reactivity is specifically only for EAAC1 but not GLAST, GLT-1, or EAAT4 immunoreactivity during development and adults (Furuta et al., 1997). The EAAT3/EAAC1 expression in the developed brain is relatively lower than in the developing stage. The developmental dependent expression reflects their major role in development possible in the regulation of biosynthesis and tropic role of GABA, which is excitatory in different brain regions during developing CNS (Nieoullon et al., 2006). This neuronal Glu transporter is also involved in the uptake of cysteine as for the *de novo* neuronal GSH synthesis. Since the application of the non-specific EAAT inhibitor threoβ-hydroxyaspartate (TBH) into primary cortical neurons inhibited cysteine uptake and reduced intracellular neuronal GSH (Chen and Swanson, 2003). The antisense oligonucleotide specific to the knockdown of the EAAT3 expression significantly reduced the cysteine uptake, neuronal GSH, and neuronal viability against oxidative stress (Himi et al., 2003). Also, EAAT4 exhibits regional and cellular specificity. Despite the expression by age, EAAT4 is mainly found in Purkinje cells of the cerebellum and much lower in the forebrain (Furuta et al., 1997). EAAT5 is exclusively expressed in the retina. Glu transport is weak in EAAT4 and EAAT5 due to their slower kinetics of capture and transport. In spite of glutamate influx, the EAAT4 and EAAT5 possess a unique co-transporter as they carry an anion influx such as Cl- down their electrochemical gradient (Wersinger et al., 2006). The characteristic of anions carried through these transporters as if they are passing through a glutamate-gated chloride channel (Danbolt, 2001; Jiang and Amara, 2011; Danbolt et al., 2016).

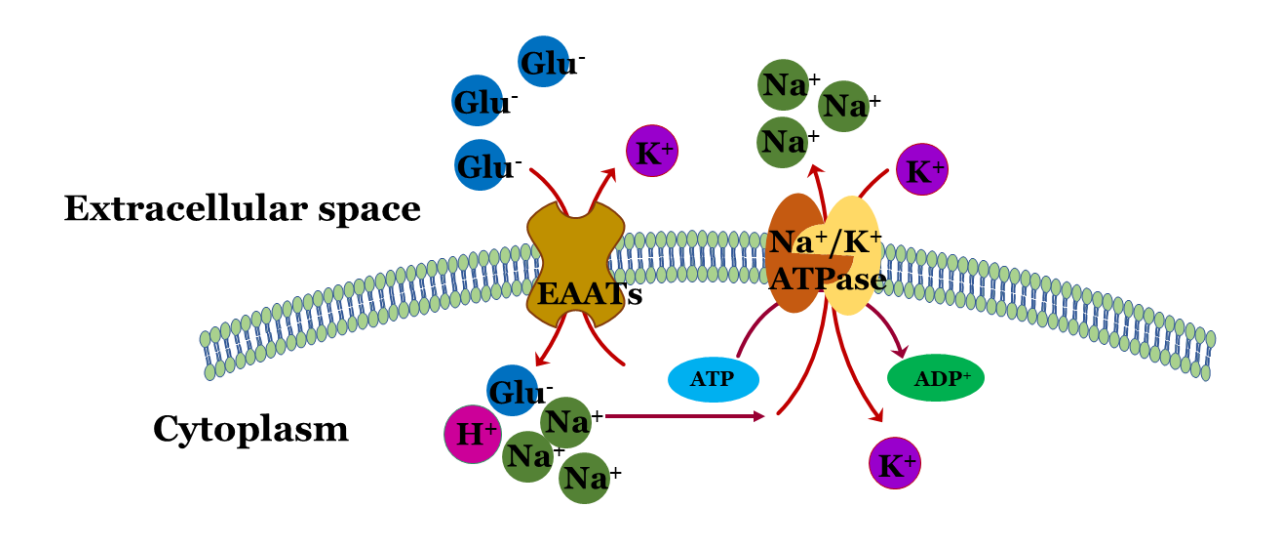


Figure 1.3 The extracellular glutamate uptake is regulated by EAATs. Upon the increase extracellular glutamate concentration during glutamatergic neurotransmission, the EAAT1 and EAAT2 in astrocytes play a prominent role in regulating extracellular glutamate homeostasis and termination of excitatory synaptic transmission by the clearance of synaptic glutamate (Otis and Dodson, 2009). The glutamate uptake depends on Na+ and K+ electrochemical gradient that is maintained through the activity of Na<sup>+</sup>/K<sup>+</sup> ATPase (Camacho and Massieu, 2006). The stoichiometry for each glutamate uptake is the co-transport of three Na<sup>+</sup>, one H<sup>+</sup> with the efflux of one K+(Zerangue and Kavanaugh, 1996a; Levy et al., 1998; Chen and Swanson, 2003; Danbolt et al., 2016). This coupling allows the net inward movement of two positive charges with each glutamate translocated into the cytoplasm (Divito et al., 2017), resulting in a large amount of ATP requirement to re-establish the Na+-gradient after glutamate uptake (Camacho and Massieu, 2006). The non-oxidative glucose utilization in astrocytes, therefore, transports glucose from the circulation via glucose transporters expressing in both capillary endothelial cells and astrocytes to establish a large amount of ATP (Bélanger et al., 2011).

The expressions of EAATs are encoded by the solute-carrier (*Slc*) gene superfamily and belong to *the Slc* family one, which is characterized as high-affinity glutamate and neutral amino acid transporter family (He et al., 2009). EAAT1/GLAST is encoded by the *Slc1a3* gene, while EAAT3/EAAC1 is encoded by *Slc1a1*. The EAAT2/GLT-1 is regulated by the *Slc1a2* gene. The EAAT4 and EAAT5 are regulated by *Slc1a6* and *Slc1a7*, respectively (O'Donovan et al., 2017).

The majority of synaptic Glu clearance is primarily responsible for astrocytic EAAT1 and EAAT2 (Rothstein et al., 1996). The dysfunction in astrocytes in the maintenance of Na<sup>+</sup>-gradience including ATP depletion as a resulting from mitochondrial damage, and or oxidative stress generation may cause the failure of these high-affinity Glu uptake systems in clearance [Glu]<sub>ex</sub> from the synapses (**see Figure 1.3**) (Emerit et al., 2004). The failure to the maintenance of Na<sup>2+</sup> due to ATP depletion contributes to astrocytic swelling and the release of Glu. Ultimately, neurodegeneration occurs due to excitotoxicity. Astrocytes exquisitely regulate the fate of [Glu]<sub>ex</sub> to prevent excitotoxicity by the Glu-Gln cycle.

#### ii. Glutamate-glutamine cycle

Glutamate (Glu) and GABA do not cross the blood-brain barrier (BBB), and they are synthesized within the CNS. Neurons, however, cannot synthesize glutamate and GABA through the tricarboxylic acid (TCA) cycle because the neuronal activity of pyruvate carboxylase is unlikely to be of quantitative significance (Yu et al., 1983; Waagepetersen et al., 2001; Sonnewald and Rae, 2010). Therefore, they depend on astrocytes for the generation of glutamate. Astrocytes generate glutamate via *de novo* synthesis or by "recycling" Gln from GABA and glutamate after reuptake. The *de novo* synthesis requires the catabolite α-ketoglutarate from the TCA cycle for glutamate synthesis and is accounts

for only 15% of astrocytic glutamate. Glutamate is later converted into Gln by GS, which predominately, if not exclusively, expressed in astrocytes (Norenberg and Martinez-Hernandez, 1979; Hampe et al., 2018). Glutamine exits astrocytes through the bidirectional amino acid flux system N transporters (sodium-coupled neutral amino acid transporter), SNAT3, and SNAT5 and enters neurons through the unidirectional system A transporters, SNAT1, SNAT2, and SNAT7 (Hampe et al., 2018). In neurons, glutamine is converted back to glutamate by phosphate-activated glutaminase, an enzyme that is highly activated in neurons than in astrocytes (Hogstad et al., 1988). The glutamic acid decarboxylase further decarboxylates glutamate to form GABA in GABAergic neurons. After release from the neurons, glutamate re-enters the astrocytes to be "recycled" to glutamine. A small portion of glutamate is oxidatively metabolized; therefore, making a de novo synthesis of glutamate is necessary to maintain adequate glutamate levels. The continuous recycling of glutamate and glutamine between neurons and astrocytes is known as the glutamate-glutamine cycle (or glutamate-glutamine shuttle) (Hampe et al., 2018). The primary role of the glutamate-glutamine cycle is to maintain glutamate homeostasis, both intracellular and extracellular domains. This cycle appears to tightly regulate with the GSH synthesis pathway between neurons and astrocytes (see Figure 1. 4).

## iii. Supply neuronal glutathione

GSH is the most abundant small non-protein thiol in cells. (Rice and Russo-Menna, 1997). GSH is intracellularly synthesized from three amino acids glutamate (Glu), cysteine (Cys), and glycine (Gly) by two consecutive ATP-dependent reactions to form the tripeptide  $\gamma$ -glutamyl-cysteinyl glycine, called GSH(Dringen, 2000). The first step is a

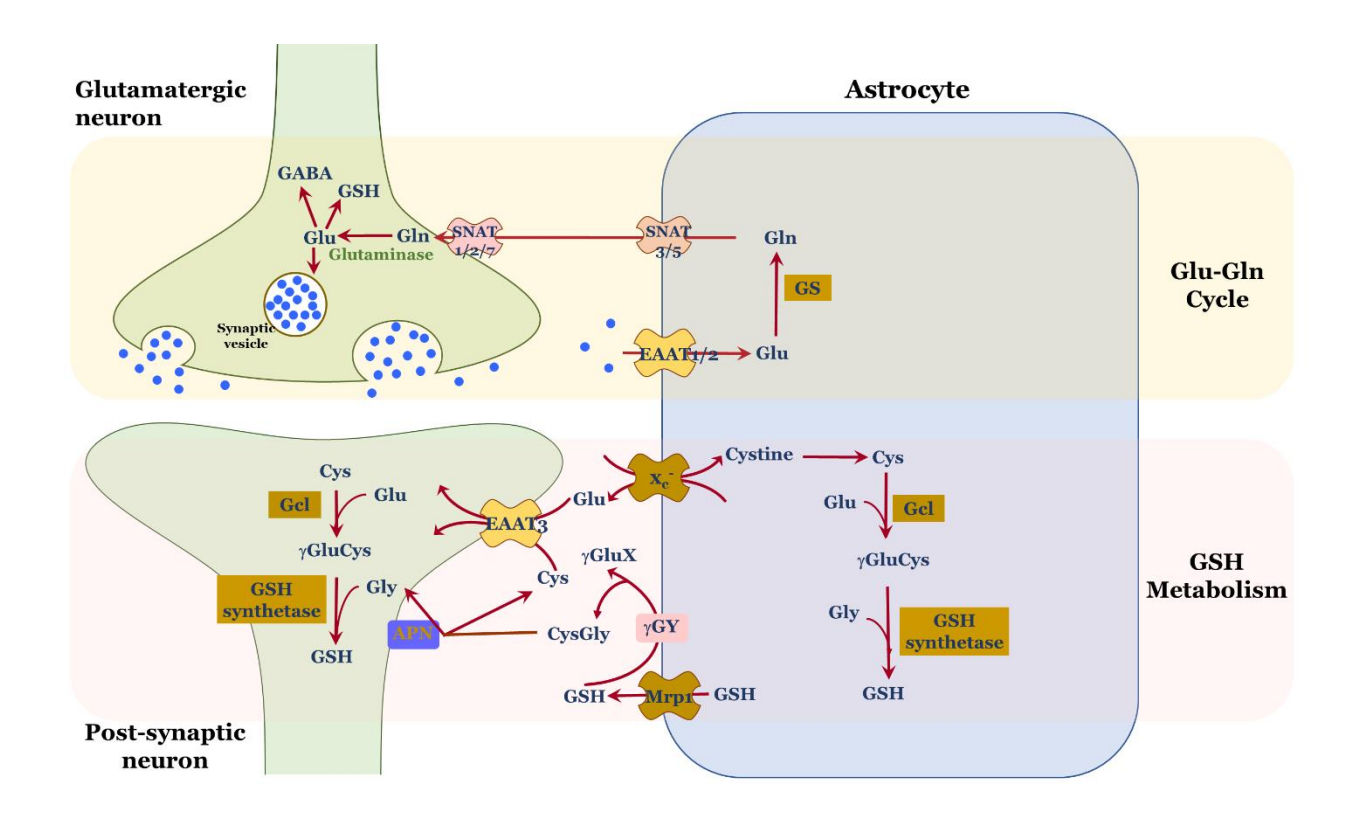


Figure 1.4 The glutamate-glutamine cycle and GSH metabolism. The interaction between neurons and astrocytes in regulating glutamate homeostasis via the glutamate-glutamine cycle (Glu-Gln cycle) (top panel) and GSH metabolism (lower panel). Upon synaptic glutamate release, astrocytes uptake glutamate through EAAT1/2, and the glutamine synthetase (GS) converts glutamate into glutamine to recycle back to neuron. This way, astrocytes can maintain synaptic glutamate concentration in a nontoxic level. In neurons, glutamine is converted back into glutamate and could be transported through a vesicular glutamate transporter (VGluT) located on the synaptic vesicle. Glutamate is also decarboxylated to form GABA or is utilized as a substrate for GSH synthesis. Metabolic interaction between astrocytes and neurons in the GSH metabolism (lower panel). Astrocytes are essential sources for neuronal GSH synthesis, primarily during oxidative stress occurs. GSH releasing from astrocytes provide a substrate precursor for neuronal GSH. Once astrocytic GSH is released via Mrp1, the ectoenzyme  $\gamma$ -glutamyltranspeptidase ( $\gamma$ -GT), which is located on the extracellular membrane of astrocytes, catabolizes GSH into glutamate with X substrate (γGluX) and cystine-glycine (CysGly). The CysGly is subsequently hydrolyzed by ectoenzyme the dipeptide by aminopeptidase (APN) located on the extracellular membrane of neurons into cysteine (Cys) and glycine (Gly). Cys and Gly are ready to uptake by EAAT3 and amino acid transporter, respectively. 'X' represents an acceptor of the y-glutamyl moiety transferred by y-GT from GSH, the most likely candidates being glutamine and H<sub>2</sub>O. (Dringen et al., 1999; Dringen and Hirrlinger, 2003).

rate-limiting step due to the involvement of the rate-limiting substrate cysteine and ratelimiting enzymes glutamate-cysteine ligase (GCL), which is composed of catalytic and modifier subunits (GCLC and GCLM). This step conjugates cysteine with glutamate resulting in  $\gamma$ -glutamylcysteine. The second step is catalyzed by GSH synthase, which adds glycine to  $\gamma$ -glutamylcysteine to form  $\gamma$ - glutamylcysteineglycine (or GSH) (Figure 1.4) (Dringen et al., 2000; Lu, 2013). This enzymatic reaction is non-allosterically feedbackregulated by the final product GSH (Kranich et al., 1998). Glutathione (GSH) has diverse functions that include detoxification, antioxidant defense, maintenance of thiol status, and modulation of cell proliferation. The primary function of GSH is cellular detoxification with non-enzymatic and enzymatic reactions. The reduced GSH (GSSG) can react non-enzymatically to remove the free radicals, particularly O<sub>2</sub>-, HO-, NO, and carbon radicals (Zeevalk et al., 2008). GSH removes hydro and organic peroxides such as H<sub>2</sub>O<sub>2</sub> from cells utilizing an enzymatic reaction of GSH peroxidase (GPx) and maintains It is involved in the enzymatic GSH in a reduced state (Zeevalk et al., 2008). detoxification of electrophilic xenobiotics to which GSH can be conjugated by the action of glutathione-S-transferases (GST) (Kranich et al., 1998).

The GSH concentration in the brain is approximately 1-3mM (Rice and Russo-Menna, 1997) with non-uniform concentration distribution in CNS cells. The GSH concentration in neurons accounts to be 2.5mM, whereas its concentration in astrocytes is relatively higher, with about 3.8mM (Rice and Russo-Menna, 1997). GSH displays differential subcellular distributions with existing in both cytosol and the mitochondria. GSH is concentrated at the nerve ending (Philbert et al., 1991) and exhibits Ca<sup>2+</sup>-dependent release upon K+-depolarization (Zängerle et al., 1992). The release of GSH was most

evident in the mesodiencephalon, cortex, hippocampus, and striatum and less observed in the pons, medulla, and cerebellum (Zängerle et al., 1992).

In the CNS, neurons highly consume oxygen for ATP generation during activation. Therefore, neurons are supplied the energy source from astrocyte when glucose expenditure exceeds availability. Astrocytes supply lactate from glycogen stores via the astrocyte-neuron lactate shuttle (Bouzier-Sore et al., 2002; Zwingmann et al., 2000). Astrocytes also have higher concentrations of antioxidant molecules such as vitamin E and GSH than neurons and can protect neurons from oxidative damage (Dringen et al., 2000; Shih et al., 2003). Astrocytes protect neurons from oxidative damage by supplying GSH precursors and GSH to neurons (Dringen et al., 1999; Dringen et al., 2000). In the CNS, astrocytes contain GSH and GPx activity higher than neurons (Dringen et al., 1999; Dringen et al., 2000). Besides, astrocytes are more efficiently synthesize de novo GSH than neurons because astrocytes are able and prefer to uptake and utilize cystine, an oxidized Cys for GSH synthesis (Dringen et al., 1999). Cystine, a disulfide forming between two cysteine molecules (Danbolt, 2001), is relatively high in extracellular synapse due to 1. cysteine is not stable and ready to be oxidized into cystine in the circulation and in cell culture media (McBean, 2002) and 2. Cystine has a greater membrane permeability through BBB than cysteine and GSH (Aoyama et al., 2012). Cystine is transported through Na+- independent system called system Xc- (McBean, 2002; Aoyama et al., 2008). System Xc- is mainly expressed on astrocytes, microglia, retinal Muller cells, and Bergmann glial cells in the cerebellum (McBean, 2002; Aoyama et al., 2008). The primary function of system Xc<sup>-</sup> is to import cystine in exchange for glutamate in a 1:1 ratio (Danbolt, 2001). Evidence reports that EAATs might support system Xc- activity and GSH synthesis (Lewerenz et al., 2009). Studies in C6 glioma cells and primary astrocyte culture indicated that extracellular glutamate concentration is directly proportional to inhibit cystine uptake and leading to GSH depletion (Cho and Bannai, 1990). EAATs support system Xc- function by reducing extracellular glutamate to maintain glutamate driving force (Danbolt, 2001; McBean, 2002), thereby, system Xccan exchange glutamate for cystine as for GSH substrate precursor cysteine. The majority of EAATs that modulate neuronal GSH synthesis and transport cysteine is EAAT3 (Zerangue and Kavanaugh, 1996b; Aoyama et al., 2012; Watts et al., 2014). Neuronal EAAT3 preferential transports cysteine over glutamate (Aoyama and Nakaki, 2013) with an affinity 10-20 greater than astrocytic EAAT1(GLAST) and EAAT2(GLT-1) (Zerangue and Kavanaugh, 1996b; Aoyama et al., 2008; Aoyama and Nakaki, 2013) which are mainly responsible for synaptic glutamate uptake (Danbolt, 2001). This finding suggests that the primary function of neuronal EAAT3 is more related to cysteine transport for GSH synthesis than synaptic glutamate clearance (Aoyama et al., 2012; Aoyama and Nakaki, 2013).

The extracellular transport of GSH from astrocytes is regulated by the family of multidrug resistance proteins (Mrp), particularly Mrp1 (Hirrlinger and Dringen, 2005; Cole, 2006; Minich et al., 2006). The regulation of GSH synthesis and GSH substrate and GSH transporters prominently regulated by the activity of Nrf2 (Hayashi et al., 2003; Hayes and Dinkova-Kostova, 2014). The activation of Nrf2 and its binding to ARE regulates a cluster of antioxidant genes, including those for GSH synthesis and those involved in GSH transport between astrocyte and neurons(Niture et al., 2014; Tonelli et al., 2018). The basal expression and activation of Nrf2-ARE are higher in astrocytes than neurons

(Ahlgren-Beckendorf et al., 1999; Murphy et al., 2001; Lee et al., 2003c; Kraft, 2004)(Kraft et al., 2004). Application of Nrf2 activators, including tert-butylhydroquinone (tBHQ) (Ahlgren-Beckendorf et al., 1999; Murphy et al., 2001)and sulforaphane to neuronal and astrocyte cultures induced the ARE-dependent genes in astrocytes, but not in neurons except those located close to astrocytes (Kraft, 2004). Presumably, neurons require an obligatory signal from astrocytes that allows the activation of the Nrf2-ARE pathway (Johnson et al., 2008; Blackburn et al., 2009).

#### iv. Regulation of neuronal glutamate receptor subunit expression

The spinal motor neuron (SMN) are more vulnerable to excitotoxicity than their neighboring neurons. The characteristic of motor neurons (MNs) that are susceptible to excitotoxicity has been hypothesized that AMPAR mediated excitotoxicity through the massive influx of Ca<sup>2+</sup>(Laslo et al., 2001), which determined by its subunit assembly (Van Damme et al., 2002). AMPAR are tetrameric assemblies of a different combination of four GluR subunits; GluR1-4. Most AMPAR are Ca<sup>2+</sup> impermeable, which depends on whether the GluR2 subunit is present within the tetramer (Wright and Vissel, 2012). The ability of the GluR2 subunit to regulate Ca<sup>2+</sup> influx, in turn, depends on the RNA editing at the position 586, a codon coding for glutamine (Q) to arginine (R) (Sommer et al., 1991; Van Damme et al., 2002; Wright and Vissel, 2012). The posttranscriptional modification from neutral glutamine to a positive charge arginine(Q/R) (Van Damme et al., 2002) attributes to AMPAR containing edited GluR2 impermeable to Ca<sup>2+</sup>(Sommer et al., 1991).

The role of astrocytes in the regulation of glutamate receptor subunit (GluR) expression was comprehensively studied by Van Damme and colleagues (2007) in the chimeric

astrocyte cell culture with MNs derived from two rat strains, which are differential susceptibility to AMPAR-mediated excitotoxicity (Van Damme et al., 2002). The MNs derived from Wistar rats contained the percent of GluR2 mRNA and protein expression lower than that MNs derived from Holtzman rats (Van Damme et al., 2002). The Wistar MNs was also vulnerable to excitotoxicity treatment with 300µM kinic acid than the Holtzman MNs (Van Damme et al., 2002). The chimeric coculture MN with astrocytes from these strains revealed that the Holtzman MN coculture with Wistar astrocytes became more susceptible to kinic acid treatment and similar susceptible levels to the Wistar MN coculture with its strain astrocytes (Van Damme et al., 2002). The characteristic of Holtzman MNs when were cocultured with Wistar astrocyte also indicated the high Ca<sup>2+</sup> conductance (Van Damme et al., 2002). Furthermore, the astrocyte condition media (ACM) from Wistar rat treated in Holzman MN caused more cell death than ACM derived from Holztman strain (Van Damme et al., 2002). The ACM from Holtzman rat lost neuroprotective properties when treated with protease and high heat, suggesting that secreted factor(s) from astrocytes mediated the protective effect of AMPR mediates Ca<sup>2+</sup> influx that contributed to excitotoxicity.

Interestingly, not all astrocytes from Holtzman strain provided MN protection except the ventral spinal cord astrocyte. This finding also demonstrated the regional specific derived astrocytes in neuronal protection (Van Damme et al., 2007). Further evidence suggested that VEGF plays an essential role in the regulation of MNs susceptibility to excitotoxicity. Treatment with VEGF protected MN from excitotoxicity, reduced Ca<sup>2+</sup> conductance, and increase % of GluR2 mRNA expression (Bogaert et al., 2010). Collectively, these studies suggested that regional-specific astrocytes, i.e., ventral spinal cord astrocytes regulated

GluR2 expression in ventral MN may be through the secretion of VEGF that results in the protection of MN from excitotoxicity mediated by AMPR mediated Ca<sup>2+</sup>influx.

## 1.1.5 Mercury species: sources, potential exposure, and toxicity

Mercury (Hg) is among the most toxic and has caused a variety of significant and documented adverse effects on human health, animals, and the environment (Diez, 2009). Hg and its compounds are highly toxic, particularly to the developing nervous system (Clarkson, 1972). The toxicity of Hg imposes on humans and other organisms depend upon its chemical form, concentration, time, and pathway of exposure and the vulnerability (Díez, 2009). Hg exists in a variety of physical and chemical forms (Clarkson et al., 2007). Three valences (oxidation) states of Hg (o, I, and II) exist in Hg<sup>o</sup>, Hg<sup>+</sup>, and Hg<sup>2+</sup>, respectively (Carocci et al., 2014). Each exhibits a specific toxic profile (Clifton, 2007). In a zero oxidation state (or oxidation number), the elemental form, Hg<sup>o</sup>, is characterized as silver-colored metal that exists as a thick liquid at room temperature (US EPA). Hg<sup>o</sup> is also called quicksilver, metallic mercury, and **mercury vapor** (Carocci et al., 2014). Hgo is found in thermometers, barometer, disk batteries, fluorescents bulbs, gas regulators, dental amalgams, topical medications, cathartics, and substances used in magico-religious practice (Clarkson and Magos, 2006; Clifton, 2007; Carocci et al., 2014). The exposure of Hg<sup>o</sup> may occur through inhalation, ingestion, and parenteral or subcutaneous administrations of these Hg<sup>o</sup> sources (Clifton, 2007). The zero oxidation state Hg<sup>o</sup> is stable in ambient air and can remain in the atmosphere for months or years (Clarkson and Magos, 2006), where it can transport and deposited globally (Carocci et al., 2014). It critically impacts global Hg cycling since it undergoes oxidation to form the two major oxidation states; oxidation state I result in Hg+ or referred to as

mercurous mercury, and oxidation state II derives Hg2+, also known as mercuric mercury (Clarkson and Magos, 2006). These oxidation states can chemically combine with other elements to form inorganic (non-carbon containing) or organic (carboncontaining) compounds (Clifton, 2007) (US EPA). Inorganic mercury compounds exist in two oxidative states (mercurous, Hg+; mercuric, Hg++), which are generally in solid states as mercurous or mercuric salts and mercury compounds with chlorine, sulfur, or oxygen. The commonly found of mercurous mercury is in the form of mercurous chloride (HgCl), whereas the most commonly found of mercuric mercury or divalent mercury is found in the form of calomel or Hg<sub>2</sub>Cl<sub>2</sub> (Clarkson and Magos, 2006). These inorganic mercury are found primarily in batteries, some disinfectants, and some health remedies and cream (Agocs et al., 1990). The industrial discharges of these inorganic mercury contaminated waste and the oxidization of Hg<sup>o</sup> in the atmosphere which later deposit in the soil, water, and ocean, are biometylated by sulfur-reducing bacteria to **organic mercury** in a primary form of methylmercury (MeHg)(King et al., 2000). MeHg is the most significant concern due to its toxicity and ability to bioaccumulate and biomagnify in the food chain (Lehnherr, 2014). The predatory fish such as swordfish, shark, king mackerel, and sea mammals are high MeHg concentrations (Carocci et al., 2014). The top food chain creature, including humans, are likely exposed to high levels of MeHg, thus they may be affected by MeHg toxicity. Table 1 summarized the physicochemical properties and toxicity of Hg species.

 $\textbf{Table 1} \ \, \textbf{The physicochemical properties and toxicokinetics of Hg species: sources, potential exposure, toxicity, and reference value and regulation limits$ 

Hg Species	Elemental Hg (Hgº)	Mercuric Hg (Hg <sup>2+</sup> )	Methylmercury (MeHg)
Sources of	Volcanic explosion, Fossil	Oxidation of Hg <sup>o</sup> ,	Fish, marine mammals,
Exposure	fuels, incineration, dental	demethylation of MeHg,	crustaceans, animals and
	amalgams, occupational	deliberate or accidental	poultry fed fish meal
	exposure,	poisoning with HgCl <sub>2</sub>	
Biological	Urine, blood	Urine, blood	Hair, blood, cord blood
Monitoring			
Toxicokinetics			
	Inhalation: approximately	Inhalation: aerosols of	<i>Inhalation:</i> vapors of MeHg
	80% of the inhaled dose of	HgCls absorbed	absorbed
	Hg <sup>o</sup> readily absorbed	<i>Oral:</i> 7-15% of ingested dosed	<i>Oral:</i> approximately 95% of
Absorption	Oral: Poor GI absorption,	of HgCl <sub>2</sub> absorbed from the GI	MeHg in fish readily absorbed
	any released vapor in GI tract	tract;	from the GI tract
	converted to mercuric sulfide	Absorption proportional to	
	and excreted	the water solubility of	

Hg Species	Elemental Hg (Hgº)	Mercuric Hg (Hg <sup>2+</sup> )	Methylmercury (MeHg)
Absorption (cont'd)	<b>Dermal:</b> Average rate of absorption of Hg <sup>o</sup> through human skin is 0.024 ng/cm <sup>2</sup> for every 1mg/m <sup>3</sup> in air	mercuric salts; uptake by neonates greater than adults  *Dermal:* In guinea pigs, 2- 3% of the applied dose of HgCl2 absorbed	<b>Dermal:</b> In guinea pigs, 3-5% of the applied dose of MeHg absorbed in 5 h
Distribution	Rapidly distribution throughout the body due to its lipophilic  Half-life is 45 days (slow phase) in the blood and dose- dependent	Highest accumulation in the kidney; a fraction of dose retain in the kidney is dosedependent; in neonate wildly distribute and not concentrate in the kidney as in adults  Half-life is 19.7-65.6 days in the blood with 24 days (1st	Distribution throughout the body due to its lipophilic; approximately 1-10% of an absorbed oral dose of MeHg distributed to blood; 90% of blood MeHg in red blood cells MeHg-Cysteine complex involved in MeHg transportation into cells

Hg Species	Elemental Hg (Hgº)	Mercuric Hg (Hg <sup>2+</sup> )	Methylmercury (MeHg)
Distribution (cont'd)	Readily cross BBB and placenta barriers	phase) and 15-30 days (2nd phase)  Does not readily cross BBB or placenta barriers; In fetus and neonate whose BBB is incompletely formed,  Hg2+concentration is higher in their brain than in adults	Half-life is 50 days in the blood; 50% of dose found in liver and 10% in the brain Readily cross BBB and placenta barriers
Biotransformation	$Hg^{o}$ in tissue or blood oxidized to $Hg^{2+}$ by catalase and $H_{2}O_{2}$ ; $H_{2}O_{2}$ production_is a ratelimiting step	Following oral administration of Hg <sup>2+</sup> in rodents, the existence of exhaled Hg <sup>0</sup> vapor occurred.  Hg <sup>2+</sup> is not methylated in the body but the microorganisms in GI can form MeHg	MeHg is slowly methylated to Hg <sup>2+</sup> Tissue macrophages, intestinal flora, and fetal liver are sites of tissue demethylation

Hg Species	Elemental Hg (Hgº)	Mercuric Hg (Hg <sup>2+</sup> )	Methylmercury (MeHg)
Biotransformation (cont'd)		Bind or induce metallothionine	Mechanisms of demethylation remain unclear in mammal cells; free radicals demethylate MeHg in vitro; bacterial demethylation enzymes involved Does not bind or induce metallothionine
Excretion	Excreted as Hg <sup>o</sup> in exhaled air, sweat, and saliva; as Hg <sup>2+</sup> in feces and urine	Excreted in urine, feces, saliva, bile, sweat, exhaled air, and breast milk	Excreted in bile and feces  (primary routes); 90%  excreted in feces and 10% in  urine as Hg <sup>2+</sup> ; 1% daily  excretion of body burden

Hg Species	Elemental Hg (Hgº)	Mercuric Hg (Hg <sup>2+</sup> )	Methylmercury (MeHg)
Excretion (cont'd)			Lactation increases clearance from blood; 16% of Hg in breast milk is MeHg
Half-life Limitation Toxicodynamics	58 days	1-2 months	70-80 days (whole-body) depending on species, dose, sex, and animal strains
Critical target organs	Brain and kidney	kidney	Brain and kidney
Causes of Toxicity	Oxidation of Hg <sup>o</sup> to Hg <sup>2+</sup>	Binding to thiols in critical enzymes and structural proteins	Demethylation of MeHg to  Hg <sup>2+</sup> and intrinsic toxicity of  MeHg

Hg Species	Elemental Hg (Hgº)	Mercuric Hg (Hg <sup>2+</sup> )	Methylmercury (MeHg)
			In Iraq, from weeks to month
			In Japan, more than a year
T atom on a suit of			Differences due to the Se in
Latency period			fish could reduce toxicity in
			Japan epidemics
			No toxic signs during latency
Mobilization	DMPS, DMSA (After oxidation	DMPS, DMSA	DMPS, DMSA
	to Hg <sup>2+</sup> )		
Possible			Se, garlic, and zinc
Antagonists			Se, garne, and zine
	RfC for chronic inhalation:	RfD for chronic oral exposure:	RfD for chronic oral exposure:
Reference values	3x10 <sup>-4</sup> mg/kg/day	3x10 <sup>-4</sup> mg/kg/day	$1x10^{-4} \text{ mg/kg/day} = 5.8 \text{g}\mu/\text{L}$
and regulatory	LOAEL: 0.009 mg/m <sup>3</sup>	LOAEL: 0.317 mg/kg/day	blood MeHg concentration
limits	(no RfD for chronic oral	(no RfC for inhalation); EPA	(no RfC for inhalation); EPA
	exposure); EPA		

Hg Species	Elemental Hg (Hgº)	Mercuric Hg (Hg <sup>2+</sup> )	Methylmercury (MeHg)
		Maximum Contaminant Level	Fish tissue-based water
		Goal (MCLG) and Maximum	quality: no more than 0.3µg
		Contaminant Level (MCL) in	Hg /g of fish (an indicator that
		drinking water; EPA	water bodies should not have
		Both MCLG and MCL	higher levels in their fish);
Reference values		in drinking water	EPA
and regulatory		=0.002mg/L (2ppb)	Commercial seafood products
limits		in water bodies = no more	no more than 1ppm
(cont'd)		than 144 ppt	(interstate shipment does not
			apply for in-state shipment
			and recreational caught fish);
	MRLs+	MRLs+	FDA
	Chronic: 0.0002mg/m3;	Acute: 0.007 mg/kg/day	MRLs+
	ATSDR	Intermediate: 0.002	Chronic: 0.0003mg/m3;
		mg/kg/day; ATSDR	ATSDR

**Note:** DMPS= 2,3-dimercapto-1-propane sulfonate, DMSA= meso 2,3-dimercaptosuccinic acid, Se= selenium, + Minimal Risk Levels (MRLs+), a health-based screening level for chronic exposures to airborne mercury; an estimate of the daily human exposure to a hazardous substance that is likely to be without appreciable risk of adverse non-cancer health effects over a specified duration of exposure, RfC=reference Concentration and RfD=Reference Dose, an estimate of the daily exposure to humans that is likely to be without an appreciable risk of deleterious effects during entire lifetime defined by US EPA Sources: (ATSDR, 1999; NRC, 2000; EPA, 2001)

#### 1.1.6 Mercury cycle and pathways of organisms exposure to mercury

Pathways of Hg entering the environments are complex. The various forms of Hg can be converted from one to the others. Hgo is released to the environment from both natural and anthropogenic sources (Clarkson and Magos, 2006). The natural sources include volcanic and geothermal activities that release an estimated 1,500 tons of Hg to the environment (Carocci et al., 2014). The anthropogenic sources derive from the various industries, fossil fuel, cement production, and incineration of solid wastes that constitute 2,320 tons of Hg emission annually (Carocci et al., 2014). The intensional extraction and utilization of Hg became primary sources of Hg emission that includes mercury mining, small scale gold and silver mining, artisanal gold mining, Chlor-alkali production, fluorescent lamps, auto headlamps, thermostats, and dental and amalgam application (Díez, 2009; Pacyna et al., 2010). Once Hg<sup>o</sup> vapor enters the atmosphere, it maintains in the atmosphere for as long as one year (Clarkson and Magos, 2006; Díez, 2009). This long atmospheric residence time of Hg<sup>o</sup> vapor ensure distributes the long travel distance from its original emission sources (Clarkson and Magos, 2006). For example, the high emission rate in the one continent might lead to Hg<sup>o</sup> transport to the remote region in the other continents (Clarkson and Magos, 2006; Díez, 2009). Based on modeling of the intercontinental Hg transport performed by the European Monitoring and Evaluation Program suggested that the annual Hg deposition to the Arctic was derived primarily from anthropogenic sources from Asia, accounting for 33% and Europe accounting for 22% (Travnikov, 2005). Most of Hg in the interior Arctic tundra is derived from Hg<sup>o</sup> deposition (70%) and an only minor contribution from Hg<sup>2+</sup> deposition (Obrist et al., 2017).

The atmospheric Hg° vapor is slowly oxidized to Hg²+ in the form of mercuric compounds, including mercuric oxide (Clarkson and Magos, 2006). Some fraction of the atmospheric Hg²+ is believed to be reduced back to the Hg°. The atmospheric mercuric compounds and Hg° return to the earth's surface mainly through the rainwater into the water, ocean, soils, and vegetation(Clarkson and Magos, 2006; UNEP, 2013). Once Hg° and Hg²+ are reaching in the aquatic ecosystems, they are transformed into MeHg via the methylation processes by the microbial communities in the sediments (Compeau and Bartha, 1985, 1987; King et al., 2000; Díez, 2009). The primary microorganisms responsible for mercury methylation are anaerobic sulfate-reducing bacteria (Compeau and Bartha, 1985, 1987; King et al., 2000). This biomethylation process is believed to be a protective mechanism since Hg²+ is more toxic to these microorganisms (Clarkson and Magos, 2006; Díez, 2009). Consequently, MeHg enters the aquatic food web and undergoes a biomagnification process. Accordingly, humans are exposed to MeHg occurring through fish and marine food consumption (Clarkson and Magos, 2006; Díez, 2009) (See the global Hg cycle and the impact on in Figure 1. 5).

The degree of biomagnification depends on the hierarchy of fish species in the food chain (Clarkson and Magos, 2006), size and age of fish, pH, and redox potential of the water (King et al., 2000; Díez, 2009). The latitude and temperature are also positively related to Hg biomagnification (Lavoie et al., 2013). Possibly, the warmer temperatures stimulate growth rates in aquatic organisms, which in turn decreases the amount of Hg per unit of body mass as opposed to colder temperatures where growth rate is diminished (Lavoie et al., 2013). The colder temperature may also reduce the MeHg excretion rate in organisms (Lavoie et al., 2013). A simpler food web at higher latitude characterized by a small

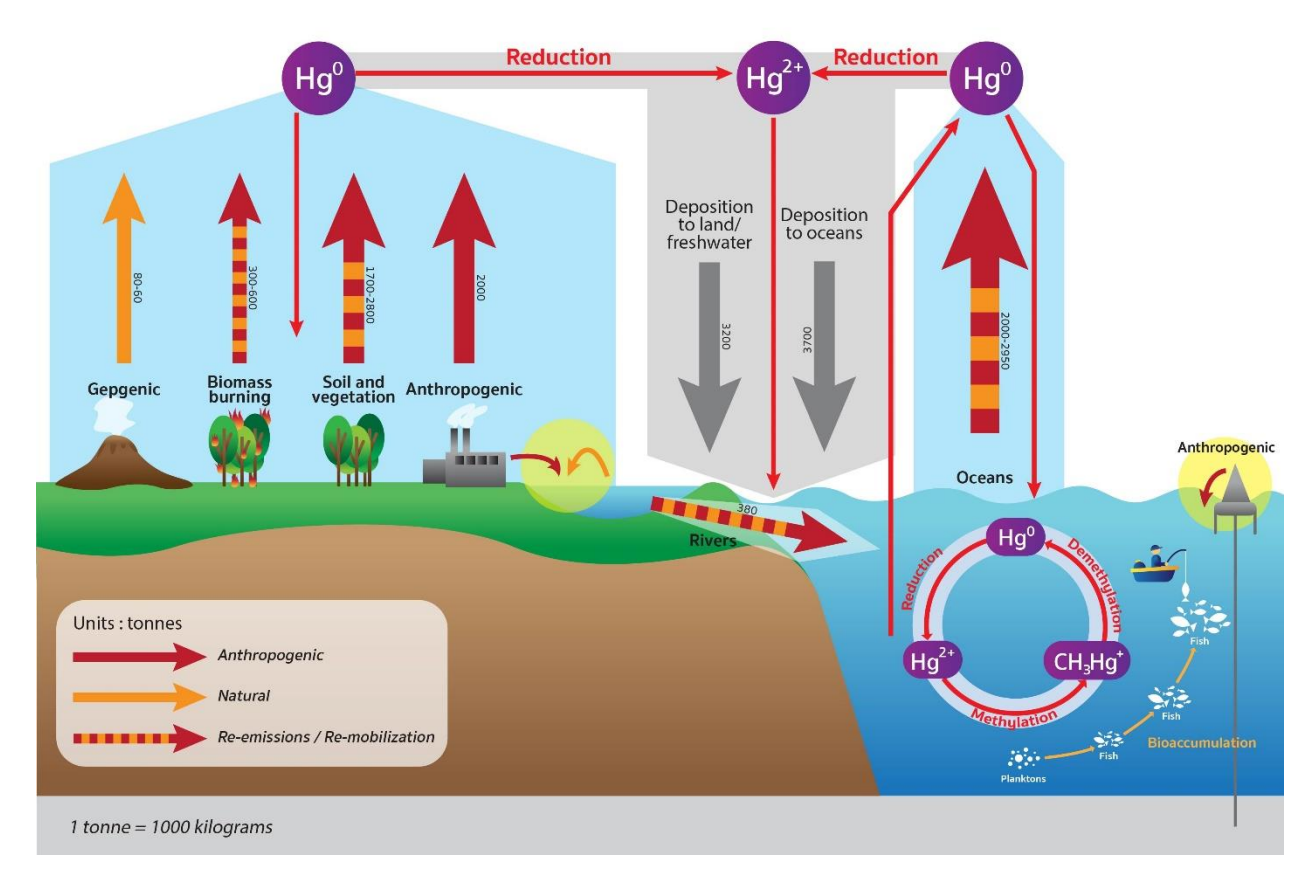


**Figure 1.5 Global cycle of Hg.** Mercury (Hg<sup>o</sup>) is released into the environment from natural and anthropogenic sources. The natural sources included the geogenic, i.e.volcano eruption, wildfire, or biomass burning. The anthropogenic sources are the exhausted and waste discharged from industries and artisanal gold mining. Once Hg<sup>o</sup> enters the environment, the atmospheric Hg<sup>o</sup> could travel long-distance from its original sources and deposits to land and water bodies after the rain. The atmospheric Hg<sup>o</sup> could be oxidized to the inorganic Hg (Hg<sup>2+</sup>). When Hg<sup>2+</sup>deposits into the sediment, the sulfurreducing bacteria metabolize Hg<sup>2+</sup> into organic Hg, i.e., MeHg (CH<sub>3</sub>Hg<sup>+</sup>), via the methylation processes. MeHg is transferred to living organisms through the aquatic food chain. The plankton, the aquatic food web producer, consumes those sulfur-reducing bacteria in the sediment, carries MeHg to its predators, primary consumers like zooplankton, small fish, and crustaceans. These primary consumers are, in turn, eaten by fish, small sharks, corals, and whales. The higher the food web's predators, the higher the MeHg concentration in the tissue, which is termed the bioaccumulation of MeHg. Human is the top predators in the food web, which consequently expose to MeHg through the consumption of seafood. The MeHg could be demethylated into Hgo, which later enters back to the atmosphere. The interchange between Hg species maintains the Hg in the environment and causes the Hg cycle (NRC, 2000; UNEP, 2013). (picture adapted from UNEP, 2013, NRC, 2000, and <a href="https://wi.water.usgs.gov/mercury/mercury-cycling.html">https://wi.water.usgs.gov/mercury/mercury-cycling.html</a>)

number of diverse species may result in higher Hg biomagnification than that in a more complex food web characterized by a large number of species diversity in lower latitude (Lavoie et al., 2013). Generally, the MeHg concentrations existing in various fish species range between 0.01 and 4mg/kg (ppm) (Díez, 2009). The higher trophic level organisms likely contain higher MeHg concentration in the muscle tissue (Clarkson and Magos, 2006; Díez, 2009). Large predatory fish such as king mackerel, pike, shark, swordfish, walleye, barracuda, large tuna, Scabbard, and marlin, as well as seals and tooth whales, contain the highest Hg concentration (Díez, 2009) that could reach as high as 4ppm (Clarkson and Magos, 2006). As such, the dietary pathway through the consumption of contaminated fish, shellfish, and sea mammals, is the primary source of human exposure to MeHg (Castoldi et al., 2008).

# 1.1.7 Historical episodes of methylmercury poisoning: Chronic high dose exposure (Minamata Bay and Agano River, Japan) and Acute high dose exposure (Iraq)

Two historical episodes of MeHg poisoning have occurred in Japan in the 1950s to 1960s and Iraq in the 1970s, classified by the high dose of MeHg exposure with the different temporal exposure. The chronic high dose exposure to humans is well illustrated in the Japanese epidemics. The first epidemic occurred in 1953 to 1956 near the Minamata Bay, Kumamoto Prefecture (Tokuomi et al., 1961), and the second epidemic occurred in 1964 to 1965 along the Agano River, Niigata Prefecture, Japan (Clifton, 2007; Carocci et al., 2014). The epidemic in Minamata occurred because the river was contaminated from the Hg containing wastes from over 36 years (1932 to 1968). The Chisso Cooperation Ltd. had been discharged MeHg associated wasted (Igata, 1993; Harada, 1995), derived from the

utilization of Hg as a catalyst for the acetaldehyde production processes into the Minamata Bay (Harada, 1995; Carocci et al., 2014). The residents living nearby these Bays ingested MeHg contaminated fish and shellfish and exhibited the neurological signs and symptoms termed Minamata disease (Eto, 1997). According to a reported studied by the Kumamoto University Research Group, the Hg level in fish in Minamata Bay was over 10μg/g (10ppm) in 1961; later in 1969, the Hg level decreased to about 0.5μg/g (0.5ppm) (Eto, 1997), which remained higher than the provisional regulatory standard in fish. A total Hg in fish is 0.4  $\mu$ g/g or less, and a MeHg in fish is not over 0.3  $\mu$ g/g according to the provisional regulatory standard in fish (Eto, 1997). The residents of Minamata Bay began to exhibit the clinical manifestation in 1950s, such as visual field constriction, sensory disturbance, and ataxia (Harada, 1995; Eto, 1997), the trias of Hunter-Russell syndrome (Eto, 1997), symptoms associated to workers who manifested from engaging in a production of MeHg compounds at a seed disinfectant plant in England (Hunter and Russell, 1954). The severity of the neurological sequelae from these MeHg exposures in Kumamoto Prefecture and Niigata Prefecture became very apparent, especially when the exposure occurred prenatally from the mothers ingesting the contaminated fish. The infants from either completely asymptomtic or mild toxic mothers exhibited or subsequent developed neurological dysfuctions including cerebral palsy, cerebellar ataxia, primitive reflexes, hyperkinesis, limb deformities, deafness, blindness, seizure, strabismus, dysarthria, and mental retardation (Clifton, 2007).

A second massive MeHg poisoning in 1971 to 1972 in Iraq involved a more acute and higher dose of MeHg poisoning than that existed in Minamata due to the consumption of a MeHg based fungicide contaminated bread (Bakir, 1973). The wheat seeds treated with

MeHg and EtHg compounds as antifungal seed dressing agents were for baking bread due to mislabelling. These incidents occurred in Iraq, Pakistan, and Guatemala (Bakir, 1973). The fungicide ethylmercury-p-toluene sulfonanilide was responsible for the outbreak in Iraq in 1956 and 1960 (Bakir, 1973). Methylmercury dicyadiamide was used to treated seeds before distribution to farmers during the growing seasons of the early 1960s—three hundred seventy cases of MeHg poisoning in Guatemala and 45 cases in Pakistan. The massive MeHg poisoning occurred in Iraq from February 1972 to August 1972. A total of 6530 cases of poisoning were admitted to hospitals throughout the country, and 459 victims died. The distribution of the Hg treated grain to farmers began in September 1971 from the southern seaport of Basra, Iraq, and delivered to all provinces in the country (Bakir, 1973). The rate of admissions to the hospitals increased in early January 1972 to several hundred per day (Bakir, 1973). There was a latent period of weeks or months between MeHg exposure and neurological symptoms. The primary signs and symptoms resembled MeHg poisoning in Japan. Due to the patients exposed to MeHg in a relatively short period, the first symptoms usually were the loss of sensation at the extremity of the hands and feet and around the mouth (paresthesia). Patients also exhibited loss of coordination in gait (ataxia), slur speech (dysarthria), diminution of vision (visual field constriction), and loss of hearing (auditory disturbance) (Bakir, 1973). The ataxia may subsequently decrease, but general recovery was poor. Severe poisoning led to blindness and death (Bakir, 1973). The clinical manifestations usually appeared after the consumption of the Hg contaminated bread has stopped. According to Hg in the blood, the mean ingestion periods ranged from 41 to 68 days and the mean latent periods ranged from 16 to 38 days (See Table 4 in Bakir, 1973). The blood Hg concentration appeared to correlate to the mean period of ingestion and the onset of the symptoms positively. The

mean half-time of blood Hg clearance was 65 days with ranging from 40 to 105 days. The first sample of blood collection were in the range of 1.1 to 3.1  $\mu$ g/ml (ppm) (Bakir, 1973). The variation of Hg clarence among individuals affected the degree of MeHg toxicity.

## 1.1.8 Recent and current investigations of methylmercury exposure: Chronic low dose exposure (the Faroe Islands and the Seychelles Islands )

The high dose of MeHg exposure, such as in Minamata or Iraq, rarely occurs, and the severely adverse neurological effects mainly occur in prenatal exposure through maternal fish consumption. As such, the current primary concern is the possible adverse effects of a chronic low dose of MeHg exposure (Clifton, 2007). According to the longitudinal studies in Kumamoto and Niigata Prefectures, the severity of neurological sequelae becomes apparent in the prenatal exposure from maternal ingesting the contaminated fish, regardless of the mother exhibiting mild or asymptomatic neurological disorders (Clifton, 2007). In Iraq, following maternal ingestion of methylmercury treated grain suggested that maternal hair mercury concentrations above 10 ppm may be related to delayed developmental milestones and neurological abnormalities. High-frequency of fish consumption could achieve a high Hg level of exposure. Two large-scale longitudinal studies evaluated the association between maternal hair MeHg levels and prenatal exposure neurological outcomes in two island populations with high seafood and fish intake. The chronic low doses of maternal dietary MeHg associated with neurotoxicity were found in the longitudinal study for seven years in the Faroe Islands cohorts. The prenatal MeHg exposure children, seven years of age, exhibited attention, language, and memory deficits. At 14 years of following up, a latency of the brain stem auditory evoked potential is associated with the maternal Hg levels with the maternal hair MeHg level

ranging 2.6 to 7.7 ppm, averagely 4ppm (Myers and Davidson, 2000), confirming a lasting effect after intrauterine MeHg exposure (Clifton, 2007). However, the 9 years (Davidson et al., 2000; Davidson et al., 2008) and 17 years (Davidson et al., 2011) of following up in evaluating the chronic low dose of MeHg exposure in prenatal in Seychelles Islands study could not detect any statistically significant adverse neurological outcomes (Davidson et al., 2000; Davidson et al., 2008; Davidson et al., 2011). Conversely, these Seychelles cohort children performed even better in specific neurological tests (Myers et al., 2000). The maternal hair MeHg levels of the Seychelles cohort ranged between 0.5 to 27 ppm, with 5.9ppm as the median (Myers and Davidson, 2000). Mayers and colleagues (2000) have compared the differences between the Faroe Islands and the Seychelles Islands in table 3 of their review that the composition of the neurological development tests and age at evaluation differences (Myers et al., 2000). However, when Davidson and colleagues (2008) applied the same testing and scoring procedure reported by the Faeroe studies to reanalyzing data at the same age of the Faroe cohort studied, the results were consistent with their previous tests that no association between the prenatal MeHg exposure and neurological development tests existed (Davidson et al., 2008). Besides the composition of the neurological test battery and age at evaluation, the differences between the Faroe Islands and the Seychelles Islands existincluding the genetic or ethnic composition, source or type of fish consumption, other environmental toxins or toxicants (Myers et al., 2000) (see detail in table 3 of Myers et al., 2000). The ethnicity of the Faroe Islands is Scandinavian, whereas the ethnicity of Seychelles is mixed, including the African and Asian (Myers et al., 2000). The Faroe cohorts consume not only fish, but the large predatory fish like the pilot whale and possible other environmental contaminants such as polycarbonate biphenyl (PCB)

synergistically contribute to the adverse neurological outcomes compared to the Seychelles cohorts who consume smaller fish and no other environmental toxicants involved (Myers et al., 2000). Perhaps, the genetic background and environmental contaminants could contribute to the MeHg susceptibility among individuals.

#### 1.1.9 Pharmacokinetics and pharmacodynamics of methylmercury

The primary route for MeHg exposure is through the dietary, which mainly is from marine food contaminated with MeHg. The biological half-time of MeHg in fish is on the order of months to years (Ballatori and Boyer, 1986). MeHg is efficiently absorbed and distributed throughout the body, including the brain, where the achieved concentration is about five times higher than that in the blood (Castoldi et al., 2008). MeHg also distributes to hair and wildly used as a biomarker of present and past exposure (Castoldi et al., 2008). The hair to blood concentration ratio is about 250:1 (µgHg/g hair to µgHg/ml blood) (WHO, 1990; Castoldi et al., 2008). The half-life of MeHg in the body is about 50 days, with a range between 20-70 days (Clarkson, 1993; Díez, 2009; Syversen and Kaur, 2012). The half-life of MeHg in the hair is approximately 65 days, while its average half-life in the blood is 40-50 days (Clifton, 2007).

Highly distribution of MeHg in the body less likely occurs through the lipid-soluble diffusion; instead, it results from the formation of complex molecules containing thiol that can transport across the plasma membrane, including BBB (Kerper et al., 1992; Simmons-Willis et al., 2002). MeHg, along with other mercuric cations, favorably react to sulfhydryl (thiol) - containing molecules, especially GSH, the most abundant non-protein thiol in cells (Clarkson, 1993). This MeHg-sulfide binding complexes, such as MeHg-GSH, highly influence toxicokinetics and toxicodynamics of MeHg. MeHg is

rapidly absorbed and eliminated by enterohepatic circulation and intestine through faces (Clarkson, 1993) and is highly accumulated in the CNS, especially the brain. After ingested MeHg contaminated diet, approximately 95% of MeHg is rapidly absorbed from the gastrointestinal tract and enters blood circulation where MeHg primarily binds to thiol molecules in erythrocytes (Clarkson, 1993; Clarkson and Magos, 2006), partly forming methylmercury-glutathione (MeHg-GSH) and methylmercury-cysteine (MeHg-Cys) complexes (Hughes, 1957; Aschner and Aschner, 1990; Kerper et al., 1992). About 90% of blood MeHg is concentrated in red blood cells (RBC) compared to the plasma in a ratio of 10-20:1 (Clarkson, 1972; Clifton, 2007). These complexes distribute to other tissues, including the brain, which reaches a steady-state within 2-3 h (Clarkson, 1972; Clarkson and Magos, 2006; Clifton, 2007). Due to its structural similarity to methionine, MeHg-Cys can cross capillary endothelial cells constitution of BBB via large neutral amino acid transporter (LAT) (Aschner and Aschner, 1990; Kerper et al., 1992; Clarkson, 1993). MeHg concentration in the brain may reach three to six times the levels in the blood (Clarkson, 1972; Clarkson and Magos, 2006; Clifton, 2007).

MeHg is eliminated from the body system partly through the MeHg-GSH transport mechanism, i.e. the ATP binding cassette transporters named multidrug resistance-associated protein (Mrp)(Gundacker et al., 2010). Some MeHg-GSH is further demethylated by intestinal microflora into poorly reabsorbed inorganic mercury (Hg<sup>2+</sup>) (NRC, 2000), which is excreted via the feces and urine (Clarkson, 1993; Clarkson and Magos, 2006). The daily net of MeHg excretion is accounted for 1% of the body burden that gives the MeHg body half-life of about 50 days (Clarkson, 1993; Díez, 2009; Syversen and Kaur, 2012), indicating that MeHg is removed from the body slowly (Díez, 2009).

Approximately 90% of MeHg is eliminated from the body by demethylation and excretion of the inorganic form Hg<sup>2+</sup> in excrement. The urinary excretion accounts for 10% of total elimination from the body (Díez, 2009).

The uptake of MeHg into the brain is slower than other organs and accounted for approximately 10% of the MeHg body burden. Approximately 20% of brain MeHg is water-soluble and mainly found as MeHg- Cys and MeHg-GSH (Kerper et al., 1992; Clarkson, 1993). Once in the brain, MeHg could be slowly biotransformed to Hg<sup>2+</sup>, accounting for 3-6% of brain Hg(Syversen, 1974), perhaps through the demethylation process (Charleston et al., 1994; Vahter et al., 1995). Both MeHg and Hg<sup>2+</sup> were relatively evenly distributed to various parts of the brain except the thalamus and pituitary that indicated the heightened increase of Hg<sup>2+</sup> level (Vahter et al., 1995). Brain Hg<sup>2+</sup> appeared to accumulate in the myelin and mitochondria more than other intracellular organelles (Syversen, 1974). The fraction of total Hg present in tissues as Hg<sup>2+</sup> depends on the duration of exposure to MeHg and the time after cessation of exposure (Friberg and Mottet, 1989). The review data from the MeHg outbreak in Iraq, where people had been exposed to high oral doses for two months, indicated that kidneys usually contained the highest fraction of Hg<sup>2+</sup>. The Hg<sup>2+</sup> in the whole blood was about 7%, in plasma 22%, in breast milk 39%, in liver 16-40%, and in urine 73% (Friberg and Mottet, 1989). Human brain biopsies detected about 87 % Hg2+ (NRC, 2000). The experimental studies of Macacus fascicularis monkeys who had been on daily oral exposure to subtoxic levels of MeHg ( 50µg Hg/Kg body weight) for 2-3 years indicated the Hg<sup>2+</sup> in the cortex accounting for 18% of total cortex Hg (Friberg and Mottet, 1989). Approximately 90% of Hg<sup>2+</sup> was found two years later in the same MeHg exposure scenario (Friberg and Mottet,

1989). Similarly, macaque monkeys with the daily oral MeHg exposure for 6 to 18 months found Hg2+ in these monkeys' brains (Vahter et al., 1994). Hg2+ constituted about 9% and 18% of total Hg in 6-12 months and 18 months of daily oral MeHg exposure, respectively (Vahter et al., 1994). After 6 months free of MeHg exposure, 74% was accounted for Hg<sup>2+</sup> of total brain Hg in monkeys exposed MeHg for 12 months (Vahter et al., 1994). The brain Hg<sup>2+</sup> levels in monkeys intravenously exposure to HgCl<sub>2</sub> were negatively related to Hg<sup>2+</sup> blood levels (Vahter et al., 1994), and Hg<sup>2+</sup> does not readily cross BBB (NRC, 2000). The brain Hg<sup>2+</sup> concentrations of MeHg exposure monkeys had several times higher than that in the brain of HgCl<sub>2</sub> exposure (Vahter et al., 1995). These results suggested that Hg<sup>2+</sup> was formed by demethylation in the brain (Vahter et al., 1994; Vahter et al., 1995). Two biotransformation processes of MeHg into Hg<sup>2+</sup> have been proposed that include the intestinal microflora and the organism tissues such as macrophages and fetal liver (Suda et al., 1991). Despite the slow rate of demethylation in rats and most other species (NRC, 2000), the enzymes responsible for the biotransformation have not been well identified in the tissue themselves. Greater emphasis has been placed on the possible role of a free radical mechanism in the biotransformation of alkyl Hg both MeHg and ethylmercury (EtHg)(Suda et al., 1991; Suda and Hirayama, 1992). The degradations of these alkyl Hg into Hg<sup>2+</sup> were achieved by using three OH radical generating systems that include Cu<sup>2+</sup> -ascorbate, xanthine oxidase (XOD)-hypoxanthine (HPX)-Fe(III)EDTA, and H<sub>2</sub>O<sub>2</sub>ultraviolet light B (Suda et al., 1991). Incubation of MeHg with HO and NADPH enhances the Hg<sup>2+</sup> formation in the liver microsome (Suda and Hirayama, 1992). In addition, the  $\gamma$ -globulin and serum albumin have shown similar degradation activity in rat liver homogenate that their activities were much stimulated further by glutathione and dithiothreitol (DTT) (Gage, 1975; NRC, 2000). The critical organ for Hg<sup>2+</sup> toxicity and somehow the biotransformation is the kideney. The biological mechasnims for removing Hg<sup>2+</sup> from the CNS are limited due to its poor membrane permability. The half-life of brain MeHg is about 37 days, whereas the half-life of brain Hg<sup>2+</sup> takes longer to 230-540 days (Vahter et al., 1995). (Counsil, 2000; Rooney, 2007). Whether MeHg or its biotransformation to Hg<sup>2+</sup> cause the CNS damage remains controversial (NRC, 2000). The intraperitoneal injection (i.p.) of a relatively high dose of MeHg or HgCl<sub>2</sub> (ranging from 0.2 to 10 mg) in Wistar rats for 2 to 50 days results in the homogenous distribution of MeHg but not HgCl2 (Møller-Madsen, 1990). The MeHg treatment indicated the massive Hg deposits in neurons, glia, and ependymal cells, whereas HgCL2 treatment mainly accumulated Hg deposits in neurons (Møller-Madsen, 1990). The motor nuclei of the rhombencephalon presented the massive Hg deposits from both compounds. While MeHg i.p. rats presented the massive Hg deposits in neurons, and lesser extent but significant in glia and ependymal cells, HgCl2 i.p. rats exhibited massive Hg deposits in neurons, a lesser degree in ependymal cells, and devoided glia (Møller-Madsen, 1990). In the cerebellum, the Purkinje cells (PKC), Golgi cells, and Golgi epithelial cells but not the granule cells, heavily deposited Hg in MeHg i.p rats, whereas the HgCl2 i.p. rats devoided the Hg deposits in PKC (Møller-Madsen, 1990). The pyramidal neurons in the cerebral cortex prominently constituted Hg deposits, as well as, glia, albeit to a lesser extent than the nerve cells (Møller-Madsen, 1990). The Hg was deposited in the gray matter of the spinal cord, particularly the anterior horn motor neurons (Møller-Madsen, 1990). Similarly, oral administrations of MeHg (20mg/L) in Wistar rats also displayed Hg depositions in neurons and later glia. There was a latent period of Hg accumulation in tissues follow MeHg administration (Møller-Madsen, 1991). The first appearance of Hg deposits was restricted to the nerve cell bodies of specific areas in the brainstem following

ten days of MeHg administration. After 16 days of the administration, the Hg depositions appeared in the spinal cord. Later following 28 days of oral administration, the even Hg distribution in the brain and spinal cord were detected, which largely deposited in the cerebellar PCK, Golgi epithelial cells, and Golgi cells and spinal motor neurons in the anterior horn (Møller-Madsen, 1991). Comparative Hg deposition at cellular levels in these rats as a function of time of oral MeHg administration suggested that the Hg deposition were first observed in neurons (day 10) later in glia (day 28) (Møller-Madsen, 1991). The clinical signs of the neurological impairments displayed on day 24 of administration with the progressive increase of locomotor and postural deficits. The ataxia and crossing the hind limbs were appeared on day 28 (Møller-Madsen, 1991). The relative lower and more chronic MeHg administration studies in M. fascicularis, the extensive depositions of Hg2+ were exhibited in astrocytes and microglia, while little deposit was seen in neurons (Charleston et al., 1995a). The presence of Hg<sup>2+</sup> deposition in neurons depends upon the concentration and duration of MeHg exposure (Charleston et al., 1995a; Syversen and Kaur, 2012). The neurons in the calcarine sulcus of adult M. fascicularis exposure to subclinical MeHg concentration (50µg/Kg/day) for 18 months appeared the increase of Hg<sup>2+</sup> accumulation in neurons than that in MeHg exposure for 6 and 12 months (Charleston et al., 1995a). While the number of neurons, astrocytes, oligodendrocytes, endothelial, and pericytes numbers were not altered, the reactive glia increased in all these treatments (Charleston et al., 1994). This increase of reactive glia appears to correlate to the increase of microglia (Charleston et al., 1995b). Moreover, the deposition of Hg<sup>2+</sup> was observed in glia during the latent phase (non-symptomatic phase), whereas Hg<sup>2+</sup> deposition was found in neurons during the symptomatic phase (Syversen and Kaur, 2012).

The cellular toxicities of Hg species are complex and intertwined. Whether the MeHg itself or its metabolites Hg<sup>2+</sup> exerts proximal neurotoxic effects in MeHg exposure, the clinical signs and symptoms are different among these Hg compounds (NRC, 2000; Syversen and Kaur, 2012). It is most likely that MeHg initially and primary causes the neurological toxicities. The biotransformation between different Hg species in MeHg toxicity also raises the complication for risk assessment.

# 1.1.10 Proposed cellular mechanisms by which methylmercury-induced toxicity

#### a. Disruption of intracellular calcium homeostasis

The intracellular calcium ([Ca²+]in) is essential for several physiological processes, including synaptic transmission, synaptic plasticity (Berridge, 1998; Augustine et al., 2003; Hidalgo and Arias-Cavieres, 2016), neuronal migration, and differentiation (Komuro and Rakic, 1996). Under resting physiological conditions, the concentration of [Ca²+]in is maintained at a small concentration in the nM range, whereas the extracellular Ca²+ concentration is in the mM range (Limke et al., 2004a). The sustained elevation of [Ca²+]in could contribute to the overstimulation of regular neuronal activity and later is detrimental to CNS cells (Mattson, 2007; Roos et al., 2012). The cellular mechanisms by which the increase in [Ca²+]in -mediated cell death is one of the critical cellular mechanisms involved in MeHg-induced toxicity. The sustained [Ca²+]in elevation has been shown in various cell types after MeHg exposure. MeHg induces the biphasic elevation of [Ca²+]in in cerebellar granule cells (CGCs) (Marty and Atchison, 1997a; Edwards et al., 2005), cerebellar Purkinje neurons (PKCs) (Edwards et al., 2005), and spinal cord motor neurons (SMNs) (Ramanathan and Atchison, 2011).

Generally, primary sources of [Ca²+]<sub>in</sub> elevation are from 1. the influx of extracellular Ca²+ ([Ca²+]<sub>ex</sub>) through plasma membrane receptors such as N-methyl-D-aspartate receptors (NMDARs) and voltage-dependent Ca²+ channels (VDCCs) and 2. the intracellular stored organelles such as mitochondria, endo/sarcoplasmic reticulum (Mattson, 2007). Several lines of evidence suggest that the first phase of Me-induced [Ca²+]<sub>in</sub> elevation has involved the release of intracellular stored calcium from the endoplasmic reticulum and mitochondria (Hare and Atchison, 1992; Hare et al., 1993; Limke and Atchison, 2002; Limke et al., 2003; Limke et al., 2004b), whereas, the second phase of [Ca²+]<sub>in</sub> elevation derived from extracellular calcium influx (Marty and Atchison, 1997a; Limke and Atchison, 2002; Edwards et al., 2005). The second phase's characteristic exhibited a gradual, sustained intracellular calcium elevation that later reaches the plateau (Marty and Atchison, 1997a; Limke and Atchison, 2002; Edwards et al., 2005). The onset of [Ca²+]<sub>in</sub> elevation is inversely related to MeHg concentration(Hare et al., 1993; Marty and Atchison, 1997a; Limke and Atchison, 2002; Edwards et al., 2005).

The intracellular stored Ca<sup>2+</sup> organelles' contribution was explained by the inhibition of the mitochondrial function or sarco/endoplasmic reticulum. Application of cyclosporin A (CsA), a mitochondrial permeability transition pore (mPTP) inhibitor (Limke and Atchison, 2002), carbonyl cyanide m-chlorophenylhydrazone (CCCP) an uncoupler of oxidative phosphorylation that depolarizes the inner mitochondrial membrane (Limke et al., 2003) delayed the onset of the first phase of the [Ca<sup>2+</sup>]<sub>in</sub> elevation. The application of thapsigargin, a non-competitive inhibitor of the sarco/endoplasmic reticulum Ca<sup>2+</sup> ATPase (SERCA) and ryanodine, a ryanodine receptor activator, reduced the contribution of the sarco/endoplasmic reticulum in the first phase of the [Ca<sup>2+</sup>]<sub>in</sub> elevation

(Limke et al., 2004b). In addition, the increase of the first phase of the  $[Ca^{2+}]_{in}$  elevation occurred before the change of mitochondrial membrane potential ( $\Psi$ m) (Hare et al., 1993) and CsA delayed the loss of  $\Psi$ m (Limke and Atchison, 2002).

The route of  $Ca^{2+}$  influx through plasma membrane receptors was examined using various receptor antagonists and extracellular  $Ca^{2+}$ chelating agents. In CGGs, both VGCCs blockers  $\omega$ -conotoxin MVIIC or nifedipine (Marty and Atchison, 1998a) and muscarinic acetylcholine receptors (mAChRs) inhibitor, atropine (Limke et al., 2004b) delayed the onset of the second phase of  $[Ca^{2+}]_{in}$  elevation. Not only VGCC blockers but also an AMPAR antagonist, CNQX, and NMDA receptor antagonists, MK-801 or AP-5 delayed the onset of the second phase of the  $[Ca^{2+}]_{in}$  elevation in SMN cell culture (Ramanathan and Atchison, 2011). These results suggested that excitatory membrane receptors are involved in  $Ca^{2+}$ -influx.

Besides excitatory glutamate receptors involved in [Ca<sup>2+</sup>]<sub>in</sub> elevation, the GABAA receptors have indicated their complex roles in the CGCs' susceptibility to MeHg toxicity. The selective GABAA receptor agonist muscimol and its antagonist bicuculline delayed the onset and reduced the magnitude of MeHg effects on Fluo-4 fluorescence, an indicator of relative changes in [Ca<sup>2+</sup>]<sub>in</sub>, in the external granule layer (EGL) and molecular layer (ML) of the rat cerebellar slice (derived from postnatal day 9) (Bradford et al., 2015). In the internal granule layer (IGL), both muscimol and bicuculline delayed the onset of MeHg-induced increases in Fluo-4 fluorescence but did not affect fluorescence magnitude (Bradford et al., 2015). The differential effects of MeHg to Fluo4 fluorescence changes among the different layers of the cerebellar slices may suggest that the more mature CGCs in the ML and IGL reacted less to MeHg than did those migrating CGCs located in EGL,

as indicated by a more considerable sustained increase in  $[Ca^{2+}]_{in}$  as an early exposure event than more mature cells (Bradford et al., 2015).

The cascade events of the [Ca<sup>2+</sup>]<sub>in</sub> elevation may contribute to cell vulnerability to a persistent of MeHg insult in MeHg exposure. Several lines of evidence in CGCs indicating the elevation of [Ca<sup>2+</sup>]<sub>in</sub> appeared to be associated with mitochondrial dysfunction and later caused cell death (Marty and Atchison, 1998a; Limke et al., 2004b; Edwards et al., 2005). The high capacity of mitochondria to sequester [Ca<sup>2+</sup>]<sub>in</sub> could eventually cause a membrane- potential collapse resulting in cessation of ATP production and ROS generation during MeHg insult (Beal, 1992). Another pathway suggested the association between [Ca<sup>2+</sup>]<sub>in</sub> elevation and cell death through the mitochondrial damage is the translocation of apoptosis-inducing factor (AIF) a key event leading to chromatin condensation and DNA degradation, characteristics of apoptosis, from the mitochondria to the nucleus in CGC exposure to MeHg (1 mM) (Fonfría et al., 2002). Mitochondrial damage can directly activate apoptosis or amplify receptor-mediated apoptotic pathways. Alterations of the outer mitochondrial membrane's permeability result in the release of mitochondrial intermembrane space proteins such as caspase or ATF (Fonfría et al., 2002). A study in mouse mitochondria indicated the release of ATF, which was initiated by the mPTP opening induced by [Ca<sup>2+</sup>]<sub>in</sub> elevation (Susin et al., 1999).

### b.Dyregulation of intracellular Zinc

Despite the  $[Ca^{2+}]_{in}$  elevation, using <sup>19</sup>Fluorine -nuclear magnetic resonance (<sup>19</sup>F-NMR) revealed that MeHg induced the intracellular zinc ( $[Zn^{2+}]_{in}$ )elevation in the rat cortical synaptosome and NG108-15 cells. The elevation of  $[Zn^{2+}]_{in}$  was not observed when applied the plasma membrane-permeable ion chelator N,N,N',N'-tetrakis (2-

pyridylmethyl)ethylenediamine (TPEN) (Denny and Atchison, 1994a). The real-time microfluorometry studies in several neuronal types using Fura-2AM also suggested the involvement of the [Zn<sup>2+</sup>]<sub>in</sub> elevation in MeHg toxicity. Application of 20µM TPEN following 3h of 10uM MeHg or mercury chloride in human neuroblastoma cell line SH-SY5Y greatly reduce the Fura-2AM (340/380 ratio) (Ohkubo et al., 2016). Application of TPEN reduced the amplitude of Fura-2AM and delayed the onset of the first phase in SMN during MeHg exposure (Ramanathan and Atchison, 2011). These studies suggested that MeHg disrupted not only  $[Ca^{2+}]_{in}$  homeostasis but also  $[Zn^{2+}]_{in}$ . Zinc is the second most abundant trace element in the body, after iron (Fe<sup>2+</sup>) (Pace and Weerapana, 2014). The neuroprotective and neurotoxic action of Zn<sup>2+</sup> depends not only on its concentration both intra-and extracellular concentration, but also cell type-specific (Takeda, 2011). Zn<sup>2+</sup> is stored in presynaptic vesicles accounting for about 10% of total Zn<sup>2+,</sup> and can be released upon activation. Co-synaptic release with glutamate, Zn<sup>2+</sup> enters postsynaptic neurons through Ca<sup>2+</sup>-permeable-α-amino-3-hydroxy-5-methyl-4-isoxazole propionicacid/ kainate receptors (Ca<sup>2+</sup>-AMPARs), VGCCs, and NMDARs (Sensi et al., 1999) and Zn<sup>2+</sup> transporters (Frazzini et al., 2006). Among these channels, Ca<sup>2+</sup>-AMPARs has the most remarkable change in intracellular Zn<sup>2+</sup> (Sensi et al., 1999). The influx of Zn<sup>2+</sup> can be buffered by the intracellular Zn<sup>2+</sup> proteins, such as metallothionine and mitochondrial (Ji and Weiss, 2018). Serie studies by Sensi and colleagues (1999 and 2000) indicated the preferential Zn2+ influx through Ca2+-AMPAR, and the increase of [Zn2+]in was concomitant with the depolarization of mitochondrial membrane potential ( $\Delta \Psi m$ ) and mitochondrial swelling (Sensi et al., 1999; Sensi et al., 2000).

Zn<sup>2+</sup> also plays a role in oxidative stress. Zn<sup>2+</sup> can trigger ROS production through mitochondrial and non-mitochondrial pathways (Sensi et al., 2000). Zn<sup>2+</sup> inhibits

complex I and III, where ROS are generated (Sensi et al., 1999). The elevation of [Zn<sup>2+</sup>]<sub>in</sub> in neurons through Ca<sup>2+</sup>-AMPAR strongly promotes the mitochondrial ROS generation. This Zn<sup>2+</sup>-triggered mitochondrial ROS generation persists more extended than that induced by Ca<sup>2+</sup> (Sensi et al., 1999; Sensi et al., 2000; Frazzini et al., 2006). MeHg has a direct inhibitory effect on respiration, which affects complex III in the culture of rat cortical neurons, cerebellar neurons, astrocytes and ologodendrocytes (Yee and Choi, 1996). Consequently, it causes ROS generation (Yee and Choi, 1996) that can further damage mitochondrial membranes by lipid peroxidation and impair mitochondrial function by the elevation of divalent cations, including Zn<sup>2+</sup> and Ca<sup>2+</sup>. MeHg induced the increase of divalent cation fluorescence Fluo-4 in the brainstem of wild type mice and amyotrophic lateral sclerosis (ALS)-mice model (transgenic human SOD1 G93A) exposure to low dose (3ppm) of MeHg through Ca2+-AMPAR. This increase in Fluo-4 fluorescence was diminished by TPEN (Johnson et al., 2011). In accordance, both wild type and transgenic humanSOD1 G93A mice exposed to 3ppm MeHg induced the increase of Zn<sup>2+</sup> fluorescence, FluoZin fluorescence (Johnson et al., 2011). Zn<sup>2+</sup> appears to contribute to the dysregulation of cation homeostasis in MeHg-toxicity through Ca<sup>2+</sup>permeable AMPAR (Johnson et al., 2011).

#### c. Dysregulation of synaptic transmission and induced excitotoxicity

MeHg has reported its effects on neurotransmitter metabolism, transmission, and receptor functions in dopaminergic, cholinergic, and glutamatergic systems.

The dopaminergic system is associated with motor functions, attention, and rewardrelated behavior. Manifestations of the dopaminergic system or MeHg toxicity exhibited Parkinsonian behaviors, attention, and cognition deficits. The study in rat offspring following in utero exposure to 1 mg MeHg/kg body weight exhibited the alternation of brain dopaminergic systems. The turnover rate and levels of dopamine (DA) were altered in these offspring at about the time of weaning (Bartolome et al., 1984), indicating the latency period of neurological disturbance of MeHg. The uptake of DA was initially inhibited and followed by the elevation of DA uptake in these offspring synaptosomes (Bartolome et al., 1984). The fluctuations of synaptic DA uptake in synaptosomes were preceded by the elevation of DA turnover rate (Bartolome et al., 1984). The perinatal MeHg exposure from gestation day (GD) 7 to PND 7, which administered orally to rat dams 1 mg MeHg/kg body weight/day, indicated the changes of monoamine oxidase B (MAO-B) activity in the cerebellum, not other brain regions, of male offspring but not female offsprings (Castoldi et al., 2006). In all offspring, MeHg enhanced the 5-hydroxyindole-3-acetic acid (5-HIAA) levels. The combination of PCBs treatment with MeHg or PCBs treatment alone in perinatal rats did not affect the cerebellar 5-HIAA level changes. This study suggested that the perinatal exposure to MeHg result in regionally and/or gender-specific alterations in the central dopaminergic systems at weaning. The PCBs did not enhance the neurotoxicity by MeHg, and apparently, these compounds possess different neurotoxic mechanisms and regional specificity (Castoldi et al., 2006). MeHg also induced the spontaneous efflux of DA in mouse striatal slices in a concentrationdependent manner (Kalisch and Racz, 1996). The K+-stimulated DA efflux markedly enhanced by 50 and 100 μM MeHg occurred either presence or absence of extracellular Ca<sup>2+</sup> (Kalisch and Racz, 1996). The notable releases of vesicular DA were also observed as the time- and concentration-dependent exposure to MeHg in PC 12 cells (Tiernan et al., 2013). MeHg-induced DA release was attenuated but not abolished in the absence of extracellular Ca<sup>2+</sup> in PC12 cells exposed to 2µM MeHg for 60 min (Tiernan et al., 2013).

Similarly, the concentration-dependent increase of striatal DA release observed in the free-moving rats exposed to 40µM to 4 mM MeHg using microdialysis coupled to liquid chromatography suggested the DA released from these rat striatal tissues were extracellular Ca²+independent (Faro et al., 2002). The increase of DA in striatal slice did not involve the DA transporter function since the inhibition of DA uptake using either nomifensine or amphetamine, DAT inhibitors, did not cause any DA level changes in MeHg coadministration (Faro et al., 2002).

The MeHg also induced the increases of the intracellular DA, and the rate of stored DA utilization accompanied by the increase of tyrosine hydroxylase activity (Tiernan et al., 2013). Besides, MeHg induced the alteration of DA metabolic mechanism by inhibiting DA metabolic enzyme aldehyde dehydrogenase (ALDH) and decreasing the intracellular 3,4-dihydroxyphenylacetic acid (DOPAC) concentration (Tiernan et al., 2015). Consequently, The intermediate metabolite 3,4-dihydroxyphenylaldehyde significantly accumulated in PC12 cells exposed to 2µM MeHg for 60min (Tiernan et al., 2015). The increase of rat striatal DA release in 400µM MeHg intrastriatal infusion was accompanied by the decrease of the extracellular levels of DOPAC and homovallinic acid (HVA) (Faro et al., 2002).

MeHg modified the dopaminergic pathway resulting in behavioral changes. The male but not female offsprings (PND 21) exposed to a low dose of MeHg (0.5 mg MeHg/kg body weight/day) in the perinatal period exhibited a reduction of dopamine-mediated locomotor activity induced by D2 receptor agonist U91356A without any changes in spontaneous locomotor activity (Giménez-Llort et al., 2001). When the offsprings were treated with apomorphine, a D1, D2, and D3 receptor agonist, the motility and locomotion

increased considerably compared to non-MeHg perinatal exposure offsprings (Daré et al., 2003). The changes of these locomotor activities were not accompanied by any changes in striatal D1 and D2 mRNA expressions, despite the reduction of D2 receptor-ligand binding in the caudate-putamen (Daré et al., 2003). Subtoxic concentrations of MeHg that induced the dopaminergic system dysfunction potentially contributed to some neurological symptoms, particularly motor functions. The toxicity of MeHg is age and gender specificity, which the subtoxic of *in utero* MeHg exposure altered the DA system in male offsprings. The latency period of neurotoxic of MeHg may underly alter the dopaminergic system, which is exhibited as some motor dysfunctions, as seen in MeHg toxicity.

Due to the critical roles in motor and cognitive functions that exhibited dysfunctions in MeHg-intoxication, the effects of MeHg on the cholinergic system were evaluated in sympathetic nerve and neuromuscular junctions (NMJ) using an electrophysiological recording for the synaptic transmission. In addition, patients suffering from a chronic high dose of MeHg intoxication in Niigata Prefecture, Japan, exhibited a reduction of the velocity of the rapid conducted motor nerve impulses (Juang and Yonemura, 1975b). Conversely, the patients suffering from an acute high dose of MeHg exposure in Iraq did not exhibit any changes in these motor nerve impulses (Juang and Yonemura, 1975b). The superior cervical ganglia from guinea pigs that were intraperitoneal injection of 1 mg/animal methylmercuric chloride exhibited the significant increase of miniature excitatory postsynaptic potentials (MEPSPs) without any changes of their amplitude following 30 min, 1 day, and 5 days of MeHg exposure (Juang and Yonemura, 1975b). The increase of MEPSP frequency gradually returned to a similar frequency of the control

MEPSP after 30 days (Juang and Yonemura, 1975b). In patients suffering from effects of Niigata methylmercury pollution in Japan, Kanbayashi et al. have found a significantly reduced value for the velocity of the most rapidly conducted impulse in the motor nerves (Juang and Yonemura, 1975b). The NMJ study in the phrenic nerve, which innervates the diaphragm, reported that relatively low MeHg concentration (4µM) did not increase miniature end-plate potential (MEPP) frequency. In contrast, the higher MeHg concentration (20 and 100 µM) increases the MEPP frequency without changing the amplitude (Atchison and Narahashi, 1982). Among these 20 and 100 µM MeHg concentrations, 100 µM MeHg did not further increase MEPP frequency, but it shortened the latency of MEPP occurring (Atchison and Narahashi, 1982). The increase of MEPPs frequency suggested that MeHg induced the release of the spontaneous synaptic vesicles. Under diminishing the quantal content using the low Ca<sup>2+</sup> and high Mg<sup>2+</sup> in Ringer's solution, MeHg initially evoked the decrease of the end-plate potentials (EPPs)' amplitude and finally ceased EPPs occurrence after exposure to 30-40 min of 20 µM MeHg and 4-5 min of 100 µM MeHg (Atchison and Narahashi, 1982). The iontophoretic

min of 100 μM MeHg (Atchison and Narahashi, 1982). The iontophoretic application of acetylcholine (ACh) to the NMJ, the EPPs' amplitude remained constant during 100 μM MeHg exposure (Atchison and Narahashi, 1982). Furthermore, 100 μM MeHg caused the marked reduction of the ACh quantal content, probability of release, and immediate available stored neurotransmitters, whereas 20 μM MeHg markedly increased the probability of release of neurotransmitters (Atchison and Narahashi, 1982). This study suggested that the effect of MeHg exposure appeared to alter the function of the nerve (presynapse) rather than the muscle fiber due to the minor alteration of the EPPs, membrane potential of the muscle fibers (Atchison and Narahashi, 1982). The *in vitro* studies of mouse brain homogenate indicated that MeHg inhibited spontaneous

choline acetyltransferase (ChA), high-affinity choline uptake, and spontaneous motor activity (Kobayashi et al., 1981). The *in vivo* studies in these mice also supported these findings that these cholinergic enzymatic activities significantly reduced in MeHg exposure mice (Kobayashi et al., 1981).

Besides the dysregulation of cholinergic synaptic transmission, MeHg affected the cholinergic receptors. MeHg and HgCl2 blocked the mAChRs binding site since they competitively bonded to the quinuclidinyl benzilate (QNB) binding sites of rat brain homogenate (Von Burg et al., 1980). Meanwhile, exposure of a low dose of MeHg (0.5 or 2 mg/kg/day in drinking water) to the adult female Sprague-Dawley rats increased the hippocampal and cerebellar, but not cerebral, AChRs densities (Coccini et al., 1999). The effect of MeHg in mAChRs elevation did not occur immediately; instead, this effect appeared after two weeks of MeHg termination (Coccini et al., 1999). These selective increases of mAChRs expressions in the adult rat hippocampus and cerebellum were preceded by a marked increase of mAChR expressions in lymphocytes (Coccini et al., 1999). This research suggested that the peripheral lymphocytes may represent a sensitive target for the interaction of MeHg with mAChRs and may be a predictive indicator of CNS mAChR responses (Coccini et al., 1999), consequently, the neurological signs and symptoms related to cholinergic system dysfunction. On the other hand, the perinatal exposure offsprings (gestation day 7 to PND 21) from dams exposed to 0.5 mg/kg/day in drinking water on 7 days of pregnancy exhibited the reduction of mAChR expressions in the cerebral and cerebellar cortex (Coccini et al., 2007). The reduction of mAChR expressions in the cerebellum preceded the reduction in the cerebral cortex in both males and females despite the lasting effect in males (Coccini et al., 2007). These offsprings (

PND 36) exhibited the marked reduction of cortical neurons exhibiting mAChR subtype 1 (M1) and subtype 3 (M3), whereas they exhibited the increase of Burgman glia expressing mAChR subtype 2 (M2) (Coccini et al., 2007). These data suggested that MeHg acts as a potent competitive inhibitor to AChR binding sites in rat brains. MeHg also affected the mAChR, mainly M3 functions in cerebellar granule cells (CGCs). The increase of [Ca<sup>2+</sup>]<sub>in</sub> in biphasic fashion occurred in CGCs involves the M3 that evokes the intracellular stored Ca<sup>2+</sup> being release and ultimately CGCs dead (Limke et al., 2004b). Since the down-regulation and desensitization of both M3 receptors and the IP3 receptor function with bethanechol protected against MeHg-induced GCG dead (Limke et al., 2004b). This protective effect was abolished by specific M3 antagonist (Limke et al., 2004b). The cellular and behavioral changes in MeHg exposure *in vitro* and *in vivo* are mimic the central cholinergic system interruption.

Both excitatory and inhibitory synaptic transmissions have reported their dysregulation in MeHg exposure. The effects of MeHg on the CA1 region in the hippocampal slice indicated the similar effects of MeHg to the inhibitory postsynaptic potentials (IPSPs) and inhibitory postsynaptic currents (IPSCs) (Yuan and Atchison, 1997b). The blockade of the IPSPs and IPSCs by MeHg occurred sooner than that occurred in the excitatory postsynaptic potentials (EPSPs) and excitatory postsynaptic currents (EPSCs). The field potential amplitude (Yuan and Atchison, 1993b), EPSPs amplitude (Yuan and Atchison, 1997b) and population spikes (Yuan and Atchison, 1997b) initially increased, subsequently decreasing during the MeHg application (Yuan and Atchison, 1993b; Yuan and Atchison, 1997b) due primarily to the activation of GABAA receptors (GABAARs)(Yuan and Atchison, 1997b). Pre-application of bicuculline, a

GABA<sub>A</sub> antagonist, prevented MeHg induced the early increase of population spike amplitude, whereas application of strychnine, a glycine receptor antagonist, failed to do so (Yuan and Atchison, 1997b). The voltage clamp of rat dorsal root ganglion neurons reported 1μM MeHg augmented the GABA-activated chloride channels by inducing a slow inward current (Narahashi et al., 1991). This event was accompanied by an increase in leakage current, resting membrane conductance, and membrane depolarization (Narahashi et al., 1991).

The correlation between the [Ca2+]in and spontaneous synaptic current frequency occurred in the molecular layer, including the CGCs of the cerebellar slice perfused with MeHg. The onset of [Ca<sup>2+</sup>]<sub>in</sub> elevation in the molecular layer induced by MeHg was concomitant to the increase of sEPSCs and sIPSCs in the PKCs (Yuan and Atchison. 2007b). The elevation of [Ca<sup>2+</sup>]<sub>in</sub> partially involved in the spontaneous synaptic responses since the elevation of [Ca<sup>2+</sup>]<sub>in</sub> remained noticeable regardless of MeHg already ceased the synaptic response (Yuan and Atchison, 2007b). The postsynaptic receptors and a release of neurotransmitters could be partially responsible for elevating  $[Ca^{2+}]_{in}$  the cerebellar molecular layer (Yuan and Atchison, 2007b). The inhibition of GABAA current (I-GABAA) in CGCs depends upon the MeHg concentration and duration of MeHg exposure (Herden et al., 2008). Due to the differential subunits combination of GABAA receptors among CGCs and PKCs, the CGCs expressing  $\alpha 6$  -subunit might confer the susceptibility to MeHg more than the PKC expressing α1 -subunit. However, the time to completely inhibit I-GABA<sub>A</sub> by MeHg did not differ among differential GABA<sub>A</sub> subunits composition (Herden et al., 2008). MeHg completely blocked or partially blocked (40% blocked) the I-GABAA in GABA<sub>A</sub> receptors expression α1- subunit similar to GABA<sub>A</sub> receptors expression α6subunit (Herden et al., 2008). This study suggested that the susceptibility of CGCs to MeHg less likely depends upon the differential α1 and α6 subunits composition in GABAA receptors (Herden et al., 2008). The auxiliary subunits of GABAA receptors might contribute to the differential susceptibility to MeHg in CGCs (Herden et al., 2008). Taken together, the rapid block of IPSPs or IPSCs exhibits sooner than the block of the EPSPs or EPSCs in MeHg exposure involves its action at GABAA receptors to decrease tonic GABAA receptor-mediate inhibitory synaptic transmission, resulting in the exaggerating the excitatory synaptic transmission (Atchison, 2005).

The effect of MeHg on the neuronal excitatory was characterized as; first, alteration of neuronal excitability threshold (Matyja and Albrecht, 1993), subsequently depolarization of the neuronal membrane and, consequently, evoke the release of neurotransmitters (Yuan and Atchison, 1995) by increase the probability of quantal content (Atchison and Narahashi, 1982). The increase of the extracellular glutamate concentration was observed in the moving rats perfused with either 10 or 100 µM MeHg examining with microdialysis (Juárez et al., 2002) and cortical synaptosomes of rats subcutaneously injected with 2mg/kg MeHg (Farina, 2003). MeHg induced a concentration-dependent increase the spontaneous release of Glu, aspartate as well as  $\gamma$ -aminobutyric acid (GABA), and taurine from mouse cerebellar slices (Reynolds and Racz, 1987). The increases of these neurotransmitters were independent on the extracellular Ca<sup>2+</sup>. The increase of these neurotransmitters releases, followed by the decrease of these neurotransmitters in cerebellar the depletion of immediate tissue. suggested available neurotransmitters and quantal contents, as seen in NMJ studied by Atchison and Narahashi, 1982. The early stimulation before the inhibiting synaptic transmission as

characteristics of MeHg cellular toxicity studies in the dorsal root ganglia neurons, CGC and PKCs, NMJ, and hippocampus suggested the effect of MeHg on synaptic transmission are complex and involve multiple synaptic activities. The synaptic activity includes an irreversible block Ca<sup>2+</sup> -, K<sup>+</sup> - and Na<sup>+</sup>-channels in a time - and MeHg concentration-dependent manner (Leonhardt et al., 1996; Yuan et al., 2005), and depression of Ca<sup>2+</sup> or voltage-dependent K<sup>+</sup> -current(Fuentes-Antrás et al., 2013). MeHg certainly affected excitatory and inhibitatory synaptic transmission which involves multilayers of toxic cellular mechansims, including the synaptic receptors and intracellular Ca<sup>2+</sup> pathway. The imbalance between excitatory and inhibitory induced by MeHg toxicity would ultimately generate the excitotoxicity and neuronal dead.

The increase of extracellular Glu not only involved the activity of membrane receptors but also involved the Glu transporters in terminating the synaptic transmission by clearance of extracellular Glu. MeHg caused a concentration-dependent inhibition of Glu and GABA uptake in mouse cortical astrocytes cell cultures (Brookes and Kristt, 1989). IC50 of MeHg for inhibiting Glu uptake is 4.6µM, whereas IC50 of MeHg for inhibiting GABA is 3.6 µM (Brookes and Kristt, 1989). Besides, Hg<sup>2+</sup> markedly inhibited the clearance of extracellular Glu by both cortical astrocytes and spinal cord cultures (Brookes, 1992a). This effect of Hg<sup>2+</sup> on inhibition of Glu uptake is more potent than that of MeHg since the IC50 of Hg<sup>2+</sup> for inhibiting Glu is lesser than 1µM (Brookes, 1992a). The inhibition of Glu uptake by MeHg is closely linked to the VGCCs as evidence by the lack of inhibition of Glu uptake in the presence of verapamil (Kim and Choi, 1995), L-type and T-type Ca<sup>2+</sup> channels blocker (Bergson et al., 2011) or the Ca<sup>2+</sup> -free medium (Kim and Choi, 1995). The Glu uptake inhibition in cortical astrocytes cell culture appeared to be affected

explicitly by mercury compounds, both MeHg and Hg<sup>2+</sup>, not other divalent metallic ions, such as Cu<sup>2+</sup>, Fe<sup>2+</sup>, and Zn<sup>2+</sup>(Kim and Choi, 1995). Nevertheless, it has been reported that MeHg affected to Glu uptake among astrocytic Glu transporters differently. The Chinese hamster ovary cells (CHO) transfected with GLAST or GLT-1 exhibited differential responses to MeHg. Following 6h of 5 µM or 10 µM MeHg exposure, GLAST mRNA expressions did not alter, whereas the GLT-1 mRNA expressions increased in both MeHg treatments (Mutkus et al., 2005). Conversely, GLAST protein expressions increased in both 5 µM or 10 µM MeHg exposure for 6h, whereas GLT-1 protein expression was reduced only with 10 µM MeHg exposure (Mutkus et al., 2005). Functional examinations of these Glu transporters in aspartate uptaking reported that 5 or 10 µM MeHg inhibited GLAST uptake of this amino acid following 5 min of MeHg exposure, despite no effects on longer time MeHg exposure. On the contrary, 10 µM MeHg induced the increase of aspartate uptake via GLT-1 following 5, 15, and 30 min of exposure, and only at 30 min of 5 μM MeHg exposure induced the increase of aspartate uptake through this transporter (Mutkus et al., 2005). The differential actions of MeHg between GLAST and GLT-1 expressions and their functions may involve several mechanisms despite their differential thiol-containing residues, specifically cysteine, which is highly reactive to oxidants (Trotti et al., 1997). The amino acid sequences of rat EAAC1, GLAST, and GLT-1 contain six, three, and nine cysteine residues in their sequence, respectively, and two of them are conserved among these Glu transporters (Trotti et al., 1997). Conversely, Hg<sup>2+</sup> inhibited all these three transporters, in reconstituted liposomes, uptaking Glu in a concentrationdependent inhibition (Trotti et al., 1997). One proposed mechanism by which Hg<sup>2+</sup> inhibits Glu uptake via these Glu transporters is its highly reactive to the thiol group in Glu transporters (Trotti et al., 1997). Since this Glu uptake inhibition by Hg<sup>2+</sup> was

reversed by application of thiol reducing agent, dithiothreitol (DTT) (Trotti et al., 1997). Similarly, in cortical astrocyte cell culture, DTT reversed the H<sub>2</sub>O<sub>2</sub>-induced inhibition of Glu uptake (Trotti et al., 1997). Hg<sup>2+</sup> may modify the SH-based redox modulatory in the Glu transporter cysteine conserved region; thereby, inhibiting Glu uptake (Trotti et al., 1997). This mechanism might not be the only case for MeHg. In the purified Glu transporters in liposomes or astrocytes cell culture expressing GLAST, thiol oxidation is applied with 5,5'-dithiol-bis(2-nitrobenzoic) acid (DTNB) possesses the opposite effect from thiol reduction DTT. DTNB diminished the Glu uptake capacity by decreasing the inward (downward) current in these astrocytes cell cultures and liposomes, while DTT enhanced the inward Glu uptake current (Trotti et al., 1997). As such, the mechanism by which MeHg induces Glu uptake via GLT-1 in CHO cells might involve a reduction of SHresidues, whereas its mechanism on GLAST could involve the oxidation of its SHresidues. Meanwhile, neither DTNB nor DTT affect changing aspartate uptake in rat cortical astrocyte cell culture expressing GLAST (Allen et al., 2001c). When acutely exposed 10µM MeHg to these rat cortical astrocyte cell cultures for 5 min, it did not affect the aspartate uptake, but Glu and Glu transporter inhibitor, threo-β-hydroxyaspartate (THA) did diminish aspartate uptake by about 70% and 99%, respectively (Allen et al., 2001c). This result suggested that MeHg did not directly inhibit Glu transport; rather, its downstream cellular toxicity was primarily involved. The 1h of 10uM MeHg exposure to this astrocyte cell culture significantly diminished aspartate uptake by about 70% of control. This inhibitory effect was reversed by coincubation with high concentration (1000U/ml) of catalase but not non-thiol containing antioxidants, α-phenyl-tert-buty nitrone (PBN) and Trolox (Allen et al., 2001c). The reversal effect of MeHg by catalase, a H<sub>2</sub>O<sub>2</sub> metabolizing enzyme, suggested that ROS particularly H<sub>2</sub>O<sub>2</sub> inhibited the Glu

transporters, specifically GLAST function in asprate uptake (Allen et al., 2001c). Prolong 10μM MeHg exposure in this cortical astrocytes for 6h, the expression of GLAST mRNA significantly reduced as well as in the THA treatment (Allen et al., 2001c) suggesting the expression of Glu transporter also affected by MeHg. However, the expressions of GLAST and GLT-1 proteins were not correlated their mRNA level in CHO cells exposing to 10μM MeHg for 6h. MeHg also did not affect the GLAST mRNA expression in CHO cells (Mutkus et al., 2005). The mechanism by which MeHg altered the expression of astrocytic Glu transporters remain unclear, and possibly may involve transcriptional, translational, and post-transcriptional processes. Certainly, the dysregulation of Glu transpoters expression and function by MeHg and Hg<sup>2+</sup> ultimately resulting in loss of Glu homeostaisis and excitotoxicity.

## d. Perturbation of redox homeostasis: oxidative damage and antioxidant pathway

Overproduction of ROS and reduction of antioxidants during MeHg exposure have been reported in neurons and glia (Kaur et al., 2006, 2007). Due to the characteristic of MeHg with high affinity to the thiol-containing molecules (Hughes, 1957), the major antioxidant in mammalian cells, GSH accounting for 90% of the intracellular non-protein thiol were reduced in a concentration-dependence of MeHg exposure in primary human neuronal cell culture, neuroblastoma cell line, and astrocytes (Sanfeliu et al., 2001). The primary cerebral cortical astrocytes cell culture exposed to MeHg exhibited the increase of cellular ROS and mitochondrial ROS formation (Shanker et al., 2004a). C57BL/6J mice exposing to multiple doses of MeHg depicted the reduction of brain and liver GSH levels, which associated with neurological disorders and progressing of death (Choi et al., 1996).

MeHg for 60 min induces a concentration-dependent increase in ROS formation in rat neonatal primary cerebral astrocytes (Shanker and Aschner, 2003b). While 5uM MeHg exposure in rat neonatal cortical astrocyte cell culture for 60 min did not elicit ROS production (Shanker and Aschner, 2003b), primary neonatal mice cerebellar neuronal or astrocyte cell cultures (Kaur et al., 2006) and rat striatal synaptosomes exposed (Dreiem and Seegal, 2007) to 5uM MeHg for 30min exhibited the marked reduction of intracellular GSH levels (Kaur et al., 2006) and increases of ROS production (Kaur et al., 2006; Dreiem and Seegal, 2007). The reduction of GSH also occurred at earliest at 1 min with 1 µM MeHg exposure in primary microglial cell culture. The reduction of GSH could also be observed within 10 min following 0.1 µM MeHg exposure in this microglial cell culture (Ni et al., 2010a). The increase of ROS formation and reduction of intracellular GSH in lower MeHg concentration suggested that the loss of redox homeostasis was attributed to the early cellular toxicity of MeHg. The reduction of GSH and the increase of ROS levels were associated with reducing cell viability (Kaur et al., 2006). The Studies in the primary human fetal neuronal cell culture, neuroblastoma cell line SH-SY5Y, and human fetal astrocytes cell culture suggested the LC50 values following 24h of MeHg exposure in these primary cell cultures were 6.5, 6.9, and 8.1 µM MeHg, respectively (Sanfeliu et al., 2001). Adding antioxidants 20 min and 24h later exposure 10 µM MeHg, 1mM GSH protected all these cell cultures from MeHg- induced toxicity (Sanfeliu et al., 2001). Not in human fetal neuronal cell culture, 8µM cysteine protected MeHg toxicity in human fatal astrocyte cell culture and SH-SY5Y cells (Sanfeliu et al., 2001). However, these protective effects were absent in pretreatments with other antioxidants, selenite, vitamin E, and catalase (Sanfeliu et al., 2001). Similarly, pretreatment of 200µM Nacetyl-L-cysteine (NAC), a GSH precursor 12h prior to MeHg exposure, protected the

reduction of GSH and attenuated the production of ROS in the primary cortical and cerebellar neuronal or astrocyte cell cultures (Kaur et al., 2006, 2007). NAC's protective effects were concomitant with the increase of cell viability in MeHg exposure in both primary neuronal or astrocyte cell cultures (Kaur et al., 2006). NAC pretreatment in cortical and cerebellar neuronal or astrocyte cell cultures confirmed protective effects against MeHg induced toxicity in these cell cultures (Kaur et al., 2007). administration of GSH-glycoside, which increases intracellular GSH, deminsihed the MeHg-toxicity and maintained the brain and liver GSH levels in mice (Choi et al., 1996). Over ROS production and significant reduction of GSH were exhibited in both the primary cortical and cerebellar neuronal and astrocytes cell cultures in 5 µM MeHg exposure (Kaur et al., 2007). Pretreatment with diethylmaleate (DEM), GSH depleting agent, exaggerated the effects of MeHg toxicity in the induction of the intracellular ROS production and attenuation of the intracellular GSH level in cortical and cerebellar neuronal or astrocyte cell cultures (Kaur et al., 2007). These finding suggested the cellular mechansims by which MeHg induced toxicity invlove the intracellular ROS over production and antioxidant reduction.

The accumulation of MeHg in the primary neuronal or astrocytic cell cultures was associated with GSH levels. When depletion of cerebellar neuronal or astrocytic GSH with DEM for 12h prior to 5  $\mu$ M MeHg exposure, significant increases of MeHg accumulations were observed in both primary cell cultures (Kaur et al., 2006). NAC pretreatment for 12 h did not enhance cellular MeHg accumulation in these cell cultures (Kaur et al., 2006). This data suggested that the reduction of intracellular GSH levels corresponded to the increase of MeHg accumulation (Kaur et al., 2006). The study in rat pheochromocytoma

cells (PC12 cells) strongly resistant to MeHg-induced toxicity suggested the positive correlation between high intracellular GSH levels and reduction of MeHg accumulation (Miura and Clarkson, 1993). PC12/TM sublines were more remarkably resistant to MeHg (8-fold higher) and accumulated MeHg lesser than the original PC12 lines (Miura et al., 1994). In chronic MeHg exposure for 10 days, PC12/TM exhibited a 10-fold more significant resistance to MeHg than the PC12 cells (Miura and Clarkson, 1993). The concentration-dependent accumulation of MeHg was positively correlated to cell growth and colony formation in both PC12 cells and PC12/TM (Miura and Clarkson, 1993). Compared to PC12 cells, the PC12/TM subline exhibited lesser retention and accumulation of cellular Hg after incubated with 5µM MeHg and washed with the MeHgfree medium for another hour (Miura and Clarkson, 1993). The lesser degree of intracellular Hg accumulation in PC12/TM was due to Hg efflux's more remarkable ability (Miura and Clarkson, 1993). About 80% of intracellular Hg was exported from PC12/TM, whereas lesser than 20% of intracellular Hg was detected in PC12 cells (Miura and Clarkson, 1993). Of note, the Hg export was mainly MeHg since the lesser than 0.3% of total Hg was inorganic Hg<sup>2+</sup> (Miura and Clarkson, 1993). The higher MeHg resistant capacity of PC12/TM was associated with the higher GSH level, with about 4.2-fold higher than the PC12 cells (Miura and Clarkson, 1993). In summary, cellular toxicity of MeHg involves the overproduction of ROS and reduction of intracellular GSH since some antioxidants such as GSH and GSH precursors could ameliorate the cellular toxicity of MeHg.

Not only perturbation of the intracellular GSH, but MeHg has also indicated its effect on the major antioxidant pathway, Keap1-Nrf2-ARE pathway, which regulates several genes involving GSH synthesis and transport. MeHg induced Nrf2 translocation into nucleus where Nrf2 activates ARE region, a promoter region of several cytoprotective genes, to synthesizing those cytoprotective mRNAs in primary astrocyte (Wang et al., 2008) and microglial (Ni et al., 2010a) cell culture. The primary rat cortical astrocytes exposed to different MeHg concentrations ranging from 0.01 to 10 µM MeHg exhibited higher MeHg concentration, which induced the ARE activity sooner than the lower MeHg concentration(Wang et al., 2008). MeHg concentrations, 1, 5, and 10 µM induced the increase of ARE activity by about 3-fold of control in 90 min exposure, while MeHg concentrations, 0.1 µM took about 4 h to induce ARE activity to be increase to 1.5- fold of control (Wang et al., 2008). At 4h Mehg exposure with 1 and 5 µM MeHg, the ARE activity started to decline, yet remained significantly higher than the control levels (Wang et al., 2008), whereas the induction of ARE activity with 10 µM MeHg was absent (Wang et al., 2008). The increase of ARE activity was accompanied by the increase of nuclear Nrf2 protein expression followed by increases of Slc7a11 and Ho-1 mRNA expressions in astrocyte and microglial cell cultures exposing to MeHg (Wang et al., 2008; Ni et al., 2010a). This data suggested that heavy metal MeHg acting as an electrophile induces Nrf2 to translocate to the nucleus and activate the ARE region resulting in activation of some cytoprotective gene expressions.

The mechanism by which MeHg directly activates the Keap1-Nrf2-ARE pathway revealed by the co-immunoprecipitation between MeHg and Keap1 protein in the study of the SH-SY5Y cells. Incubation of 50µg MeHg with 2 µg recombinant Keap1 resulted in about a 25:1 ratio of their binding interaction (Toyama et al., 2007). Using the ultra-performance liquid chromatography-tandem mass spectrometer indicated that MeHg and MeHg-GSH

modified the cysteine residues (Cys) of Keap1 at the Cys151 and Cys319, respectively (Yoshida et al., 2014). Using luciferase activity assay, both MeHg and intracellular MeHg-GSH adduct induce the increase of the ARE activity depending upon their concentrations and exposure time (Toyama et al., 2007; Yoshida et al., 2014). Determinations of some cytoprotective gene expression levels such as Gclc, Gclm, Ho-1, and Slc7a11, as well as their protein expression levels, indicated that the levels of these genes and protein synthesis depended upon the concentrations of MeHg and MeHg-GSH adduct (Toyama et al., 2007; Yoshida et al., 2014). The expression of GCLC protein increased following nuclear Nrf2 protein increase in 12 h of 0.5 µM MeHg, while the expression of GCLC protein started to decline with 24h of this MeHg concentration, which corresponded to the reduction of nuclear Nrf2 expression (Toyama et al., 2007). Consistently, GCLM and HO-1 protein expression increased depending upon MeHg and MeHg-GSH concentrations (1, 2, and 4 µM). Of note, the extracellular MeHg-GSH concentrations with 1 and 2 µM did not cause SH-SY5Y cells dead, whereas these MeHg and intracellular MeHg-GSH concentrations markedly induced SH-SY5Y cells dead (Yoshida et al., 2014). The extracellular GSH might reduce the availability of cellular toxicity of MeHg, and the MeHg-GSH could not permeate the SH-SY5Y cell membrane.

The vital role of Keap1 and Nrf2 in cellular defense ROS generation and MeHg toxicity has been demonstrated in the manipulation of Nrf2 expression levels. Overexpression of Nrf2 in SH-SY5Y cells protected 0.5  $\mu$ M and 2  $\mu$ M MeHg induced cell death (Toyama et al., 2007), meanwhile diminishing Nrf2 expression with siRNA exacerbated the effect of MeHg induced cell death (Toyama et al., 2007; Ni et al., 2010a). The knockdown of Nrf2 expression in primary microglial cell culture with siRNA also exacerbated the reduction

of Ho-1, Ngo-1, and Slc7a11 mRNA expressions in 5µM MeHg exposure (Ni et al., 2010a) and appeared to contribute to the reduction of mitochondrial activity and increase cell death (Ni et al., 2010a). Besides, the primary hepatocytes derived from Nrf2 knockout mice exhibited more susceptibility to MeHg than those derived from the wild type (Toyama et al., 2007), partly due to the higher MeHg accumulation in these Nrf2 knockout hepatocyte cells (Toyama et al., 2007). The higher MeHg accumulation in Nrf2 knockout hepatocytes is associated with reducing Mrp1 and Mrp2 expressions (Toyama et al., 2007). The MRP1 and Mrp2 possess a critical role in export xenobiotics, including heavy metals, and GSH and its conjugated (Cole, 2006). Nrf2 regulates these transporters' expressions (Hayashi et al., 2003; Vollrath et al., 2006). Thereby, lacking Nrf2 in this hepatocyte cell culture would reduce the Mrp1 and Mrp2 expression, consequently increases the cellular MeHg accumulation and exacerbates MeHg cellular toxicity. Meanwhile, the conditional Keap1 deficient hepatocytes were more tolerant of MeHg toxicity than the wild-type hepatocyte cell culture (Toyama et al., 2007). The conditional Keap1 deficient hepatocytes also expressed Mrp1 and Mrp2 greater and accumulated Hg lesser than wild-type control (Toyama et al., 2007). These findings indicated that not only ROS overproduction but also the Keap1-Nrf2-ARE pathway are directly affected by MeHg.

The loss of redox homeostasis is also tightly associated with the dysregulations of the Ca<sup>2+</sup> signaling and mitochondrial function. The Nrf2 regulated several cytoprotective gene expressions, including the cytosolic enzymes SOD1 (Cu<sup>2+</sup>/Zn<sup>2+</sup> SOD), cytosolic thioredoxin reductase 1 (Txnrd1) and mitochondrial enzymes SOD2 (Mn-SOD) and the mitochondrial thioredoxin reductase 2 (Txnrd2). Both Trx1 and Trx2 activities were

reduced significantly when human hepatoma cells (HepG2) were exposed to MeHg (Branco et al., 2014). The inhibition of Txnrd2 activity appeared to be more pronounced than the Txnrd1 activity, and it is the primary target of Hg2+ cellular toxicity in HepG2 (Branco et al., 2014). The selective inhibition of SOD2 by MeHg was also exhibited in the mouse brains (Shinyashiki et al., 1996). Mice subcutaneous exposure to 10mg/kg MeHg resulted in a time-dependent decrease in the SOD2 activity with about 60% of the control level but without any effect of SOD1 activity (Shinyashiki et al., 1996). When direct incubation 10U each SOD isozyme with 0.2mM MeHg (1:600 ratio) for 24h, only SOD2 but not SOD1 activities reduced considerably relative to control level (Shinyashiki et al., 1996). The isoelectric focusing-agarose gel electrophoresis and synchrotron radiation Xray fluorescence analysis revealed the mechanism by which MeHg affects the reduction of SOD2 activity is due mainly to the modification of thiol group in SOD2 by MeHg (Shinyashiki et al., 1996). This study also indicated that mRNA and protein expression levels for SODs were unaffected by MeHg administration (Shinyashiki et al., 1996). Meanwhile, the overexpression of *SOD2* in Hela cells reduced the susceptibility to MeHg (Naganuma et al., 1998). This protective effect was absent in the overexpression of either GPx or SOD1 (Naganuma et al., 1998). Moreover, the susceptibility of CGC to MeHg appeared to be associated with the instinctive SOD2 expression in these cerebellar neurons compared to PKCs and molecular layer neurons (Fujimura and Usuki, 2014). Not only is its basal SOD2 mRNA expression lower, but also the Txnrd1 and GPx1 mRNAs are significantly expressed lower in the CGCs relative to their neighboring cells that are resistant to MeHg (Fujimura and Usuki, 2014). Meanwhile, the basal levels of SOD1 and catalase mRNAs were similar among these three types of cerebellar neurons (Fujimura and Usuki, 2014). As such, not only the direct and indirect advese effects of MeHg to the

mitochondria function and mitochondrial ROS generation, but also the intrinsic vulnerability of CGCs with lower expressing antitoxidant genes contribute to neuronal degeneration.

ROS overproduction and mitochondrial dysfunction may be causally linked. ROS could potentially impair mitochondrial function and vice versa. Whether MeHg induced ROS generation resulting in disruption mitochondrial activity is required more pieces of evidence. Rat striatal synaptosomes exhibited an increase of 2',7'-dichlorofluorescein (DCF), a fluorescent ROS indicator, depending upon MeHg concentrations. MeHg concentration, ranging from 5 to 15 µM but not 1 and 2.5 µM, for 30 mins induced the elevation of DCF in these rat striatal synaptosomes (Dreiem and Seegal, 2007). These MeHg concentrations also reduced formazan production, a catalytic byproduct of methyl thiazole tetrazolium (MTT) by mitochondrial succinate dehydrogenase (Dreiem and Seegal, 2007). While the vitamin E analog Trolox reduced MeHg induced the increase of DCF, Trolox did not protect striatal synaptosomes from MeHg-induced a reduction of formazan (Dreiem and Seegal, 2007). This study suggested that ROS did not cause mitochondrial damage in striatal synaptosome exposure to MeHg. Instead, ROS generation as a consequence of mitochondrial damage from MeHg toxicity (Dreiem and Seegal, 2007). The elevation of [Ca<sup>2+</sup>]<sub>in</sub> in these striatal synaptosomes also linked to the mitochondrial disruption by MeHg since the elevations of Fura-2AM, a cytosolic divalent cation fluorescent indicator, and Rhod-2AM, a mitochondrial Ca<sup>2+</sup> fluorescent indicator, were appeared to be positively correlated (Dreiem and Seegal, 2007). ROS and [Ca<sup>2+</sup>]<sub>in</sub> also appeared to be involved in neuronal susceptibility to MeHg. The Comparative susceptibility to MeHg between cortical neurons and CGCs showed increased ROS

generations in both these neuronal types in a concentration and time of MeHg exposure with the significantly higher ROS generation in immature neurons than the mature neurons (Mundy and Freudenrich, 2000). Both immature and mature cortical neurons and CGCs also exhibited the increase of [Ca<sup>2+</sup>]<sub>in</sub> in a concentration and time of MeHg exposure similarly (Mundy and Freudenrich, 2000). With only relatively high MeHg concentration (10uM), it caused a significant increase of [Ca<sup>2+</sup>]<sub>in</sub> in immature cortical neurons compared to the mature cortical neurons (Mundy and Freudenrich, 2000). Meanwhile, the increases of [Ca<sup>2+</sup>]<sub>in</sub> in immature and mature CGCs were equally affected by MeHg (Mundy and Freudenrich, 2000). The age-independent effect to MeHg in [Ca<sup>2+</sup>]<sub>in</sub> elevation in CGCs suggested that the intrinsic characteristic might contribute to this neuronal type's susceptibility (Mundy and Freudenrich, 2000). Interestingly, the age-dependence of basal ROS and mitochondrial function exhibit in rat striatal synaptosomes, which greater basal ROS levels and lower mitochondrial function present in the younger rat striatal synaptosomes (Dreiem et al., 2005). MeHg induced ROS generations and reduced mitochondrial activities in all ages of striatal synaptosomes, with the most remarkable changes in younger striatal synaptosomes (Dreiem et al., 2005). Indeed, ROS overproduction and dysregulation of the antioxidant Keap1-Nrf2-ARE pathway are involved in cellular toxicity by MeHg. MeHg-induced ROS overproduction appeared to be generated primarily from mitochondria, contributing to loss of [Ca<sup>2+</sup>]<sub>in</sub> homeostasis and results in neuronal degeneration. Besides, the intrinsic antioxidant system contributes to neuronal susceptibility to MeHg. The basal SOD2, Txnrd1, and Gpx1 mRNA and protein expressions in CGCs are lower than that in the PKCs and molecular neurons (Fujimura and Usuki, 2014).

#### 1.2 Research rationale, hypothesis, aims, and techniques:

#### 1.2.1 Rationale, hypothesis, and aims

The neurological signs and symptoms of Minamata and Iraq patients caused by MeHg exposure have a primary characteristic of sensory disturbances such paresthesias and motor disorders such as tremor, upper or lower limbs incoordinate (Tokuomi et al., 1961; Joselow et al., 1972; Bakir, 1973; Okajima et al., 1976; Skerfving and Copplestone, 1976) that resemble signs and symptoms of motor neuron disease (MNDs) including ALS. Despite the postcentral gyrus and spinal dorsal root ganglia (DRG) (Chang, 1972; Schiønning et al., 1991; Schiønning et al., 1993), the degeneration of the precentral gyrus where corticomotor neurons are reside was reported as one of the most susceptible brain regions of the post mortem of Minamata and Niigata patients (Sakai et al., 1975; Igata, 1993; Harada, 1995; Eto, 1997; Eto et al., 2010). Although The susceptibility of SMNs to MeHg remains in conflict. The high susceptibility of SMNs to MeHg demonstrated by the low concentrations of MeHg (0.1uM to 2uM) caused CGCs death, but not PKCs, also caused SMNs (Ramanathan and Atchison, 2011) and hiPSC- derived MNs degenerations (Colón-Rodríguez et al., 2017) and dysregulated [Ca<sup>2+</sup>]<sub>in</sub> homeostasis (Ramanathan and Atchison, 2011). Moreover, the non-toxic MeHg exposure in human tgSOD1 G93A mouse through the drinking water hastens the onset of neurologic motor dysfunctions exhibited the concomitant with the dysregulation of [Ca<sup>2+</sup>]<sub>in</sub> homeostasis in these mice brainstem MNs (Johnson et al., 2011). The elevation of [Ca<sup>2+</sup>]<sub>in</sub>, a hallmark of excitotoxicity, involves the over glutamate receptor stimulation that the elevations of [Ca<sup>2+</sup>]<sub>in</sub> inducing by MeHg in brainstem MNs (Johnson et al., 2011) and SMN (Ramanathan and Atchison, 2011) were diminished when applying NMDARs and AMPARs antagonists (Johnson et al., 2011; Ramanathan and Atchison, 2011). The elevation of [Ca<sup>2+</sup>]<sub>in</sub> in the lumbar spinal cord's

ventral horn, where this region also displayed a significant overall increase in network excitability, indicating through increases in a spontaneous action potential firing, and increases the sensitivity to current injection during MeHg exposure (Sceniak et al., 2020). The increase of EPSCs frequency in lumbar SMNs was blocked by the GluA<sub>2</sub> lacking Ca<sup>2+</sup>-permeable AMPAR antagonist, 1-naphthyl spermine (NAS) (Sceniak et al., 2020). Similarly, the elevation of [Ca<sup>2+</sup>]<sub>in</sub> in the brainstem MNs was blocked by NAS (Johnson et al., 2011). MeHg perturbed the synaptic transmission in lumbar SMNs by which MeHg induced the increase of sEPSCs and IPSCs frequency and sEPSCs amplitude of lumbar SMNs (Sceniak et al., 2020). Likewise, MeHg induced the increase of both excitation and inhibition in the cerebellar slice (Yuan and Atchison, 2003; Yuan and Atchison, 2007b) and hippocampal slices (Yuan and Atchison, 1993b; Yuan and Atchison, 1997b).

Besides presynaptic neurons, astrocytes also control synaptic transmission by reuptake synaptic Glu via the astrocytic EAAT1/2 to control synaptic Glu concentration and termination the synaptic processes. ROS (Trotti et al., 1997) and MeHg (Brookes, 1992b; Allen et al., 2001b; Shanker et al., 2001a) also inhibited the EAAT1/2 functions by blocking the reuptake of aspartate and Glu (Brookes, 1992b; Trotti et al., 1997; Allen et al., 2001b; Shanker et al., 2001a). Prolonged 10µM MeHg exposure for 6 h in the astrocytic culture system that facilitates only EAAT1 expression indicated reduced EAAT1 mRNA expression (Allen et al., 2001c). The consequence of inhibiting EAAT1/2 function, or reducing EAAT expression, is the elevation of [Glu]<sub>ex</sub>, which subsequently reduces glutamate/cystine antiporter (system Xc<sup>-</sup>) function(Danbolt, 2001; McBean, 2002). Ultimately, neuronal degeneration occurs due to ROS overproduction and excitotoxicity.

During MeHg exposure, not only the cerebral and cerebellar neurons but astrocytes also lose their redox homeostasis characterized as the overproduction of ROS and reduction of the GSH, and antioxidant proteins and gene expressions. MeHg perturbed the Keap1-Nrf2-ARE pathway in the cortical astrocytes (Wang et al., 2008), microglia (Ni et al., 2010b), SH-SY5Y cells (Toyama et al., 2007), hepatocytes (Branco et al., 2014), and kidneys (Bridges et al., 2011, 2012a). The effects of MeHg to Keap1-Nrf2-ARE pathway include the direct interaction with Keap1 (Toyama et al., 2007), alteration of enzymes involving GSH synthesis (GCLC, GCLM, GST, MRPs) (Toyama et al., 2007; Vanduyn and Nass, 2014), alteration of cytoplasmic and nuclear Nrf2 protein level (Toyama et al., 2007; Wang et al., 2008; Ni et al., 2010b), and ARE activity (Toyama et al., 2007; Wang et al., 2008), including Ngo1, Ho-1, Gpx, Txnrd1, Mpr, and system Xc- expressions (Wang et al., 2008; Ni et al., 2010b; Bridges et al., 2011, 2012a; Branco et al., 2014; Vanduyn and Nass, 2014). The increase or decrease of these antioxidant enzymes and proteins in this pathway depend upon MeHg concentrations (Wang et al., 2008; Ni et al., 2010b; Branco et al., 2014), and duration of exposure (Wang et al., 2008). The differential response to MeHg exposure is also dependent on cell types. In primary cortical astrocytes cell culture, the increase of system Xc- expression began at 1µM MeHg and Ngo1 and HO-1 expression began to induce at 5µM MeHg (Wang et al., 2009a), in microglia, system Xcexpression was induced at 5M MeHg, and Nqo1 and HO-1 expression began to induced at 1µM MeHg(Ni et al., 2010b). Ultimately, the reduction of Nrf2 and antioxidant gene and protein expressions have positively corresponded to cell viability reduction (Toyama et al., 2007; Vanduyn and Nass, 2014) and negatively corresponded to the intracellular Hg accumulation (Toyama et al., 2007; Bridges et al., 2011, 2012a; Vanduyn and Nass, 2014).

Nevertheless, the contribution of CNS damage mediated by MeHg to the neurological symptoms onset and progression in specific cell types of the spinal cord has not yet been cleared. MeHg mediated the degeneration of the DRG (Chang, 1972; Schiønning et al., 1991; Schiønning et al., 1993) in the dorsal horn of the spinal cord where was one of the MeHg primary target regions (Eto, 1997; Korogi et al., 1998; Eto et al., 2010). Meanwhile, MN in the ventral horn of the spinal cord was observed as a primary target site and Hg accumulation when exposed to a high dose of MeHg (10mg CH3HgCl/kg bodyweight for 10 days) in rats (Su et al., 1998) and a chronic low dose of inorganic Hg i.p. injection (0.6µg HgCl<sub>2</sub>/g bodyweight for 12 months) in mouse (Pamphlett and Waley, 1996). Several lines of evidence in rodents (Chang, 1972; Leyshon-Sørland et al., 1994), non-human primates (Friberg and Mottet, 1989; Charleston et al., 1994; Charleston et al., 1995a; Vahter et al., 1995), and human (Sakai et al., 1975; Leyshon-Sørland et al., 1994; Eto, 1997) also suggested that microglia, astrocytes, and Bergmann glia are the primary Hg accumulation site in the brain (Sakai et al., 1975; Eto, 1997). However, the level of Hg accumulation was inversely related to the severity of cell damage since neurons, especially CGCs, the most susceptible to MeHg toxicity, show small or absent Hg accumulation compared to their neighboring neurons, PKCs which Hg primarily accumulated and exhibit little signs of neuronal damage (Sakai et al., 1975; Møller-Madsen, 1990, 1991; Eto, 1997). The time function of Hg granules appearance studied in the Wistar rats with 20mg CH3HgCl/L oral administration reported that the Hg granules were exclusively accumulated in the nerve cells' cell bodies in the brainstem as early as 10 days of MeHg administration (Møller-Madsen, 1991). Hg granules first appeared in the cortex and cerebellum on 14 days of MeHg administration. In the cerebellum, Hg granules were detected in the deep nuclei on day 14, and after 20 days or more of MeHg administration, Hg granules

appeared in PKCs and inhibitory interneurons of the cerebellar granular layer (Møller-Madsen, 1991). The Hg granules were undetected in the CGCs even after up to 84 days of MeHg administration, despite the fact that the PCKs, Bergman glia, and protoplasmic astrocytes were heavily loaded with Hg (Møller-Madsen, 1991). In the gray matter of the spinal cord, Hg granules appeared on day 16 with the prevalent deposits in MNs in Rexed's lamina IX (Møller-Madsen, 1991). The spinal cord laminae IV, V, and X, located on the anterior horn, were also detected the Hg granules on 16 days of MeHg administration (Møller-Madsen, 1991). The Hg granules were first appeared in glia on day 20 of MeHg administration (see data summary in Table 1 of Møller-Madsen, 1991). The clinical signs of locomotor and postural deficits were exhibited after 24 days, and ataxia started on day 28 of MeHg administration in these Wistar rats (Møller-Madsen, 1991). The time function of Hg granule accumulation in this study in accordance to the neurological sign and symptom exhibitions suggested that the latent period (non-symptomatic phase) is associated with Hg accumulation in neurons, while the symptomatic phase starts following Hg accumulation in glia. The mechanism(s) involving the latent period of MeHg toxicity has not yet been fully explained. MeHg may overwhelm astrocytic functions in neuronal protection since astrocytes provide GSH to neurons for combating against oxidative stress occurring during normal physiological conditions and oxidative insults. Loss of GSH content render neurons vulnerable to MeHg toxicity, and the increase of GSH appears to protect MeHg toxicity. PC12 cells containing four times of basal GSH level are resistant to MeHg-toxicity and increase of MeHg efflux rate (Miura and Clarkson, 1993; Miura et al., 1994; Goyer et al., 2000). In addition, intrinsic antioxidative enzymes also play a role in determining the selective vulnerability to MeHg

toxicity. The CGCs are more vulnerable to MeHg than PKCs and MLNs due to an intrinsic lower expression of SOD2 (Mn-SOD), Gpx1, and Txnrd1 (Fujimura and Usuki, 2014). Furthermore, MeHg reduces the uptake of GSH precursors, including CySS (Allen et al., 2001b), Cys (Shanker et al., 2001a), and Glu (Albrecht et al., 1993; Allen et al., 2001c) through blocking the system Xc- (Allen et al., 2001a; Shanker and Aschner, 2001) and (Allen et al., 2001a; Shanker et al., 2001b; Shanker and Aschner, 2001) **EAATs** transporting of these amino acids. These cytoprotective and antioxidant proteins are regulated by the Keap1-Nrf2-ARE pathway, which is more confer in astrocytes (Murphy et al., 2001; Liddell, 2017), besides their GSH and Gpx activity higher than in neurons (Dringen et al., 1999; Dringen et al., 2000). Astrocytes are predominantly expressed the systemXc- (McBean, 2002) and EAAT1/2 (Danbolt, 2001). The loss of redox and glutamate homeostasis during MeHg exposure potentially affects astrocytic functions in neuronal protection. Under oxidative stress causing neuronal degeneration induced by H<sub>2</sub>O<sub>2</sub> could be attenuated by co-culture with astrocytes (Drukarch et al., 1997). Converesely, the GSH depleted astrocytes could not protect neurons from H<sub>2</sub>O<sub>2</sub> induced oxidative damage (Drukarch et al., 1997). Similarly, GSH depleted astrocytes failed to increase the neuronal intracellular GSH level (Gegg et al., 2005). Incubation of both SOD and catalase ameliorated NO-induced neuronal degeneration in GSH depleted astrocyte coculture (Drukarch et al., 1998). Thus, the dysfunction of this antioxidant pathway which tightly coregulated with the EAATs in SCAs would render SMNs and DRGs susceptible to MeHg toxicity, which later exhibited neuropathology. Consequently, neurological signs and symptoms such as paresthesia and ataxia occur. See Figure 1.6 overarching hypothesis and the proposed cellular mechanisms by which MeHg indued toxicity in the CNS.

My working hypothesis was that MeHg dysregulated SCAs function by altering the Keap1-Nrf2-ARE pathway, which also cooperates with the EAATs function. As such, MeHg also altered astrocytic EAAT1 or EAAT2 expression that later resulted in dysregulation of their function (Figure 1.7). Three subworking hypotheses were 1. MeHg affected SCAs depending upon the maturity (age) of SCAs as well as MeHg concentration and time of exposure. 2. MeHg affected the Keap1-Nrf2 -ARE by reduced the expression of GSH synthesis pathway and transporter as well as EAAT1 and EAAT2. 3. The antioxidant would ameliorate MeHg-induced cytotoxicity in SCAs.

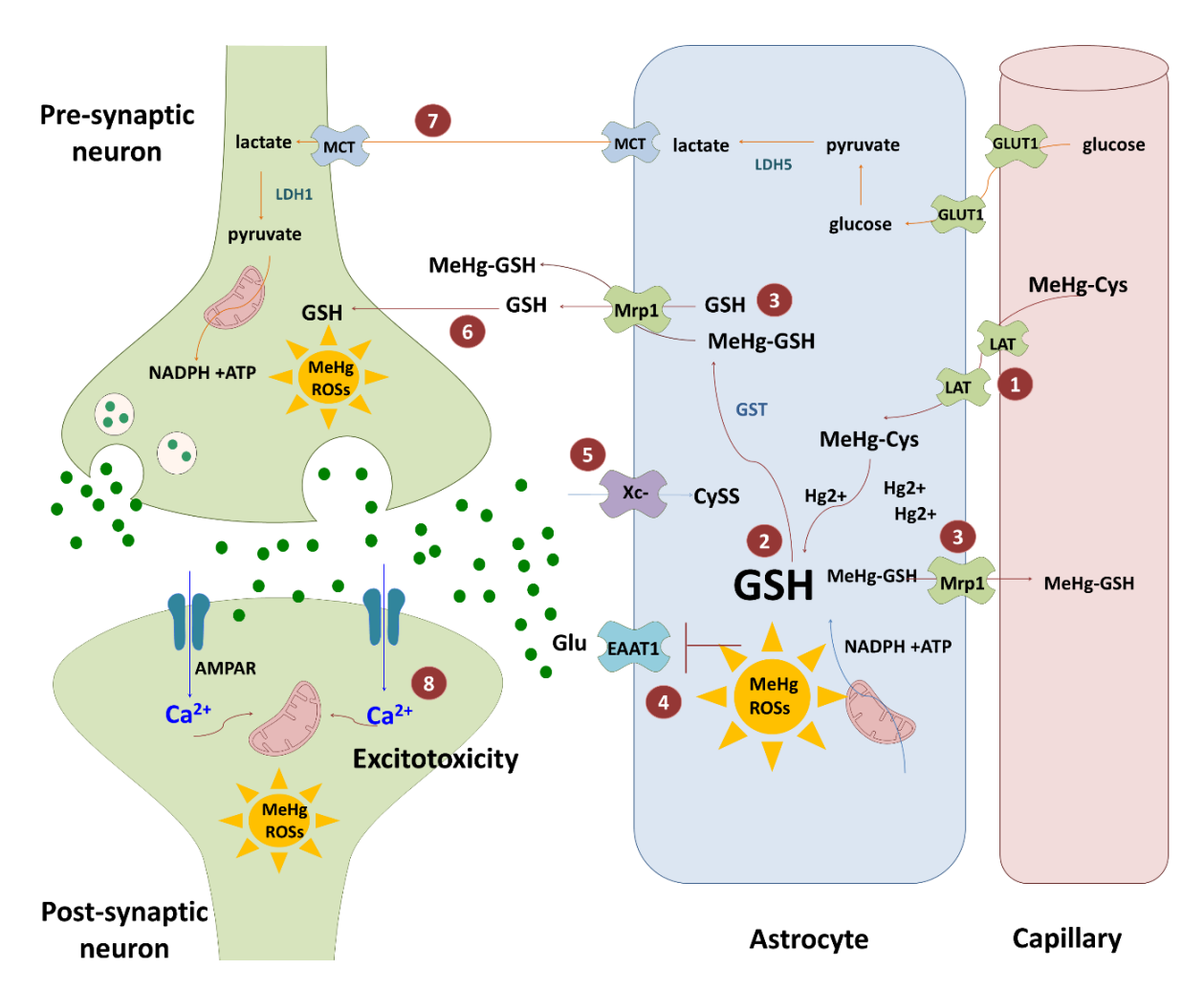
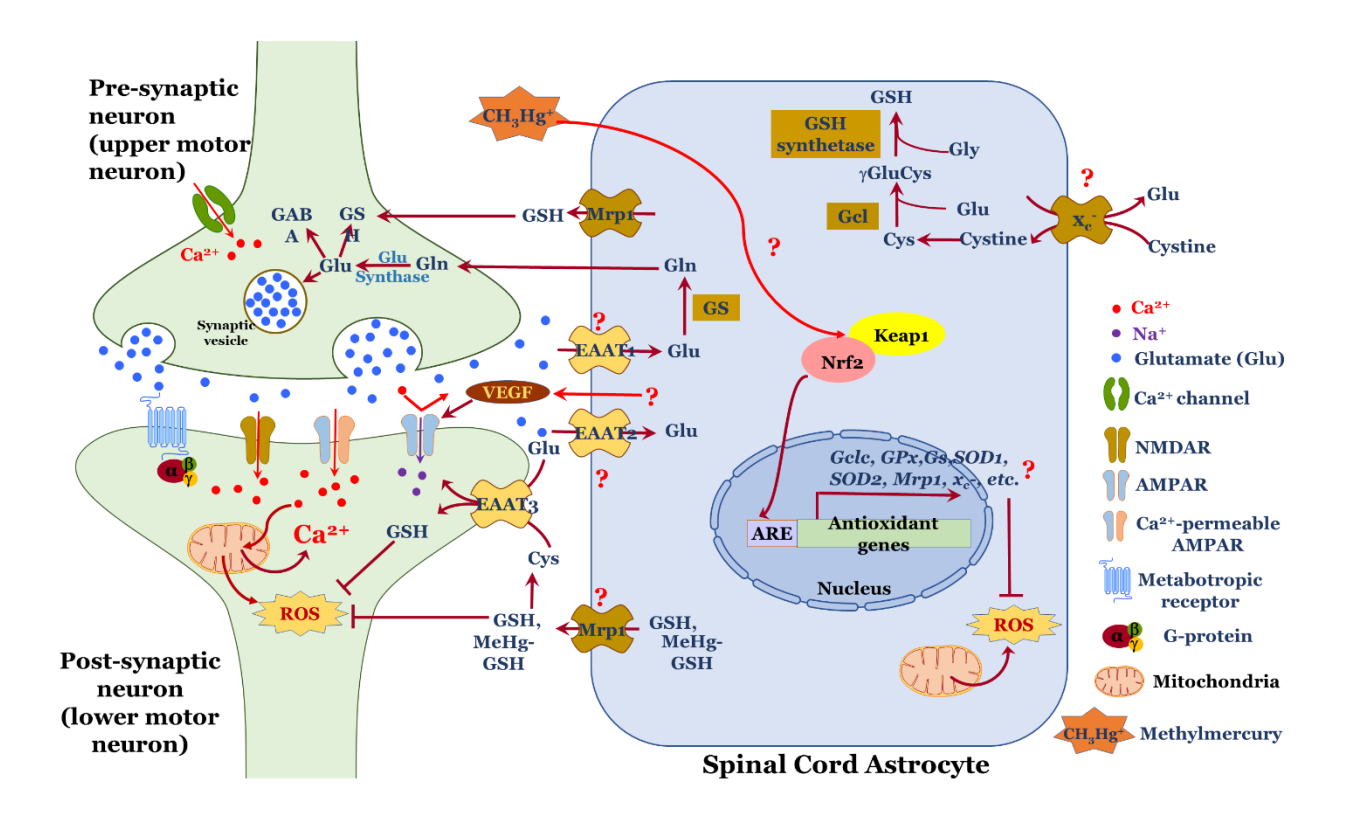


Figure 1.6 Proposed cellular mechanisms by which MeHg induced toxicity in the CNS: the interaction between astrocytes and neurons (overarching **hypothesis**). The pathogenic mechanism by which MeHg induced neuronal generation is imitated by astrocytic antioxidative defense failure, subsequently render neurons vulnerable to oxidative stress and excitotoxicity. Multistep induced this pathogenesis are as follows; 1) MeHg enters the brain through LAT due to it forming a complex with cysteine (MeHg-Cys), which has a similar structure to methionine. LAT is expressed in endothelial cells and astrocytes. Therefore, astrocytes are the first brain cells exposed to MeHg. 2) Once in astrocytes, MeHg-Cys is detoxified by GSH and export from cells through the Mrp, a xenobiotic and GSH transporter. 3) During detoxification, astrocytes require NADPH and ATP for recycling GSH generated by mitochondrial oxidative phosphorylation, which in turn generated ROSs as a byproduct. 4) ROSs, as well as MeHg, alters sulfhydryl bonding in EAATs that causes the reduction of glutamate uptake. concentration Thereby. extracellular glutamate [Glu]<sub>ex</sub> is heightened. Glutamate/Cytine (Glu/CySS) antiporter later decrease CySS uptake due to the transporter function depends upon [Glu]<sub>ex</sub>. High [Glu]<sub>ex</sub> reduces the driving force for exchanging Glu for import CySS into the cells. 6) Reduction of CySS uptake resulting in de novo GSH synthesis reduction since CySS is a precursor for cysteine (Cys) a rate limiting substrate for GSH synthesis.

**Figure 1.6 (cont'd)** Consequently, GSH content in astrocytes is insufficient to detoxify MeHg and also insufficient to supply for neurons. 7) During MeHg detoxification in astrocytes, lactate an essential substrate for neuronal TCA, and oxidative phosphorylation is insufficiently produced in astrocytes. Therefore, neurons are unable to generate ATP from TCA and unable to control redox homeostasis. ROSs later occurs. 8) The excessive [Glu]<sub>ex</sub> as a consequent of EAAT inhibited, overly stimulate postsynaptic excitatory amino acid receptors, particularly Ca2+ -permeable AMPAR which lacking GluR2 or lacking RNA editing GluR2. Subsequently, the excessive influx of Ca<sup>2+</sup> impairs mitochondrial function, ROSs later occurs. Oxidative stress and excitotoxicity, therefore, induced neuronal degeneration.



**Figure 1.7 Working hypothesis.** MeHg impaired the redox homeostasis in SCAs by exacerbating the ROS production and dysregulation of the Keap1-Nrf2-ARE pathway. Thereby, SMN and DRG are susceptible to ROS overproduction during MeHg exposure resulting from the loss of antioxidant GSH supplied by SCAs. MeHg dysregulated Nrf2 by reducing the Mrp1 expression. Due to the ROS overproduction and MeHg insult, cystine is imperative for *de novo* GSH synthesis, therefore, the upregulation of system Xc- would increase the transport of GSH substrate precursor. Meanwhile, MeHg and ROS also inhibited EAAT1/2 expressions. The intertwined between redox and excitotoxicity occurring through the dysregulation of system Xc- and EAAT1/2 in SCAs. Ultimately, SMN and DRG were susceptible to MeHg due partly to oxidative stress and excitotoxicity occur. MeHg might also reduce *Vegfa* expression in SCAs, which later contributed to increased Ca<sup>2+</sup>-permeable through the AMPAR, consequently induced neuronal excitotoxicity.

## Aim1: Determination of SCAs' sensitivity during MeHg exposure and the cellular mechanisms involving the redox and glutamate homeostasis.

The functions of time and concentrations of MeHg exposure were comparatively determined the susceptibility to MeHg between the developmental stage (DIV14) and fully developmental stage (DIV30). Whether the Keap1-Nrf2-ARE pathway was dysregulated in the aged related susceptibility was determined in the SCAs DIV30. Furthermore, whether the intertwined between redox and glutamate homeostasis occurring in MeHg exposure SCAs, the dysregulation of *Slc7a11* expression and astrocytic glutamate transporters *Slc1a3* and *Slc1a2* were determined their correlation of expressions.

### Aim2: Characterization of the role of Nrf2 in the regulation of MeHg-induced toxicity in SCAs.

Nrf2 regulates several cytoprotective enzymes and proteins (Muramatsu et al., 2013; Hayes and Dinkova-Kostova, 2014; Tonelli et al., 2018). To identify which biomolecules underlying Nrf2 regulation are involved in MeHg-induced the dysregulation of the Keap1-Nrf2-ARE pathway in SCAs, the Nrf2-knockout derived SCAs were compared with the wildtype-derived SCAs for their susceptibility and the expression of genes involving the GSH synthesis and transport, the glutamate transporters including the system Xc- and EAAT1/2.

# Aim3: Assessment of the role of antioxidant compound N-acetyl-L-cysteine (NAC) during MeHg exposure in SCAs.

Since MeHg induced the dysregulation of genes involving GSH synthesis and transport as well as glutamate transporters in SCAs. These genes are primarily regulated by the Nrf2 pathway. Therefore, when applying antioxidant compounds such as NAC in SCAs during

MeHg exposure, these compounds would have benefit in protecting SCAs against MeHg induced toxicity. Besides its thiol-containing antioxidant property, NAC acts as a cysteine precursor for GSH synthesis (Dringen and Hamprecht, 1999). However, the role of NAC in the protection of SCAs during MeHg has not been assessed and elucidated its mechanism(s). Several antioxidant molecules regulate nrf2; therefore, NAC might exert its protective effect through the activation of Nrf2, resulting in induction of genes underlying Nr2 activation, such as GSH synthesis and transport genes.

#### 1.2.2 Research model system: Primary spinal cord astrocyte cell culture

### a. Primary astrocyte cell culture as an experimental model system for understanding astrocytes in health and diseases

During the past few decades, astrocytes has become increasing their significant roles in central nervous system both in health and diseases. The increasing of astrocytic roles has raisen together with the development of astrocytic models that includes the development of primary astrocytes cell culture techniques for characterizations of their functions and interaction to other cell types such as neurons. Since these significant roles of astrocytes involved in interaction to different cell types, some limitations in employing primary cell culture system raise awareness if the *in vitro* systems truly mimic the astrocytic characteristics and functions *in vivo* systems and to which degree results obtained in cell culture could be translated into astrocytic functions *in vivo* system (Lange et al., 2012). Despite different primary cell culture methods, several astrocytic characteristics contribute to the discrepancy results between studies *in vitro* and *in vivo*. To define and characterize astrocytes is complicated and not straightforward since astrocytes posse morphological and functional diversities. The heterogeneity of astrocytes is involved

several aspects that include intrinsic factors (gene and protein expressions), extrinsic factors (extracellular milieu), and locations of their origin and distribution (Lange et al., 2012; Li et al., 2016). These factors greatly contribute to gliogenesis to a different degree in spatiotemporal manners. Furthermore, the astrocyte cell culture protocols, including cell isolation stage, culture medium composition, a substrate for cell adhesion, subculture, and day in vitro (DIV), which varies among different research labs, influence the heterogeneity of astrocyte cell culture.

#### b. The astrocyte cell culture protocol factors

In the mammalian brain cortex, a cell with typical astrocytic morphology accounts for about 30% of the volume with regional and species variability. In mice and rats, astrocytes can undergo mitosis (division) at the time of birth while, most neurons are already in the postmitotic stage (Hertz et al., 1998). The majority of primary astrocyte cell culture protocols obtain astrocytes from newborn mice or rats, ranging from postnatal day 0-7. Few protocols for primary astrocytes from adult rodents (Norton and Farooq, 1989; Sun et al., 2017) and bovine (Norton et al., 1988) have developed. Since the heterogeneity of astrocyte is partly involved in giologensis. Besides, species of animal contribute to astrocytic heterogeneity; the developmental stage of animal for cell culture is involved. Culturing astrocytes from neonates which progenitor cells are plastic and labile to stimuli could achieve in fully developed or mature astrocytes. Whereas culturing astrocytes from older animals when astrocytic development is complete, the cell culture results mainly in immature astrocyte stem cells, not mature astrocytes since they were immunoreactive to GFAP and immature neuroectodermal cell markers (Norton and Farooq, 1989).

However, maturation of astrocyte in culture could be achieved by the addition of trophic factors and/or compounds that induce astrocyte maturation in cell culture media.

Despite some of the discrepancy results from *in vivo*, employing primary astrocyte cell culture in research studies provide a significant contribution to a better understanding of astrocytic roles in physiological and pathological conditions that include maintaining CNS homeostasis, neurovascular coupling, synaptic formation/removal, and synaptic transmission/modulation as discussed previously.

#### 1.2.3 Research Techniques:

#### a. The principle of real-time cell viability assay

The real-time cell viability assay (RealTime-Glo<sup>TM</sup> MT Cell Viability Assay, Promega, Madison, WI.) consists of two compounds, a luciferase enzyme (NanoLuc® luciferase) and prosubstrate (Figure 2.2), which are added to cell culture media. The prosubstrate is cell-permeant compound, while the luciferase enzyme remains in the cell culture media. The prosubstrate is reduced intracellular by active metabolic cells into active luciferase substrate, NanoLuc® substrate. The active luciferase substrate diffuses from intracellular to cell culture media where it rapidly catabolized by NanoLuc® luciferase enzyme. The reaction between active luciferase substrate and luciferase enzyme exhibits illumination, which corresponds to a number of the metabolic active cells (viable cells). Due to the properties of active luciferase substrate that it does not accumulate in cell culture media and is rapidly catabolized, a real-time detection of cell viability is attainable. In addition, both prosubstrate and the luciferase enzyme are stable in cell culture media for > 96h, and they are non-toxic to cells since the luminescent intensity remains higher than basal intensity over than 96h (Duellman et al., 2015).

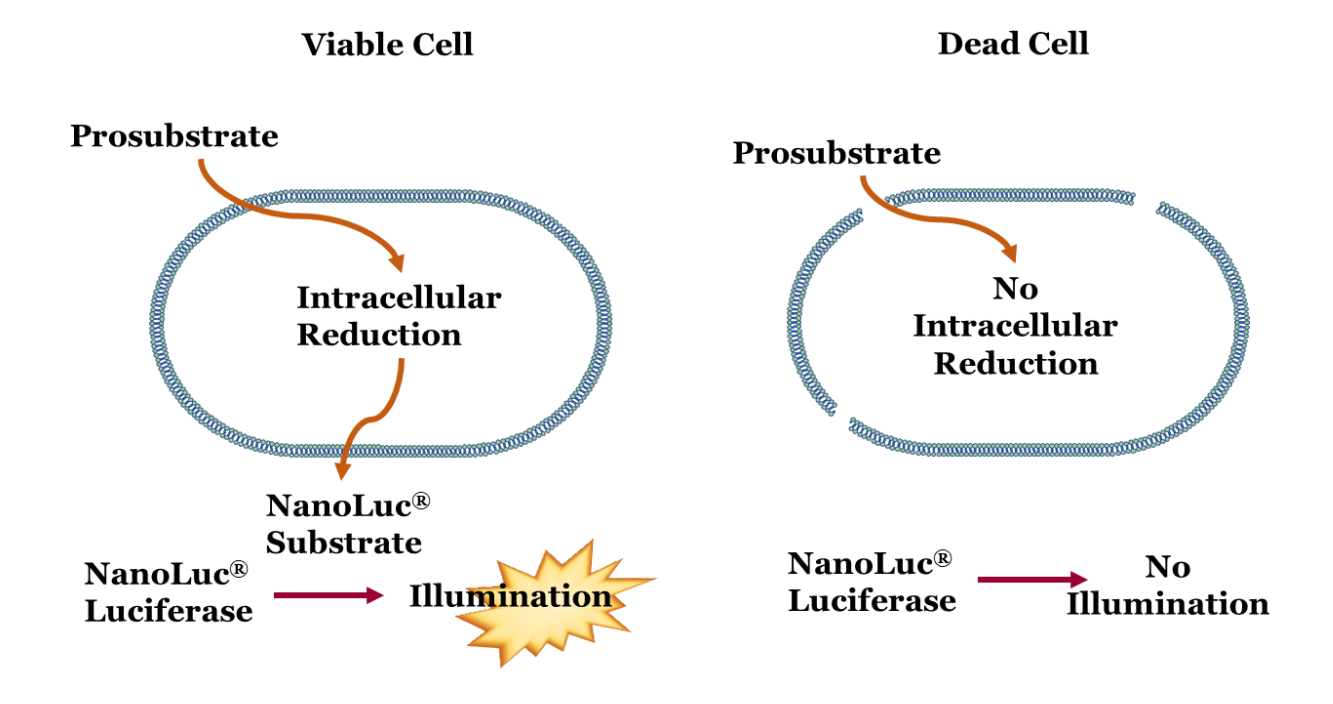


Figure 1.8 The principle of the Real-Time Cell Viability Assay (RealTime-Glo<sup>TM</sup> MT Cell Viability Assay, Promega, Madison, WI.) A cell-permeable prosubstrate is intracellularly reduced into NanoLuc® substrate by active metabolic cells. Subsequently, NanoLuc® substrate diffuses through the cell membrane into the cell culture media where it is rapidly catabolized by NanoLuc® luciferase. The reaction between NanoLuc® luciferase and NanoLuc® substrate exhibits illumination, which can be determined using a spectrophotometer and microplate reader for luminescent intensity. The luminescent intensity corresponds to a number of viable cells. The higher luminescent intensity, the higher number of viable cells (high metabolic activity) (Technical Manual and (Duellman et al., 2015)).

A kinetic assay, as well as concentration-response curve, is achievable in monitoring the luminescent signal over time in each treatment compared to control. The fold change of cell metabolic activity (change in cell viability) is presented in concentration-response curve, and each value of time point is achieved using equation is as follows:

$$\textit{Change in cell viability (Fold change to control)} = \left(\frac{\left((\textit{LITtA}) - \left(\textit{Average LICtA}\right)\right)}{\textit{Average LIC tA}}\right)$$

LI TtA = Luminescent intensity of treatment at time point A

Average LI CtA = Average luminescent intensity of control at time point A

To measure the potency of substances such as MeHg in inhibiting a specific biological or chemical function termed a half-maximal inhibitory concentration (IC50) is obtained from the kinetic relationship between the substance concentration and cell biological activity. In real-time cell viability assay, IC 50 is to determine a concentration of substance where the response (cell metabolic activity in converting prosubstrate into active luciferase substrate) is reduced (inhibited) by half of the maximum response. This quantitative measurement IC50 is determined from a concentration-response curve which examines the effect of different concentrations of substances on biological or chemical function. The half-maximal response IC50 is derived from the maximum fold change (top), and minimal fold change (bottom) from the concentration-response curve where the values of response relative to control are calculated from the equation mentioned previously.

#### b. Real-time quantitative polymerase-chain-reaction (qPCR)

Real-time quantitative polymerase-chain-reaction (qPCR) becomes a gold standard for gene expression analysis since it provides a plethora of applications in fundamental research and biomedical diagnostics. The advancement of qPCR compared to conventional PCR is that it allows amplification and simultaneous quantification of targeted DNA as the reaction progress in real-time. This advancement allows quantifying the initial amounts of targeted template molecules by comparing the cycle threshold (Ct). The Ct value is defined as the number of amplification cycles that are required for the fluorescent signal to cross the threshold. Ct values are inversely proportional to the amount of targeted nucleic acid in the sample. The more copies of a nucleic acid template are presented at the beginning, the fewer PCR cycles (relatively lower Ct value) is observed, and this condition is referred to as the up-regulation of targeted gene expression. In contrast, the term downregulation represents a condition that fewer copies of DNA templates are subjected to the reaction, which indicates more PCR cycle (relatively higher Ct value).

Several strategies were developed to quantify targeted DNA molecules, which are mainly based on measuring the emission of the fluorescent reporter dye. DNA binding dye, i.e., SYBR green dye: it binds the double-stranded DNA (dsDNA). SYBR green exhibits little fluorescent signal in free solution, while it increases 100-fold fluorescent intensity when it binds to dsDNA. As a new copy of dsDNA is created, the fluorescent intensity increases, corresponding to the SYBR dye binding. Therefore, the fluorescent signal proportional to the amount of dsDNA generation and will increase as the target is amplified. The SYBR green dye is widely used due to no probe requirement, ease of use, cost-efficiency, and

generic detection (Pabinger et al., 2014). The primary disadvantage of SYBR dye is that it may generate false-positive signals. Since SYBR dye binds to any dsDNA, including nonspecific reaction products, this might overestimate the targeted gene expression. Another SYBR dye issue is that multiple dye molecules bind to a single amplicon and the fluorescent signal depends upon the mass of amplicons produced in the reaction. The longer amplicons will generate more fluorescent signal than the shorter one. In contrast to the probe-based methods such as TagMan, which relies on the sequence-specific detection of a targeted DNA. Using a fluorogenic probe, the fluorescent signal is generated from a single fluorophore that is released from the probe when a specific full amplicon is generated regardless of its length. Therefore, the single amplicon is determined from one fluorophore emission after a full specific target sequence is generated. In addition to a better specificity and sensitivity for quantitative targeted DNA analysis, the probe-based method also allowed to detect multiple targeted sequences in a single reaction using the different fluorogenic probes to distinguish the different targeted amplicons. This technique is referred to as multiplex PCR. The advantage of TaqMan multiplex PCR is the cost and time efficiencies over the single tube/well TagMan PCR because reagents and cDNA or RNA templates are reduced for the assay application. In addition, the internal control is in the same reaction tube that reduces variability as opposed to determining targeted sequences and endogenous control in separated reaction tubes. The multiplex PCR, however, might reduce sensitivity as a consequence of different targeted primers competing for the limited cDNA or RNA template (Pabinger et al., 2014).

Two commonly used methods to analyze data from qPCR are absolute quantification and relative quantification. *Absolute quantification* determines the input copy number of

the targeted transcript (amplicon) by comparison with a standard curve (Livak and Schmittgen, 2001). The standard curve is presented in a relationship between a logarithm of a serial dilution of known nucleic acid concentrations and its Ct value. The result of the analysis is represented in the quantity of nucleic acid (copy number; µg) per amount of given sample (per µg of total RNA). The reliability of the absolute quantification analysis depends on the amplification efficiencies for the target and standard curve (Pabinger et al., 2014). **Relative quantification** describes the change in target gene expression relative to some reference group such as untreated control or a sample at time zero in a time-course study (Livak and Schmittgen, 2001). This analysis does not require a standard curve because the target gene is normalized to a single or multiple internal reference genes (a.k.a endogenous control gene) such as glyceraldehyde-3-phosphate dehydrogenase (*gapdh*), β-actin (*actb*) or 18srRNA which represents in a fold- difference change. The relative quantification  $2^{-\Delta\Delta Ct}$  method by Livak and Schmittgen (2001) is widely used and easy to perform. This method assumes that both target and reference genes are amplified with efficiencies close to 100% and variable within 5% of each other. To determine the relative target gene expression, a few steps are as follows:

First, normalize the Ct value of the target gene (Ct target) to that of the reference gene (Ct ref) for both the test sample (treatment sample) and the control sample (ctrl). This normalized step is to compensate for any difference in the amount of tissue sample. The result is delta Ct ( $\Delta$ Ct)

$$\Delta Ct (test) = Ct (target, test) - Ct (ref, test)$$

$$\Delta Ct(ctrl) = Ct (target, ctrl) - Ct (ref, ctrl)$$

Second, normalize the  $\Delta$ Ct (test) to the  $\Delta$ Ct (ctrl). The result is deltadeltaCt ( $\Delta\Delta$ Ct)

$$\triangle \Delta Ct = \Delta Ct (test) - \Delta Ct (ctrl)$$

Finally, calculate the expression ratio

$$2^{-\Delta\Delta Ct}$$
 = Normalized expression ratio

The obtained result is the fold increase (or decrease) of the target gene in the test (treatment) sample relative to the control (vehicle) sample. The relative gene expression level can be compared across multiple qPCR experiments (Livak and Schmittgen, 2001; Pabinger et al., 2014).

#### **CHAPTER TWO**

THE MECHANISM BY WHICH METHYLMERCURY INDUCES SPINAL CORD ASTROCYTE CELL CULTURE DEGENERATION THROUGH THE DYSREGULATION OF THE KEAP1-NRF2-ARE PATHWAY AND GLUTAMATE TRANSPORTER EXPRESSIONS

#### 2.1 Abstract

The mechanism by which SMN degeneration occurs following MeHg exposure remains unknown. Previous studies in brainstem slices and SMN primary cell culture suggested that the dysregulation of intracellular Ca<sup>2+</sup> homeostasis was involved in the activation of AMPARs to permit Ca<sup>2+</sup> entry. Astrocytes participate in regulating Ca<sup>2+</sup>-impermeability of AMPARs by induced GluR2 subunit expression in motor neurons through secretion of vascular endothelial growth factor (VEGF). Astrocytes also play significant roles in regulating neuronal redox, and glutamate homeostasis against oxidative stress and subsequent excitotoxicity. As such, dysregulation of SCA function could be detrimental to SMNs. In this study, a major antioxidant pathway, Keap1-Nrf2-ARE, was examined as a potential mechanism by which MeHg affected SCA function. Expression of astrocytic glutamate transporters (EAAT1/GLAST and EAAT2/GLT-1) and Vegfa mRNAs were determined whether the dysregulation of these molecules occurred in SCAs during MeHg exposure. The results indicated the concentration and time course of MeHg exposure that affected SCAs' metabolic activities as determined by a RealTime-Glo<sup>TM</sup> MT cytotoxicity assay. The differential susceptibility of SCAs between mature DIV 14 and fully mature SCAs DIV30 was examined. Metabolic activity of SCAs DIV 30, but not SCAs DIV 14, significantly decreased following 0.1µM MeHg for longer than 12h exposure. Degeneration of SCAs DIV 14 was a consistent observation after 24h of treatment with 0.5, 1.0, 2.0, and 5.0, but not with 0.1µM MeHg. Subsequent experiments all utilized a 0.5µM MeHg to examine the mechanisms involved in SCAs DIV 14 and DIV 30 susceptibility to MeHg. Expressions of Keap1, Nrf2, Gclc, Abcc1 mRNAs increased significantly starting at 6h of 0.5µM MeHg exposure in SCAs DIV3 and later declined to basal control levels. Expressions of antioxidant genes Gclc and Abcc1 and AMPAR-

permeable regulator Vegfa mRNAs appeared to increase in a bi-phasic fashion during 24h of MeHg exposure. The cystine/glutamate transporter (system Xc-) Slc7a11 mRNA increased in a tri-phasic manner with the first, second and third peaks occurring at 30min, 6h, and 21 h of MeHg exposure, respectively. The expression of astrocytic Glu transporters EAAT1/GLAST Sla1a3 and EAAT2/GLT-1 Slc1a2 mRNAs was increased following 3h of MeHg exposure, but later returned to basal control levels. Immunocytochemistry indicated reduction of Mrp1, system Xc- as well as GLT-1 following 18h of MeHg exposure in SCAs. In conclusion, the mechanism by which MeHg induced toxicity in SCAs involved dysregulation of the Keap1-Nrf2-ARE pathway, particularly GSH rate-limiting enzyme (Gclc) and the the GSH and GSH precursor transporter (Abcc1 and Slc7a11). Mechanisms involved in MeHg-induced toxicity in SCAs appear to be intertwined between oxidative stress and excitotoxicity, as demonstrated by its effect on glial Glu transporters system Xc- and EAATs. Induction of Vegfa mRNA expression following MeHg exposure remined unclear whether it involved in the regulation of blood-brain barrier permeability or its protective role in the regulation of Ca<sup>2+</sup> impermeability through AMPAR in SMN during MeHg exposure.

#### 2.2 Introduction

The temporary exposure to the low level of MeHg through marine food consumption remains a public health concern, especially for susceptible populations such as pregnant or nursing women (Mahaffey, 1999). Additionally, exposure to heavy metals, including MeHg, has been postulated to be a risk factor for neurodegenerative diseases such as amyotrophic lateral sclerosis (ALS) and Parkinson's disease (PD) (Portaro et al., 2019). The incidence of these neurodegenerative diseases increases with age (Costa, 2017). Typical clinical signs and symptoms of MeHg intoxication such as peripheral neuropathy (paresthesia), visual impairment (visual filed constriction), auditory disturbance, cerebellar-based ataxia (dysmetria, adiadochokinesis, dysarthria, and gait disturbances), hyperreflexia, and mental deterioration (intellectual and emotional disabilities) (Igata, 1993; Harada, 1995) are often preceded by lengthy asymptomatic periods (Igata, 1993; Harada, 1995; Weiss et al., 2002a, b). For example, chronic low dose MeHg exposure through a fish consumption in Minamata patients did not exhibit the adverse observable symptoms for several years (Igata, 1993; Harada, 1995; Weiss et al., 2002a) This "silent latency" characteristic associated with MeHg exposure (Weiss et al., 2002a; Bailey et al., 2017) may only be severely exhibited in "susceptible individuals" in later life.

Some epidemiology studies (Mangelsdorf et al., 2017; Parkin Kullmann and Pamphlett, 2018; Portaro et al., 2019) suggested that mercury intoxication is associated with some common clinical symptoms exhibited in ALS, upper MN signs: hyperreflexia and spasticity and lower MN signs: muscle weakness and atrophy (Sienko, 1990). The study by Sienko *et. al.* (1990) suggested a correlation between the frequency of fish consumption and ALS patients in a small Wisconsin community. Sienko suggested that

consumption of contaminated fish may be a risk factor for ALS onset (Sienko, 1990). Investigation of the correlation between mercury exposure and ALS has reported a positive correlationship between mercury content in the toenail, and ALS patients. The increase of toenail mercury level in these patients was associated with fish consumption (Andrew et al., 2018). Some studies, however, reported the no correlation between mercury exposure and ALS (Parkin Kullmann and Pamphlett, 2018). More longitudinal with case-control studies are required to investigate further the potentially positive correlation between the cause (MeHg or mercury) and the effect (ALS). Nevertheless, exposure to mercury or MeHg indicated the pathophysiology and cellular mechanisms similar to ALS patients (Barber, 1978; Callaghan, 2011; Mangelsdorf et al., 2017) and ALS mouse models(Johnson et al., 2011). Common cellular mechanisms that are well characterized in both MeHg-toxicity and ALS have included the disruption of intracellular Ca<sup>2+</sup> homeostasis (Marty and Atchison, 1997b, 1998b; Vanselow and Keller, 2000; Limke and Atchison, 2002; Edwards et al., 2005; Johnson et al., 2011; Ramanathan and Atchison, 2011; Meszlényi et al., 2020), redox homeostasis (Amonpatumrat et al., 2008; Barber and Shaw, 2010; Xu et al., 2012b), as well as a dysregulation of Glu transmission and excitotoxicity (Yuan and Atchison, 1993a, 1995, 1997a; Xu et al., 2012b). The loss of upper and lower MNs are distinct pathologies in ALS (Rezania and Roos, 2013), and these are one of the primary targets of MeHg-toxicity (Korogi et al., 1998). The loss of the upper MNs in the primary motor cortex have been documented in a postmortem examination of Minamata Disease patients (Korogi et al., 1998), while the loss of the lower MNs located in the ventral spinal cord (anterior horn of the spinal cord) remains a controversy. The summary of a report from moderate cases of Minamata Disease patients indicated an absence of primary lesions in the spinal cord, but the secondary degeneration was found

in the spinal tract. This is likely due to degeneration of the nerve fibers of the upper MNs from the premotor cortex (the primary lesion area) (Eto, 1997; Korogi et al., 1998). Conversely, MeHg exposure in rodent models indicated the primary and severe loss of neurons in the anterior horn of the spinal cord (Su et al., 1998; Johnson et al., 2011) where the lower MNs are located. Degeneration of lower MNs remains unclear as to whether or not they are a primary target of MeHg in addition to the sensory neurons in the spinal DRG. The differential susceptibility of particular neurons in the certain brain or spinal cord regions might be due partly to its intrinsic susceptibility or the attribution of their neighboring cells, particularly astrocytes. Not only do the astrocytes play an important role in providing energy and nutrients to neurons, but their role in the regulation of Glu transmission is also critical for glutamate hemostasis for the CNS(Rothstein et al., 1996; Mahmoud et al., 2019; Pajarillo et al., 2019). The "non-cell-autonomous mechanism of MN death" in ALS was initiated from Clemen et al. (2003) studies using chimeric mice expressing mutant SOD1 (G37R or G85R or G93A) (Clement et al., 2003) and further confirmed in chimeric cell culture studies using motor neurons coculture with astrocytes (Clement et al., 2003; Di Giorgio et al., 2007; Nagai et al., 2007). Primary cultures of spinal cord MNs or embryonic MN stem cells carrying either the nonpathological human SOD1 (hSOD1) transgene or the hSOD1 G93A mutant showed neurodegenerative characteristics (neuronal loss and SOD1 aggregates) when cocultured with hSOD1 G93A astrocytes (Di Giorgio et al., 2007; Nagai et al., 2007). However, cocultures of hSOD1 G93A astrocytes with spinal GABAergic or DRG neurons or embryonic interneuron stem cell did not cause the neuronal death (Nagai et al., 2007). The astrocyte generated from fibroblast induce pluripotent stem cells (iPSCs) from patients with sporadic ALS (sALS) were also toxic to Mns as were in astrocyte-derived iPSC from familial ALS (fALS) (Meyer

et al., 2014). These findings suggested that astrocytes may play a role in the specific degeneration of spinal MNs in ALS (Nagai et al., 2007). However, the mechanism by which astrocytes specifically induced motor neuron death has not been fully understood. The growing evidence also suggests that astrocytes did not initiate neuronal toxicity, but they were involved in progression of pathologies. Deletion of some neuroinflammatory cytokines which activates quiescent astrocytes to become reactive astrocytes extends survival in SOD1 G93A mice (Guttenplan et al., 2020). Tripple knockout of *IL-1a*, *TNFa*, and *C1q* in this ALS mouse model delayed but not completely inibited MNs death of these mice compare to SOD1 G93A mice (Guttenplan et al., 2020). Astrocytes from these SOD1 G94A mice reach high levels of reactivity at much lower dose of these cytokine exposures than in the WT (Guttenplan et al., 2020). Mutant SOD1 G93A perhaps attribute astrocytes primed to subtle toxic insults, including these cytokines that would not sufficiently respond to aberent MN viability or function (Guttenplan et al., 2020).

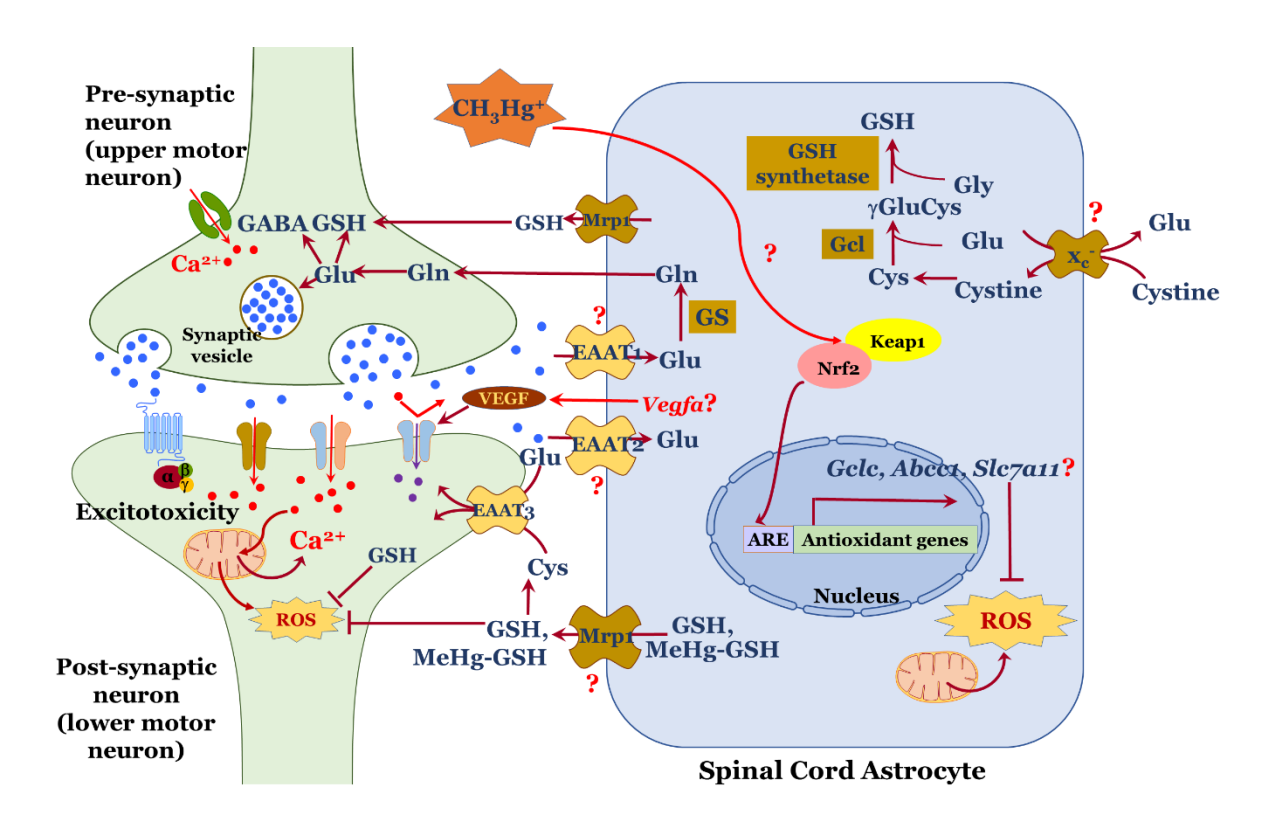
MeHg-induced toxicity is associated with the specific susceptibility of certain neuronal types in specific brain areas. The intrinsic properties of those susceptible neurons may contribute to the differential effects of pathogenic mechanisms. For example, in the highly susceptible area in the brain, the cerebellum, CGCs are more vulnerable to MeHg than are their neighboring Purkinje cells and molecular layer neurons (Yuan and Atchison, 1999; Edwards et al., 2005; Yuan and Atchison, 2007a). A comparative study of the expression of the basal antioxidant genes using laser microdissection to isolate these neurons from wild type rat cerebellar slices indicated that the basal level of gene encoding the mitochondria superoxide dismutase (MnSOD, also know as SOD2), glutathione

peroxidase (GPx1), and thioredoxin reductase (Txnrd1) were all significantly lower in CGC than that in Purkinje cells and molecular layer neurons (Fujimura and Usuki, 2014). Oxidative stress (Lebel et al., 1990; Pamphlett et al., 1998; Shanker et al., 2004a) and excitotoxicity (Reynolds and Racz, 1987; Matyja and Albrecht, 1993; Yuan and Atchison, 1997a, 2007b; Xu et al., 2012b; Liu et al., 2014) have long been associated with the pathogenesis of MeHg toxicity (Xu et al., 2012a). MeHg inhibits the ability of astrocytic EAATs to take up the amino acids cystine (Cyss) (Allen et al., 2001b), cysteine (Cys) (Shanker et al., 2001a), and Glu (Allen et al., 2001c), which are all precursors to GSH. Inhibiting EAATs uptake of these amino acids in astrocytes has several deleterious consequences. First, elevation of extracellular Glu ([Glu]<sub>ex</sub>) levels, resulting in excessive activation of Glu receptors, including the AMPARs increasing the influx of Ca<sup>2+</sup>, and induction of excitotoxicity in neurons, and second, de novo GSH synthesis in the astrocytes is reduced. Since neurons rely on astrocytes for GSH, astrocytic depletion of GSH renders neurons more vulnerable to MeHg-induced oxidative stress (Desagher et al., 1996). The master antioxidative pathway through Keap1-Nrf2 -ARE regulates the production of enzymes required for GSH synthesis and transport (Mrp1), Cyss transporter (system Xc-), EAAT3 (Escartin et al., 2011b), and other antioxidative enzymes (Lee et al., 2003b). This Keap1-Nrf2 -ARE pathway is more prominant in astrocytes than neurons partly due to Nrf2 which is more abundant in astrocytes than in neurons (Ahlgren-Beckendorf et al., 1999; Murphy et al., 2001), and neurons contain higher Cul3dependent Nrf2 degradation capacity (Baxter and Hardingham, 2016).

In addition, astrocytes increase Ca<sup>2+</sup>-impermeable AMPARs expression by secreting VEGF (Van Den Bosch et al., 2004) to increase GluA2 (also named GluR2) subunit expression (Bogaert et al., 2010). The ability of GluA2 to regulate Ca<sup>2+</sup>-permeable AMPA depends upon the posttranscriptional modification by the RNA editing process (Sommer et al., 1991). Brain *Gria2* mRNA, encoding GluA2 subunit, practically undergoes RNA editing at glutamine (Q) codon to arginine (R) codon (Sommer et al., 1991) and only 1% are unedited (Wright and Vissel, 2012). RNA editing enzyme called adenosine deaminase that act on RNAs (ADAR2) responsible to changing the neutral amino acid Q to positive amino acid R contributes to a selective Ca<sup>2+</sup> impermeability entering GluA2 containing AMPARs (Kallman, 2003; Pachernegg et al., 2015).

In this study, the proposed hypothesis was that the loss of redox homeostasis, together with the reduction of Glu transporter expression in SCAs during MeHg intoxication, would contribute to spinal cord motor neurons (SMNs) degeneration from dysregulation of redox and Glu homeostasis. Loss of redox and glutamate homeostasis in SCAs would be detrimental to neighboring cells, including SMNs in MeHg toxicity by means of development of oxidative stress and excitotoxicity. Specifically, MeHg might perturb the Keap1-Nrf2-ARE pathway in SCAs and result in insufficient levels of antioxidants such as GSH to supply for SMNs. SMN, which already suffer from oxidative stress and Glu over activation, causing subsequent degeneration. The role of the Keap1-Nrf2-ARE pathway induced astrocyte toxicity was examined through the expression level of antioxidant genes. For example, glutamylcysteine ligase (Gclc, a rate-limiting enzyme for GSH synthesis), GSH peroxidase (Gpx1 and Gpx4), xenobiotic and GSH transporter (Multidrug-resistant associated protein1, Mrp1, Abcc1),

cystine/glutamate transporter (systemXc-), which are underlying of Nrf2 activation were examined. The effect of exposure time and MeHg concentration at submicromolar levels were tested. In addition, the interplay between the oxidative stress and EAAT1(GLAST) or EAAT2 (GLT-1) was determined as a function of expression of time of MeHg exposure. Furthermore, whether *Vegfa* expression was dysregulated in SCAs during MeHg exposure was investigated. To examine these hypotheses, the function of MeHg concentrations and time of exposure were first determined and were used to compare the susceptibility of SCAs in different days of *in vitro* culture as for age-related susceptible comparison. The dysregulation of antioxidant genes and transporters expression were later investigated in SCAs as a function of time of MeHg exposure.



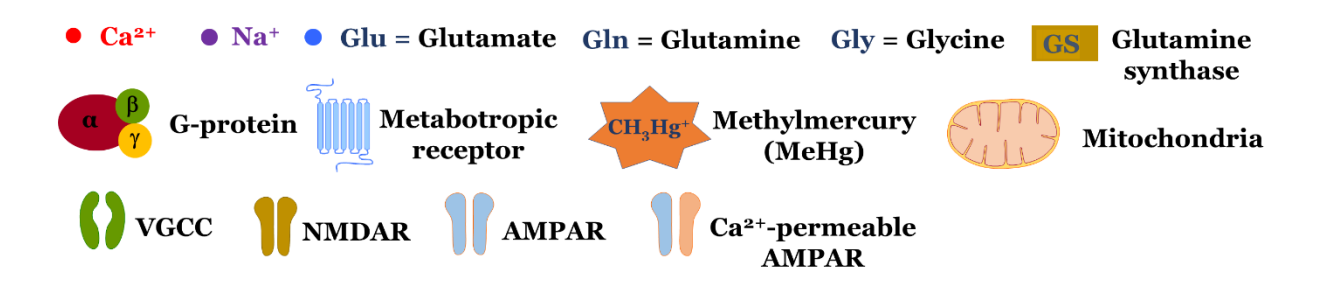


Figure 1. 1 Research aims 1: Determination of SCAs' sensitivity during MeHg exposure and the cellular mechanisms involving the redox and glutamate homeostasis. Sub aim1. Characterizing the relative contributions of MeHg-exposed duration and concentration as a function of SCAs development (DIV14 and DIV30). Sub amim2. To determine if MeHg dysregulated the antioxidant Keap1-Nrf2-ARE pathway in SCAs. Sub aim3. To determine if MeHg affected the expression of astrocytic glutamate transporters, EAAT1/GLAST1, and EAAT2/GLT-1 and *Vegf* in SCAs.

#### 2.3 Material and methods

#### 2.3.1 Chemical and solutions

Methylmercuric chloride was obtained from Aldrich Chemical (Milwaukee, WI) and was dissolved in sterilized distilled water at 10mM concentration as for stock MeHg solution. The stock MeHg was kept in a secondary container in the refrigerator and protected from light.

#### 2.3.2 Primary spinal cord astrocyte cell culture

Spinal cord astrocyte cell culture was prepared from C57BL/6J mice pups with postnatal day (PND) 1-7 following the protocol for Neural Tissue Dissociation Kit (using Trypsin for dissociation (T)) from Miltenyi Biotec Inc., San Diego CA. Trypsin was used for dissociation because the antibody for the astrocyte isolation kit is sensitive to other digestion enzymes such as papain. Spinal cords from cervical C<sub>3</sub> to lumbar section L<sub>5</sub> were dissected and minced in Hanks' Balanced Salt Solution (HBSS) without Ca2+ and Mg<sup>2+</sup>. Minced tissues were further digested with 37 °C prewarmed trypsin buffer (Enzyme mix 1; Miltenyi Biotec Inc., San Diego CA) in a 37 °C shaker for 15 min. After trypsinization, the DNase buffer (Enzyme mix 2; Miltenyi Biotec Inc.) was added to reduce cell clumping and to digest nucleic acids from damaged cells. Clumping cells were gently dissociated with fire-polished Pasteur pipette and later incubated at 37 °C in a shaker water bath for 15 min. To complete tissue digestion, cells were dissociated using a fire-polished Pasteur pipette until tissue-pieces were not observed. Upon complete digestion, tissue was filtered ofcell debris using 70µm nylon mesh filter (Miltenyi Biotec Inc.) and HBSS with Ca<sup>2+</sup> and Mg<sup>2+</sup> applied to inactivate trypsin activity. Digesting buffer and HBSS buffer were removed by centrifugation 300X g for 10 min. Dissociated cells were resuspended in culture media consisting of DMEM (Gibco®) supplement with v/v 10% Fetal Bovine Serum (FBS) (Atlanta Biologicals Inc., GA), 1% MEM Non-Essential Amino Acid (Gibco®, Thermo Fisher Scientific, MA), 2mM L-Glutamine, and 100 units/mL penicillin and 100  $\mu$ g/mL streptomycin (Gibco®). The cell was determined density of suspension in order to establish the concentration of antibody for immunopanning in the astrocyte purification step.

#### 2.3.3 Astrocyte purification using an immunopanning technique

Following dissection and digestion, resuspended spinal cord cells were further purified using Anti-GLAST (ACSA-1) MicroBead Kit (Miltenyi Biotec Inc., San Diego CA) according to the company protocol. Briefly, the cell suspension was rinsed with an icecold phosphate buffer saline (PBS) containing: 137 mM NaCl, 2.7 mM KCl, 1.4 mM NaH<sub>2</sub>PO<sub>4</sub>, and 4.3 mM Na<sub>2</sub>HPO<sub>4</sub>, at pH 7.4 and 0.5% (w/v) bovine serum albumin (BSA). Later, cell pellets were resuspended gently in PBS with 0.5% BSA and an Anti-GLAST primary antibody with a concentration appropriate to the cell density. Cells were incubated with the antibody in the refrigerator (2-8 °C) for 10 min. They were subsequently washed with PBS buffer and centrifuged at 300xq for 10 min. After complete aspiration of the supernatant, cell pellets were resuspended gently in PBS buffer. Anti-Biotin Microbeads were added and incubated in the refrigerator for 15 min. Next, the PBS buffer was added to wash cells and later centrifuge at 300xg for 10min. Cell pellets were resuspended in PBS containing 0.5% BSA. The cell suspension was filtered through a 70µm nylon mesh filter (Miltenyi Biotec Inc., San Diego CA), which was adapted to connect the top of the magnetic column (MACS Column, Miltenyi Biotec Inc.). Cells labeled with Anti-Biotin Microbead against Anti-GLAST were trapped in the magnetic column and were eluted using astrocyte cell culture media and a plunger to push them through the magnetic column. The cell density and viability of the suspension was counted for subsequent seeding and cell culture.

#### 2.3.4 Cell culture plating

Following astrocyte purification, SCAs were stained using 0.4% (w/v) Trypan blue solution (Gibco®) to determine cell viability. The percent of cell viability was obtained from automated cell counting (TC20<sup>TM</sup> model, Bio-Rad, Hercules, CA, USA), and SCA suspension was diluted to 1x10<sup>5</sup> viable cells/ml. One ml, 0.5ml, and 0.1ml of 1x10<sup>5</sup> viable cells/ml were seeded per well in 12-, 24- and 96- well plates, respectively. Plates were precoated with 100μg/ml (w/v) poly-D-lysine (PDL). Cell cultures were maintained at 37 °C in a 95% O<sub>2</sub> and 5% CO<sub>2</sub> incubator. After 24h of cell seeding, seeding media were removed and replaced with new astrocyte cell culture media. SCAs were replenished with astrocyte cell culture medium every 2 days until used for experiments (DIV 14 or DIV30).

#### 2.3.5 Cell culture treatments

The primary SCAs culture derived from C57BL/6J mice pups (PND 1-7) were cultured and maintained in replenishing astrocyte media every 2 days for 28-30 days in vitro (DIV). Some research groups have suggested that primary astrocyte cell culture when cultured without neuron, will not express GLT-1. Despite traditional astrocyte media, the astrocyte media for SCAs were developed containing non-essential amino acids, one of the ingredients for the SMN cell line NSC34. This medium provided healthier SCAs which developed into typical star-shaped astrocytes when grown for an extended period of time. SCAs DIV 28-30 indicated high cell confluence and maturation of astrocytes by a high level of GLT-1 expression. Thus, between DIV 28-30, SCAs were exposed to 0.5, 1, 2, or 5 µM MeHg concentrations in astrocyte media without FBS. Omitting FSB in the treatment

medium aims to reduce cysteine-containing proteins to bind nonspecifically to MeHg and thereby potentially reduce MeHg toxicity. The function of the time of MeHg exposure was monitored to determine the effect of time of exposure to a toxic effect of MeHg on SCAs.

To determine if MeHg induced SCAs degeneration was involved in the disturbance of redox and glutamate homeostasis, SCAs were exposed to 5  $\mu$ M MeHg for 18h. This concentration and time point indicated significant cell degeneration, and some SCAs remained in cell culture dishes resulting from the determination of MeHg toxicity in the function of time and different MeHg concentrations. A concentration and time relationship has been extensively demonstrated for MeHg.

#### 2.3.6 Real-time cell viability assay

To determine the effect of MeHg in cell viability, the Real-Time  $Glo^{TM}$  MT Cell Viability Assay from Promega (Madison, WI, USA) was used. This assay allows determining the toxicity of MeHg over time >96h (Duellman et al., 2015). The assay could be used with cell culture media; therefore, it minimizes any cell culture response to new environmental conditions (buffer) rather than to the test compound. Two assay compounds, a cell viability probe, termed prosubstrate, and luciferase enzyme were added into the cell culture with the test compounds, including MeHg, according to the assay protocol. The concentrations of MeHg for test in this assay were 0, 0.1, 0.5, 1, 2 and 5  $\mu$ M which are 0, 0.0216, 0.108, 0.216, 0.438 and 1.08ppm, respectively. These concentrations are considered relatively low concentrations that have little or no adverse effects when humans consume seafood, such as canned tuna (Tollefson and Cordle, 1986; Grandjean et al., 2010). SACs were cultured in an opaque clear bottom 96-well plate with 100 $\mu$ l of cell density 1x105 cell/ml in each well. This cell density was tested if two requirement assay

compounds were sufficient to monitor cell viability overtime prior to pursuing any experimental assays. The luminescence intensity, which indicates a viable cell response, was determined after 30min of adding MeHg and assay compounds and continued to monitor every 3h over 24h with a luminescent plate reader, BoTek, Synergy Neo2, (Winooski, VT, USA).

### 2.3.7 Cell morphology and structure determination with coomassie brilliant blue staining

The method using coomassie brilliant blue to determine cellular structure and morphology applied from Mochizuki and Furukawa (1987) (Mochizuki and Furukawa, 1987) with minor modifications as follows. Following MeHg treatment, SCAs were fixed with 4% (v/v) paraformaldehyde for 20 min and rinsed with PBS. The cell later stained using coomassie brilliant blue solution; 0.02% (w/v) coomassie brilliant blue R-250 in methanol: acetic acid: water, 46.5: 7: 46.5 (v/v/v), respectively, for 20 min. The cells were rinsed with PBS at least three times or until blue background staining disappeared. The staining cells were examined under a light microscope, Leica Microsystems (Welzlar, Germany).

#### 2.3.8 Immunocytochemistry and confocal imaging analysis

SCAs cultured on coverslips were fixed in Zamboni's fixative reagent (PBS containing 4.0% (v/v) paraformaldehyde and 0.2%v/v picric acid; American MasterTech Scientific Laboratory Supplies, Inc., Lodi, CA, USA) for 15 min. SCAs were rinsed in ice-cold PBS three times or until the yellow color disappeared. Later, SCAs were incubated for 30 min in blocking buffer; PBS containing 0.3% (v/v) Triton-X and 5% (v/v) normal goat serum (NGS, Vector Laboratories, Inc., Burlingame, CA, USA). After removing the blocking buffer, SCAs were rinsed with ice-cold PBS three times. They were next incubated in PBS

buffer containing 0.1% (v/v) Triton-X, 5% (v/v) NGS, and primary antibodies for 18-20h in a humidified chamber at 2-8 °C. SCAs were rinsed three times with ice-cold PBS after aspiration of primary antibody buffer. The secondary antibodies were diluted in ice-cold PBS buffer. SCAs were incubated in a secondary antibody buffer for 2h in a humidified chamber at the ambient room temperature. After 2h, the secondary antibody buffers were removed and rinsed off with ice-cold PBS buffer. The detailed information and dilution for primary and secondary antibodies employed in this study were indicated in the appendix. The SCAs on coverslips were mounted with ProLong<sup>TM</sup> Diamond Antifade Mountant (Invitrogen<sup>TM</sup>). The images were acquired from Nikon C2 Confocal Microscope (Nikon, USA) using the same setting for each channel. Fluorescence intensity was analyzed using NIS Element Advanced Research software (Nikon, USA).

#### 2.3.9 Real-Time Quantitative Reverse Transcription-PCR

Total RNA was isolated from the SCAs using the Direct-Zol RNA Microprep (Zymo Research, Irvine, CA, USA) and converted to cDNA using the High Capacity cDNA Reverse Transcription kit (Applied Biosystems, Foster City, CA, USA). Quantitative PCR was analyzed using TaqMan® premade gene-specific probes designed against target genes with FAM/MGB reporter dye (Applied Biosystems, Foster City, CA), as indicated in Table A1, of the appendix. The mouse glyceraldehyde-3-phosphate dehydrogenase (*Gapdh*) endogenous control VIC TM/MGB probe with primer limited (catalog number: 4352339E; Applied Biosystems, Foster City, CA) was used as an endogenous control for the multiplex PCR. Gene expression data were obtained from the QuantStudio TM 7 Flex-Real Time PCR system (Applied Biosystems, Foster City, CA, USA) using the TaqMan Fast Advance cycle. The relative gene expression was determined using the 2-ΔΔCT method (Livak and

Schmittgen, 2001), and the data were presented as a fold change of target gene expression levels in SCAs.

#### 2.4 Results

#### 2.4.1 Aged-related SCA degeneration by MeHg induced toxicity

The silent latency characteristic associated with MeHg toxicity (Weiss et al., 2002b) exhibited in both chronic MeHg exposure through the fish consumption in Minamata and Niigata Prefecture patients (Rice, 1996), and acute MeHg exposure through the accidental ingestion of wheat flour from seed treated with methyl-and ethyl mercury compound in Iraq patients (Bakir, 1973). The mechanisms involved in this silent latency remain unknown, and it severely exhibits in some susceptible individuals in later life. In the present study, the SCAs were used to determine if their developmental stages would contribute to MeHg susceptibility and, if so, what concentration and time would significantly affect SCAs degeneration. Two different developmental stages of SCAs were used 1. early developmental stage (DIV14) and 2. fully developmental stage (DIV30) indicated with the highly expressed EAAT 2 (Roybon et al., 2013), were exposed to different MeHg concentration (0, 0.1, 0.5, 1, 2 and 5 µM MeHg) and different durations of exposure. The metabolic activity of SCAs, which is related to the viability of cells, was determined using a RealTime-Glo™ MT cell viability assay (Promega, Madison, WI). The assay requires adding sufficient cell-permeant prosubstrate and luciferase enzymes in order to monitor cell viability over a 96h experimental period. (The condition was optimized to a specific cell type by the experimenter.) To determine the temporal relationship between cell viability and duration of MeHg exposure, different concentrations of MeHg ranging from 0, 0.1, 0.5, 1.0, 2.0, and 5.0 µM MeHg were determined in a function of time to generate a concentration-response curve. Figure 2.2

A (DIV 14) and 2.3 A (DIV 30) displayed the kinetics of different MeHg concentrations in the induction of SCAs degeneration. With the Real-Time Glo Viability assay compared to control, SCAs DIV14 (Figure 2.2 A) exposed to 1, 2, and 5 µM MeHg exhibited a significant reduction of cell metabolic activity starting at 30 min and at every through time point assayed. Exposure to 0.5 µM MeHg caused a significant reduction in metabolic activity starting from 2h, whereas 0.1 µM MeHg did not affect the SCAs at DIV 14. The concentration-dependence of SCAs degeneration was also exhibited in DIV 30 (Figure 2.3 A) by which 5µM MeHg caused a significant reduction of cell metabolic activity starting at 2h exposure. Lower concentrations 0.5, 1, and 2 µM MeHg produced significant effects at 6h exposure. While 0.1 µM MeHg did not affect SCAs DIV 14 degeneration, it did for SCAs DIV30 when exposed for longer than 12 h. These results suggested even though SCAs DIV 14 and DIV 30 were both affected by MeHg as a function of MeHg concentration and time of exposure, the susceptibility was different between the maturity of SCAs (Figure 2.4 table). The IC50 of SCAs DIV 14 (Figure 2.2 B) and DIV 30 (Figure 2.3B) indicated the lower the MeHg concentration, the higher was the effect on SCAs degeneration when increasing the exposure time (Figure 2.4). The onset of cell metabolic reduction occurred sooner in DIV 14 (30min with 1, 2, and 5 µM MeHg) than in DIV 30 (6h with 0.5, 1, and 2 µM MeHg). Interestingly, The IC 50 of SCAs DIV 30 degeneration was about half of IC50 of SCAs DIV 14 when exposed longer than 12h. These differential effects of MeHg toxicity to different SCAs maturity might suggest the differential cellular mechanisms of MeHg-toxicity in the onset and progression.

# 2.4.2 The concentration and time-dependent MeHg-toxicity to the pathologic morphology of SCAs.

The morphological changes of SCAs were observed in a function of time and MeHg concentrations in SCAs DIV 14. The simple staining with coomassie brilliant blue enhanced the differences between cell morphology and the background. The 3h and 24 h of different MeHg concentrations and exposure regimen were observed the effect of early stage and prolonged MeHg exposure, respectively. The 0.1 µM MeHg did not affect the SCAs DIV 14 in morphological changes in either short-term (3h) or relatively longer-term (24h) exposure (Figure 2.5). The non-toxic effect of 0.1 µM MeHg was relevant to the cell viability assay data as this concentration did not affect SCAs DIV14 viability (Figure **2.2)** while it caused SCAs DIV 30 degeneration at exposures longer than 12 h (Figure 2.3). The IC50 for SCAs DIV 14 degeneration curve (Figure 2.2 B) following 3 h suggested the o.6µM MeHg would reduce cell viability by 50%. Morphologically following 3h of 0.5µM MeHg, SCAs exhibited punctate processes, and this characteristic was a more prominent appearance with higher MeHg concentration (1, 2, and 5µM). The 5µM MeHg exposure for 3h already exhibited the loss of synaptic contact in some SCAs. When these SCAs were exposed to different MeHg concentrations longer (for 24h), the morphology of SCAs was more greatly affected with the loss of processes, synaptic contact, and cell degeneration compared to the same concentration for 3h exposure. The higher MeHg concentration caused a pronounced significant reduction of cell viability as observed a few SCAs remained in the cell culture dish. These morphological change data supported the cell viability, and IC 50 curve is that the function of time and MeHg concentrationdependent affected to SCAs.

# 2.4.3 Sub-micromolar MeHg (0.5 $\mu$ M) dysregulated the expression of *Keap1* and *Nrf2* mRNA in SCAs

The potential role of *Keap1* and *Nrf2* mRNA expression in greater susceptibility of mature SCAs (DIV 30) was next examined. The 0.5µM MeHg was used because this was the lowest concentration that exhibited toxicity in both DIV 14 and DIV30 SCAs (**Figure 2.4 table**). The function of time of MeHg exposure was used to investigate the expression profile of these mRNA. At 6h of 0.5µM MeHg exposure, the *Keap1* mRNA expression was increased about 1.9-fold and later decreased in about 0.74-fold following 18h exposure (**Figure 2.6**). Nrf2 mRNA expression was increased about 1.3-fold and 1.2-fold increase at 6h and 9 h, respectively. It was then followed with a decrease of its expression level relatively similar to baseline (vehicle exposure) (**Figure 2.7**).

# 2.4.4 Sub-micromolar MeHg (0.5μM) affected the expression of *Gclc* mRNA encoding to a rate-limiting enzyme for GSH synthesis in a bi-phasic induction.

MeHg has been reported to reduce intracellular GSH and activate Nrf2 (Feng et al., 2017) in both neurons and astrocytes (Shanker et al., 2005a; Robitaille et al., 2016). MeHg might affect only the intracellular GSH content, or MeHg might affect *de novo* GSH synthesis. Determination of the *Gclc* mRNA expression could explain if MeHg affected the Nrf2-ARE pathway by determining its downstream mRNA, driven by the ARE promotor region of Gclc mRNA. It could also explain if MeHg affected the pathway of *de novo* GSH synthesis. During 24h 0.5μM MeHg exposure, the *Gclc* mRNA was increased starting from 6h exposure (1.51-fold) and reached its peak at 9h exposure (2.1-fold). Later, after 12h exposure, *Gclc* mRNA gradually declined, but still significantly increased to

about 1.52-fold of vehicle control (**Figure 2.8**). At 15h of MeHg exposure, *Gclc* mRNA expression level returned to the baseline (vehicle treatment level) and was later increase with 1.38 and 1.47-fold following 18h and 21h 0.5µM MeHg exposure, respectively (**Figure 2.8**). Following 24h of MeHg, the *Gclc* mRNA expression returned to its baseline level.

# 2.4.5 MeHg induced a time-dependent increase of the detoxification transporter Mrp1 and antioxidant precursor transporter system Xc- mRNA expressions.

If MeHg perturbed the Keap1-Nrf2-ARE pathway, the expression of its downstream mRNA, such as Mrp1 and system Xc- could reveal the specific antioxidant genes involved. Both *Abcc1* mRNA encoding for Mrp1 and *Slc7a11* encoding for system Xc- are regulated by the Nrf2 activity by initiation of these mRNA syntheses through the Nrf2 binding site at the ARE promotor region of these mRNAs (Maher et al., 2007; Habib et al., 2015). Mrp1 is involved in the export of the GSH and xenobiotics as part of the detoxification process, while system Xc- is involved in the transport of cystine as a cysteine prosubstrate for *de novo* GSH synthesis. MeHg induced a significant increase of *Abcc1* mRNA expression following 6 h with 1.54-fold of increase and 9h with 1.59-fold of increase. The relative reduction of Abcc1 to its peak occurred at 12 h of MeHg exposure. Although the level of Abcc1 mRNA at 12h appeared to be higher than baseline (vehicle treatment), this was not significant from either the baseline or peak levels (at 9h). The *Abcc1* level was increased significantly later at 15h MeHg exposure (about 1.51-fold of increase, p> 0.5) after that declined to the baseline at 21h of exposure (Figure 2.9).

While the *Abcc1* mRNA expression profile was increased following MeHg exposure starting from 6h and was later decline after 21h, the *Slc7a11* mRNA expression profile fluctuated following MeHg exposure. MeHg increased *Slc7a11* at the earliest time point (1h) of MeHg exposure and peaked with an 8.65-fold increase (Figure 2.10). While the *Slc7a11* expression level returned to its baseline later at 3h, it subsequently increased following 6h of MeHg exposure. *Slc7a11* started to decline and returned to its baseline during 9 to 15h of MeHg exposure, but started to increase following 18h exposure. The increase of *Slc7a11* expression levels was 4.94-fold and 5.30-fold of increase following 21 and 24h exposure, respectively.

## 2.4.6. MeHg induced the increase of EAAT1/GLAST and EAAT2/GLT-1 mRNA expression during early exposure.

MeHg has been reported to dysregulate excitatory synaptic transmission by it increasing the synaptic Glu concentration (Reynolds and Racz, 1987; Farina, 2003) and inhibiting EAAT1/GLAST and EAAT2/GLT-1 function (Brookes and Kristt, 1989; Kim and Choi, 1995; Mutkus et al., 2005; Yin et al., 2007a). A reduction of EAAT expression in astrocytes could also attribute to dysregulation of Glu homeostasis. System Xc- and EAATs work in concert to regulate both redox and Glu homeostasis, and dysregulation of either of these transporters will likely affect the function of the others. The mRNA expression of *Slc1a3* (encoding for EAAT1/GLAST) and *Slc1a2* (encoding for EAAT2/GLT-1) in SCAs could also be used to determine the relationship between these transporter expressions. The expression profile of *Slc1a3* (Figure 2.11) and *Slc1a2* (Figure 2.12) in SCAs were similar during MeHg exposure. MeHg induced a significant increase in both *Slc1a3* and

*Slc1a2* with 3.3-fold and 2.2-fold at 3h of exposure, respectively **(Figure 2.13).** These increases later returned to baseline level at 6h to 12h of exposure.

## 2.4.7 MeHg induced Vegfa mRNA expression in SCAs in a bi-phasic fashion

The vulnerability of MN degeneration to excitotoxicity is partly due to the regional specific astrocytes regulating GluR2 subunit expression. VEGF has been indicated its role in the protection of MNs (Lunn et al., 2009) against excitotoxicity by regulating GluR2 subunit expression in AMPAR (Bogaert et al., 2010). To examine if MeHg dysregulated VEGF in SCAs at its transcriptional level, the *Vegfa* mRNA expression was determined as a function of time of MeHg exposure. MeHg increased *Vegfa* in a biphasic manner. *Vegfa* significantly increased (1.9-fold) following 6h of MeHg exposure, which reached its peak (2.5-fold) at 9h (Figure 2.14). The expression of *Vegfa* decreased following 12h of MeHg exposure and returned to baseline (vehicle treatment) at 15 h. After 18h exposure, *Vegfa* expression was significantly induced to 1.8-fold of increase. The induction of *Vegfa* was appeared to increase following 21 to 24 h of exposure, but these expression levels were not significantly different from baseline (vehicle treatment).

# 2.4.8 Immunocytochemistry indicated a reduction of Mrp1, system Xc- and EAAT2/GLT-1 expression following 5µM MeHg exposure in SCAs

Besides the mRNA expression, MeHg could affect the Mrp1, system Xc- and EAAT2/GLT- 1 transporter protein expression in SCAs. Immunocytochemistry against the Mrp1, systemXc- and GLT-1 was used to examine these transporters' abundance in SCAs when exposed to  $5\mu$ M MeHg for 18 h compared to the vehicle (H<sub>2</sub>O) treatments. Following MeHg exposure, SCAs showed cell atrophy (white arrowhead  $\triangle$ ), process disintegration (white arrow  $\Re$ ), and degeneration. Some SCAs started to retract their process as they

showed punctuated on the processes (yellow arrow (Figure 2.15). The relative mean immunofluorescent intensities of each specific transporter antibodies were determined using NIS-Element Advanced Research software from Nikon. Individual single SCAs were traced as regions of interest (ROI) for fluorescence intensity determination. Two-Way ANOVA with Sidak multiple comparison *post hoc* indicated differential expression between vehicle and MeHg treatments with the diminution of about 28% Mrp1, 25% system Xc- and 48% GLT-1 relative to the vehicle treatments (Figure 2.16).

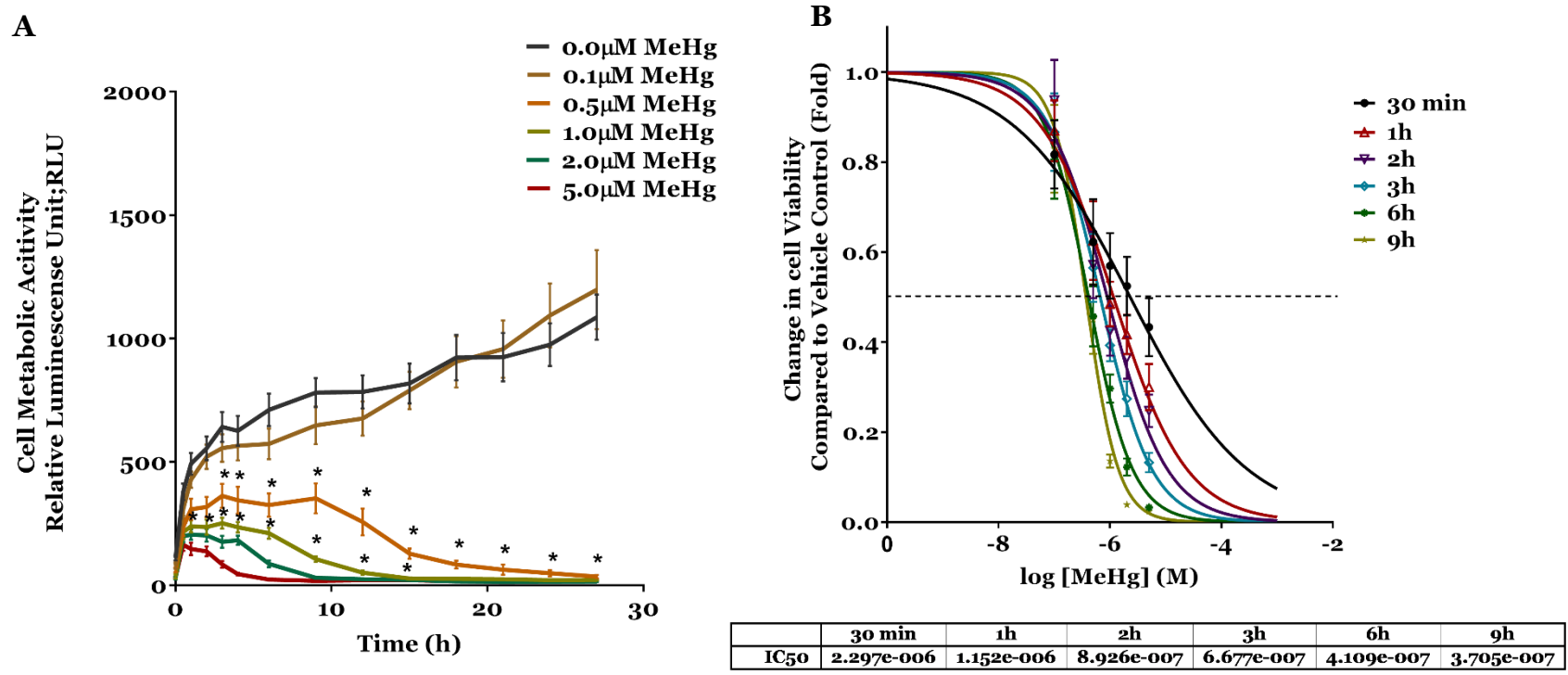


Figure 2.2 SCA Cell Culture (DIV14) exposed to 0, 0.1, 0.5, 1, 2, and 5 μM MeHg from 30 min to 27 h. The function of time of MeHg exposure presented in A. The concentration and duration of MeHg exposure contributed to SCAs metabolic activity (viability). With the Real-Time Glo<sup>TM</sup> MT Viability assay compared to control, SCAs at DIV14 exposed to 1, 2, and 5 μM MeHg indicated a significant reduction of cell metabolic activity (cell viability) starting from 30 min across all-time points of the assay. Exposure to 0.5 μM MeHg caused a significant reduction starting from 2h, while 0.1 μM MeHg did not affect these SCAs. B. The Concentration Response Curves of MeHg to SCAs in the early phase of MeHg exposure (30min to 9h). The concentration-response curve shifted to the left as a result of longer cell exposure to MeHg. In addition, the half-maximal inhibitory concentration (IC50) decreased for longer times of exposure. The asterisk (\*) indicated p<0.05 compared to vehicle control treatments., N= 9 biological replications. Two-Way ANOVA with repeated measurements, and Tukey's Multiple Comparisons post hoc test were performed using GraphPad Prism 8.02 for data analysis.

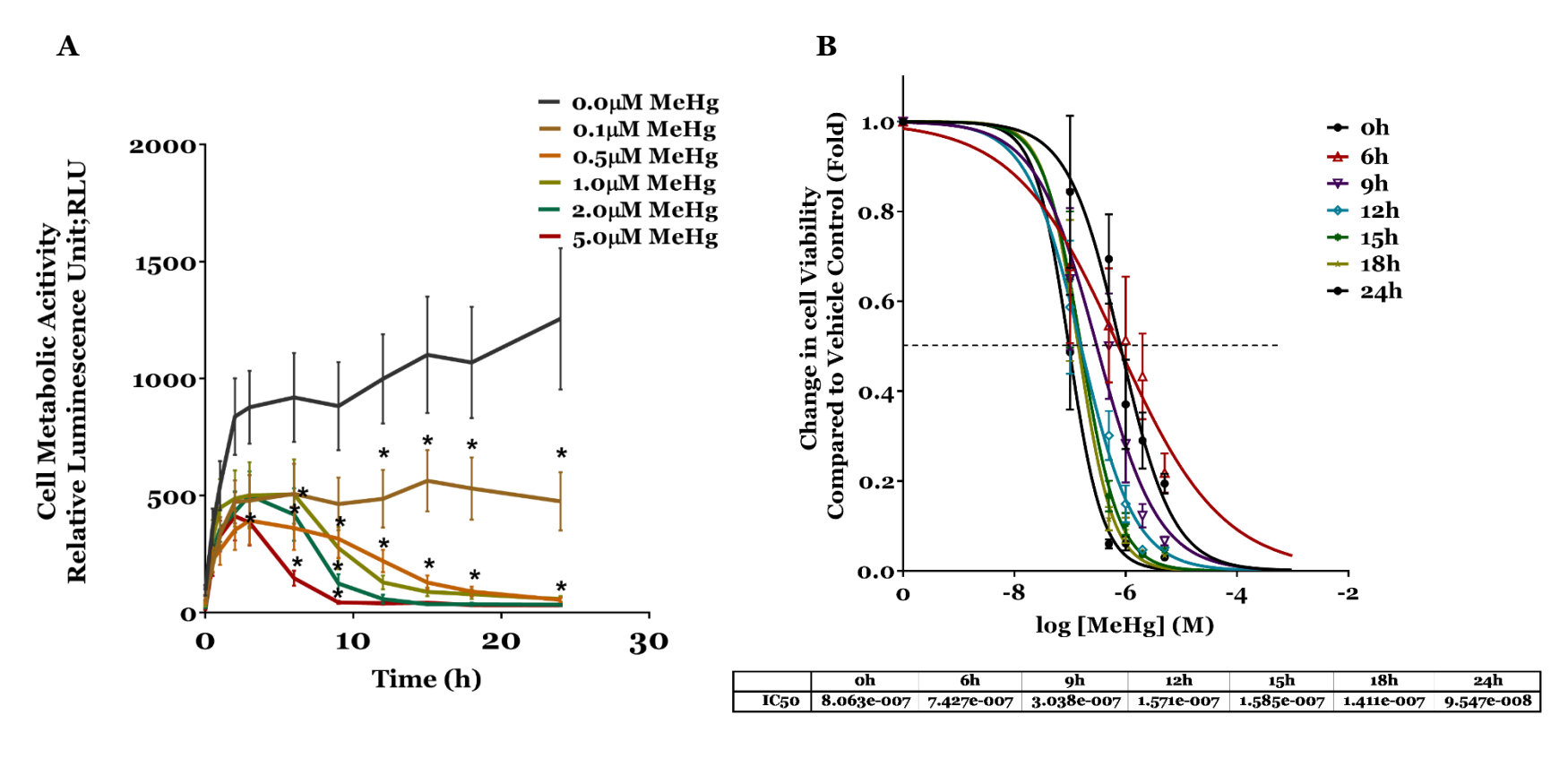


Figure 2.3 SCA cell culture (DIV30) exposed to 0, 0.1, 0.5, 1, 2, and 5 μM MeHg from 30 min to 27 h. The function of time of MeHg exposure presented in A.) *The concentration and duration of MeHg exposure contributed to SCAs metabolic activity (viability)*. SCAs DIV30 exposed to 5 μM MeHg indicated a significant reduction of cell viability (\*) starting from 2h, while 0.5, 1, and 2 μM MeHg indicated a significant reduction following 6h exposure. Following exposure to 0.1 μM MeHg, SCA cell viability reduced significantly following 12 h exposure. B.) *The Concentration-response curves of MeHg to SCAs from oh to 24h*. The curve shifted to the left due to longer exposure to MeHg, which resulted in a decrease of half-maximal inhibitory concentration (IC50). N= 7 biological replications. Two-Way ANOVA with repeated measurements and Tukey's Multiple Comparisons *post hoc* test were performed using GraphPad Prism 8.1. for data analysis.

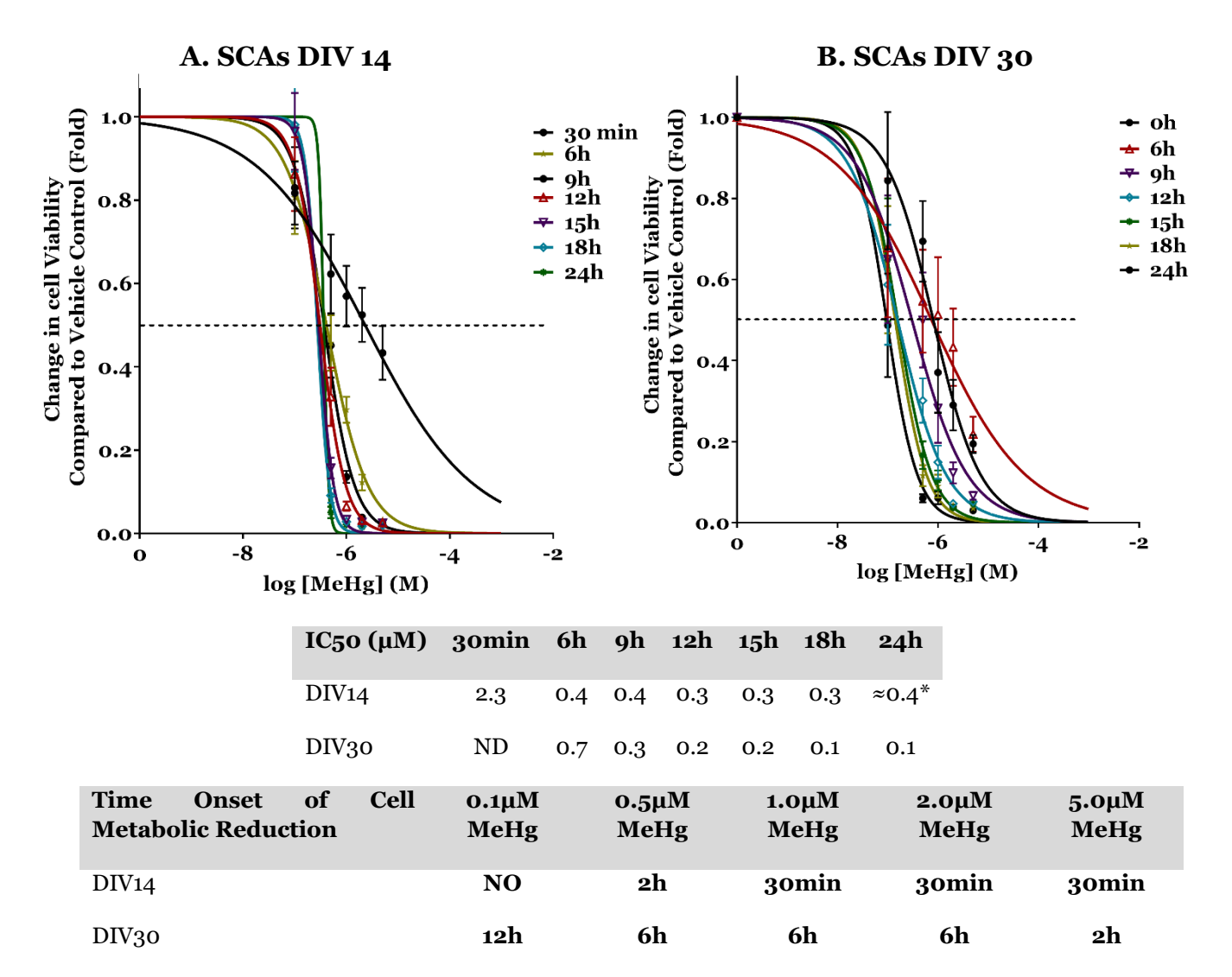


Figure 2.4 Comparison of the susceptibility to MeHg between SCAs DIV14 (early developmental stage) and DIV 30 (fully developed stage). SCAs were exposed to 0, 0.1, 0.5, 1, 2, and 5 μM MeHg, and cell metabolic activities were determined over 24h of exposure. *Concentration-response curves of MeHg to SCAs DIV 14* (A) and *DIV 30* (B). During the early phase of MeHg exposure 30min to 6h, SCAs DIV14 were more susceptible to MeHg based on the IC50 at 6h which was higher than that in DIV30. The time onset of metabolic reduction occurred sooner than that in SCAs DIV30. Nevertheless, the longer MeHg exposure affected SCAs DIV 30 more than in SCAs DIV14 as the IC50 of SCAs DIV30 during more prolonged MeHg exposure was lower than that in SCAs DIV14. The lowest MeHg concentration (0.1 μM) did not affect SCAs DIV 14 but did affect SCAs DIV 30 following 12h of exposure. IC50 values were obtained from a concentration-response curve and determined from the halfway between the maximal response (Top) and the maximally inhibited response (bottom) using GraphPad Prism version 8.1. (ND= Not Determined; NO= No Effect Observed)

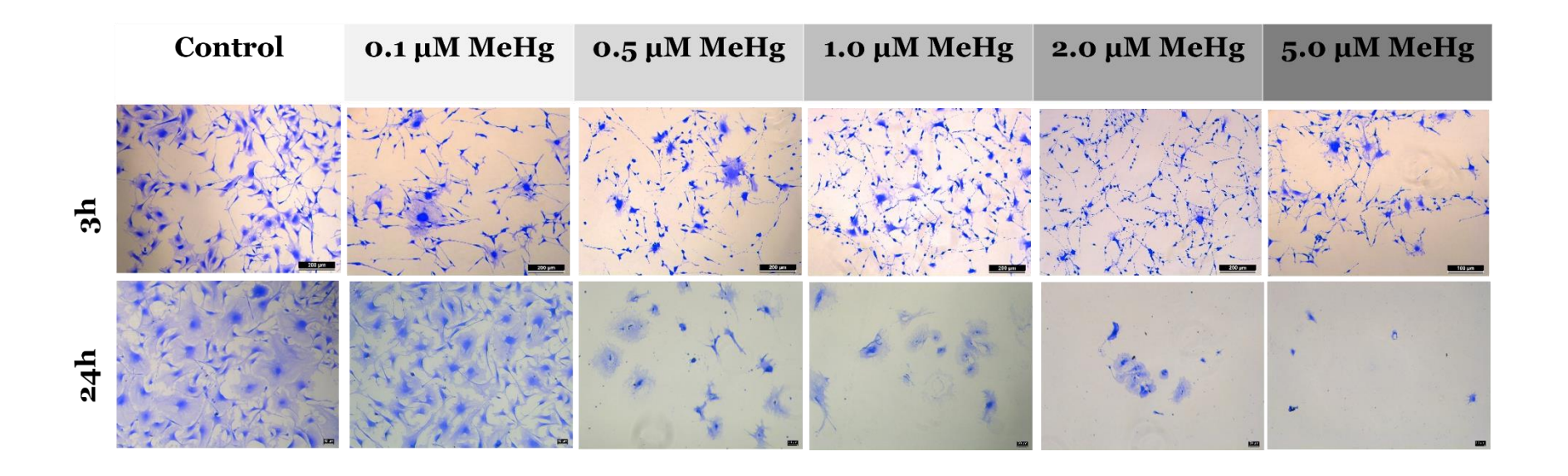
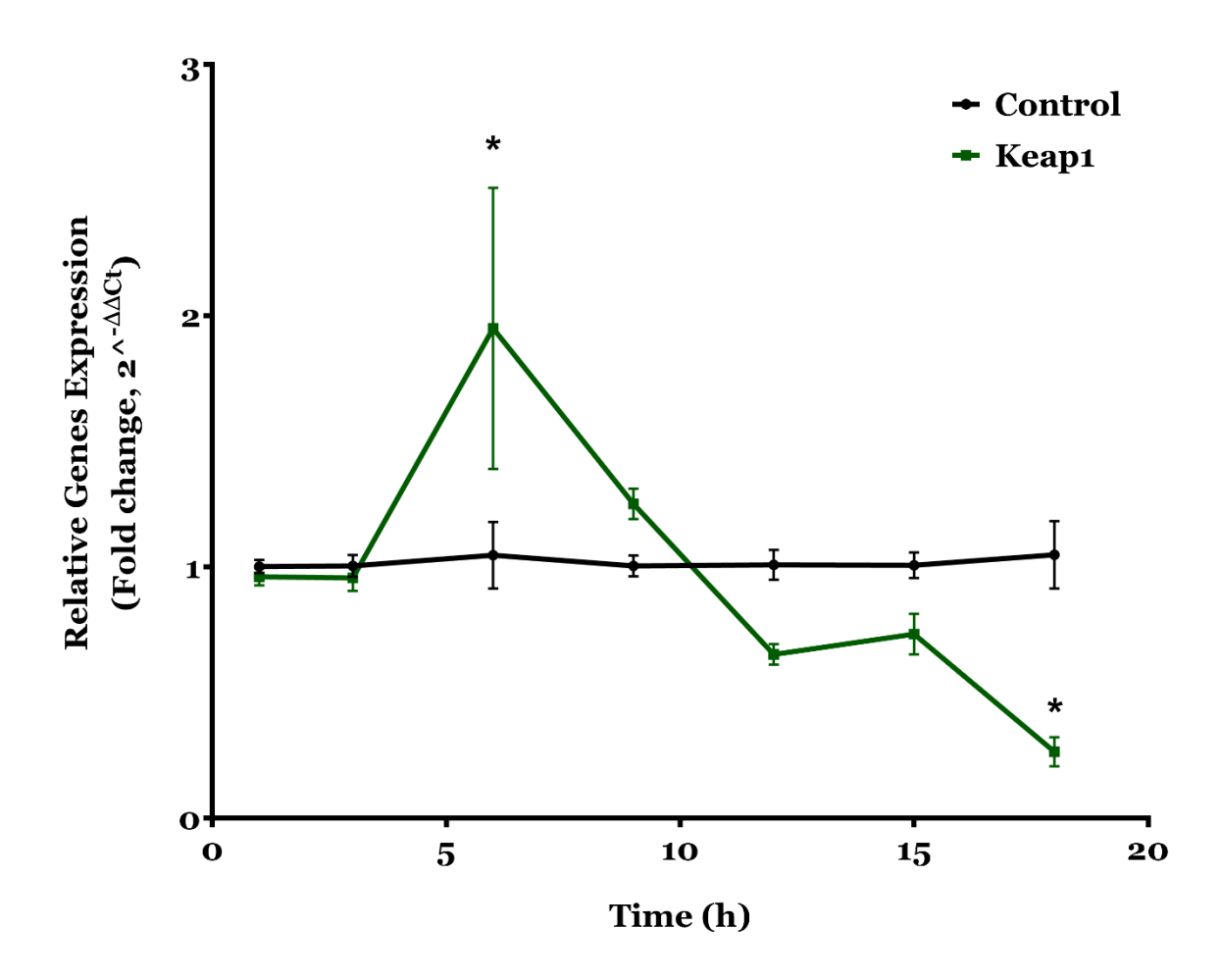
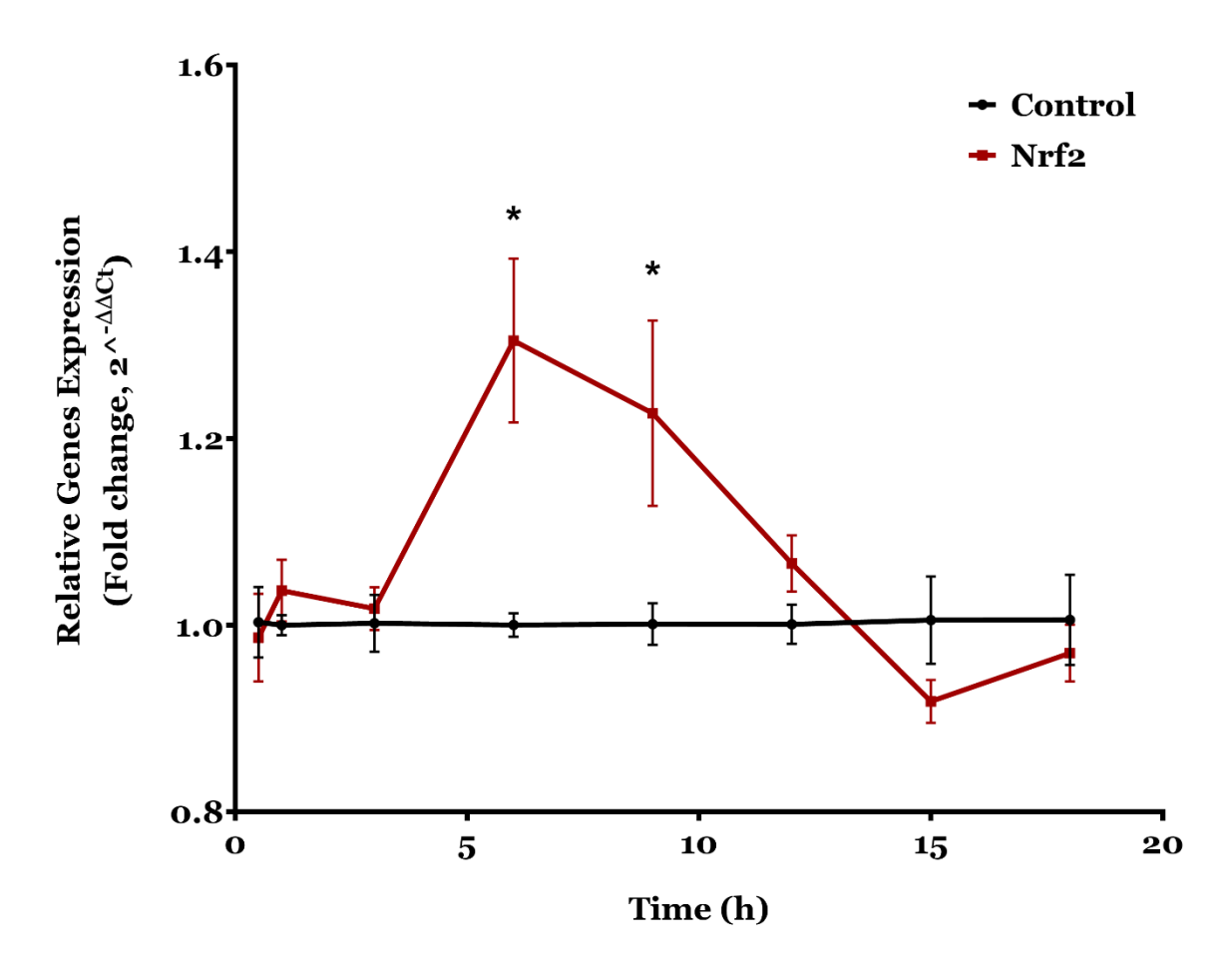


Figure 2.5 Pathological and morphological features of SCAs at DIV 14 exposed to different MeHg concentrations for 3h and 24h. The giant flat cell astrocytes appeared to be more resistant to MeHg compared to small process bearing astrocytes. The control SCAs processes remained in contact with each other and were about twice the cell body dimension in length. The processes in 0.5, 1, 2, and 5  $\mu$ M MeHg-treated SCAs presented fragmentation of processes as well as an apparent loss of synaptic contact and degeneration. At higher concentrations of MeHg, a greater severity of fragmentation of processes was observed. Despite following 3h exposure, exposure to 0.1  $\mu$ M MeHg for 24h resulted in a loss of synaptic contact in small process-bearing astrocytes and damage to the cytoarchitecture in some large flat cells with smaller cell diameter. Small process bearing astrocytes exposed to 5  $\mu$ M MeHg for 24h severely degenerated while at 3h exposure, several small process-bearing cells remained intact. The morphologies were observed under brightfield with a light microscope (Leica, Microsystem) with the same magnification (20X). Note at 3h, the scale bar is 200 $\mu$ m, and at 24h the scale bar is 50 $\mu$ m.



**Figure 2.6 The expression profile of** *Keap1* mRNA during **0.5μM MeHg exposure to SCAs for 18 h.** The Keap1 mRNA expression indicated the significant increase (1.9-fold induction) at 6h which is the peak of expression. Its expression level later declined to control level and further decrease its expression lower than control level. At 18h, Keap1 mRNA was significantly reduced relative to control level (0.7-fold reduction). The statistical analysis using Two-Way ANOVA with Sidak's Multiple Comparison *post hoc* indicated \*; p<0.05. N=3 biological replications with two replications/N.



**Figure 2.7 The expression profile of** *Nrf2* mRNA during **0.5μM MeHg exposure to SCAs for 18 h.** Following MeHg exposure, *Nrf2* mRNA expression indicated a significant increase from 6h to 9h (1.3-fold and 1.2-fold induction, respectively). Later, its expression gradually decreased and returned to the control level. The statistical analysis using Two-Way ANOVA with Sidak's Multiple Comparison *post hoc* indicated \*; p<0.05. N=3 biological replications with two replications/N.

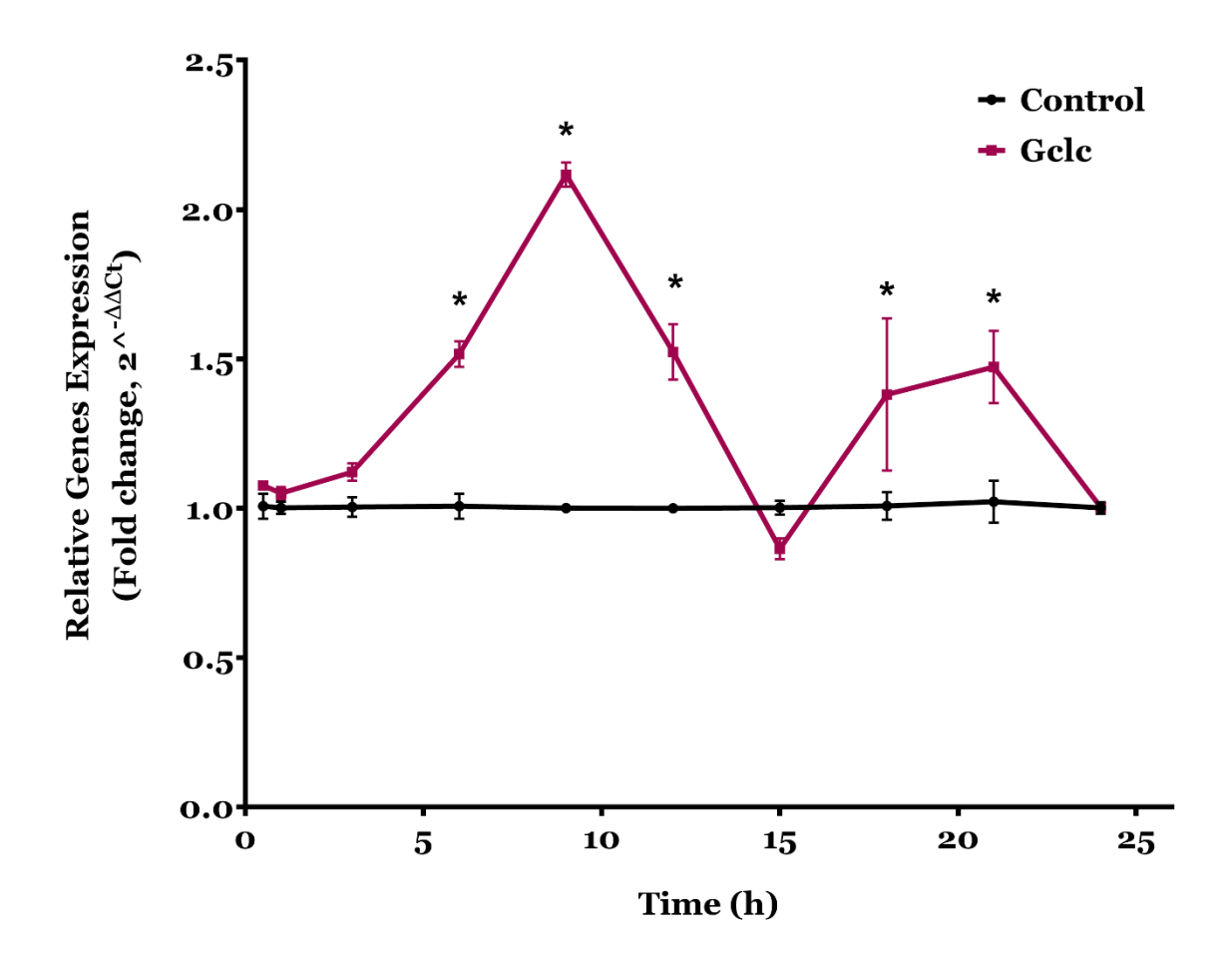


**Figure 2.8 The biphasic expression profile of** *Gclc* mRNA during **0.5μM MeHg exposure to SCAs for 24 h.** The first phase of Gclc mRNA expression indicated a significant increase starting from 6h to 12h, with 9h as the peak of its expression (2.1-fold induction). Later, its expression returned to the control level at 15h of exposure and then increased its expression significantly relative to control at 18 and 21h (1.3-1.4-fold induction). The decline of Gclc expression returning to the control level was later observed. The statistical analysis using Two-Way ANOVA with Sidak's Multiple Comparisons indicated \*; p<0.05. N=5 for control and N= 6 for MeHg treatments. Each N was performed in two replications.

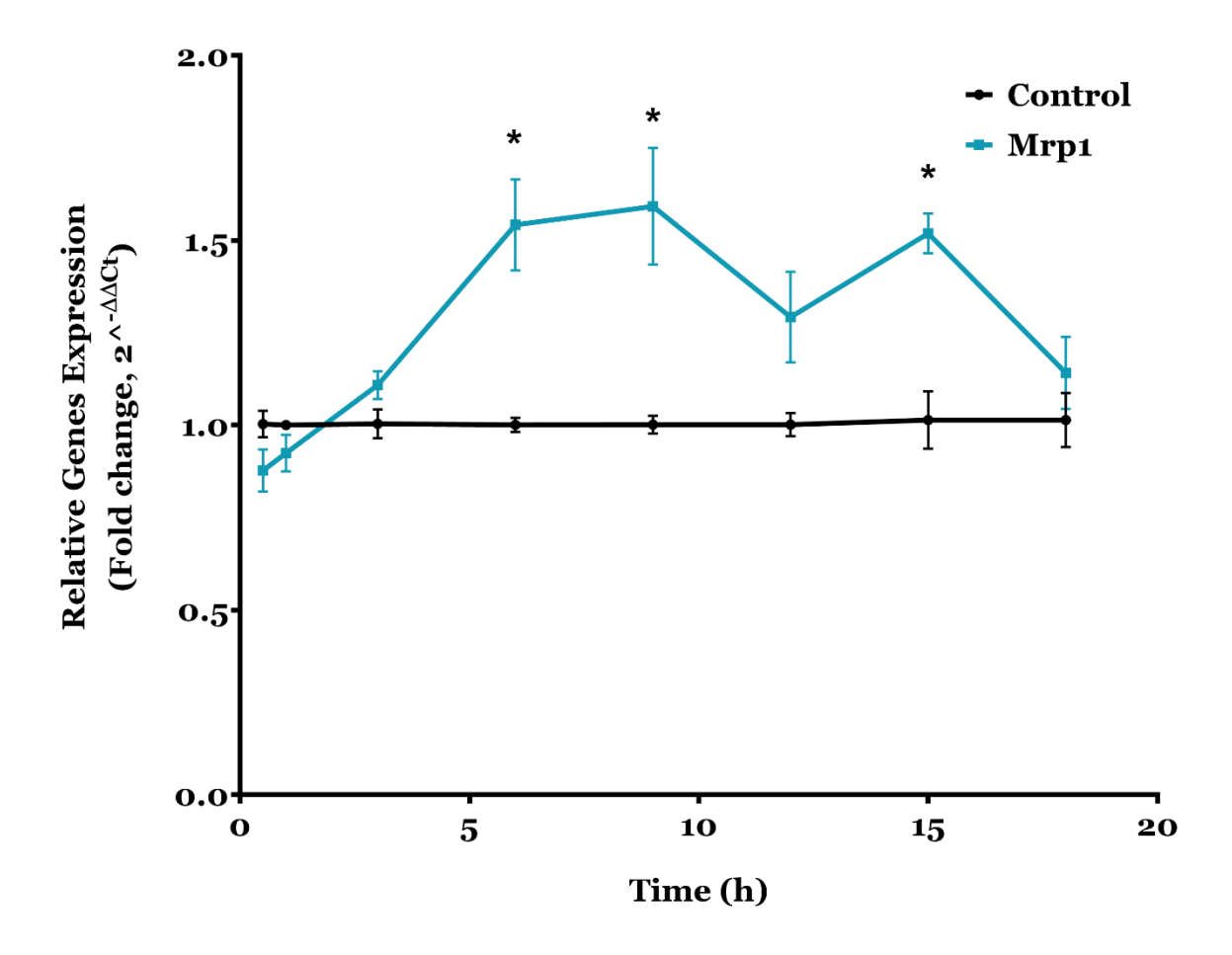
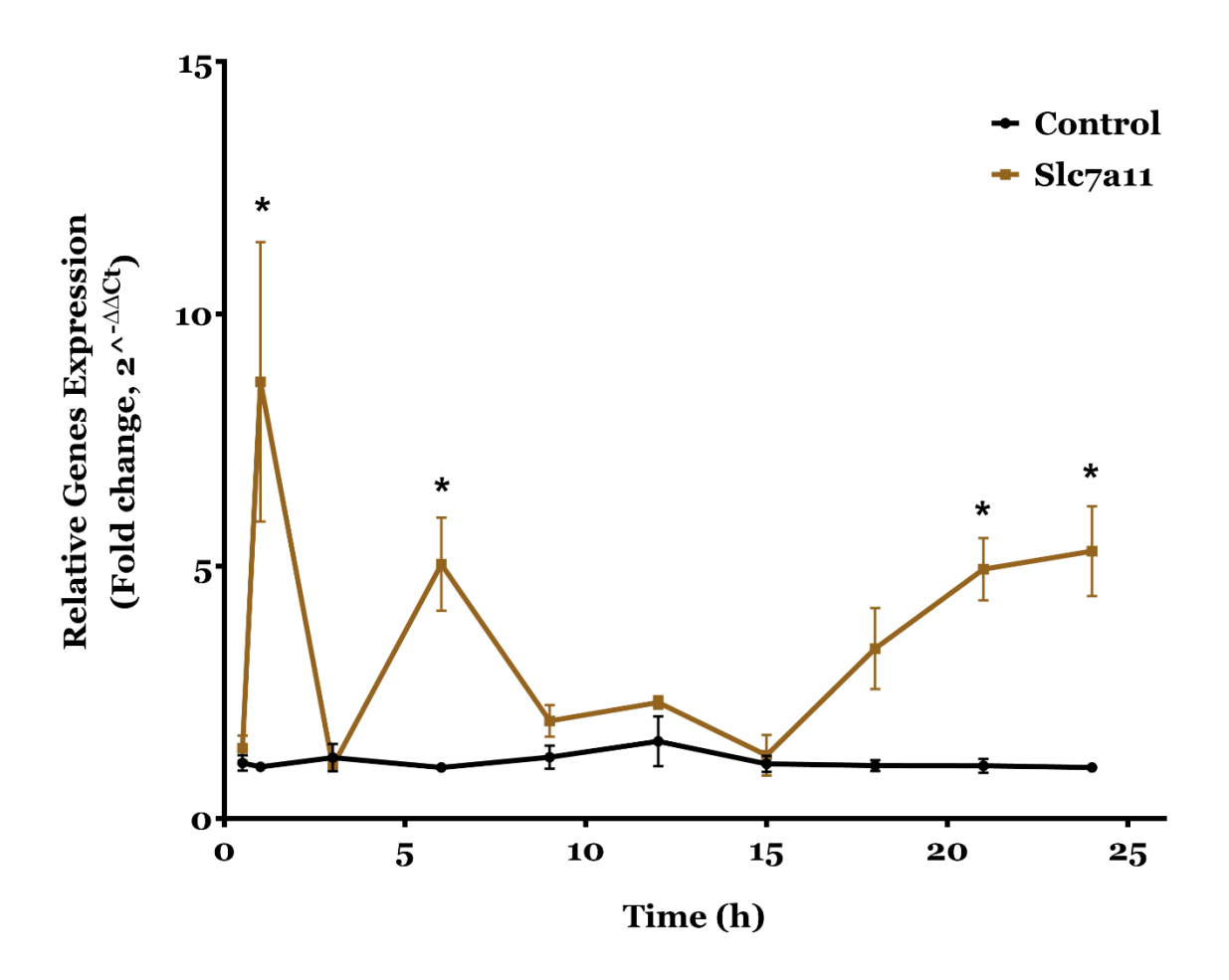


**Figure 2.9 The expression profile of** *Abcc1* (**Mrp1**) **mRNA during 0.5μM MeHg exposure to SCAs for 18 h.** The *Abcc1* mRNA expression appeared to increase during MeHg exposure, and significant increased starting from 6h to 9h (1.5 to 1.6-fold induction). At 12 h exposure, the *Abcc1* mRNA declined but remained higher than the control level (1.3-fold induction) and later increase (1.5-fold induction) at 15h. Later, its expression returned to the control level at 18h of exposure. The decline of Gclc expression to the control level was later observed. The statistical analysis using Two-Way ANOVA with Sidak's Multiple Comparison *post hoc* indicated \*; p<0.05. N=3 biological replications with two replications/N.



**o.5μM MeHg exposure to SCAs for 24 h.** The early phase of *Slc7a11* mRNA expression indicated a significant increase following 30min of MeHg exposure with 8.6-fold induction. This induction was returned to the control level following 3h of MeHg exposure, and later *Slc7a11* was significantly induced to 5-fold increase at 6h. The expression of *Slc7a11* subsequently declined to the control level from 9h to 15 h exposure and started to increase following 18h exposure. During 21h to 24h exposure, *Slc7a11* indicated a significant increase (4.9 to 5.2-fold indication, respectively) relative to the control level. The statistical analysis using Two-Way ANOVA with Sidak's multiple comparison *post hoc* indicated \*; p<0.05. N=5 for control and N=6 for MeHg treatments. Each N was performed in two replications.

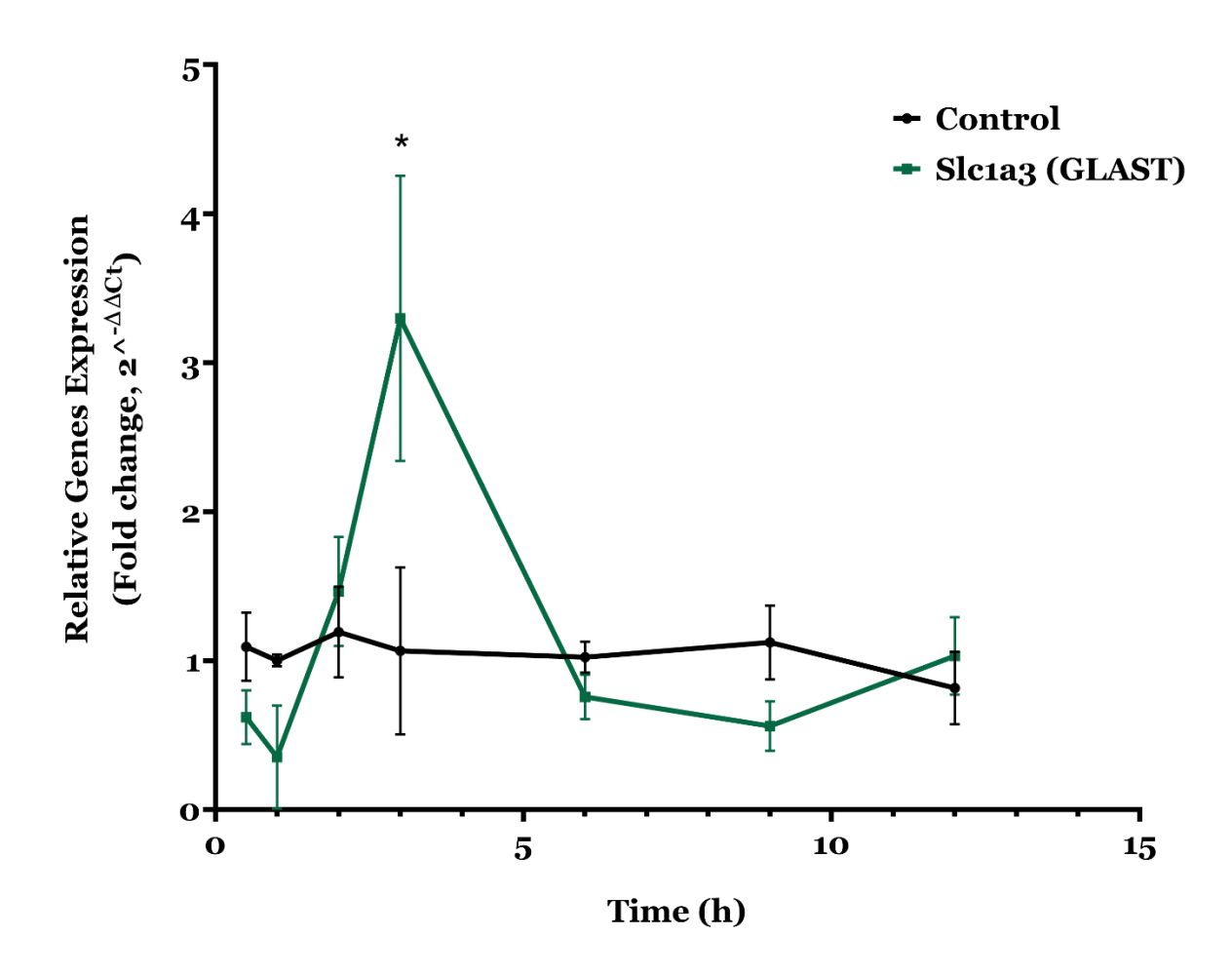


**Figure 2.11 The expression profile of** *Slc1a3* (GLAST in murine or EAAT1 in human) mRNA during 0.5μM MeHg exposure to SCAs for 12 h. Following MeHg exposure for 3h, the expression *of Slc1a3* mRNA was induced to increase significantly relative to the control level (3.3-fold induction). The expression of *Slc1a3* subsequently declined to the control level following 9h to 12 h exposure. The statistical analysis using Two-Way ANOVA with Sidak's multiple comparison *post hoc* indicated \*; p<0.05. N=5 biological replications. Each N were performed in two replications.

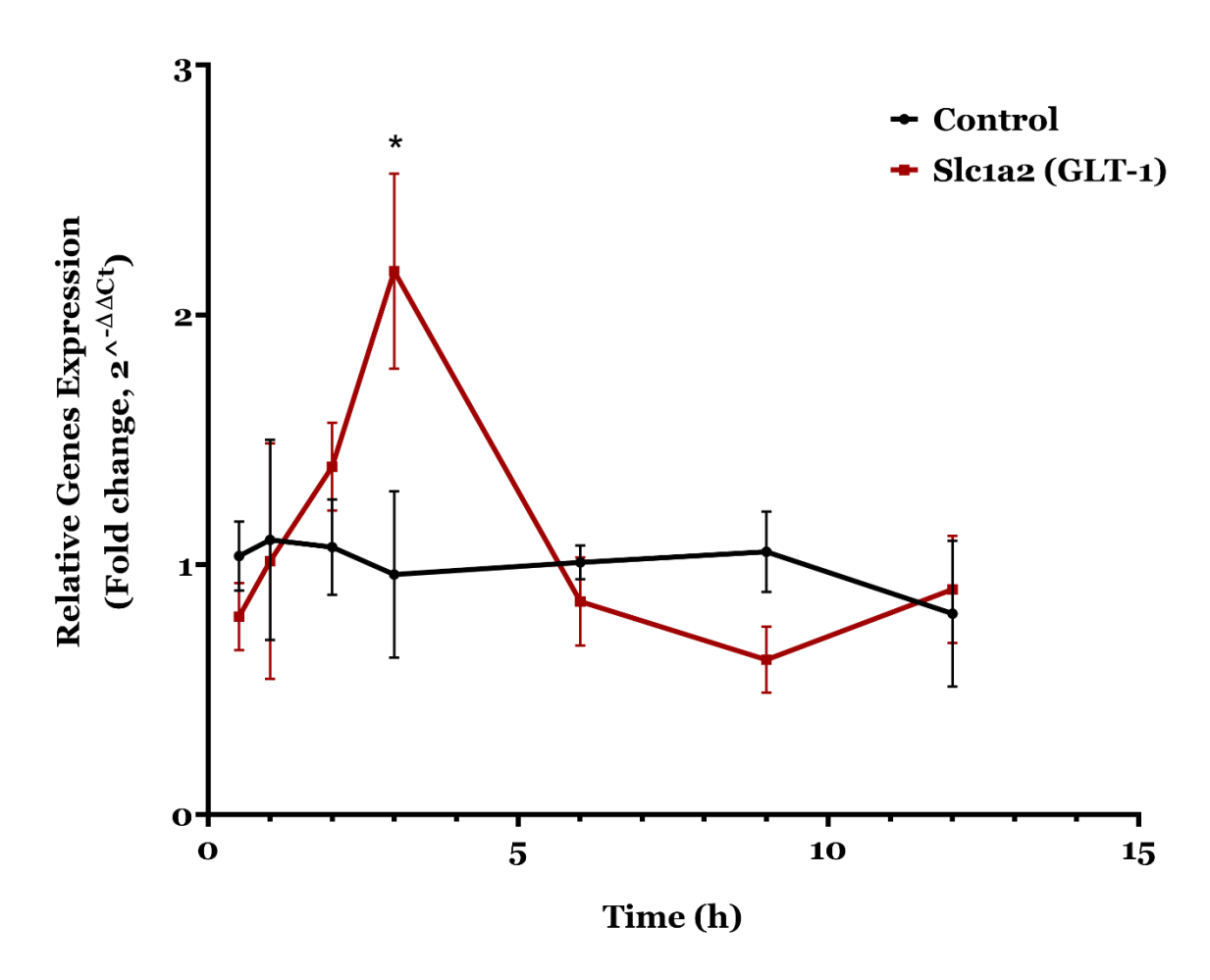


**Figure 2.12 The expression profile of** *Slc1a2* **(GLT-1 in murine or EAAT2 in human) mRNA during 0.5μM MeHg exposure to SCAs for 12 h.** Following MeHg exposure for 3h, the expression *of Slc1a2* mRNA was induced to increase significantly relative to the control level (2.2-fold induction). The expression of *Slc1a2* mRNA subsequently declined to the control level following 9h to 12 h exposure. The statistical analysis using Two-Way ANOVA with Sidak's multiple comparison *post hoc* indicated \*; p<0.05. N=5 biological replications. Each N was performed in two replications.

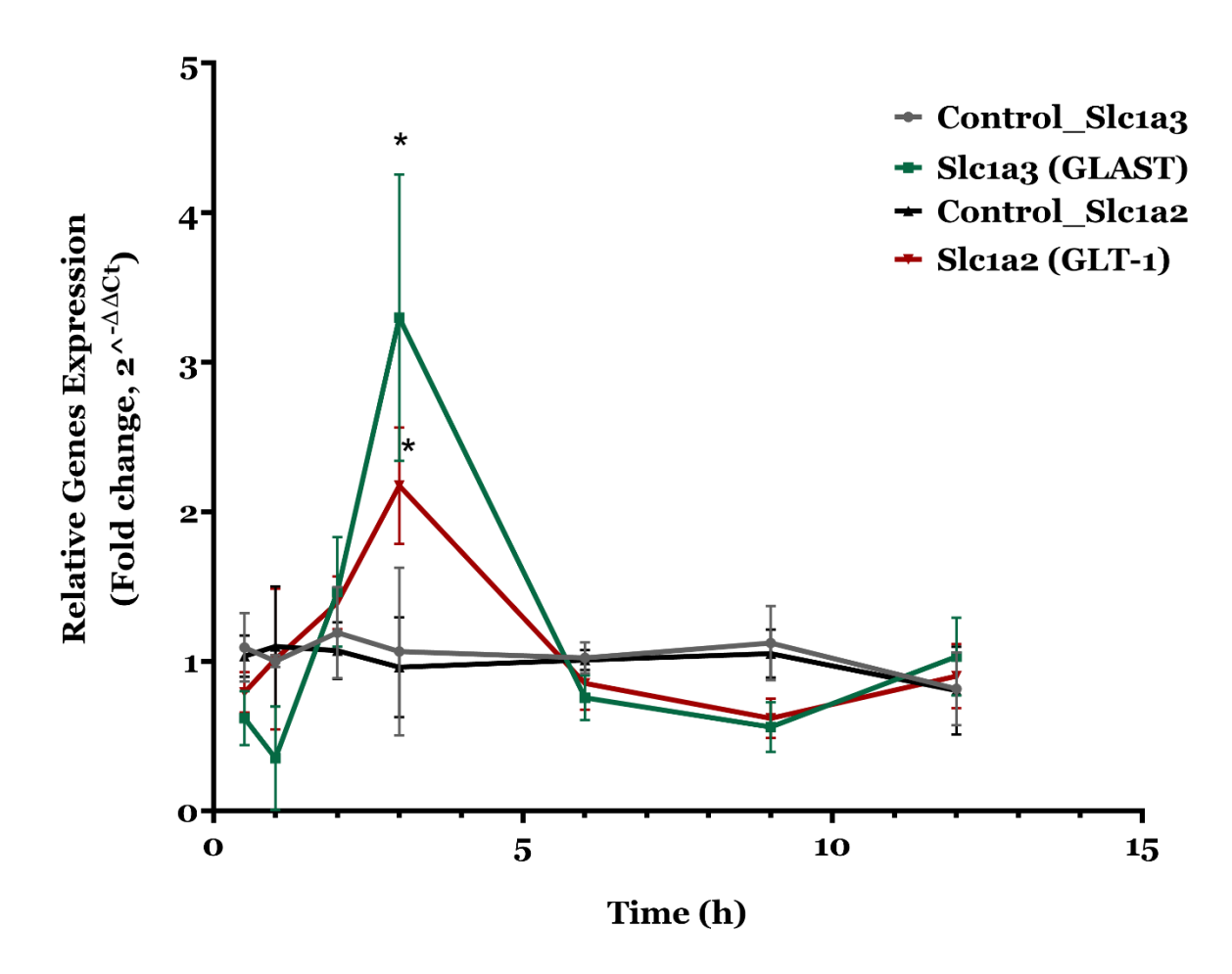


**Figure 2.13 Comparision of the expression profiles of** *Slc1a3* **and** *Slc1a2* **during 0.5μM MeHg exposure to SCAs for 12 h and their control.** The expression profiles of Slc1a3 and Slc1a2 mRNA during MeHg exposure were similar, which indicated the significant induction of these mRNA expressions following 3h of MeHg exposure, which later declined to (basal) control levels. The basal control levels of these mRNA expressions were also similar. The statistical analysis using Two-Way ANOVA with Sidak's multiple comparison *post hoc* indicated \*; p<0.05. N=5 biological replications. Each N was performed in two replications.

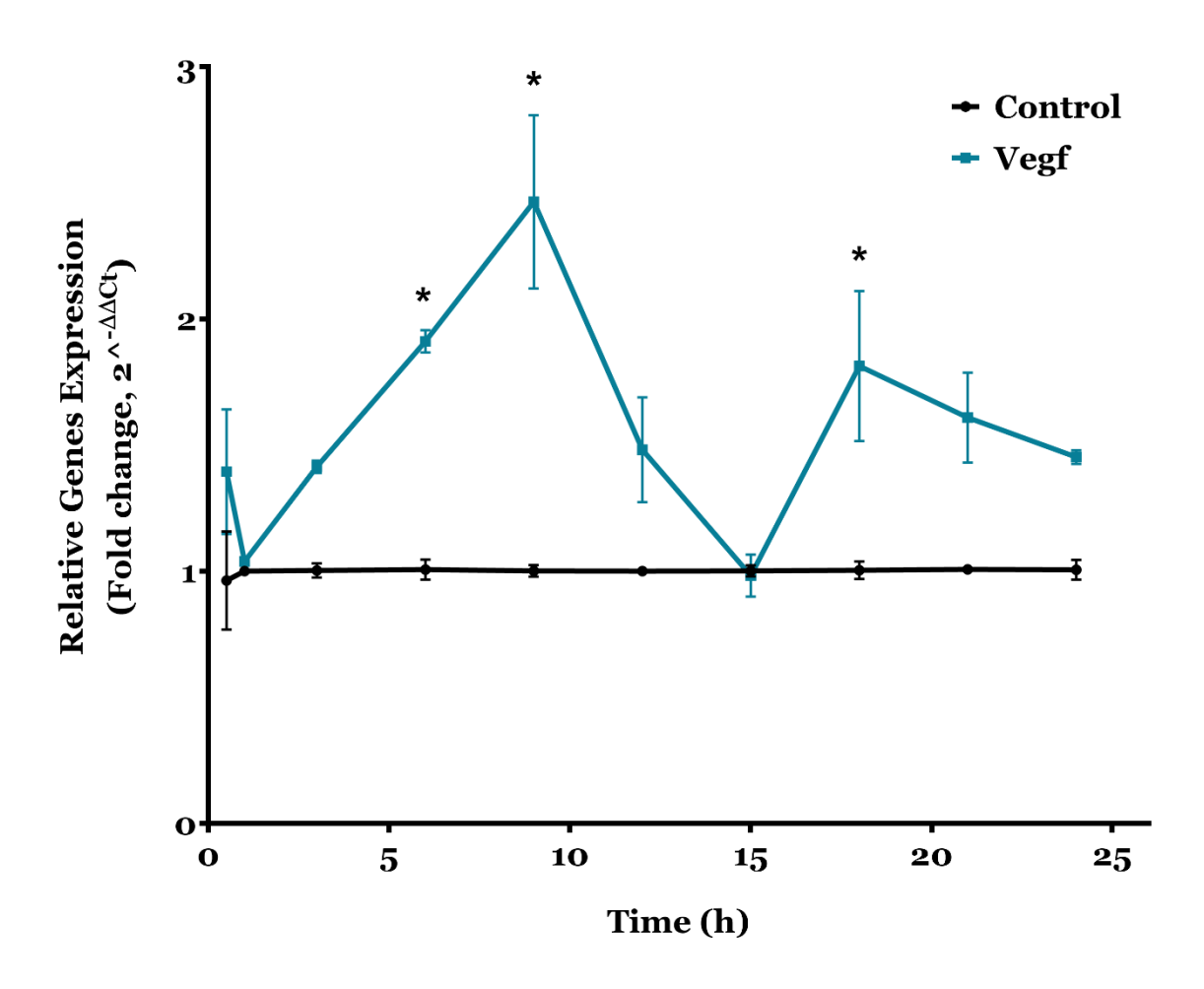


**Figure 2.14 The biphasic expression profile of** *Vegf* mRNA during **0.5**μM **MeHg exposure for 24 h.** The first phase of *Vegf* mRNA expression indicated a significant increase starting from 6h to 9h, with 9h is the peak of its expression (2.5-fold induction). Its expression subsequently returned to the control level following 12h to 15 h exposure. The *Vegf* mRNA later was induced to increase its expression significantly relative to control (1.8-fold induction) following 18h and gradually declined to the control level. The statistical analysis using Two-Way ANOVA with Sidak's multiple comparison *post hoc* indicated \*; p<0.05. N=5 for control and N=6 for MeHg treatments. Each N was performed in two replications.

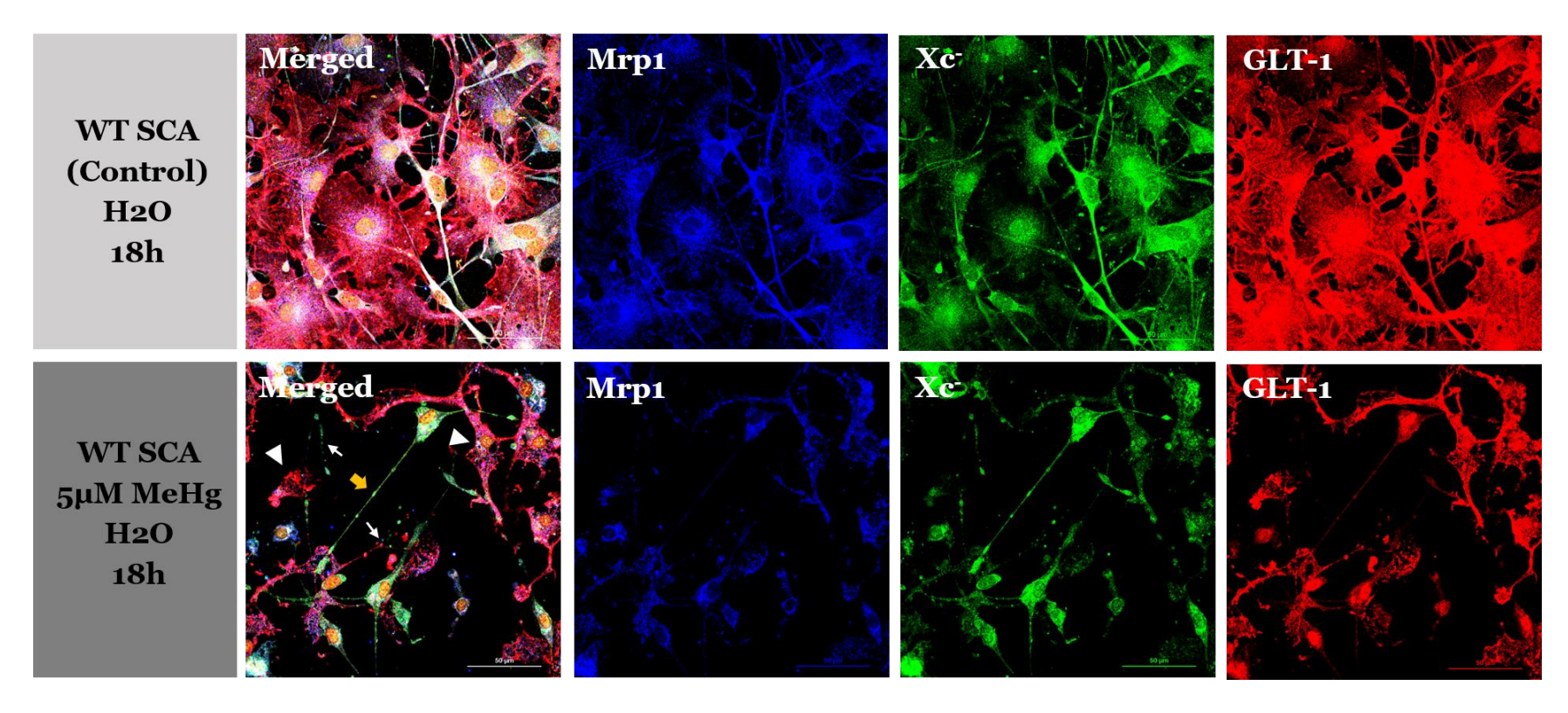
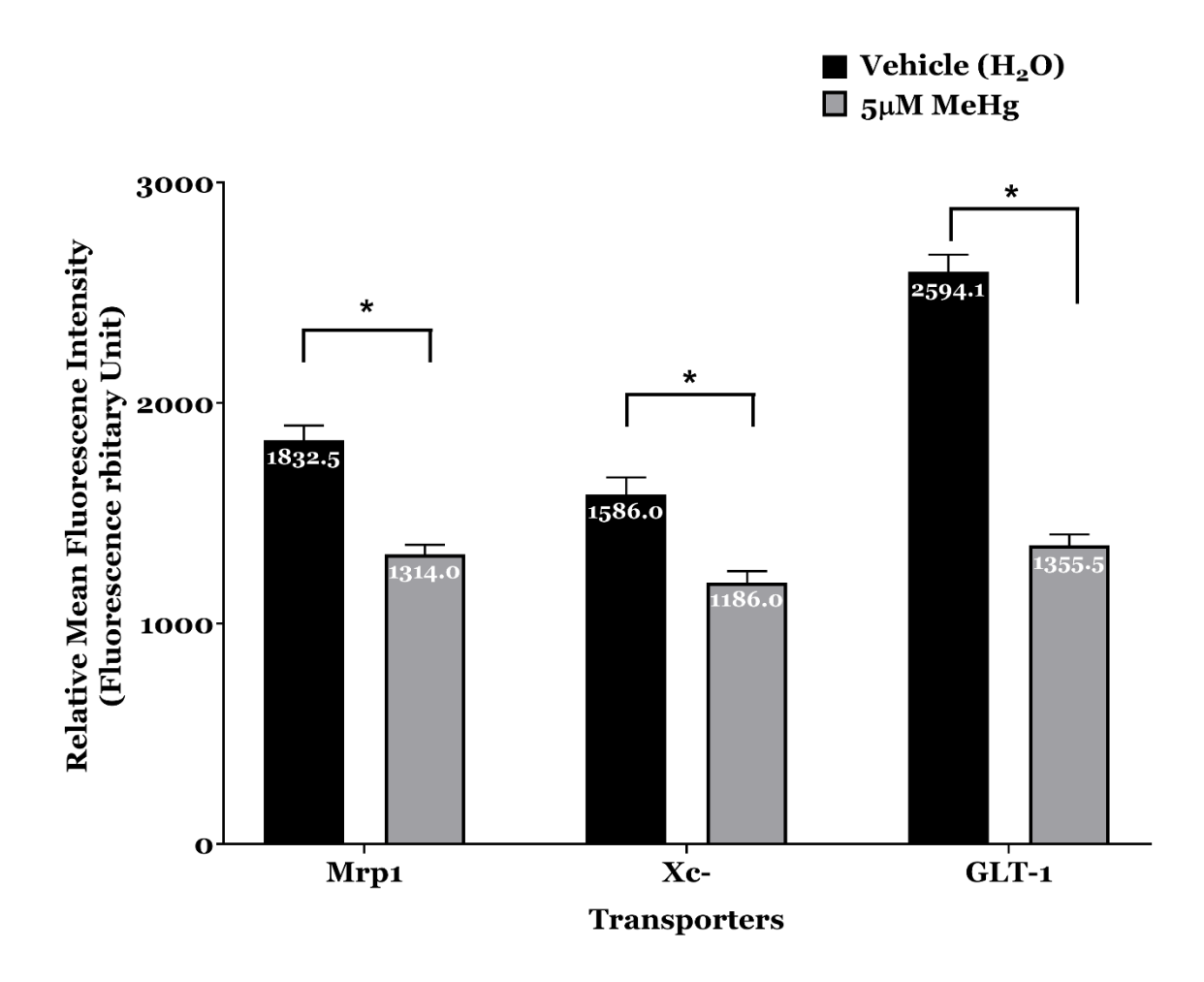


Figure 2.15 Comparision of morphological features and transporter protein expressions of SCAs following 5μM MeHg exposure for 18h. Following MeHg exposure, SCAs showed cell atrophy (white arrowhead Δ) and processes disintegration (white arrow μ) and degeneration. Some SCAs started to retract their process as they showed punctuated on the processes (yellow arrow μ). The multidrug-resistant associated proteins were labeled with mouse-monoclonal Mrp1 antibody, which was detected by anti-mouse Alexa Fluor 647. The system Xc- (cystine/glutamate antiporters) were detected using a rabbit-polyclonal SLC7A11 antibody, which was observed with anti-rabbit Alexa Flour 488. The glutamate transporter (GLT-1 in murine or EAAT2 in human) were detected using anti-guinea pig glutamate transporter (GLT-1) antibody, which was determined using anti-guinea pig Alexa Flour 594. The images were acquired from Nikon C2 confocal microscope using 60X oil objective lenses with the same exposure setting for each laser channel across all different treatments.



**Figure 2.16 The reduction of Mrp1, system Xc- and GLT-1 proteins in SCAs following 5μM MeHg for 18h.** The expression of these transporters following MeHg exposure was diminished by 28.2% (Mrp1), 25.2% (Xc-), and 47.7% (GLT-1) from vehicle treatment. The relative mean fluorescence intensity of these transporters was determined using NIS-Element Advanced Research software from Nikon. Individual single SCAs cells were traced as regions of interest for fluorescence intensity determination. Two-Way ANOVA with Sidak Multiple Comparison *post hoc* indicated differential expression between vehicle and MeHg treatments with \*; p<0.05. Values are presented as mean average +/- SEM from N=12-24 biological replications with 3 independent experiments.

### 2.5 Discussion

Several lines of evidence characterize the neurotoxicity of MeHg with a delayed onset, a long interval (latency period) between the time of exposure and the onset of neurological symptoms (Nierenberg et al., 1998). In children, MeHg exposure during pregnancy (in utero) has been associated with delays in reaching developmental milestones (e.g., age at first walking) and decreases in intelligence. These developmental milestones increase in severity with increasing exposure (Gilbert and Grant-Webster, 1995; Pletz et al., 2016). In adults, toxic effects of environmental levels of MeHg caused neurotoxic signs and symptoms that included weight loss, blurred vision, and paresthesia, following by visual field constriction and ataxia after several weeks to years of cessation (Rice, 1996; Ke et al., 2019). The latency period preceding neurotoxicity induced by MeHg is correlated to the concentration-response relationship (Pletz et al., 2016), species involved (Wobeser et al., 1976) and developmental stages (Sakamoto et al., 2018). Therefore, minimal doses of MeHg exposure to susceptible individuals may cause extensive adverse effects later in life. This study, therefore, initially determined the lowest toxic effect of MeHg in SCAs and compared the susceptibility between the early developmental stage (DIV14) and full developmental stage (DIV30). The susceptibility to MeHg toxicity in SCAs displayed the concentration and time relationship (C x T relationship) at both cell maturity stages. Realtime viability assays were used to determine the level of susceptibility with MeHg concentration ranging from 0.1 μM (0.02ppm) to 5 μM (1ppm) MeHg; the range that is lower than the maximum of MeHg content in commercial fish and seafood (1ppm) according to the World Health Organization (WHO) (WHO, 1990). The US National Research Council (USNRC) recommended that maternal blood Hg concentration is not over 5.8 µg/L or 1mg/kg (1.0 ppm) as the US Environmental Protection Agency (USEPA)

reference dose in hair (Hsi et al., 2016). Susceptibility of CxT response in these cells suggested that SCAs are also affected by MeHg in a concentration that has previously been studied in primary spinal cord motor neurons cell culture (Ramanathan and Atchison, 2011), spinal cord motor neuron cell line (NSC34 cells) (Rivera-Caraballo et al., 2017), CGCs (Marty and Atchison, 1998b; Sirois and Atchison, 2000; Limke and Atchison, 2002), PKCs (Edwards et al., 2005), cortical astrocytes(Allen et al., 2001b; Shanker et al., 2005a; Yin et al., 2007b; Yin et al., 2011), cerebellar astrocytes (Kaur et al., 2006) and microglia (Ni et al., 2011).

It is well documented that the prenatal and neonatal stages are the most susceptible for MeHg toxicity. The relative susceptibility of mature DIV 14 and fully mature SCAs DIV30 could explain the differential susceptibility of neurons in the spinal cord. Interestingly, 0.1 µM MeHg exposure did not affect DIV14 cell metabolic activity of SCAs; however, this concentration caused the DIV 30 SCAs to degenerate when exposure was longer than 9h (Figure 2.2). The onset of metabolic reduction (cell viability) of the SCAs DIV114 occurred sooner than that in SCAs DIV30 (see Figure 2.3 for the comparative summary), yet the IC50 in SCAs DIV14 was higher than that in SCAs DIV 30 with a more extended interval of MeHg exposure starting from 9h to 24h. The earlier appearance of the reduction of cell viability, but higher IC50 in DIV14 could be explained with their ability to recover from MeHg insult being better than the DIV30 (aged cells). The resilience of SCAs DIV14 could be because their antioxidant pathways are more active and well-regulated than the aged DIV30 SCAs. Oxidative stress and chronic inflammation are hallmarks of aging. The oxidative damage of macromolecules, including proteins and nucleic acids, increases with age, leading to a decline in cell and tissue functions (Frazzini

et al., 2006). Loss of balance between oxidants and antioxidants in aged cells like SCAs DIV30 could render DIV30 more vulnerable to MeHg than relatively immature cells DIV14SCAs. It has been reported that a chronic low dose of MeHg exposure (40µg/kg/day by oral gavage for 60 days caused rat (90- days old) to display oxidative stress, a neuronal marker (NeuN) and astrocytic marker (GFAP) positive cells degeneration in the motor cortex and impairment of some motor skills (Santana et al., 2019). This level of hair Hg 2µg/g is commonly found in Amazonian (Malm, 1998). The differential susceptibility between the mature SCAs DIV 14 and fully mature SCAs DIV30 to MeHg toxicity could be partly due to increased oxidative stress with aging.

Several studies suggested that the efficiency of mitochondrial functions, particularly oxidative phosphorylation (OXPHOS) declines with age as a result from the accumulative mutation of mitochondrial DNA (mtDNA) damaged from ROS (Frazzini et al., 2006). Wallace (2005) proposed that the delayed-onset and progressive course of age-related diseases result from the accumulation of somatic mutations in the mtDNAs of post-mitotic tissues. The tissue-specific manifestations of these diseases may result from the varying energetic roles and needs of the different tissues (Wallace, 2005). Therefore, the susceptibility of DIV 30 SCAs to MeHg may be explained by a decline in OXPHOS, and mitochondrial function with age and result in a MeHg manifestation at a concentration that has no adverse effect  $(0.1\mu\text{M})$  on the DIV14 SCAs.

Mitochondria and the OXPHOS are not only responsible for ATP production but are also involved in a variety of cellular processes, including Ca<sup>2+</sup> homeostasis, cAMP/protein kinase A (PKA) signaling, inflammation, and apoptosis (Bergman and Ben-Shachar, 2016). The changes of Ca<sup>2+</sup> homeostasis during MeHg exposure are associated with

mitochondrial dysfunction (Hare et al., 1993; Marty and Atchison, 1997a; Limke and Atchison, 2002). As such, the latency period preceding neurotoxicity induced by MeHg and age-related susceptibility may involve mitochondrial dysfunction and loss of Ca<sup>2+</sup> and redox homeostasis.

One of the hallmarks of aging is reduction of a cellular redox capacity characteristic with a more oxidized status (Cheng et al., 2011), thereby increasing the susceptibility to any ROS generation and toxicological and pathological insults (Suh et al., 2004). reductions of antioxidant SOD1, catalase, and GPx activity in blood samples were correlated with aging subjects, 65–90+ years of age, compared to subjects at the beginning of aging, 55–59 years of age (Kozakiewicz et al., 2019). SOD1 activity was the most explicit decrease related to age regardless of healthy or hypertensive subjects (Rybka et al., 2011). The GSH level, as well as GCLC and GCLM activities, declined significantly in the aging rat's liver (Suh et al., 2004). This was a result of the reduction of Nrf2 activity in the aged rats (Suh et al., 2004). The experimental mimetic aging model induced with chronic administration with D-galactose (D-Gal) in rats exhibited pathologies with increased oxidative stress, dysfunction of mitochondria, and damage of neurons (Ho et al., 2003; Li et al., 2018). The reductions of the Keap1-Nrf2-ARE signaling pathway were characteristics of associated aged reductions of nuclear Nrf2 expression and Ngo1, Ho-1, and Sod2 (MnSOD1) mRNA expressions in the auditory cortex of this aging rat model (Li et al., 2018). Interestingly, control rats treated with normal saline in that experiment also exhibited aged associated increase of Keap1 and reduction of Nrf2 and those Nrf2 regulated genes (Li et al., 2018). Besides this, Nrf2 has its role in the neurogenesis of neuronal stem progenitor cells (NSPCs) in the subventricular zone of the dentate gyrus of

the rat hippocampus. The NSPCs exhibited regenerative and neuronal density compromises with age as well as the decline of *Nrf2* and *Gclm* (Ray et al., 2018). Overexpression of Nrf2 in middle-aged rats, a critical period that showed a marked reduction of NSPC neurogenesis and cognitive behavior decline, the neurogenesis in these Nrf2 treated rats was enhanced, compared to untreated middle-aged rats (Ray et al., 2018). As such, the increase of SCAs DIV 30 susceptibility to MeHg may involve dysregulation of the Keap1-Nrf2 -ARE pathway in more mature cells. Further study of a comparative expression of the Keap1-Nrf2 -ARE pathway and antioxidant activity between SCAs DIV 14 and DIV30 may explain the mechanism underlying the differential susceptibility.

Whether the Keap1-Nrf2 -ARE pathway was involved in MeHg-induced toxicity in DIV 30 SCAs, the expression of Keap1, Nrf2, and downstream genes under Nrf2 activity were determined using gene expression assays as a function of time of exposure with 0.5µM MeHg, the lowest concentration exhibiting toxicity to both SCAs DIV 14 and DIV 30 in this study. Expressions of *Keap1*, *Nrf2*, *Gclc*, *Abcc1* mRNAs obviously increased at 6h of MeHg exposure and declined at 15h of MeHg exposure. While the expression of Keap1 continued to decline and became significantly lower than the control treatment, the expression of Nrf2 appeared to return to the control level at 18h exposure. The level of *Nrf2* mRNA expression was not significant at a time at which *Keap1* mRNA was significantly reduced (18h). Perhaps the cellular bioavailability of Nrf2 protein was sufficient to combat oxidative stress and MeHg insults. Cellular Nrf2 protein might also regulate the increase of *Gclc* and *Abcc1* expression at this time point. At 18h of MeHg exposure, both *Gclc* and *Abcc1* were increased (Figure 2.8 and 2.9) with a significantly

reduction of Keap1 (Figure 2.6). The biphasic induction of Gclc and Abcc1 mRNA expressions during MeHg exposure in SCAs could be explained by the nature of Nrf2 activity and MeHg. MeHg is highly reactive with the sulfhydryl group (Simpson, 1961), and Keap1 is a cysteine-rich protein (Dinkova-Kostova et al., 2002). MeHg has been shown to bind to recombinant Keap1 protein with an SDS-PAGE assay (Toyama et al., 2007). Therefore, MeHg would potentially interrupt the bonding between Keap1 and Nrf2, which leads to the regulation of genes underlying ARE expression. The gradual induction of Gclc and Abcc1 mRNA expressions (Figure 2.8 and 2.9) in the first phase could be due to activation of Nrf2 by MeHg, which later declined due to the loss of Nrf2 activity and availability of cellular Nrf2 protein. The Nrf2 half-life is about 20 min under basal conditions (Ma, 2013). It is rapidly degraded under ubiquitin-proteasome degradation (Ma, 2013). Nrf2 is also activated by other metals such as Zn2+(Silbajoris et al., 2014; Wages et al., 2014). The second phase of Nrf2 activity, as seen in the induction of Gclc, Abcc1, and slightly Nrf2, could be partially due to Zn2+ activation of this pathway, in addition to the decline of Keap1. Elevation of Zn<sup>2+</sup> is involved in the cellular mechanism by which MeHg induced toxicity in the synaptosome (Denny and Atchison, 1994b), neuronal cell line (Denny and Atchison, 1994b), cerebellar neurons(Limke, 2004; Edwards et al., 2005), and brainstem (Johnson et al., 2011). That peak of the second phase was lower than the first phase could be related to multiple factors, such as the cell survival stage or lower affinity to thiols for Zn<sup>2+</sup> than MeHg (Kensler et al., 2007).

Besides Keap1, additional negative Nrf2 regulators are presented in the nucleus that indicate the Keap1-independent regulation of Nrf2 pathway. These regulators include Src subfamily members Fyn, Src, Yes, and Fgr, which phosphorylate Nrf2 at tyrosine 568 that

results in nuclear export and later degradation of Nrf2 in the cytoplasm (Niture et al., 2014). The nuclear activity of Fyn is regulated by a glycogen synthase kinase 3 beta (GSK-3β) and its negative effector protein kinase B (Akt) (Hayes, 2016). The regulation of Nrf2 activity is also controlled by a Keap1-independent pathway by which the IGF-1-PI3K-Akt pathway regulates the ARE underlying gene expression. The increase of Akt dramatically increased in Nrf2 KO mice in the presence of insulin, which activates the IGF-1 receptor (Meakin et al., 2014). The active Akt antagonizes the inhibition of Nrf2 expression by GSK-3\beta activity in the phosphorylation of Fyn (Jain and Jaiswal, 2007). Low concentration (0.5-1.0 µM) of MeHg or HgCl2c induced the activation of phosphoinositide 3-kinases (PI3K)/Akt signaling pathway in mouse pancreatic β-cell which corresponded to mouse pancreatic β-cell dysfunction and ROS generation after 1h exposure (Chen et al., 2006). Exposure of human neuroblastoma SH-SY5Y-cells with 0.5uM MeHg for 6h increased the cytoplasmic and nuclear Akt, CREB, and anti-apoptotic Bcl-1, which were regulated by PI3K (Unoki et al., 2016). Under this MeHg treatment also phosphorylated GSK-3β and activated Nrf2 (Unoki et al., 2016). These data might suggest that exposure to low MeHg concentration induced the cellular protective molecules such as Bcl2 and Nrf2 in the Keap1-independent pathway. With higher MeHg concentration, the cortical astrocyte cell culture exposure to 5µM MeHg for 6h exhibited the nuclear translocation of Nrf2 which was associated to the reduction of nuclear Fyn (Culbreth et al., 2017). This research group concluded that MeHg sustained the Nrf2 expression in cortical astrocytes by down regulation of Src kinases pathway which activated Fyn through inactivation of GSK-3\beta and phosphorylated Akt (Culbreth et al., 2017). Perhaps, MeHg induced toxicity in SCAs in the same way as it did in cortical astrocyte cell culture (CAC) and SH-SY5Y-cells by which at 6h of Nrf2 mRNA increase may correspond to the

inactivation of GSK-3β and phosphorylated Akt. However, MeHg concentration in this study was 1/10 of that CAC study. In addition, the differential susceptibility to MeHg between CAC and SCAs existed. The comparison of the susceptibility between the CAC and SCAs to 5μM MeHg for 18h revealed that the SCAs were more susceptible than CAC according to morphological pathologies. SCAs exhibited the loss of processes and degeneration, while CAC were intact (data do not show). Perhaps, MeHg regulated the GSK-3β and Fyn pathway in regulation of Nrf2 in SCAs different from that in the CAC. MeHg might induce the increase of inactive GSK-3β in CAC resulting in the sustained Nrf2 activity leading to CAC are more resistant to MeHg. Conversely, MeHg might induce the active GSK-3β up-regulation which later enhances Nrf2 degradation. The regional astrocytes could play a role in MeHg susceptibility as well as differential cytotoxicity pathway attributed to the susceptibility.

Not only was a loss of redox homeostasis involved in MeHg-induced CNS toxicity, but excitotoxicity was also indicated. The fluctuation of cystine/glutamate (systemXc-) *Slc7a11* mRNA expression exhibited in SCAs exposure to 0.5uM MeHg with three cycles of increase (Figure 2.9). The earliest peak was following 30min exposure and the second peak at 6h. The third phase was gradually increased, starting from 18h, and a significant increase was observed at 21h and 24h of MeHg exposure. The earliest induction of *Slc7a11* mRNA expression might suggest the response of SCAs to MeHg exposure, which activated Nrf2 activity to combat MeHg- insults by inducing the expression of *Slc7a11*. The increase of *Slc7a11* could also suggest the imbalance of intracellular GSH to combat against MeHg-toxicity. Interestingly, the increases of the 1st peak at 30 min of *Slc7a11* mRNA expression was followed by the increase of *Slc1a3* and

Slc1a2 mRNA expression at 3h of MeHg exposure (Figure 2.10 and 2.11). This result might support the co-operative function between system Xc- and EAAT1/2 activity. Since the systemXc- exchanges extracellular cystine with intracellular Glu (with 1:1 ratio) (Warr et al., 1999) for de novo GSH synthesis (Murphy et al., 1989). This exchange, however, would cause the increase of extracellular Glu, which is required to be maintained at a nontoxic level as well. As such, SCAs responded to the imbalance of redox and glutamate homeostasis by inducing the increase of EAAT1 and EAAT2 expression. The immunocytochemistry also demonstrated the correlation of expression between systemXc- and EAAT2, which were reduced when extended MeHg exposure with higher MeHg concentration (5μM) (Figure 2.16 and 2.17). This increase of Slc7a11 mRNA expression, but the reduction of system Xc- protein expression suggested that MeHg also affected the post-transcriptional processes, thereby reduction of protein expression. Protein synthesis was inhibited early during MeHg-intoxication in vivo (Yoshino et al., 1966). As such, low MeHg concentration exposure in SCAs exerted the toxic effect through the dysregulation of redox and glutamate homeostasis by interfering with the expression of system Xc- and EAAT1/2 expression at both transcriptional and translational processes.

The effect of MeHg to *Vegf* expression was determined in SCAs because the astrocytic VEGF role plays a role in the regulation of AMPAR-GluR2 subunit expression in MNs (Bogaert et al., 2010). The neuroprotective functions of VEGF are an increase of axonal outgrowth anneurogenesis and inhibition of neuronal apoptosis (Rosenstein, 2004; Rosenstein et al., 2010). For example, the motor neuron-like cell NSC 34 cells incubated with cerebrospinal fluid (CSF) from ALS patients exhibited a reduction of aerobic

respiration and neurofilament, and VEGF co-incubation with ALS-CSF reduced these adverse effects (Kulshreshtha et al., 2011). Mice with deletion of promotor region of Vegf, resulting in a reduction of Vegfa expression, exhibited adult-onset progressive motoneuron degeneration, with many neuropathological and clinical signs reminiscent of human ALS (Lambrechts et al., 2003). In this study, however, the results showed that MeHg induced the expression of *Vegfa* mRNA in SCAs in a biphasic increase fashion. The increase of Vegfa mRNA expression was similar to the results in the human brain microvascular endothelial cells and pericytes cell cultures exposed to MeHg (1, 2, 3 µM) for 12h and 18h (Hirooka et al., 2013). The expression of VEGF receptor 1 and 2 (VEGFR-1 and VEGFR-2, respectively) also increased in endothelial cells but not in the pericytes (Hirooka et al., 2013). The primary pathway to regulate VEGF expression is hypoxia inducing factor (HIF) since the hypoxia response element (HRE) is located within the promoter of the VEGF gene to restore the oxygen acquisition by enhancing angiogenesis and tissue perfusion (Lambrechts et al., 2004). MeHg neither induced the increase of HIF-1a nor HIF-2a, transcriptional factors that regulate HIF pathway, in either human endothelial cells or pericytes (Hirooka et al., 2013). This research group suggested that MeHg activated the VEGF system in brain microvessels in a paracrine fashion (Hirooka et al., 2013). The elevation of VEGF is not only associated with vascular plasticity related to angiogenesis in developing CNS but is also associated with BBB permeability in mature CNS (Argaw et al., 2009). The increase of VEGF following MeHg exposure could increase the microvascular tissue permeability and cause an edematous change around this tissue (Hirooka et al., 2013). The edematous changes in white matter have been suggested as the cause of the localization lesion (Hirooka et al., 2013). Chronic MeHg exposure in adult Minamata cases indicated the local damage of the CNS, while the global CNS damages

were observed in fetus and infant cases (Korogi et al., 1998; Eto et al., 2010). The neuropathological damages were predominantly in selective areas, including the calcarine region, the postcentral and precentral gyri, and the temporal transverse gyrus (Hunter and Russell, 1954; Eto, 1997). (Hunter and Russell, 1954; Eto, 1997). These changes were most advanced in the depths of the sulci (Eto, 1997). Perhaps, selective CNS damage in adult MeHg exposure may involve the brain edemas resulting from abnormal accumulation of the perivascular tissue caused by the increase of BBB permeability. The elevation of astrocytic VEGF might take part in BBB permeability in MeHg toxicity since the permeability barrier formed by cerebral endothelial cells is supported by trophic factors secreted by other cells in the BBB, including pericytes, and astrocytes (Demeuse et al., 2002). Astrocytes cover approximately 90% of endothelial cells, and communication between endothelial cells and astrocytes is essential to maintain the BBB properties (Minagar and Alexander, 2003). For example, astrocytes coculture with endothelial cells induced the increase of MnSOD (SOD2) expression and activity in endothelial cells (Schroeter, 2001).

In conclusion, the dysregulation of SCAs functions significantly contributes to MeHg-induced cellular pathologies. These cellular mechanisms included the perturbation of the Keap1-Nrf2-ARE pathway and astrocytic Na<sup>2+</sup>-dependent glutamate transporters such as GLT-1/EAAT2 expression. Perturbation of the antioxidant pathway and glutamate expression could contribute to oxidative stress and excitotoxicity generation. The increase of *Vegfa* expression in SCAs may involve in the mechanism by which specificity of MeHg susceptibility in the CNS, including the gracile fasciculus (a tract of Goll) in the spinal

cord as well as calcarine sulcus and gyrus in the cerebrum and cerebellum (Eto, 1997) as a resulting from blood-spinal cord barrier (BSCB) and BBB disruption.

### **CHAPTER THREE**

CHARACTERIZATION OF AN NRF2 ROLE IN THE REGULATION OF METHYLMERCURY- INDUCED TOXICITY IN PRIMARY SPINAL CORD ASTROCYTES DERIVED FROM C57BL/6J MICE AND NRF2 KNOCKOUT MICE

### 3.1 Abstract

The cellular and molecular mechanisms of MeHg induced SCAs degeneration has involved the dysregulation of the Keap1-Nrf2-ARE pathway, as observed in chapter 2. Since Nrf2 regulated a variety of cellular detoxification/antioxidant genes and some antioxidant transporters' functions are associated with the function of glutamate transporters such as EAAT1 or EAAT2. The dysregulation of system Xc- and EAAT1/2 transcripts exhibited in SCAs during MeHg exposure. To determine whether MeHg induced SCAs degeneration through the Keap1-Nrf2-ARE pathway is solely due to Nrf2 activity, SCAs derived from wild type C57BL6J (WT), and Nrf2 knockout (Nrf2 KO) mice were compared. Furthermore, whether the regulation of system Xc- and EAAT1/2 expressions were associated, and this association was involved in the Nrf2 activity, the expression of these gene transcripts was compared among these genotypes.

The Nrf2-ARE pathway regulates redox homeostasis. Oxidants and MeHg activate the Nrf2-ARE pathway to increase the expression of antioxidant genes such as the rate-limiting enzyme in GSH synthesis (Gclc), GSH peroxidase (Gpx), cystine/ glutamate antiporter (system Xc-), and multidrug-resistant associated protein (Mrp). In the central nervous system, the Nrf2-ARE pathway in astrocytes is relatively active compared to neurons. Consequently, neurons require the antioxidants supplied by astrocytes, mainly when oxidative stress occurs. Thus, dysregulation of the Keap1-Nrf2-ARE pathway in astrocytes might be detrimental to neurons. The perturbation of this pathway has been reported in MeHg-induced toxicity in cortical and cerebellar astrocytes, as well as neurons. The effects of MeHg on viability and expression levels of redox homeostasis genes were first examined. The real-time viability results showed that the Nrf2 KO-

derived SCAs were more susceptible to MeHg compared to WT-derived SCAs. A one-hour exposure of 5 μM MeHg significantly reduced cell viability of Nrf2 KO derived SCAs by 60% compared to WT derived SCAs. With vehicle treatment, *Gclc*, *Gpx1*, and *GPx4* mRNAs were reduced in Nrf2 KO SCAs significantly compared to WT SCAs, whereas expressions of *Keap1*, *Abcc1* (Mrp1) and *Slc7a11* (system Xc-) mRNA were significantly higher than in WT SCAs. MeHg treatment for 18 h reduced the expression of most of these antioxidant genes except *Slc7a11* in both WT and Nrf2 KO derived SCAs when compared to their genotype treated with vehicle. Following 18h MeHg treatment, the *Slc7a11* mRNA was significantly increased in WT SCAs (5-fold induction); however, it was slightly affected in the Nrf2 KO SCAs compared to their genotype treated vehicle. MeHg slightly affected the expression of *Keap1* in WT SCAs, but it significantly induced the reduction of *Keap1* mRNA expression in Nrf2 KO SCAs. The differential effects of MeHg on the expressions of *Keap1* and *Slc7a11* in WT and Nrf2 KO could demonstrate the genetic background played a role in response to MeHg.

Glutamate homeostasis is one of the critical mechanisms in MeHg- induced toxicity. In this study, the expression of excitatory amino acid transporter 1 (*Slc1a3*) and 2 (*Slc1a2*) were measured. In both WT and Nrf2 KO derived SCAs, *Slc1a2* was significantly reduced following MeHg exposure for 18h compared to their same genotype treated with the vehicle. *Slc1a3* was significantly reduced only in Nrf2 KO derived SCAs, but only slightly affected in the WT SCAs. There was a differential expression of *Slc1a3* and *Slca1a2* in Nrf2 KO SCAs in which the *Slc1a3* expression was significantly higher than WT SCAs (4-fold higher), and *Slc1a2* expression was about 2-fold higher than WT SCAs. The increase of *Slc1a3* and *Slc1a2* expression in the Nrf2 KO derived SCAs could be due to their role in

cooperative modulation of glutamate homeostasis with system Xc-, which was highly expressed in Nrf2 KO derived SCAs. However, the immunocytochemistry revealed that expression of Mrp1, system Xc- and GLT-1 protein in Nrf2 KO derived SCAs was significantly lower than that in WT derived SCAs. MeHg further reduced the expression of these proteins in both WT and Nrf2 KO SCAs when compared to their genotype treated with the vehicle. When compared to different genotypes, Nrf2 KO derived SCAs had a severe reduction of these transporters following 18h 5µMMeHg exposure, suggesting that MeHg affects transcriptional levels but also the translational processing of these proteins.

It is well documented that MeHg effects the regulation of [Ca<sup>2+</sup>] in homeostasis. One of these effects involves the activation of Ca<sup>2+</sup> permeable AMPAR. VEGF has reported a role regulating Ca<sup>2+</sup> impermeability of AMPAR via induction of GluR2 subunit expression, which results in the channel Ca<sup>2+</sup> impermeable. Previously, a low concentration of MeHg exposure (0.5μM) in SCAs exhibited a bi-phasic induction of *Vegf* mRNA expression over 24h. To understand the mechanism by which MeHg causes the dysregulation of *Vegf* mRNA expression, this study aimed to characterize if Nrf2 was involved in the dysregulation of *Vegf* mRNA expression. There was an increase in *Vegf* mRNA expression in Nrf2 KO (12-fold increase) compared to WT derived SCAs. Interestingly, MeHg induced the increase of *Vegf* mRNA expression in WT derived SCAs (2.7- fold increase), while it induced the reduction of this mRNA (7.7-fold decrease) in Nrf2 KO derived SCAs.

In this study, the results suggested that the Nrf2 gene plays an essential role in MeHginduced toxicity in cells such as SCAs through alteration of redox homeostasis, glutamate signaling, and intracellular calcium homeostasis. The genetic predisposition also plays a vital role in MeHg susceptibility.

### 3.2 Introduction

MeHg-induced neuronal degeneration may be caused by complex interactions between three important signals: [Ca<sup>2+</sup>] in, redox signaling molecules, and glutamate These three signaling pathways are intertwined. For example, MeHg-induced spontaneous neurotransmitter release is dependent on [Ca<sup>2+</sup>] in (Hare et al., 1993). The disruption of [Ca<sup>2+</sup>] in during MeHg toxicity exhibited a biphasic increase of [Ca<sup>2+</sup>] in. The first phase involved the [Ca<sup>2+</sup>] in stored in organelles such as the endoplasmic reticulum and dysregulation of mitochondrial function. The dysregulation of mitochondrial function could also contribute to reactive oxygen species (ROS) overproduction leading to loss of redox homeostasis when the antioxidant system is saturated. Finally, ROS (Trotti et al., 1997; Trotti et al., 1998) and mercury (Hg and MeHg) also inhibit glutamate transporter function, blocking the uptake of aspartate and glutamate into the cells and astrocytes (Brookes, 1988; Brookes and Kristt, 1989; Trotti et al., 1997).

The electrophilic/ antioxidant pathway Keap1-Nrf2-ARE pathway is involved in MeHg induced toxicity. MeHg activates the antioxidant Nrf2-ARE pathway due to its electrophilic property. MeHg induces the Nrf2 activation in cortical astrocytes (Wang et al., 2008) and microglia (Ni et al., 2010b) as well as neurons (Toyama et al., 2007; Vanduyn et al., 2010; Yoshida et al., 2014) that results in downstream antioxidant gene expression (Wang et al., 2008; Kumagai et al., 2013). Dysregulation of antioxidant genes in the Nrf2-ARE pathway occurs during MeHg exposure in SCAs (chapter 2) and NSC34 motor neuron-like cells (refs). The Nrf2-ARE in astrocytes plays a prominent role in neuronal protection, particularly during oxidative stress occurring in the CNS (Vargas et al., 2008) mainly because the Nrf2-ARE pathway is more activated in astrocyte than that

in neurons (Murphy et al., 2001). Therefore, a loss of redox homeostasis in astrocytes could be detrimental to neurons, including SMNs.

MeHg exposure induces dysregulation of [Ca<sup>2+</sup>]<sub>in</sub> in primary SMNs cell culture (Ramanathan and Atchison, 2011) and MNs in the brainstem derived from WT and hTg SOD G93A ALS mice (Johnson et al., 2011). Specific overexpression of Nrf2 in astrocytes prevented motor neuron degeneration in astrocytic-neuronal cocultures derived from hTg SOD G93A mice, and delayed neuromuscular junction denervation and extended hTg SOD G93A mice survival (Vargas et al., 2008). When overexpression of Nrf2 was restricted to neurons or type II muscle fibers, the ALS onset was delayed but not the survival rate (Vargas et al., 2013). These results support the hypothetical model that the onset of motor neuron disease is due to the dysfunction of motor neurons, and the progression of the disease is due to the dysfunction of astrocytes. However, the pathogenic mechanisms of MNDs, as well as MeHg induced MNs degeneration, remains unclear. The dysregulation of the Nrf2-ARE pathway in SCAs may instigate the progression of SMNs degeneration due to insufficient antioxidant supplied from SCAs to SMNs during MeHg exposure. To determine if Nrf2-ARE pathway has a role in MeHg-induced toxicity in SCAs, I investigated the expression of antioxidant genes underlying Nrf2-ARE pathway in the WT and Nrf2 KO derived SCAs during exposure to MeHg.

The Nrf2-ARE regulates the expression of enzymes involved in GSH synthesis, including the GSH synthesis, Gclc, and GSH peroxidase (Gpx; isoforms Gpx1, Gpx2, and Gpx4). Gpx1 (Gardaneh et al., 2011) and Gpx4 (Bellinger et al., 2011) have a role in neuronal protection. The Gpx1 knockout mice are highly susceptible to the oxidant paraquat, and hydrogen peroxide (De Haan et al., 1998). Overproduction of human Gpx1 in the SK-N-

MC neuroblastoma cell line provides resistance to 6-hydroxydopamine (6-OHDA) toxicity (Gardaneh et al., 2011). Furthermore, human Gpx1 overexpressing SK-N-MC cells cultured with conditioned media from human Gpx1 overexpressing astrocytes are even more resistant to 6-OHDA induced cell death (Bellinger et al., 2011). Glutathione peroxidase4 (GPx4) is the most widely expressed isoform in the brain (Cardoso et al., 2017). An observed reduction in GPx4 expression in the substantia nigra in Parkinson's Disease patients compared to the control subjects supports its role in neuroprotection in dopaminergic neurons (Bellinger et al., 2011). Moreover, the tamoxifen-inducible conditional Gpx4 ablation mice exhibited pathological paralysis with dramatic MN degeneration in the spinal cord but not in adult mice's cerebral cortex (Chen et al., 2015). Overall, GPx1 and Gpx4 expression, particularly in astrocytes, has an essential role in neuronal protection.

Regulation of GSH import and export is via the multidrug resistance-associated protein (Mrp1) member of the ATP-binding cassette (ABC) transporter superfamily (Cole, 2006) encoded by the *Abcc1* mRNA (Cole, 2014b). The expression of *Abcc1* mRNA is regulated by Nrf2 activation (Maher et al., 2007). Mrp1 can also transport the oxidized disulfide form of GSH, GSSG (or reduced GSH). GSSG increases when the cells are under oxidative stress, and the efficient reduction of this molecule with antioxidant is essential for cellular redox homeostasis. Unlike GSH, GSSG does not facilitate the transport of the other Mrp1 substrates (Cole, 2014a) but instead inhibits their transportation (Leier et al., 1996; Cole, 2014a). Mrp1 also excretes xenobiotics and electrophilic compounds that can conjugate to GSH by the GSH-S-transferase (Leier et al., 1996) enabling exportation of the GSH-electrophile compound (Cole, 2006, 2014a). A study in the Mrp2 knockout rat suggested

that inorganic mercury (Hg<sup>2+</sup>) and MeHg were excreted through the Mrp2 from the kidney and liver since there was higher mercury accumulation in the kidney and liver in the Mrp2 knockout rats and lower mercury accumulation in the urine and feces of these rats compared to the wildtype rat (Bridges et al., 2011). In addition, over expression of Mrp2 in the Sf9 cells indicated the larger transport of mercury than that in the Sf9 cell control (Bridges et al., 2011). It appeared that Mrp plays important role in excrete mercury and its compounds from cells.

The cystine glutamate antiporter (system Xc-) has a significant role in importing extracellular cystine into astrocytes and neurons in exchange for Glu, which leads to de novo intracellular GSH synthesis. Structurally, system Xc- is composed of a light-chain subunit xCT, encoded by the Slc7a11 gene that is regulated by Nrf2-ARE pathway (Habib et al., 2015) that confers substrate specificity, and a glycosylated heavy-chain subunit (4F2hc or rBAT) that targets the transporter to the plasma membrane (Jackman et al., 2010). The system Xc- is expressed in both neurons and astrocytes (Lewerenz et al., 2012). However, mature neurons exhibit little or no system Xc- function due to their lack/small ability of cystine uptake (Shih et al., 2006). Thus, to synthesize intracellular GSH, mature neurons use the EAAT3/EAAC1 (Aoyama et al., 2006; Watts et al., 2014) to import cysteine. The extracellular cysteine is usually in the form of two cystine molecules (Cyss=Cyss) bonded with a disulfide bond; however, this cysteine form is relatively unstable and is easily oxidized into cystine (Aoyama and Nakaki, 2015). Astrocytes import extracellular cystine as a cysteine pro-substrate for GSH synthesis, and cystine is transported through system Xc-(Aoyama and Nakaki, 2015). Therefore, system Xc- has its role in the regulation of redox as well as glutamate homeostasis.

MeHg inhibited GSH precursors cystine and cysteine uptake in cortical astrocyte cell culture but not in the neurons. Comparative the transport of cystine and cysteine in cortical neurons and astrocytes during MeHg exposure reported that MeHg inhibited the uptake of these GSH precursors in cortical astrocyte cell culture but not in the neurons (Allen et al., 2001a; Shanker et al., 2001b) via the Na+-dependent transport system, i.e., the EAATs (Allen et al., 2001a; Shanker and Aschner, 2001). However, the prominant role of EAATs in astrocytes is the uptake of extracellular synaptic Glu, whereas the system Xcplays a significant role in transport cystine in astrocytes (Bridges et al., 2012b). Furthermore, the system Xc- and EAAT function in concert to regulate Glu and GSH homeostasis (Lewerenz et al., 2006). The cooperative function of these transporters is driven by the electrochemical gradients of Glu and cystine (Lewerenz et al., 2006; Bridges et al., 2012b). Overexpression of either system Xc- or EAAT3 in mouse hippocampal neuron cell line (HT22) enhanced the intracellular GSH content and increased the cell survival threshold to glutamate-induced excitotoxicity and H2O2-induced oxidative stress (Lewerenz et al., 2006). When overexpressed both system Xc- and EAAT3, these HT22 cells exhibited the highest intracellular GSH content and highest threshold of Glu induced excitotoxicity as well as were more resistant to H2O2-induced oxidative stress and increase survival rate (Lewerenz et al., 2006). It is possible that the expression of system Xc- and EAATs levels are correlated due to their cooperative function. In addition, EAAT3/EAAC1 expression is regulated by the Nrf2-ARE pathway in rat C6 glioma cells as well as mice brain (Escartin et al., 2011a). The cellular mechanisms of MeHg-induced neuronal degeneration involve the increase of synaptic transmission (Juang and Yonemura, 1975a; Atchison and Narahashi, 1982; Yuan and Atchison, 2003, 2005; Yuan and Atchison, 2007b) and extracellular Glu elevation (Juárez et al., 2002; Farina, 2003)

as well as GSH depletion. MeHg could perturb the glutamate and GSH homeostasis in the CNS by reducing the expression of these genes, subsequently contributing to the excitotoxicity-induced neuronal degeneration.

The increase of synaptic transmission and elevation of extracellular Glu following MeHg exposure also increases [Ca<sup>2+</sup>]<sub>in</sub> via the ionotropic Glu receptors such NMDARs (Ramanathan and Atchison, 2011) and AMPARs (Johnson et al., 2011). The AMPARs mediated [Ca<sup>2+</sup>]<sub>in</sub> elevation in hTgSOD1G93A derived motor neurons following MeHg exposure was diminished by the Ca<sup>2+</sup>-permeable AMPAR antagonist, 1-naphthyl acetyl spermine (NASPM) (Johnson et al., 2011). This result suggests that MeHg increases the susceptibility of MNs by enhancing Ca<sup>2+</sup> permeability through AMPARs (Johnson et al., 2011). Among the four GluR1-4 subunits of AMPAR, GluR2 possesses a role in Ca2+ impermeability as a result of RNA editing from a glutamine (Q) to arginine (R) in this subunit (Sommer et al., 1991). Therefore, the presence of GluR2 subunit combination as well as the RNA editing process in this subunit determines the Ca<sup>2+</sup>-impermeability of AMPAR (Sommer et al., 1991; Vandenberghe et al., 2000; Wright and Vissel, 2012). Motor neurons are susceptible to toxicity because they have a high number of GluR2lacking AMPA receptors leading to intracellular calcium increases (Laslo et al., 2001; Mennini et al., 2002; Van Damme et al., 2002; Corona and Tapia, 2007). The regulation of GluR2 subunit expression in motor neurons is attributed by regional-specific astrocytes (Van Damme et al., 2007). The presence of SOD1 mutation in astrocytes suppressed the regulation of GluR2 expression in motor neurons (Van Damme et al., 2007). It has also been suggested that VEGF regulates GluR2 expression and reduction of Ca2+influx in motor neurons (Bogaert et al., 2010). These lines of evidence led me to hypothesize that

MeHg could perturb the expression of *Vegf* in SCAs, which later contributes to the reduction of GluR2 subunit expression in SMN. Consequently, Glumediated AMPAR activation and increased Ca<sup>2+</sup> permeability occur during MeHg-induced toxicity. In addition, I hypothesize that genetic impairment of the antioxidant Nrf2/ARE pathway (Nrf2 KO) alters the *Vegf* expression in this genotype, contributing to exacerbating MeHg-toxicity. The elevation of [Ca<sup>2+</sup>]<sub>in</sub> following MeHg has a significant impact on cellular metabolisms, including mitochondrial function (Denny and Atchison, 1994a; Marty and Atchison, 1997a; Limke and Atchison, 2002; Limke et al., 2004b), and ROS generation (Liu et al., 2014) that later render cells more susceptible to Glu and MeHg toxicity even if the concentration of these agents are considered non-toxic.

In this study, Nrf2 KO derived SCAs were compared with the WT genotype counterpart to determine: 1) their susceptibility to MeHg compared to the WT derived SCAs, 2) the role of Nrf2-ARE pathway in the regulation of the antioxidant genes involved in MeHg induced toxicity, 3) the effect of cooperative expression of system Xc- and EAAT1,2, and 4) the role of Nrf2 in the regulation of *Veqf* in SCAs following MeHg exposure.

## 3.3 Materials and methods

The material and method for SCAs cell culture, qPCR, and immunocytochemistry assays are described in chapter 2.3. The Nrf2 KO mice pups were generously obtained from Dr. Cheryl Rockwell's laboratory (Pharmacology and Toxicology Department, Michigan State University, East Lansing, MI).

### 3.4 Results

# 3.4.1 The susceptibility of SCAs derived from neonatal wild type C<sub>57</sub>BL/6J and Nrf2 knockout mice to MeHg

The susceptibility of SCAs to MeHg-toxicity was determined using a Real-time glow viability assay. Viability measurements were obtained every 3 h over 24 h time course to monitor the kinetics of MeHg toxicity as a function of time. The data were normalized to the vehicle control (water) for each genotype. The viability was significantly reduced in SCAs derived from Nrf2 KO mice compared to WT mice when exposed to 5µMeHg (Figure3.1). While 1h exposure to 5µMeHg did not have any effect on cell viability in WT derived SCAs, the viability of the Nrf2 KO derived SCAs was significantly reduced. The significant reduction in viability in Nrf2 KO derived SCAs continued until 18h. There was no significant difference among the genotypes at 21h and 24h, as all SCAs had died at this timepoint. The results suggest that SCAs derived from Nrf2 KO mice were more susceptible to MeHg than SCAs derived from wild type mice, indicating a potential role of or the Nrf2 pathway in cell toxicity.

# 3.4.2 MeHg exposure reduces *Nrf2* mRNA expression in both WT and Nrf2 KO derived SCAs but has differential effects on *Keap1* mRNA in these genotypes.

I next determined if MeHg reduces Nrf2 mRNA expression and/or affects the Nrf2 negative modulator, Keap1 mRNA using the gene expression assay comparing wild type and Nrf2 KO derived SCAs. There was a reduction of *Nrf2* mRNA in Nrf2 KO derived SCAs (about 0.6-fold decrease) when compared to the WT derived SCAs control treatment (Figure 3.2). MeHg reduced *Nrf2* mRNA by about 32% (0.32-fold decrease) in wild type

and 24% (0.24-fold decrease) in Nrf2 KO when compared to the control in the respective genotype (Table 3.1). The expression of *Nrf2* mRNA in Nrf2KO derived SCAs was significantly 43% lower (0.43-fold decrease) compared to the WT derived SCAs with MeHg treatment. Due to the reduction of *Nrf2* mRNA in Nrf2 KO, this rendered Nrf2 KO derived SCAs more susceptible to MeHg than the WT derived SCAs.

The Nrf2 negative modulator Keap1 plays a critical role in redox homeostasis in cells. Keap1 negatively regulates antioxidant gene expression by binding to Nrf2 and undergoes proteasome degradation to maintain the antioxidant level. Interestingly, the expression of *Keap1* mRNA from Nrf2 KO derived SCAs was 3.2-times higher than the wild type SCAs (3.2-fold increase) (**Figure 3.3**). These results suggest that both a reduction in Nrf2 mRNA and a higher basal level of *Keap1* mRNA contributed to the susceptibility of Nrf2 KO derived SCAs to MeHg. MeHg significantly reduced Keap1 mRNA (0.26-fold decrease) in Nrf2 KO derived SCAs compared to its genotype treated vehicle. In contrast, Keap1 mRNA was not significantly affected by MeHg exposure in WT derived SCAs (p=0.0594). The differential effects of MeHg to Keap1 mRNA expression in WT and Nrf2 KO derived SCAs could explain the greater susceptibility of Nrf2 KO derived SCAs.

# 3.4.3 MeHg reduces *Gclc*, *GPx1*, and *GPx4* mRNA expression in both WT and Nrf2 KO derived SCAs.

Nrf2 regulates the expression of major antioxidant genes such as glutathione (GSH) synthesizing enzymes glutamate-cysteine ligase catalytic subunit enzyme (Gclc) and GSH peroxidase (GPx). To determine if MeHg interferes with the Nrf2-ARE pathway and subsequent expression of *Gclc*, *GPX1* and *GPX4*, *I measured* mRNA levels in WT and Nrf2 KO derived SCAs.

The expression of *Gclc* mRNA level was about 1.5- times lower in Nrf2 KO SCAs when compared to WT SCAs (**Figure 3.4**) as expected. Expression of *Gclc* mRNA levels from both WT and Nrf2 KO derived SCAs were significantly reduced following 18 h of 5µM MeHg exposure (0.58-fold decrease and 0.24-fold decrease, respectively) compared to its vehicle treatment. The level of *Gclc* mRNA expression from Nrf2 KO derived SCAs following 18h of 5µM MeHg exposure was significantly lower by about 3.6 times WT *Gclc* mRNA (0.25-fold decrease). MeHg exposure contributed to a significant reduction of *Gclc* mRNA expression in both WT (1.72 lower than its vehicle treatment) and Nrf2 KO (4.1-times lower than its vehicle treatment). The greater effect of MeHg on *Gclc* expression in Nrf2 KO derived SCAs could contribute to the greater sensitivity to MeHg exposure in Nrf2 KO derived SCAs. The reduction of *Gclc* mRNA expression could later contribute to the reduction of *de novo* GSH synthesis in SCAs during MeHg exposure. Consequently, the imbalance of redox homeostasis would contribute to SCAs death.

In the brain, glutathione peroxidase (GPx) enzymes are expressed in both neurons and astrocytes. Both *GPx1* and *GPx4* mRNAs from both WT SCAs and Nrf2 KO SCAs were down-regulated following MeHg exposure (**Figure 3.5 for** *GPx1* **and Figure 3.6 for** *GPx4*). Similar to *Gclc* mRNA expression in Nrf2 KO derived SCAs, *Gpx1* and *Gpx4* mRNAs were significantly down-regulated in this genotype when compared to WT control (1.5- time and 1.47-time lower, respectively). These data suggested that deletion of the Nrf2 gene affected its downstream regulatory gene expression, including Gclc, *Gpx1*, and *Gpx4*. Therefore, the reduction of these antioxidant genes expression could contribute to Nrf2 KO derived SCAs susceptible to MeHg toxicity.

3.4.4 Nrf2 KO derived SCAs express *Abcc1* mRNA to a greater extent than the WT derived SCAs; however, a greater *Abcc1* mRNA expression did not provide greater resistance to MeHg than the WT.

To reduce xenobiotic compounds such as MeHg in cells, the transporter called multidrug-resistant associated protein (Mrp) plays an essential role in export MeHg through the covalent bonding with GSH. Mrp1 is one of multidrug-resistant transporter in the central nervous system. It is encoded by *Abcc1* mRNA by the regulation of Nrf2. Surprisingly, the *Abcc1* mRNA expression level in Nrf2 KO was 2.3- time greater than WT SCAs (**Figure 3.7**) as opposed to diminishing its expression level. This result suggests a compensatory expression of antioxidant genes (detoxification mechanisms) in Nrf2 KO mice. Indeed, both WT and Nrf2 KO SCAs *Abcc1* mRNA was reduced following 18h of 5µM MeHg exposure. This reduction of *Abcc1* mRNA in Nrf2 KO following MeHg exposure was greater than WT *Abcc1* mRNA. This significant reduction of *Abcc1* in Nrf2 KO SCAs could suggest the susceptibility to MeHg in Nrf2 KO partly due to the greater effect of MeHg to a reduction of *Abcc1* mRNA expression than that in the WT derived SCAs. The lower of *Abcc1* mRNA expression could contribute to lower expression of Mrp1, subsequently, reduce the export of MeHg from SCAs.

3.4.5 Nrf2 KO derived SCAs expressed *Slc7a11* mRNA greater than the WT derived SCAs, and MeHg affected *Slc7a11* mRNA expression in these genotypes differently.

In addition to GSH synthesis pathways, the cystine/glutamate antiporter (a.k.a. system Xc-) is regulated by Nrf2 (Habib et al., 2015) to induce its *Slc7a11* gene. System Xc-imports the amino acid cystine, the oxidized form of cysteine, in exchange to the export

of glutamate with 1:1 ratio. MeHg induced toxicity involves both glutamate-induced excitotoxicity and a reduction of intracellular GSH. Therefore, the expression of system Xc- could involve in the dysregulation of [Glu]<sub>ex</sub> and *de novo* GSH synthesis. Surprisingly, SCAs derived from Nrf2 KO mice exhibited an increase of Slc7a11 mRNA expression compared to WT derived SCAs (**Figure 3.8**). The increase of *Slc7a11* mRNA could be a compensatory response from Nrf2 gene deletion because in most tissues, cysteine is a rate limiting substrate for GSH synthesis and cysteine is transported in its oxidized form via system xc- (Lewerenz et al., 2006). The increase of Slc7a11 mRNA in Nrf2 KO mice may enhance the transport of cysteine for de novo GSH synthesis in a system that lacks a master regulator of antioxidant pathway, i.e., Nrf2. Interestingly, following 5µM MeHg exposure for 18h, WT derived SCAs expressed Slc7a11 mRNA 5.3-times higher than the WT SCAs treated with vehicle. Conversely, the expression of Slc7a11 mRNA in Nrf2 KO derived SCAs was reduced (about 2.6 lower but statistical insignificance) relative to its genotype treated with vehicle. When comparing the effect of MeHg on WT- and Nrf2 KO derived SCAs, the expression level of *Slc7a11* mRNA in WT derived SCAs was significantly higher (about 4.0-higher) than that in the Nrf2 KO derived SCAs. The different responses between WT and Nrf2 KO derived SCAs to MeHg in the induction of Slc7a11 mRNA could suggest different signaling pathways may contribute to these differential responses.

3.4.6 Nrf2 KO derived SCAs exhibit higher basal levels of *Slc1a3* and *Slc1a2* mRNAs relative to WT derived SCAs and MeHg reduces the mRNA expression in both WT and Nrf2 KO derived SCAs.

A mechanism of MeHg toxicity is the induction of [Glu]<sub>ex</sub> elevation as well as inhibition of EAAT1/GLAST and EAAT2/GLT-1 function. The elevation of [Glu]<sub>ex</sub> could not only be due to the dysfunctional EAATs but also the level of their expression. The reduction of Slc1a3 and Slc1a2 mRNA could reflect the ability of SCAs in [Glu]<sub>ex</sub> clearance during MeHg exposure. It has also been reported that the Keap1-Nrf2-ARE pathway regulated EAAT3 expression in neurons and rat C6 glioma cells (Escartin et al., 2011a). To further analyze if the Keap1-Nrf2-ARE pathway also regulates the expression of EAAT1 and EAAT2 transcripts, Slc1a3 and Slc1a2 mRNA expression levels were compared between WT and Nrf2 KO derived SCAs. Surprisingly, both basal Slc1a3 and Slc1a2 mRNA expression level were higher in Nrf2 KO derived SCAs than in WT derived SCAs. The Nrf2 KO derived SCAs exhibited the basal level of *Slc1a3* mRNA was 4.0- higher (**Figure 3.9**) and Slc1a2 mRNA was 1.9- higher (Figure 3.10) than that in the WT derived SCAs. However, following 5µM MeHg exposure for 18h, the expression of *Slc1a2* mRNA in both WT and Nrf2 KO derived SCAs were reduced from their genotype control treated with vehicle (**Figure 3.10**). MeHg induced the reduction of the *Slc1a1* mRNA expression in Nrf2 derived SCAs while it slightly diminished Slc1a1 mRNA expression in WT derived SCAs (**Figure 3.9**). In summary, the basal levels of *Slc1a1* and *Slc1a2* mRNAs in Nrf2 KO derived SCAs were significantly higher than the WT derived SCAs. MeHg slightly affected to Slc1a1 mRNA expression in WT derived SCAs but did so in the reduction of Slc1a2 mRNA expressions in both WT and Nrf2 derived SCAs.

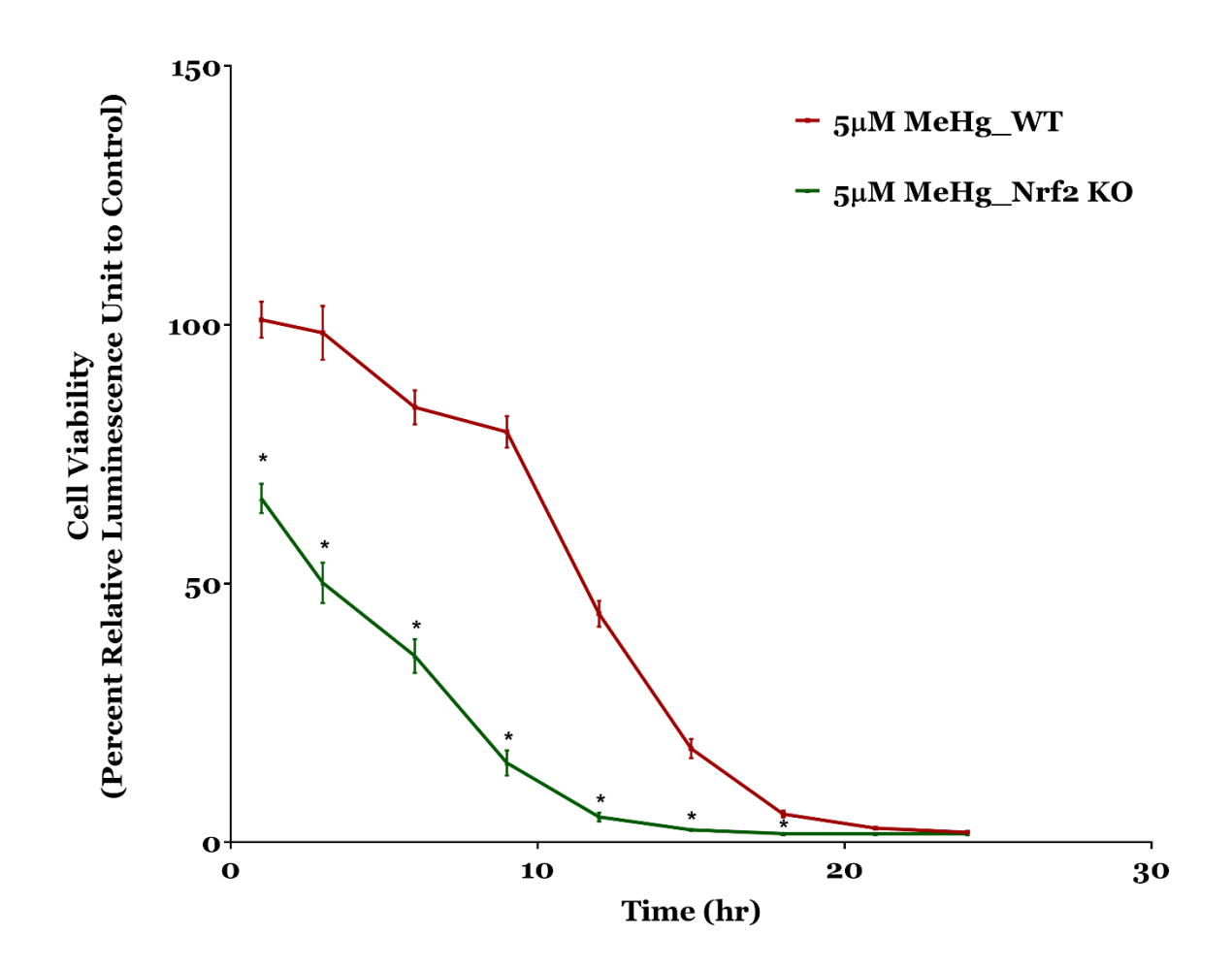
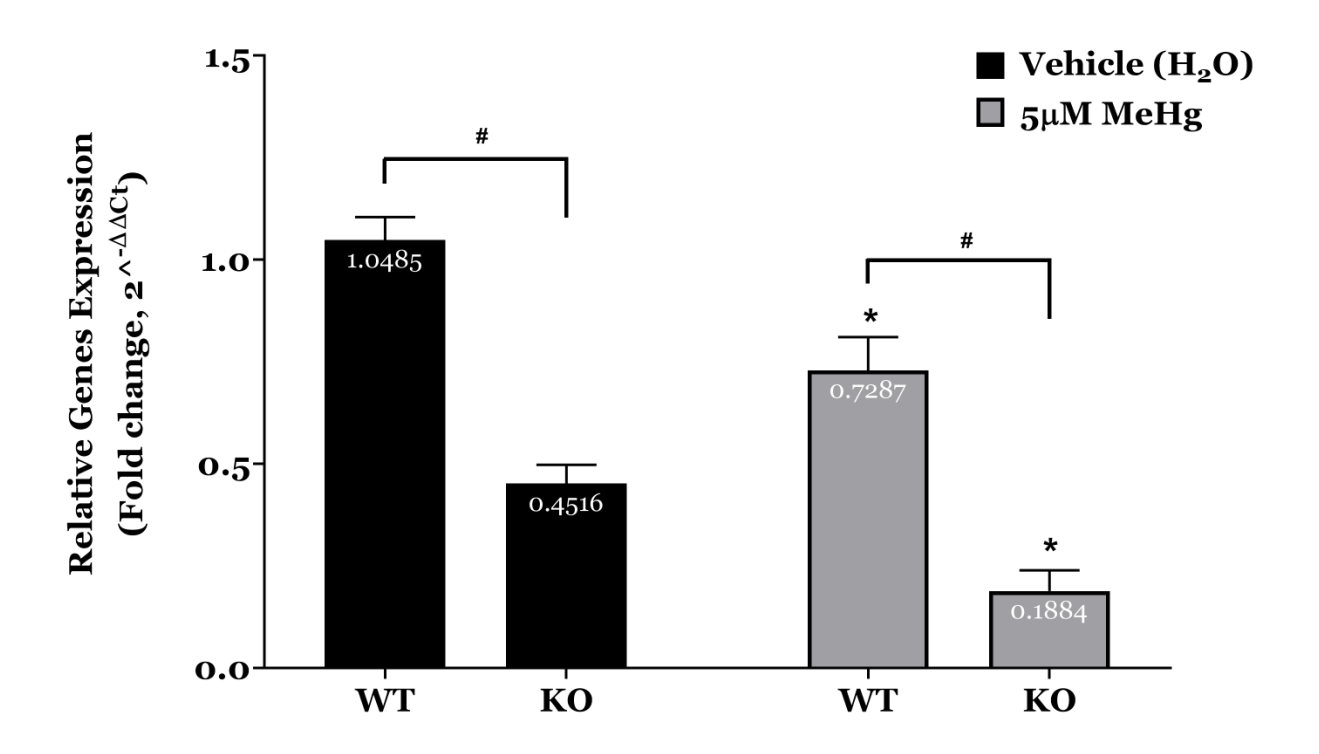
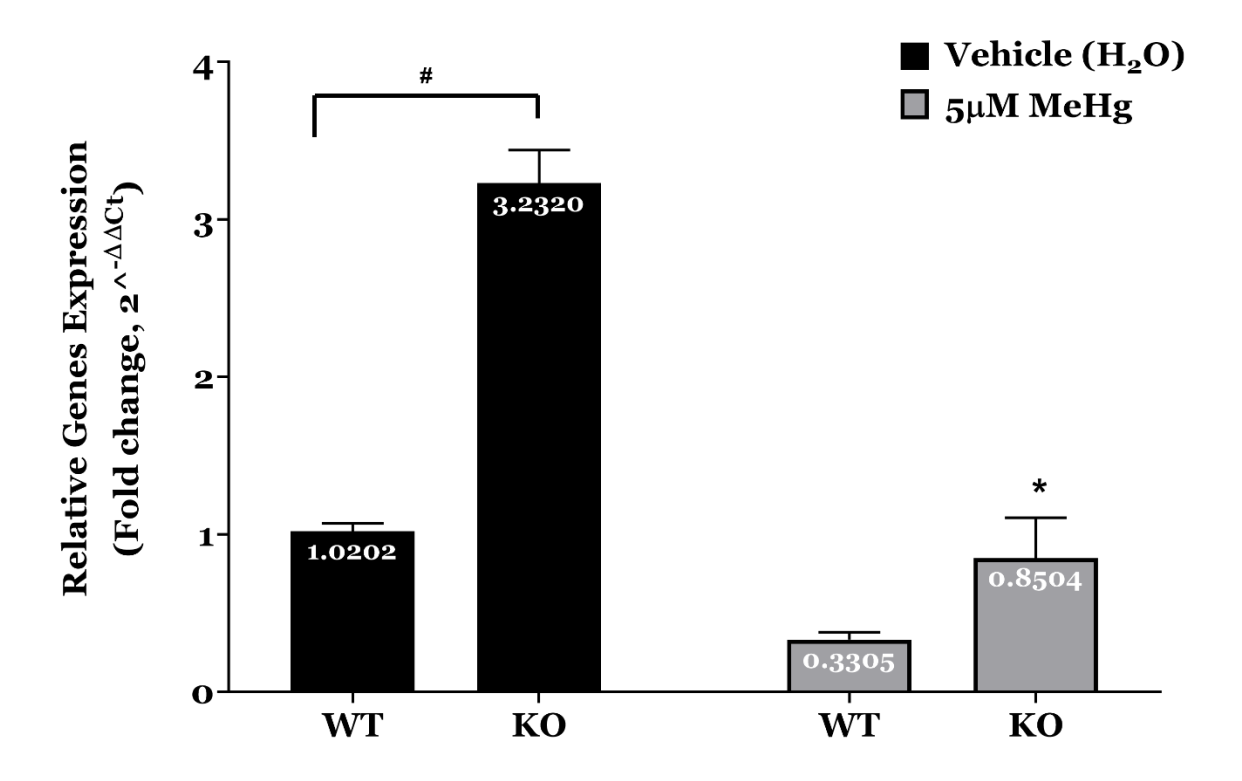


Figure 3.1 Comparison of the susceptibility of DIV 30 SCAs to MeHg between SCAs derived from wild type C57BL/6J mice pups and Nrf2 knockout mice pups. SCAs were exposed to 5μM MeHg over 24h time course. Real-time viability assays were employed to monitor the kinetic of MeHg-toxicity as a function of time. Each data was normalized to its control (vehicle) treatment. The results suggest SCAs derived from Nrf2 KO ( — , green line) were more susceptible to MeHg than SCAs derived from wild type ( — , red line). Two-Way ANOVA with Sidak multiple comparison *post hoc* indicating SCAs derived from Nrf2 KO showed a significant reduction of cell viability greater than SCAs derived from WT starting from 1h MeHg exposure. (\* indicates p<0.05 when compared to WT) N=24 biological replications with four independent experimental studies.



**Figure 3.2 Relative mRNA expression of** *Nrf2* **mRNA derived from wild type SCAs (WT) and Nrf2-KO SCAs (KO) when exposed to 5μM MeHg for 18h.** Nrf2-KO SCAs expressed *Nrf2* mRNA about 0.57-fold decrease relative to wild type SCAs. Expression levels of Nrf2 mRNA from both WT and Nrf2 KO compared to its vehicle treatment were significantly reduced following 18 h of 5μM MeHg exposure with about 0.30-fold and 0.58-fold decrease, respectively. When compared among different genotypes, following 5μM MeHg exposure, the level of Nrf2 mRNA from Nrf2 KO was lower than WT Nrf2 mRNA, about 0.74-fold decrease. The statistical analysis was derived from Two-Way ANOVA with Tukey's multiple comparison *post hoc.* (\* indicates p<0.05 when compared to vehicle (control) treatment from the same genotype, # indicates p<0.05 when compare between different genotypes; WT vs. KO); N=12 biological replications with 2 replications/N



**Figure 3.3 Relative mRNA expression of** *Keap1* **mRNA derived from wild type SCAs (WT) and Nrf2-KO SCAs (KO) when exposed to 5μM MeHg for 18h.** Nrf2-KO SCAs expressed *Keap1* mRNA about 3.1- fold increase relative to wild type SCAs. MeHg did not affect *Keap1* mRNA in WT SCAs; however, it caused a significant reduction of *Keap1* mRNA expression in Nrf2 KO SCAs, about a 0.74-fold decrease compared to its genotype control. The statistical analysis was derived from Two-Way ANOVA with Tukey's multiple comparison *post hoc.* (\* indicates p<0.05 when compared to vehicle (control) treatment from the same genotype, # indicates p<0.05 when compare between different genotypes; WT vs. KO); N=12 biological replications with two replications/N

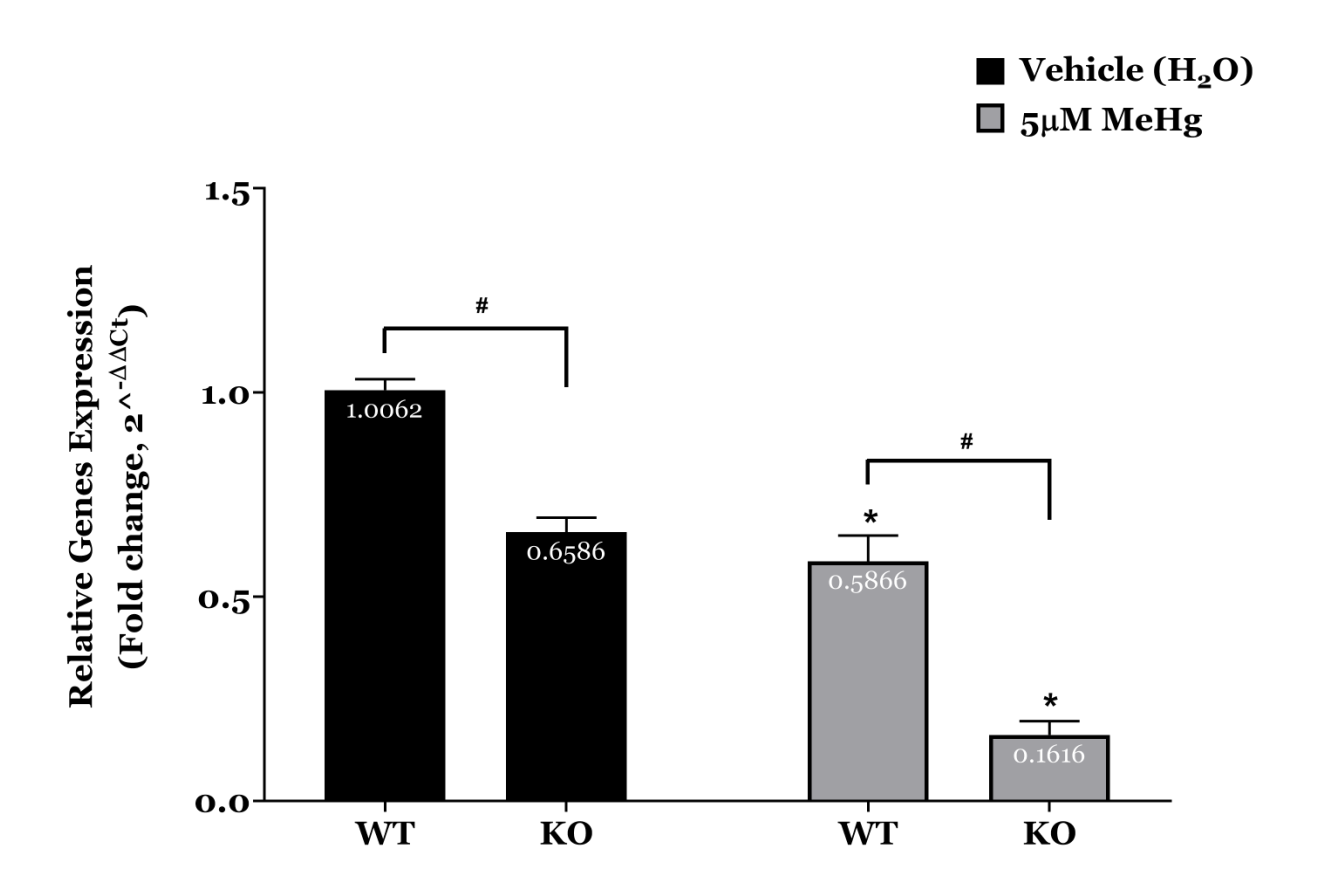


**Figure 3.4 Relative mRNA expression of** *Gclc* **mRNA derived from wild type SCAs (WT) and Nrf2-KO SCAs (KO) when exposed to 5μM MeHg for 18h.** Nrf2-KO SCAs expressed *Gclc* mRNA about 0.34-fold decrease relative to wild type SCAs. Expression levels of *Gclc* mRNA from both WT and Nrf2 KO compared to its vehicle treatment were significant reduced following 18 h of 5μM MeHg exposure. MeHg caused a significant reduction of Gclc mRNA expression in WT SCAs (0.42-fold decrease) and Nrf2 KO (0.75-fold decrease). When comparing the effect of MeHg between these genotypes, *Gclc* mRNA expression from Nrf2 KO is lower than WT SCAs with about 0.72-fold decrease. The statistical analysis was derived from Two-Way ANOVA with Tukey's multiple comparison *post hoc.* (\* indicates p<0.05 when compared to vehicle (control) treatment from the same genotype, # indicates p<0.05 when compare between different genotypes; WT vs. KO); N=12 biological replications with two replications/N

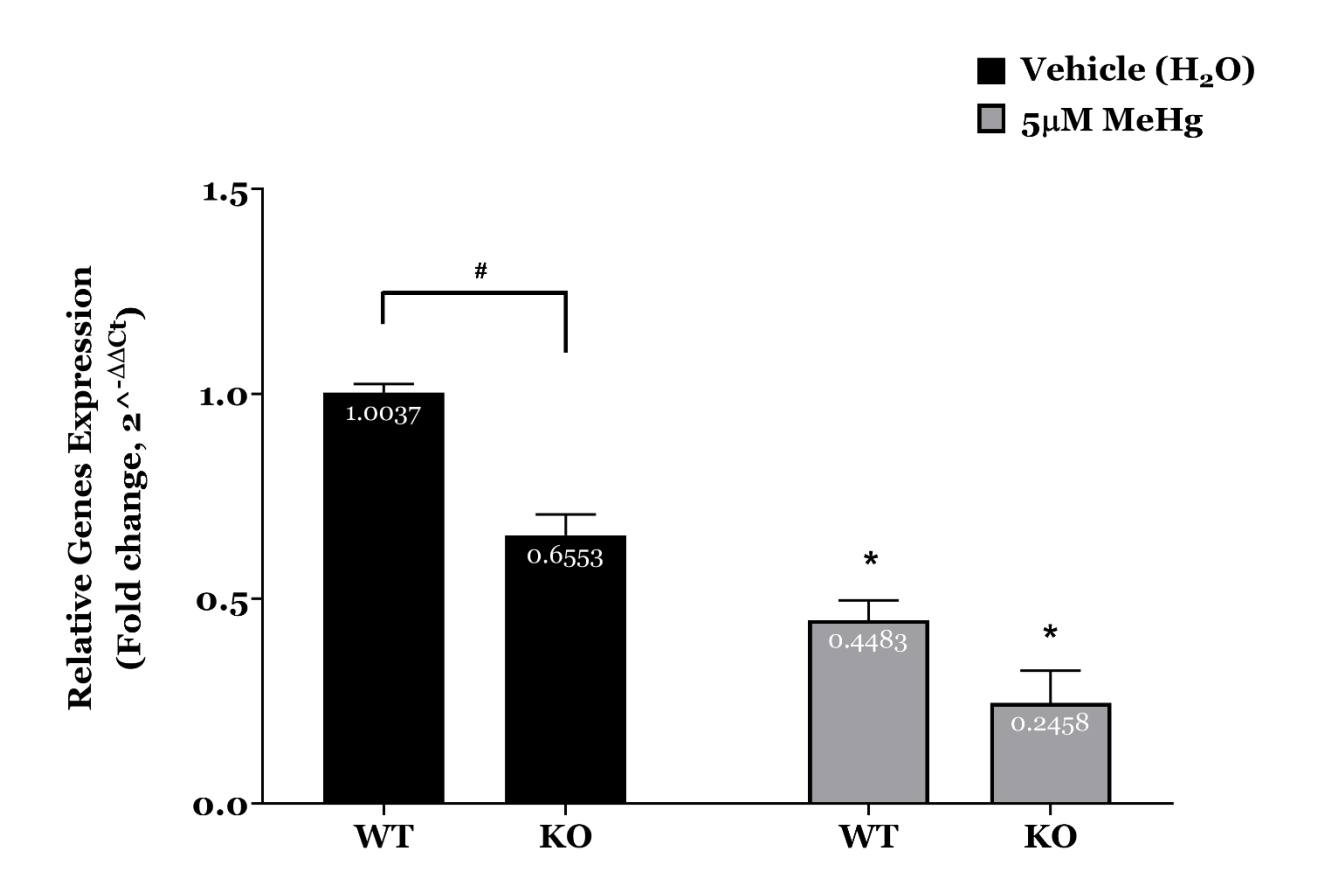


**Figure 3.5 Relative mRNA expression of** *GPx1* **mRNA derived from wild type SCAs (WT) and Nrf2-KO SCAs (KO) when exposed to 5μM MeHg for 18h.** Nrf2-KO SCAs expressed *GPx1* mRNA about 0.35-fold decrease relative to wild type SCAs. Expression levels of *GPx1* mRNA from both WT and Nrf2 KO compare to its vehicle treatment were significant reduced following 18 h of 5μM MeHg exposure (0.55-fold and 0.62-fold decrease, respectively). The statistical analysis was derived from Two-Way ANOVA with Tukey's multiple comparison *post hoc.* (\* indicates p<0.05 when compared to vehicle (control) treatment from the same genotype, # indicates p<0.05 when compare between different genotypes; WT vs. KO); N=12 biological replications with 2 replications/N

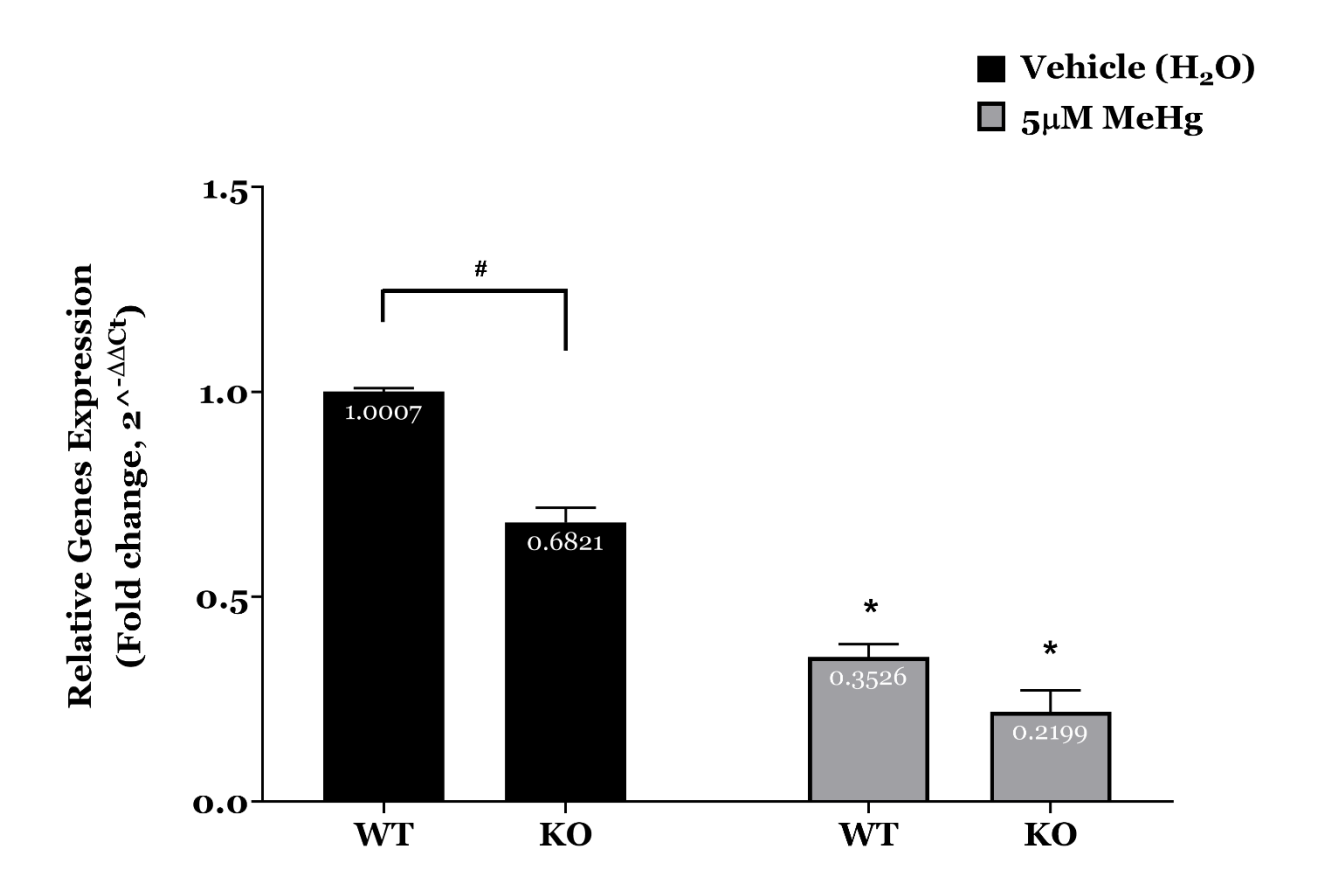


**Figure 3.6 Relative mRNA expression of** *GPx4* mRNA derived from wild type SCAs (WT) and Nrf2-KO SCAs (KO) when exposed to 5μM MeHg for 18h. Nrf2-KO SCAs expressed *GPx4* mRNA about 0.32-fold decrease relative to wild type SCAs. Expression levels of *GPx4* mRNA from both WT and Nrf2 KO compare to its vehicle treatment were significant reduced following 18 h of 5μM MeHg exposure (0.65-fold and 0.67-fold decrease). Following 18h of MeHg exposure, no significant differences among these genotypes were observed. The statistical analysis was derived from Two-Way ANOVA with Tukey's multiple comparison *post hoc*. (\* indicates p<0.05 when compared to vehicle (control) treatment from the same genotype, # indicates p<0.05 when compare between different genotypes; WT vs. KO); N=12 biological replications with 2 replications/N

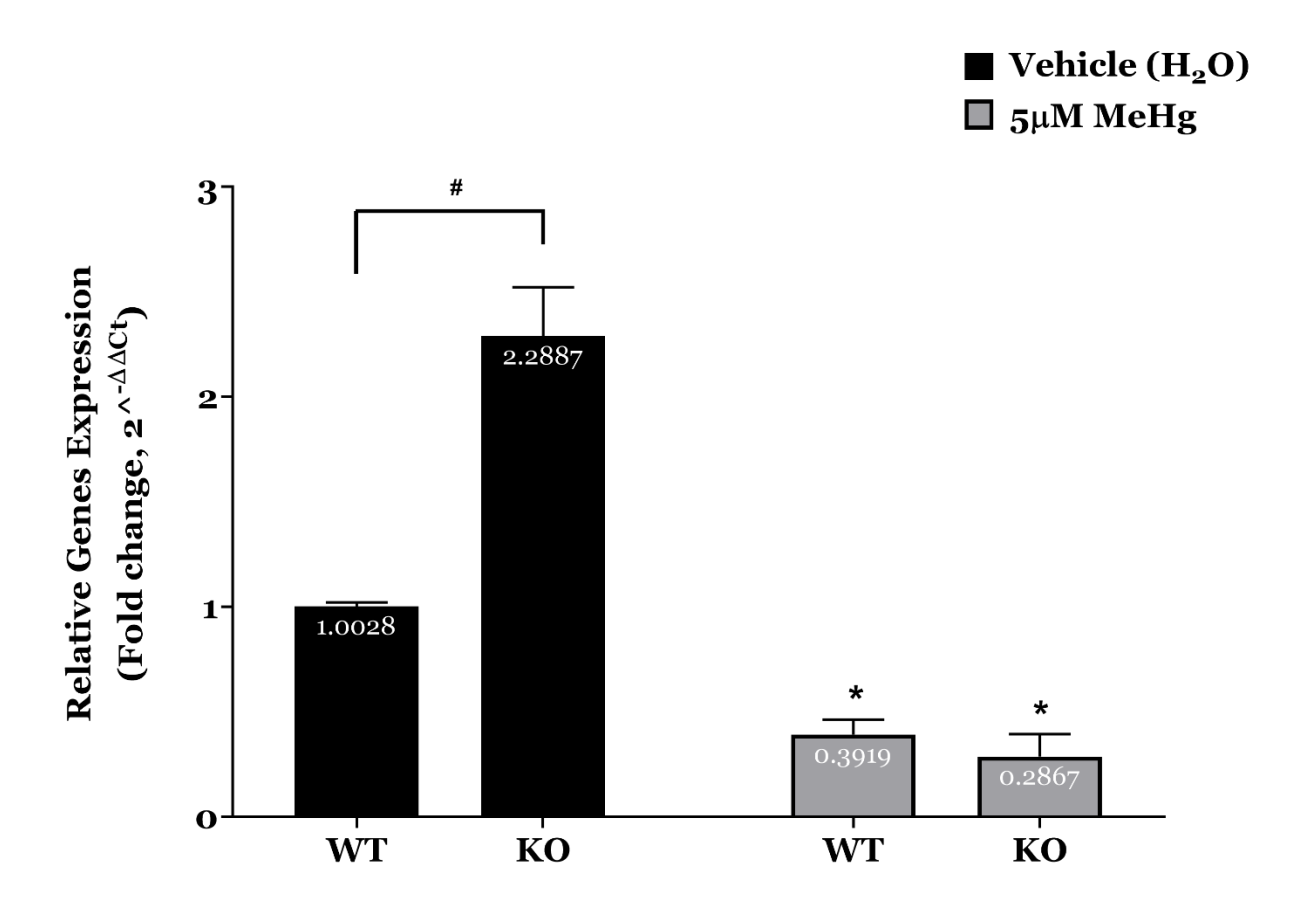
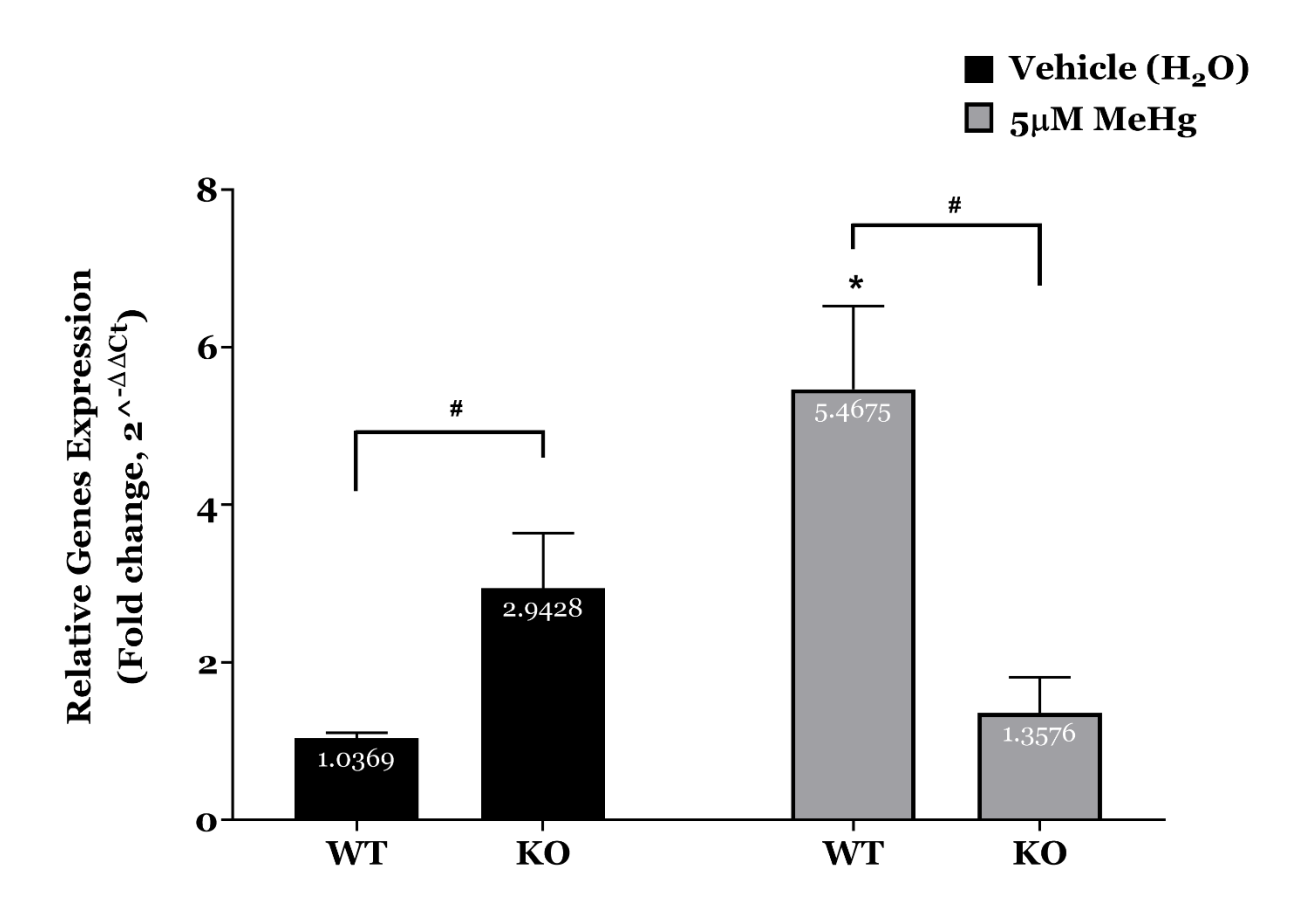
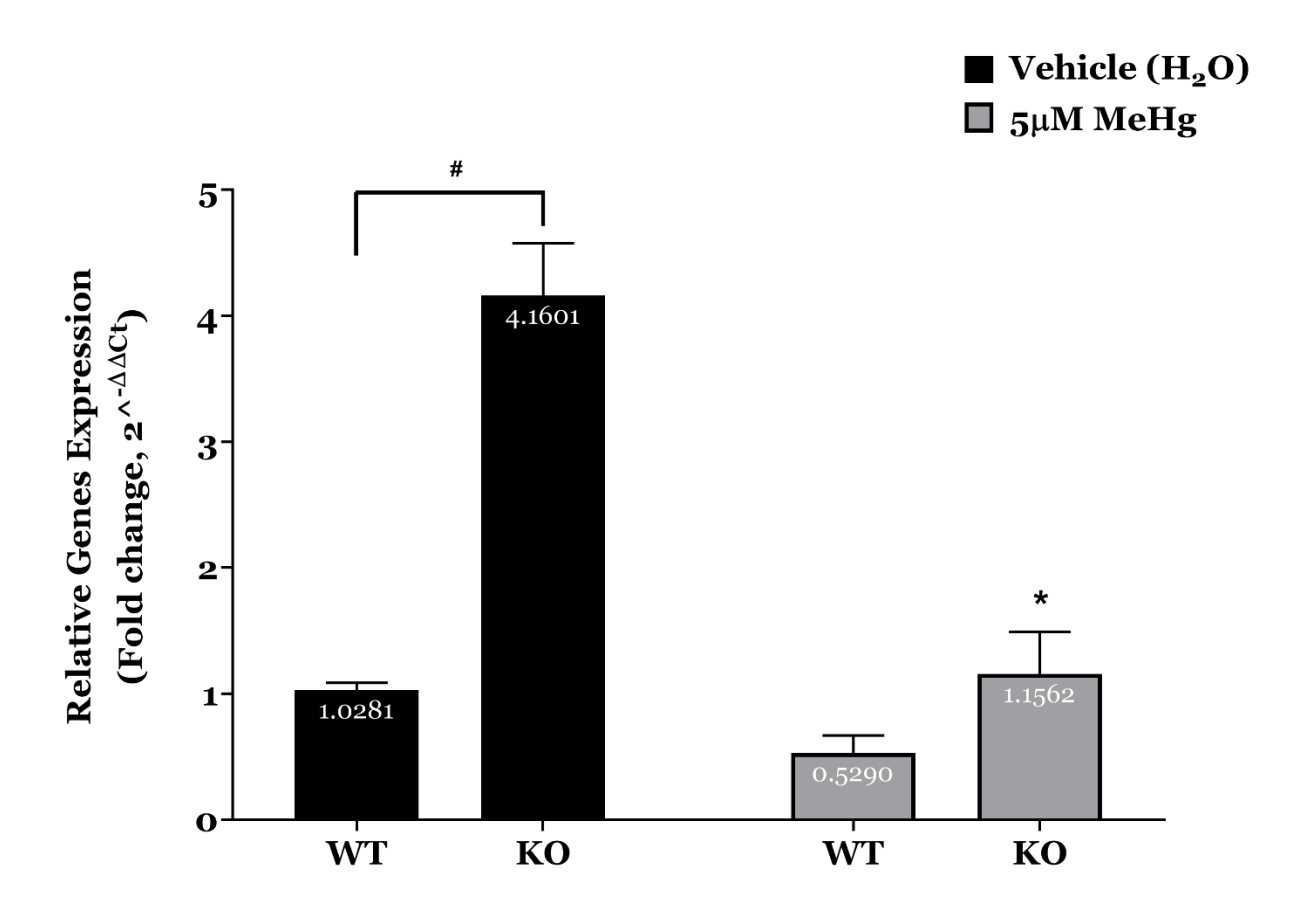


Figure 3.7 Relative mRNA expression of *Abcc1* mRNA derived from wild type SCAs (WT) and Nrf2-KO SCAs (KO) when exposed to 5μM MeHg for 18h. Interestingly, Nrf2-KO SCAs expressed *Abcc1c* mRNA about 2.3 – fold increase relative to wild type SCAs. Expression levels of *Abcc1* mRNA from both WT and Nrf2 KO compared to its vehicle treatment were significantly reduced following 18 h of 5μM MeHg exposure with 0.61-fold and 0.87-fold decrease, respectively. There was no statistical difference among different genotypes following 5μM MeHg exposure for 18h. The statistical analysis was derived from Two-Way ANOVA with Tukey's multiple comparison *post hoc.* (\* indicates p<0.05 when compared to vehicle (control) treatment from the same genotype, # indicates p<0.05 when compare between different genotypes; WT vs. KO); N=12 biological replications with two replications/N



**Figure 3.8 Relative mRNA expression of** *Slc7a11* **mRNA derived from wild type SCAs (WT) and Nrf2-KO SCAs (KO) when exposed to 5μM MeHg for 18h.** Nrf2-KO SCAs expressed *Slc7a11* mRNA about 2.8-fold increase relative to wild type SCAs. Interestingly, expression levels of *Slc7a11* mRNA following 18 h of 5μM MeHg exposure from WT increased significantly about 5.3-fold increase relative to the WT vehicle treatment, while expression levels of *Slc7a11* mRNA were diminished in Nrf2 KO compared to its vehicle treatment with a 0.54-fold decrease. When compared the effect of MeHg to these genotypes, the Slc7a11 mRNA in Nrf2 KO SCAs was lower than WT treated with MeHg with a 0.75-fold decrease. The statistical analysis was derived from Two-Way ANOVA with Tukey's multiple comparison *post hoc.* (\* indicates p<0.05 when compared to vehicle (control) treatment from the same genotype, # indicates p<0.05 when compare between different genotypes; WT vs. KO); N=12 biological replications with two replications/N



**Figure 3.9 Relative mRNA expression of** *Slc1a3* **mRNA derived from wild type SCAs (WT) and Nrf2-KO SCAs (KO) when exposed to 5μM MeHg for 18h.** Interestingly, Nrf2-KO SCAs expressed *Slc1a3* mRNA about 4.45-fold increase relative to wild type SCAs. While expression levels of *Slc1a3* mRNA from both WT and Nrf2 KO compared to its vehicle treatment reduced following 18 h of 5μM MeHg exposure, the MeHg had a significant effect on Nrf2 KO on *Slc1a3* mRNA expression (about 0.72-fold decrease). The statistical analysis was derived from Two-Way ANOVA with Tukey's multiple comparison *post hoc.* (\* indicates p<0.05 when compared to vehicle (control) treatment from the same genotype, # indicates p<0.05 when compare between different genotypes; WT vs. KO); N=12 biological replications with two replications/N

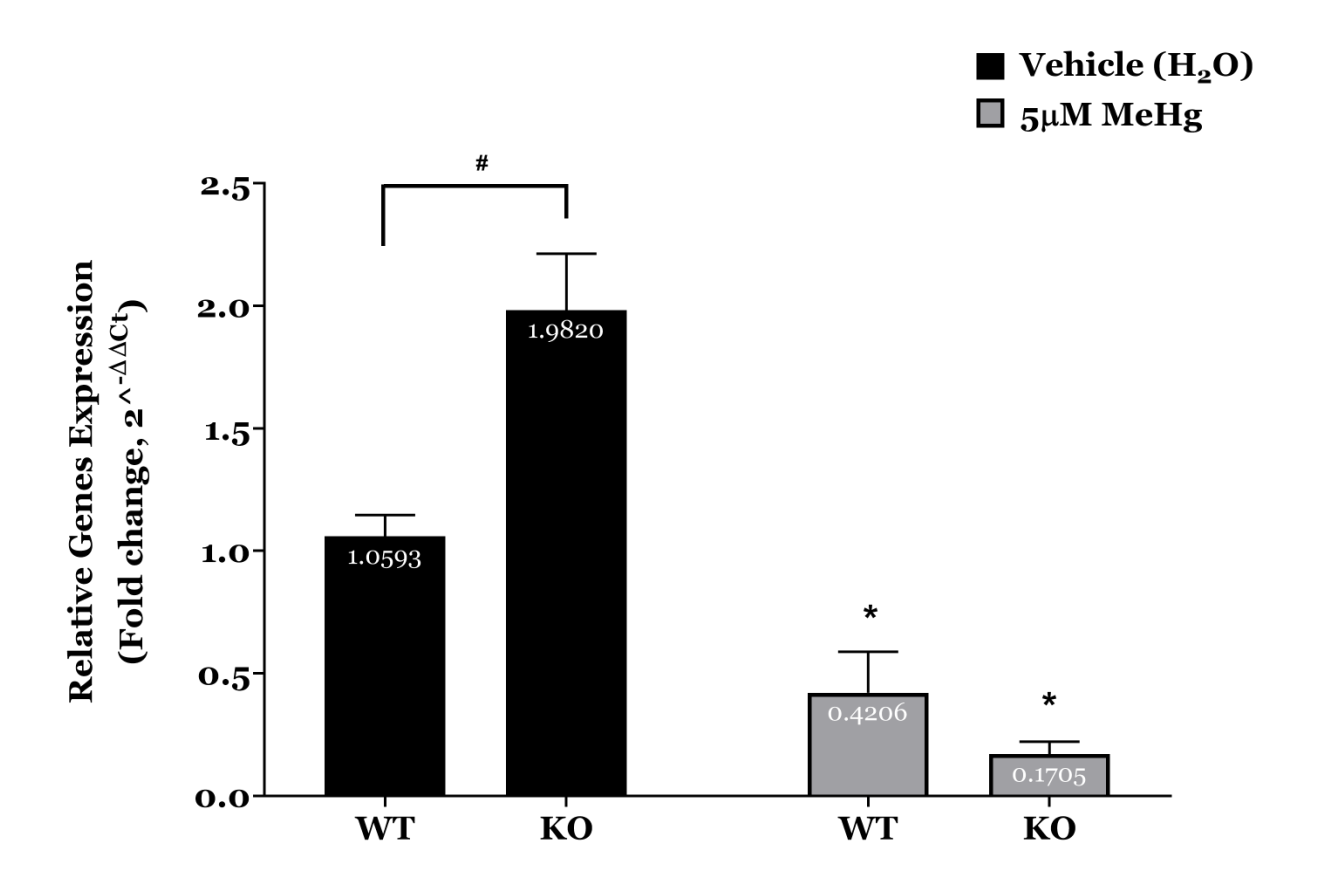


Figure 3.10 Relative mRNA expression of *Slc1a2* mRNA derived from wild type SCAs (WT) and Nrf2-KO SCAs (KO) when exposed to 5μM MeHg for 18h. Nrf2-KO SCAs expressed *Slc1a2* mRNA about 1.8-fold increase relative to wild type SCAs. Expression levels of *Slc1a2* mRNA from both WT and Nrf2 KO compared to its vehicle treatment were significantly reduced following 18 h of 5μM MeHg exposure with a 0.6-fold and a 0.91-fold decrease, respectively. The statistical analysis suggested there were no differences in expression of *Slc1a2* mRNA levels following 18h MeHg exposure among these genotypes. The statistical analysis was derived from Two-Way ANOVA with Tukey's multiple comparison *post hoc.* (\* indicates p<0.05 when compared to vehicle (control) treatment from the same genotype, # indicates p<0.05 when compare between different genotypes; WT vs KO); N=12 biological replications with two replications/N

## 3.4.7 MeHg induced the reduction of transporter proteins, Mrp1, system Xcand EAAT2/GLT-1 expression in both WT and Nrf2 KO derived SCAs.

In addition to examining the effect of MeHg on the transcriptional level of *Abcc1*, *Slc7a11* and *Slc1a2* mRNA, the protein levels of these transporters in SCAs were determined using immunocytochemistry. The fluorescent intensity of Mrp1, system Xc- and GLT-1 were diminished following 5µM MeHg exposure for 18h in both WT (Figure 3.11) and Nrf2 KO (Figure 3.12) derived SCAs relative to the vehicle treatments. The quantitative fluorescent intensity of these transporters indicated the significant reduction of the basal Mrp1, system Xc- and GLT-1 expression in Nrf2 KO derived SCAs compared to their basal expression levels in WT derived SCAs (Figure 3.13). MeHg induced the reduction of these transporter expressions significantly when compared to their genotyped with vehicle treatments (Figure 3.13 and Figure 3.14).

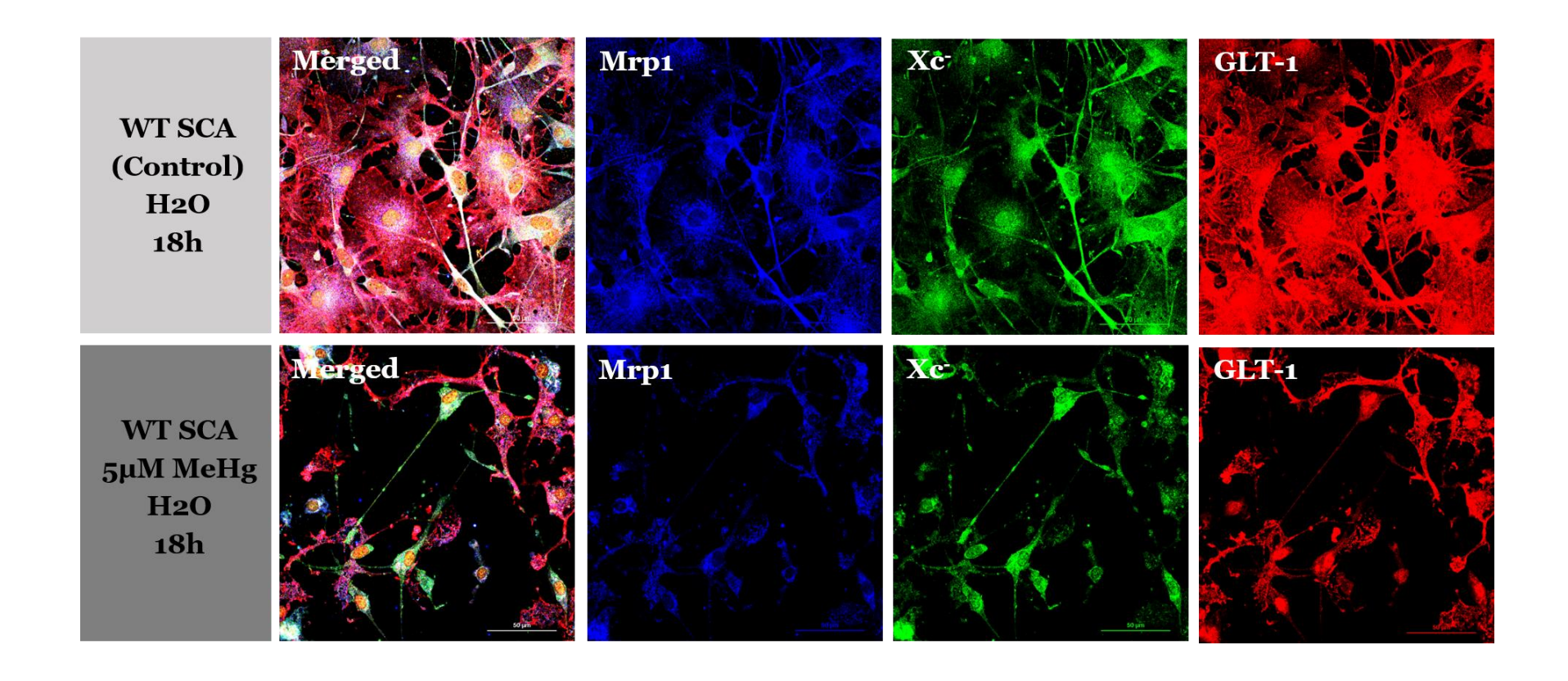


Figure 3.11 Comparative morphologies and transporter protein expressions of SCAs derived from WT following 5μM MeHg exposure for 18h. The multidrug-resistant associated proteins were labeled with Mrp1 mouse-monoclonal antibody and were detected by Alexa Fluor 647 anti-mouse. The system Xc- (cystine/glutamate antiporters) were detected using SLC7A11 rabbit-polyclonal antibody, which was observed with Alexa Flour 488 anti-rabbit. The EAAT2 were detected using anti-guinea pig glutamate transporter (GLT-1) antibody, which was determined using Alexa Flour 594 anti-guinea pig. The images were acquired from Nikon C2 confocal microscope using 60X oil objective lenses with the same exposure setting for each laser channel across all different SCAs genotypes and treatments.

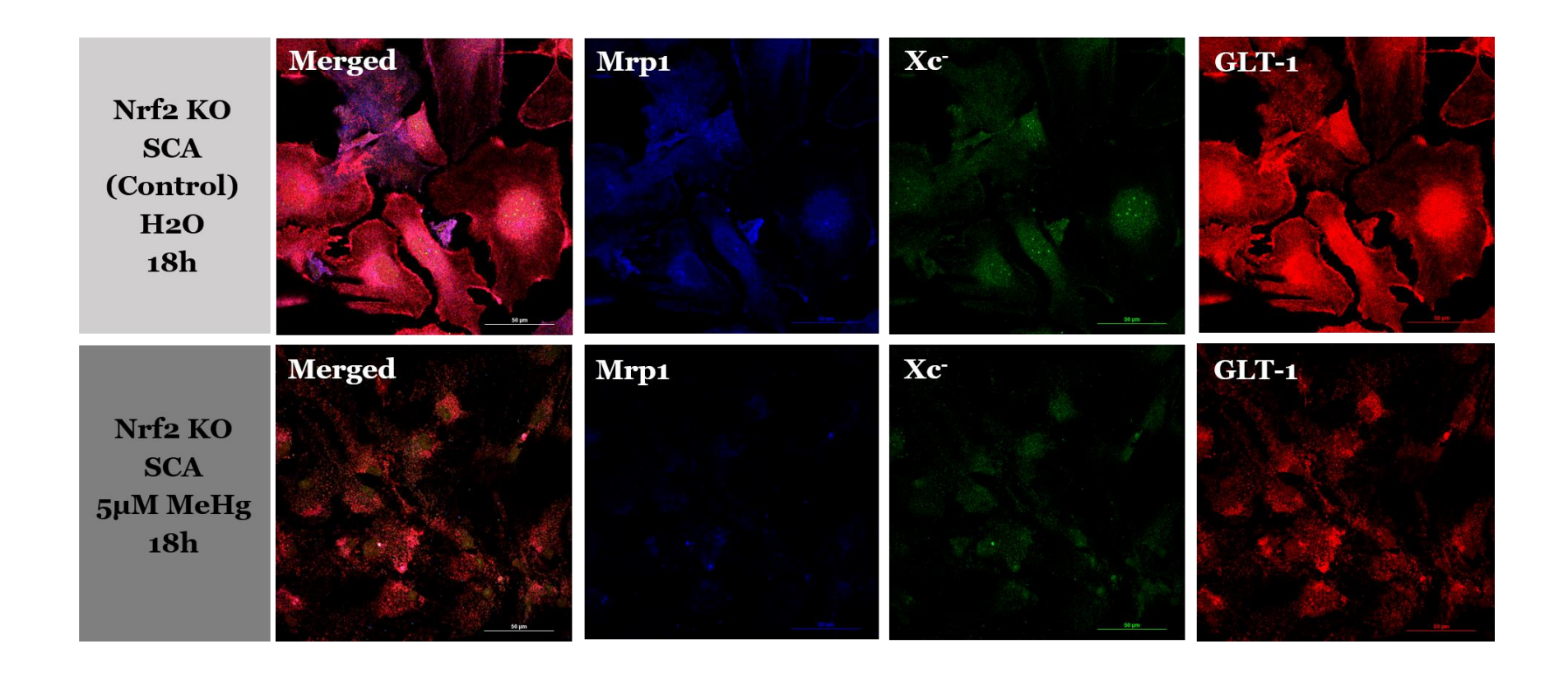


Figure 3.12 Comparative morphologies and transporter protein expressions of SCAs derived from Nrf2 KO following 5μM MeHg exposure for 18h. The multidrug-resistant associated proteins were labeled with Mrp1 mouse-monoclonal antibody and were detected by Alexa Fluor 647 anti-mouse. The system Xc- (cystine/glutamate antiporters) were detected using SLC7a11 rabbit-polyclonal antibody, which was observed with Alexa Flour 488 anti-rabbit. The EAAT2 were detected using anti-guinea pig glutamate transporter (GLT-1) antibody, which was determined using Alexa Flour 594 anti-guinea pig. The images were acquired from Nikon C2 confocal microscope using 60X oil objective lenses with the same exposure setting for each laser channel across all different SCAs genotypes and treatments.

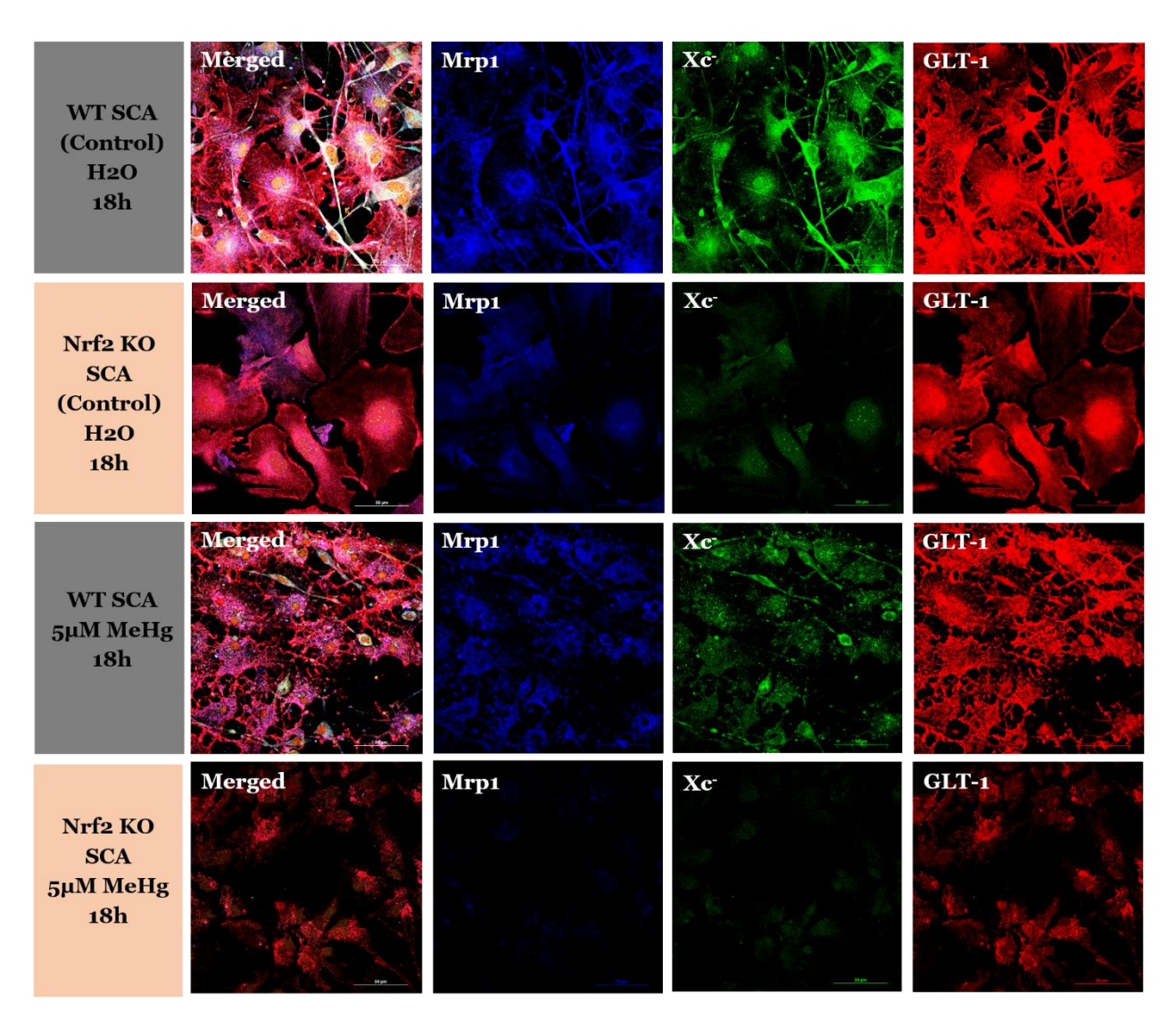


Figure 3.13 Comparative effect of 5μM MeHg to SCAs from WT and Nrf2 KO following 18h exposure. The SCAs DIV 30 were exposed to 5μM MeHg for 18h (C. and D.) compared to vehicle control treatments (A and B.) The multidrug-resistant associated proteins were labeled with Mrp1 mouse-monoclonal antibody, which was detected by anti-mouse Alexa Fluor 647 (displayed in blue as pseudocolor). The system Xc-(cystine/glutamate antiporters) were detected using rabbit-polyclonal SLC7A11 antibody, which was observed with Alexa Flour 488 anti-rabbit. The EAAT2 were detected using anti-guinea pig glutamate transporter (GLT-1) antibody, which was determined using Alexa Flour 594 anti-guinea pig. The images were acquired from Nikon C2 confocal microscope using 60X oil objective lenses with the same exposure setting for each laser channel across all different SCAs genotypes and treatments.

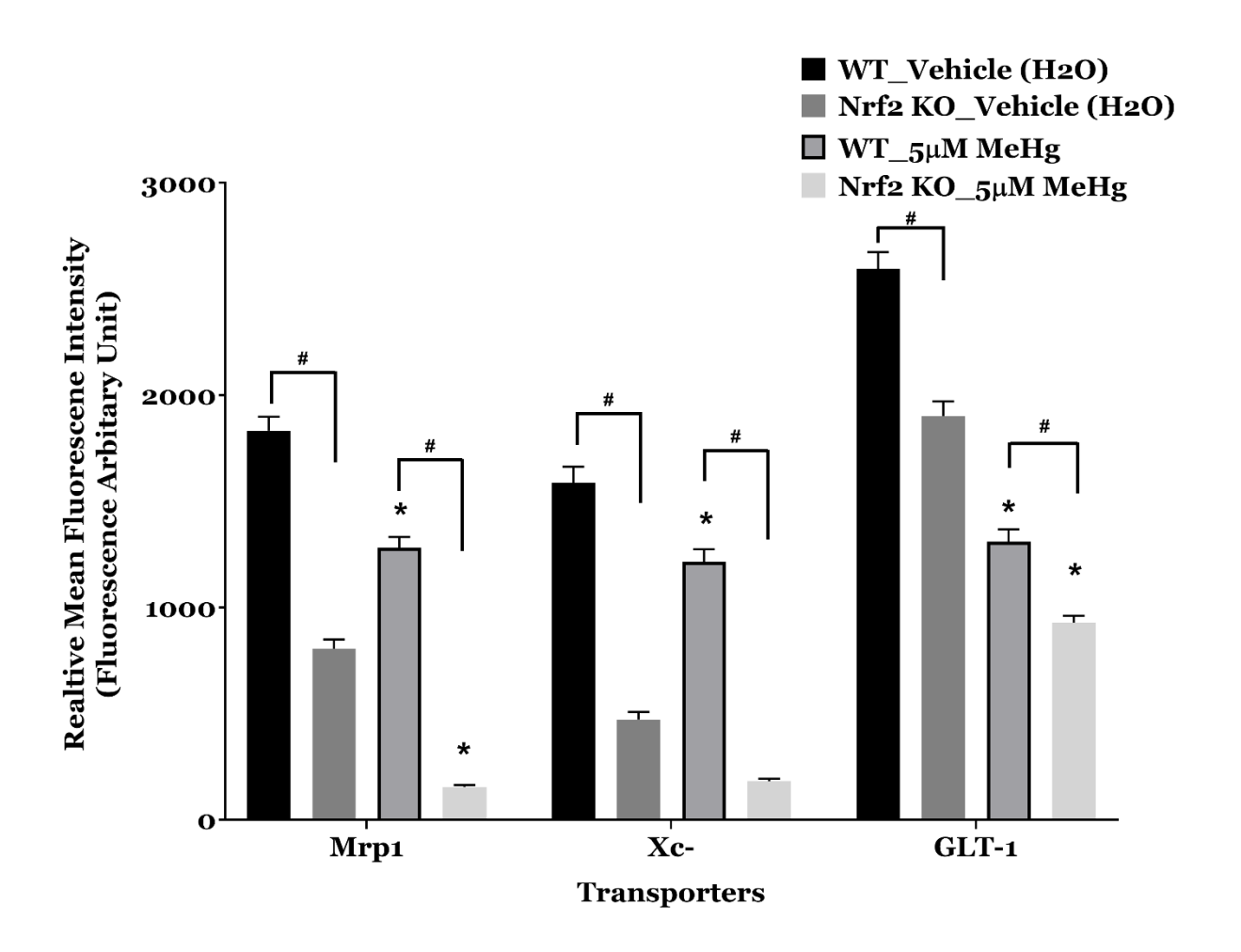
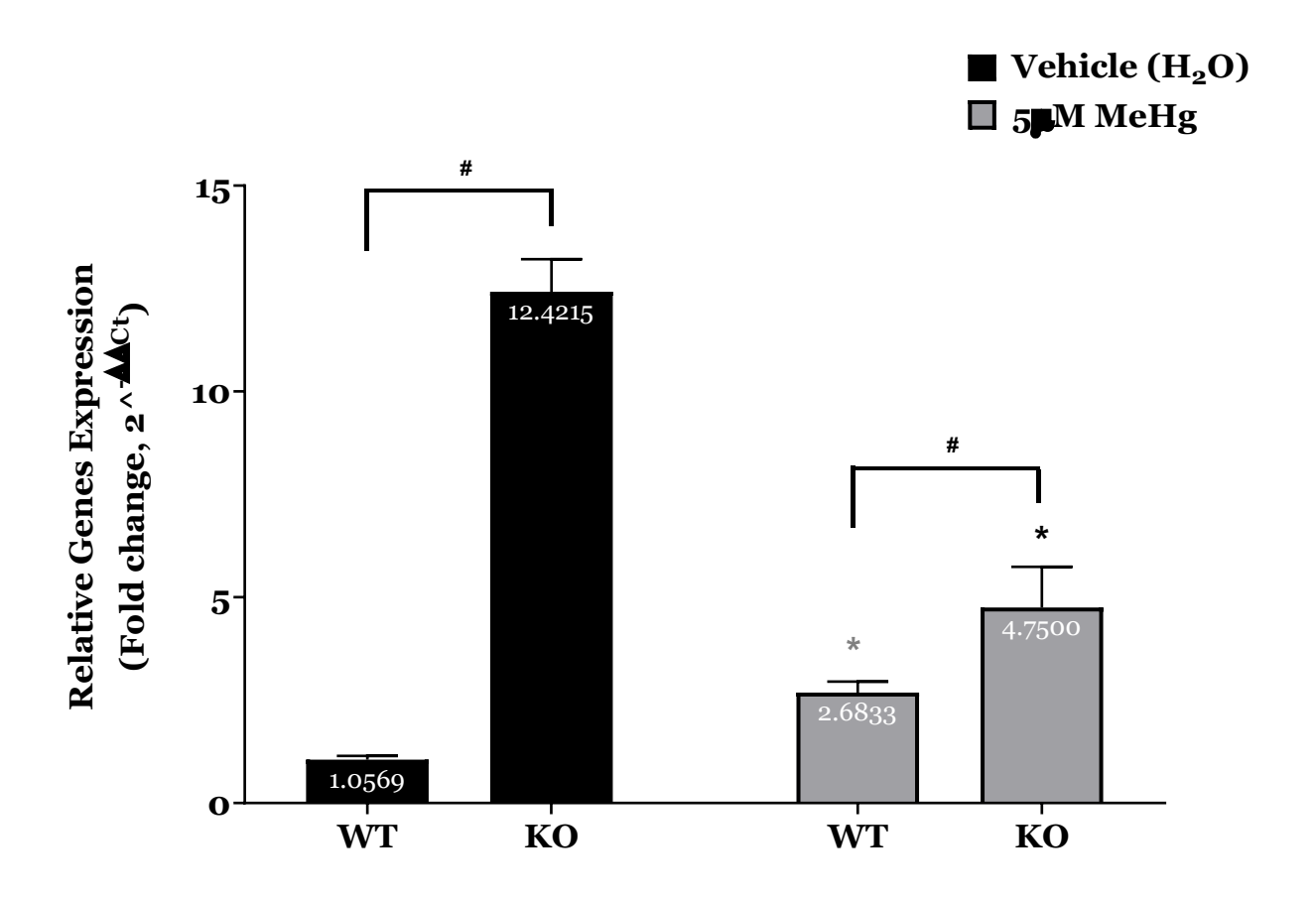


Figure 3.14 Comparative effect of 5µM MeHg to the expression of transporter proteins in SCAs derived from WT and Nrf2 KO following 18h exposure. The expression of Mrp1, system xc- and GLT-1 transporters derived from Nrf2 KO showed lower expression relative to wildtype control. When Nrf2 KO SCAs was exposed to MeHg, there were greater and significant reductions of these transporters than in the wildtype SCAs exposed to MeHg. The relative mean fluorescent intensity of SCAs DIV 30 exposed to 5µM MeHg for 18h was compared to vehicle control treatments. The relative mean multidrug-resistant fluorescent intensity of associated proteins cystine/glutamate antiporters (system Xc-), and glutamate transporter (GLT-1 or EAAT2) were determined using NIS-Element Advanced Research software from Nikon. Two-Way ANOVA with Sidak multiple comparison post hoc indicated different expression among different genotypes with #; p<0.05 and among different treatments with \*; p<0.05.

# 3.4.8 MeHg differential regulated *Vegfa* mRNA expression in WT and Nrf2 KO derived SCAs.

Since a low MeHg concentration (0.5µM) induced Vegfa upregulation in WT derived SCAs in a biphasic fashion as a function of time of MeHg exposure for 24 h (Figure 2.13) in chapter 2). However, the mechanism underlying this Vegfa expression during MeHg exposure is unknow in SCAs. To examine whether Nrf2 directly regulated Vegfa mRNA expression and whether MeHg induced the alteration of *Vegfa* expression was underlying the regulation of Nrf2 pathway, the expression levels of Vegfa mRNA were compared between WT and Nrf2 KO derived SCAs. The basal levels of Vegfa mRNA expression between WT and Nrf2 derived SCAs were different where the expression level of Vegfa mRNA in Nrf2 KO derived SCAs was about 12-time higher than WT derived SCAs (Figure 3.15). The effect of 5µM MeHg to these genotype derived SCAs are different. Whereas 18 h MeHg exposure induced Vefga mRNA in WT derived SCAs increased about 2.53-fold of WT vehicle treatment, MeHg induced Vegfa mRNA in Nrf2 derivd SCAs decreased about 2.6-fold of Nrf2 KO vehicle treatment (Figure 3.15). These results demonstrated the differential genetic background exhibited different response of Vegfa expression to MeHg.



**Figure 3.15 Relative mRNA expression of** *Vegfa* **mRNA derived from wild type SCAs (WT) and Nrf2-KO SCAs (KO) when exposed to 5μM MeHg for 18h.** Nrf2-KO SCAs pronouncedly expressed *Vegfa* mRNA, which is about an 11.75-fold increase relative to the wild type SCAs. Expression levels of *Vegfa* mRNA from WT, when treated with MeHg, were significantly increased about 2.5-fold increase compared to WT control treatment. Conversely, the expression of *Vegfa* mRNA from Nrf2 KO SCAs compared to its vehicle treatment significantly reduced approximately 2.62-fold decrease following 18 h of 5μM MeHg exposure. Even though *Vegfa* mRNA was reduced in Nrf2 KO SCAs following MeHg exposure, its expression level was higher than WT treatment with MeHg by about 1.77-fold. The statistical analysis was derived from Two-Way ANOVA with Tukey's multiple comparison *post hoc.* (\* indicates p<0.05 when compared to vehicle (control) treatment from the same genotype, # indicates p<0.05 when compare between different genotypes; WT vs. KO); N=12 biological replications with two replications/N

## 3.5 Discussion

The primary objective of this study was to examine the role of the Keap1-Nrf2-ARE pathway in MeHg induced SCAs degeneration. It is well established that MeHg induces the increase of [Glu]<sub>ex</sub> in the synapses leading to excitotoxicity-induced neuronal death. MeHg also induces ROS overproduction and impairs antioxidant systems such as GSH and Keap1-Nrf2-ARE pathway. The mechanisms inducing excitotoxicity and oxidative stress are intertwined since the synaptic glutamate clearance is predominantly responsible by the EAAT1/2, which are sensitive to ROS (Trotti et al., 1998). Both ROS and MeHg inhibit EAATs ability to transport Glu and aspartate. Additionally, the cystine/glutamate transporter (system Xc-) transports amino acid cystine in exchange with exporting Glu to increase the intracellular cysteine for de novo GSH synthesis. System Xc- transports these amino acids depending upon the Glu concentration gradient. Therefore, during glutamate transmission and particularly during excitotoxicity when [Glu]<sub>ex</sub> concentration is relatively high, system Xc- cannot transport cystine into the cells, resulting in the reduction of de novo GSH synthesis and overproduction of ROS. The comparison between WT derived SCAs and Nrf2 KO derived SCAs in this study showed that there was a greater susceptibility of Nrf2 KO derived SCAs to MeHg. This data was consistent with the study in the primary hepatocytes derived from Nrf2 KO mice. The primary hepatocytic viability from Nrf2 KO was significantly reduced by approximately 70% when exposed to 5µM MeHg for 24h while the WT derived hepatocytic viability was spared (Toyama et al., 2007). The greater susceptibility of Nrf2 KO derived cells, including SCAs and hepatocytes, could be explained by the overproduction of ROS in the Nrf2 KO mice. The susceptibility of Nrf2 KO SCAs could be due to the over production of ROS. The comparison of basal ROS level in glial-cortical neuronal co-culture derived from

WT, Nrf2 KO and Keap1 knockdown (Keap1 KD) found that the level of ROS was dramatically increased in Nrf2 KO derived glial-cortical neuronal co-culture relative to WT derived glial-cortical neuronal co-culture, whereas the basal ROS level from Keap1 KD were similar to WT glia-cortical neuronal co-culture (Kovac et al., 2015). Even though homozygous Nrf2 KO mice are fertile, reduction of Keap1-Nrf2-ARE pathway activity potentially enhances ROS production due to the imbalance of redox homeostasis and renders this genotype more susceptible to any insult. The evidence supporting this finding is that the primary cortical astrocyte cell culture derived from Nrf2 KO had an increased susceptibility to oxidants (hydrogen peroxide) compared to the WT derived astrocytes (Bell et al., 2015). Nrf2 KO derived neurons in mixed culture system (90% neuron and 10% glia) were more sensitive to mitochondrial toxins (1-methyl-4-phenyl-1,2,5,6tetrahydropyridine (MPTP) or rotenone compared with WT derived neurons that exhibited apoptosis marker caspase 3 elevation (Lee et al., 2003a). The sensitivity of Nrf2 KO derived neurons was suggested by the microarray data that the reduction of GSH as well as some antioxidant genes, Ngo1, Gst, and Gclc, were significantly reduced (Lee et al., 2003a). Besides, Nrf2 KO derived neurons exhibited the significant reduction of genes involving the Ca<sup>2+</sup> homeostasis, including visinin-like 1, calbindin-28K, synaptotagmin-1 and 5, calmodulin III and ryanodine receptor 3(Lee et al., 2003a). The important role of Nrf2 in regulation of Ca2+ homeostasis was also supported by a marked reduction of Nrf2 KO neuronal viability when exposed to a Ca<sup>2+</sup> ionophore ionomycin or an endoplasmic reticulum Ca<sup>2+</sup>-ATPase inhibitor dtBHQ, whereas these compounds did not affect WTderived neuron viability (Lee et al., 2003a). The microarray data from Nrf2 KO derived cortical astrocytes also indicated a great reduction of detoxification and antioxidant enzymes including the known ARE containing genes such as Sod1, Gclc and Gclm (Lee et

al., 2003b). Interestingly, the *Gclm* expression level was not affected by the absence of Nrf2 in cortical neurons (Lee et al., 2003a) but did so in cortical astrocytes (Lee et al., 2003b). The reduction of *Gclc* mRNA expression was consistent with results from Bell et al. (2015) in cortical astrocytes which derived from Nrf2 KO (Bell et al., 2015). The reduction of *Gclc* mRNA expression was also characteristic of Nrf2 KO derived SCAs from this study.

Both GCLC and GCLM are involved in the rate-limiting step of GSH synthesis. Gclcdeficient mice (Gclc-/-) exhibited more severe effects than *Gclm*-deficient (Gclm-/-) mice. The intracellular GSH was absent in Gclc-/- mice and these mice die during embryogenesis (Dalton et al., 2000) whereas 10-25% GSH were remained in Gclm<sup>-</sup>/-mice and they are normally viable (McConnachie et al., 2007). The reduction of basal Gclc mRNA in Nrf2 KO derived SCAs renders these SCAs more susceptible to ROS generation as well as MeHg intoxication. This result also supports the critical role of Nrf2 in regulation of Gclc transcripts. Therefore, loss of Nrf2, a master regulator of antioxidant genes, could be detrimental to a cell's ability to survive MeHg exposure, as the toxicological mechanism involves the increase of ROS generation and impairment of mitochondrial function. Nrf2 KO derived SCAs lack the antioxidant system s which results in the inability to combat ROS generation as efficiently as the WT derived SCAs. In addition to the reduction of Gclc mRNA in Nrf2 KO derived SCAs, the GPx1 and GPx4 were greatly reduced in Nrf2 KO derived SCAs compare to WT SCAs. The reduction of Gpx1 mRNA expression following MeHg in SCAs was consistent with the sexual dimorphism study in C57BL/6J mice that exposure to 5ppm MeHg through drinking water from early gestational period until postnatal day 21(Ruszkiewicz et al., 2016). The

expression of *GPx1* mRNA expression was reduced in both male and female cerebrum but not cerebellum (Ruszkiewicz et al., 2016). Swiss adult male mice exposed to 40ppm MeHg in drinking water during 21 day demonstrated a significant reduction of GPx1 and GPx4 activities with western blotting analysis in the cerebellum and cortex when compared to untreated animals (Zemolin et al., 2012). These data support the important role of Nrf2 in a regulation of redox homeostasis, particularly in the regulation of GSH synthesis and metabolism.

Despite the reduction of mRNAs involving GSH synthesis and metabolism, the study by Lee et al (2003) to confirm the absence of Nrf2 mRNA in Nrf2 KO revealed that the expression of *Nrf2* mRNA was slightly detectable in primary cortical neurons with the primer specific to exon 1-3 but it absent with the primer specific to the exon5 (Lee et al., 2003a). This was because Nrf2 KO mice were generated by the selective deletion of 4.2kp DNA containing part of axon 4 and all of axon5 of *Nrf2* gene which was replaced by a 5.5 kb fragment DNA of the bacterial LacZ gene and neomycin resistant cassette (Chan et al., 1996). This DNA fragment replacement was effectively nullifying the *Nrf2* gene function because of the deletion of CNCbZIP region (Chan et al., 1996), the conserved region of a family of basic leucine zipper transcription factors (Sykiotis and Bohmann, 2010). Therefore, the detectable mRNA level of Nrf2 in Nrf2 KO derived SCAs in this study is due to the primers using in this study targeted specific to exon 1-2 (TaqMan gene expression assay; ThermoFisher Scientific, catalogue number Mmo0477784-m1).

Although in Nrf2 KO derived SCAs, the expression of genes involved in GSH synthesis, *Gclc* and activity *GPx1* and *GPx4* were greatly reduced compared to WT SCAs, the expression of phase III detoxification (transporter) gene *Abcc1* encoding for Mrp1 (Hayes,

2016) was largely increased in Nrf2 KO. Similarly, the cystine/glutamate transporter encoded by Slc7a11 mRNA also increased in Nrf2 KO derived SCAs. The increase of these transporters could be a compensatory regulation to by CNCbZIB family transcription factor such as Nrf1 (Sykiotis and Bohmann, 2010). Nrf1 also plays important role in cellular defense oxidative damage. Overexpression of Nrf1 induces the upregulation of cytoprotective gene Ngo1. Nrf1 is critical for erythrocyte since Nrf1 null mice die in utero due to the decreased number of enucleated red blood cells and severe anemia (Niture et al., 2010). Nrf1 and Nrf2 however, exhibit distinct roles in activation of antioxidant gene expression. For example, Nrf1 deficiency results in the up-regulation of Nrf2 target genes such as Ngo1, Gst, Gclc and Ho1 (Ohtsuji et al., 2008). Specific knockdown Nrf1 in mice liver also exhibited dramatic increase of GSH level in liver. While the GSH synthesizing enzymes, Gclc, Gclm mRNA were not affected in these Nrf1 KD mice, the system XcmRNA was greatly increased (Tsujita et al., 2014). Overexpression of Nrf2 in combination with Nrf1 protein inhibited Gclc and Gclm expression determined by the increases of luciferase activity located downstream of the electrophilic response element (EpRE or ARE) linked with Gclc and Gclm genes (Chepelev et al., 2013). These results suggest negative competitive binding of EpRE /ARE by Nrf1 in regulation of Nrf2-dependent antioxidant genes such as Gclc. The compensatory increase of Abcc1 and Slc7a11 in Nrf2 KO derived SCAs could be partly to a down regulation of Nrf1 activity. Alternatively, other signaling molecules play prominent role in induction of these transporters' expression in Nrf2 KO derived SCAs. Particularly, the pro-inflammatory cytokines would be activated in Nrf2 KO mice whose basal ROS level are high. The pro-inflammatory cytokine interleukin-1β (IL-1β) which specifically up-regulated system Xc- in astrocytes but not in neurons or microglia (Jackman et al., 2010) might be induced in Nrf2 KO derived SCAs.

The effect of IL-1β on system Xc- expression was found to be mediated through the activation of NF-kB (Yang et al., 2005; He et al., 2015) and activator protein 1 (AP1) (Yang et al., 2005). It could be possible that the up-regulation of *Slc7a11* mRNA in Nrf2 KO derived SCAs was activated through the activity of IL-1β and NF-kB, and/or AP1. Additionally, the promoter region of *Slc7a11* gene could be regulated by STAT3/STAT5, growth factors, neuronal activity and amino acid (AA) starvation (Massie et al., 2015) (see Figure 3.16) (comprehensive reviewed by Massie et al. 2005).

The mechanism by which MeHg induces system Xc- mRNA expression is complex and genetic predisposition also contributes to the differential toxicity. The effect of MeHg to Slca7a11 mRNA expression could be direct activation of Keap1-Nrf2-ARE and/or indirectly through ROS activity. MeHg (18h of 5µM) induced the increase of Slca7a11 mRNA expression in WT derived SCAs. This increase is consistent with the study in a human blastoma cell line (HeLa S3 cells) where MeHg (12h of 8uM) induced a 2.1-fold increase of Slc7a11 mRNA (Amonpatumrat et al., 2008). In contrast, MeHg slightly reduced Slc7a11 mRNA in Nrf2 KO derived SCAs. This slight effect could be caused by MeHg-induced Slc7a11 mRNA elevation either through Nrf2-ARE pathway, therefore no effect for induction was noticeable, or alternative pathways such as the IL-1β which might be involved in the reduction of *Slc7a11* mRNA expression. Recently, Shi et al. (2016) confirmed the role of IL-1β in mediating the system Xc- expression through the activation of NF-kB in primary cortical astrocytes culture (Shi et al., 2016). The regulation of system Xc- expression and activity in astrocytes through IL-1β implicates that hypoxic injury occurs (Jackman et al., 2010). Under hypoxic conditions, the hypoxia inducing factor-1a (HIF-1α) pathway is activated and has been reported to regulate expression of some

antioxidant genes such as Abcc1 mRNA (Lv et al., 2015). In addition, another transcription factor, the activating transcription factor 4 (ATF4), may regulate system Xcexpression through its binding to the AA response element (AARE) at the upstream region of Slc7a11 mRNA (Lewerenz et al., 2014). The effectors of ATF4 activity are involved in the activation of phosphoinositide 3-kinases (PI3Ks) pathway which induces glycogen synthase kinase 3β (GSK3β). GSK3β later phosphorylates eukaryotic initiation factor 2a (peIF2α), which results in the activation of ATF4. The induction of system Xc- expression is regulated by the PI<sub>3</sub>K-peIF<sub>2</sub>α-ATF pathway in glioblastoma (Lewerenz et al., 2014). The increase of the Slc7a11 mRNA expression in Nrf2 KO relative to WT SCAs could be explained by these alternative pathways that activate system Xc- transcripts. MeHginduced increase of system Xc- transcripts in WT derived SCAs compare to the vehicle treatment could be due to the activities not only of Nrf2 but also these alternative pathways. The expression of Slc7a11 mRNA in Nrf2-KO derived SCAs appeared to be lower (but insignificant) in MeHg treatment compared to its genotype treated with vehicle. Several possible explanations are as follows. 1. Nrf2 pathway was not a major regulator since the slightly affected by MeHg to Nrf2 KO derived SCAs was observed in the expression of *Slc7a11* mRNA. 2. Nrf2 pathway was the major regulator in activation of Slc7a11 mRNA since MeHg could not induce the increase of Slc7a11 mRNA in Nrf2 KO SCAs. 3. Alternatively, MeHg affected WT- and Nrf2- derived SCAs differently via those alternative pathways (non-Nrf2) in regulation of system Xc- transcripts. To better understand the difference between WT- and Nrf2- derived SCAs in the regulation of system Xc- expression further experiments to elucidate the involvement of these alternative pathways are required. The expression of those cytokines and proteins including IL-1β, NF-kB, PI3K GSK3b and ATF4 would be compared between WT and Nrf2

KO derived SCAs following MeHg exposure as well as compare to their own genotype treated vehicle.

In addition to the MeHg-induced increase in *Slc7a11* mRNA in WT SCAs, inorganic Hg²+could affect this alteration. MeHg could slowly undergo demethylation to inorganic mercury that cannot usually cross the BBB via the L-type neutral amino acid carrier transport (LAT) system. Consequently, Hg²+ is trapped inside the CNS. The mechanism by which Hg²+ induces neurological damage is still unclear. Nevertheless, Hg²+ disruption of cell cycle progression and/or induction of apoptosis in several tissues is well recognized. Moreover, Hg-induced neurotoxicity is known to be mediated by ROS in different models by altering Na+/K+ ATPase activity and mitochondrial function (Mieiro et al., 2011). Indeed, at the synapse, glutamate transport through astrocytes is dependent mainly on the Na+ electrochemical gradient, which is established by Na+/K+ ATPase activity (Camacho 2006). An alteration in the Na+/K+ ionic and electrochemical gradient is intimately associated with astrocyte regulation of glutamatergic activity (Kinoshita et al., 2016), which includes EAAT2/GLT-1 function and ultimately affects the system Xcactivity. The alteration of the expression of these transporters could also contribute to the functional dysregulation of these transporters.

A marked reduction of GLT-1 and system Xc- expression following 18h of 5µM MeHg exposure as measured with immunocytochemistry occurs in both WT and Nrf2 KO derived SCAs. The reduction of system Xc expression could contribute to the reduction of *de novo* GSH synthesis. Total GSH was considerably reduced in both cortical neuronal cell culture (Kaur et al., 2007) and cerebellar astrocytes (Kaur et al., 2006) after exposure to MeHg. The effect of Hg<sup>2+</sup> on GSH content has been reported as well. Hg<sup>2+</sup> causes the

depletion of GSH content as a result of the interaction between Hg<sup>2+</sup> and sulfhydryl groups. Hg<sup>2+</sup> interacts with the thiol group of GSH, leading to the formation of an excretable GS-HgCH<sub>3</sub> complex, and all these compounds inhibit glutathione reductase and glutathione peroxidase (GPx) activities. This is characteristic of Hg<sup>2+</sup> neurotoxicity (Mieiro et al., 2011). The effect of MeHg to system Xc- is complex due to the increase of system Xc- transcript but reduction of the system Xc- protein in WT derived SCAs. Conversely, MeHg appears to induce the reduction of system Xc- transcript, as well as dramatic decrease of system Xc- protein in Nrf2 KO, derived SCAs. These results suggest that genetic predisposition also contributes to the differential regulation of glutamate transport systems in MeHg induced toxicity with both transcriptional and posttranslational levels.

In the CNS, astrocytes play an essential role in regulating glutamate homeostasis by taking up extracellular glutamate through EAAT1/GLAST encoded by the *Slc1a3* gene and EAAT2/GLT-1 encoded by *Slc1a2* genes. Other than the EAAT3/EAAC1 in rat C6 glioma cells (Escartin et al., 2011a), these two genes have not been reported to be regulated through Nrf2 activation. However, these transporters work cooperatively with system Xcto maintain redox homeostasis as well as glutamate homeostasis. In this study, both *Slc1a3* and *Slc1a2 mRNA* expression levels in Nrf2-KO SCAs were up-regulated compared to WT SCAs (Figure 3.9 and 3.10, respectively). The up-regulation of *Slc1a3* and *Slc1a2*mRNA corresponded to the increase of *Slc7a11* mRNA expression in Nrf2-KO SCAs, which supports the fact that these transporters work cooperatively to maintain extracellular glutamate, especially in the system that lacked Nrf2. In addition, the regulation of *Slc1a2* expression was induced by several pathways, such as the PIK3, NF-

kB, and PKA (Su et al., 2003). It is possible that these signaling pathways positively regulated the EAAT2 expression at the transcriptional level in Nrf2 KO derived SCAs. Following MeHg exposure, Slc1a3 and Slc1a2 mRNA expression levels were lower in both WT and Nrf2 KO SCAs. While MeHg had significant effects on the reduction of both Slc1a3 and Slc1a2 mRNA in Nrf2-KO SCAs, only Slc1a2 mRNA showed a significant reduction in WT SCAs (Figure 3.10). The reduction of Slc1a3 and Slc1a2 mRNA expression could contribute to a reduction of EAAT1 and EAAT2 expressions. Consequently, extracellular glutamate clearance by these transporters are restricted. Ultimately, excitotoxicity occurs and leads to SCAs death. Several lines of evidence suggest that Hg<sup>2+</sup> (Brookes, 1988; Brookes and Kristt, 1989) and MeHg (Brookes and Kristt, 1989; Kim and Choi, 1995) inhibit glutamate uptake in primary cortical astrocyte cell culture (Brookes, 1988; Brookes and Kristt, 1989; Kim and Choi, 1995) and spinal cord cell culture (Brookes, 1992a). The effect of Hg<sup>2+</sup> on Glu uptake inhibition was selective and concentration-dependent, whereas the mechanism by which MeHg inhibits Glu uptake is closely related to voltage-gated Ca<sup>2+</sup> channels due to the lack of inhibition in the presence of Ca<sup>2+</sup> channel blocker verapamil (Kim and Choi, 1995). The decrease of Slc1a3 and Slc1a2 expression in SCAs following MeHg exposure could be attributed to the decrease of extracellular Glu uptake and results in the Glu induced excitotoxicity. The significant reduction of EAAT2/GLT-1 protein expression (Figure 3.13 and 3.14) in WT (Figure 3.11) and Nrf2 derived SCAs (Figure 3.12) following 18 h of 5μM MeHg were observed from immunocytochemistry. Therefore, the reduction or inhibition of Glu uptake could not only be because MeHg affected EAAT1/2 transporter function but also affected the transcriptional and translational process of these transporters.

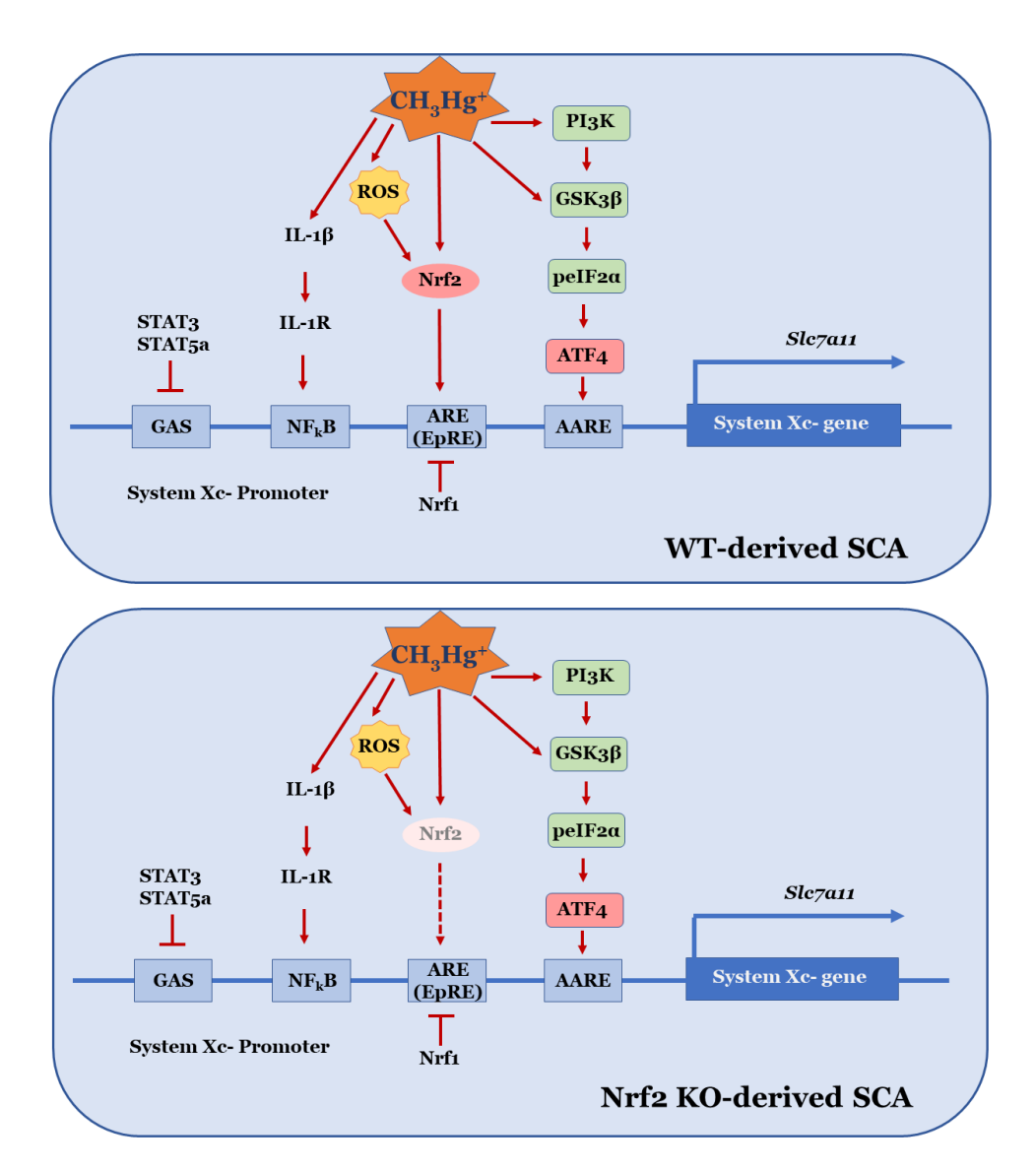


**Figure 3.16 Proposed mechanisms involved in the regulation of** *Slc7a11* **in Nrf2 KO derived SCAs.** Not only Nrf2 is involved in the regulation of *Slc7a11* expression, several signaling molecules, due to the promoter region of the *Slc7a11* gene, possesses a binding region for these molecules. While ATF4 regulated by the PI3K GSK3β pathway, and cytokines IL-1β positively regulate *Slc7a11* expression, transcriptional factor Nrf1 and STATs exert the negative regulation of the *Slc7a11* expression. The upregulation of *Slc7a11* expression in Nrf2 KO derived SCAs could be due to the compensatory mechanisms by which to enhance a positive regulation pathway and diminish the negative regulation pathways. The differential effect of MeHg between WT and Nrf2 derived SCAs could be explained by the differential genetic background that possesses different basal signaling activity. In the WT-derived SCAs in which the Nrf2 pathway is activated as well as a positive regulation pathway following MeHg. The activations of these positive regulation mechanisms of *Slc7a11* expression would enhance the *Slc7a11* expression in WT, whereas lacking Nrf2 in Nrf2 KO derived SCAs, the *Slc7a11* expression was diminished following MeHg exposure.

MeHg treatment not only affected Glu transport but also the transport of xenobiotic or toxicants. Multidrug resistance proteins (MRPs) are involved in transporting exogenous and endogenous compounds such as GSH across cellular membranes because these transporters are a subset of the ATP-binding cassette genes that are phase III detoxification proteins (Leier et al., 1996). Following MeHg exposure to WT and Nrf2 KO derived SCAs, there were significant reductions of *Abcc1* mRNAs (Figure 3.7). The immunocytochemistry also indicated the reduction of Mrp1 protein expression in these genotypes following 18h of 5µM MeHg exposure (Figure 3.13 and 3.14). The reduction of Mrp1 protein in both WT and Nrf2 KO-derived SCAs may initially contribute to the accumulation of Hg and later generate cellular and molecular toxicity to SCAs. The in vivo study comparing Nrf2 KO mice to WT mice demonstrated a more significant total cellular Hg accumulation in the cerebrum, cerebellar, and liver of Nrf2 KO mice than WT mice following the oral administration of MeHg (5 mg/kg/day for 8 days) (Toyama et al., 2011). The accumulation of Hg in Nrf2 KO mice was concurrent with the increase of hindlimb flaccidity and mortality, whereas WT control was not affected by this MeHg exposure paradigm (Toyama et al., 2011). The accumulation of cellular Hg following MeHg exposure was linked to the diminished expression of Mrp1 and Mrp2 in Nrf2 KO primary hepatocyte cell culture, which corresponds to the greater susceptibility to MeHg compared to WT (Toyama et al., 2007). As such, the susceptibility of Nrf2 KO derived SCAs could be partly due to the reduction of Mrp1 expression (as exhibited in **Figure 3.12**), which plays an essential role in the excretion of xenobiotics including MeHg as well as GSH from the cells. MeHg could be conjugated with GSH through non-enzymatic processes and/or enzymatic processes through GSH-S-transferase (GST) processes to form a polar MeHg-GSH adduct (Rabenstein and Fairhurst, 1975). The MeHg-GSH could be transported through the Mrp1 due to its structural similarity to GSH. A reduction of Mrp1 expression could cause cells to accumulate Hg that later contributes to cellular toxicity to SCAs and the neighboring neurons such as SMN. Perhaps, a reduction of Mrp1 in SCAs following MeHg exposure could contribute to the susceptible of SMN to MeHg due to insufficient GSH export.

The increase of Mrp1 transcript (Abcc1 mRNA) in Nrf2 KO derived SCAs compared to WT derived SCAs was observed in this study (Figure 3.7). Nrf2 activity may regulate the expression of Mrp1 transcript in mouse embryonic fibroblast (Hayashi et al., 2003) as well as the expression of Mrp2 (Vollrath et al., 2006), Mrp3 and Mrp4 transcripts in mouse liver (Maher et al., 2007). Nevertheless, the expressions of Mrp2, Mrp3, and Mrp4 mRNAs were relatively spared in Nrf2 KO compared to WT mouse liver (Maher et al., 2007). In a colon cancer cell line, hypoxia response element (HRE) loci were in the proximal promoter of *Abcc1* gene, and hypoxia inducing factor-1α (HIF-1α) can directly bind to this site and directly regulate Mrp1 expression (Lv et al., 2015). Suppression of HIF-1α with siRNA resulted in the reduction of Mrp1 mRNA (Lv et al., 2015). A transcriptional factor HIF-1, a heterodimer of HIF-1α and HIF-1β subunits (Semenza, 2007), induces genes required for the adaptation to hypoxia. In normoxia, HIF-1α is continuously degraded by the proteasomal system, and upon hypoxia, HIF-1a is stabilized and translocate to the nucleus, where it dimerizes with HIF-1\beta and regulates the expression of genes involved in angiogenesis, glucose transport, glycolysis, survival, and cell migration (Yang and Jackson, 2019). The breast cancer cell lines without Nrf2 were treated with a ROS inducer menadione exhibited the induction of HIF- 1a mRNA expression (Lacher et al., 2018). This result suggests that lacking Nrf2, the HIF-1a

remains activated by ROS and perhaps contributes to the induction of Abcc1 mRNA elevation. The studies in colorectal, gastric, and bladder cancer tissues found the expression of HIF-1 and Mrp1 was significantly correlated (Toth and Warfel, 2017) and ROS or a pro-oxidant, NADPH oxidase (NOX) may act as an intermediate molecule between Nrf2 and HIF-1 pathway. The study of molecular mechanisms underlying chronic intermittent hypoxia (IH), a pathological characteristic of sleep apnea, revealed multiple pathways involved in regulating HIF activities. These include 1. Ca<sup>2+</sup>/calmodulin kinase (CaMK) dependent pathway, 2. PI3K-mTOR pathway, and 3. ROS evokes a stabilized HIF-1\alpha pathway (Yuan et al., 2008). All these pathways are regulated by the effector NOX (Yuan et al., 2008) as a major ROS producer (Kovac et al., 2015). In cortical neuron-astrocyte co-culture and mouse embryonic fibroblasts that are Nrf2 deficient, Nox2 mRNA was dramatically increased while Nox4 mRNA was decreased compared to WT (Kovac et al., 2015). Furthermore, IH induced NOX2 activation with xanthine oxidase (XO), ROS inducer in PC 12 cells. NOx2 activation required [Ca<sup>2+</sup>]<sub>in</sub> which was evoked by XO via stimulation of protein kinase C (PKC) (Nanduri et al., 2015). NOX2 subsequently stimulated HIF-1 (Nanduri et al., 2015). The regulation of *Nox* mRNA expression by Nrf2 appears to be cell type-specific. For example, Nrf2 negatively regulates Nox4 expression in endothelial cells. Conversely, Nrf2 induces Nox4 elevation in the mouse and human lung endothelium in response to hyperoxia (Kovac et al., 2015). Perhaps, the elevation of Mrp1 transcripts in Nrf2 KO derived SCAs is regulated by cross talk between the Nrf2 and HIF pathways whereby NOX2 acts as an intermediate mediator regulating the elevation of Mrp1 transcripts through the activation of HIF-1 pathway as a compensatory antioxidant mechanism (see Figure 3.17).

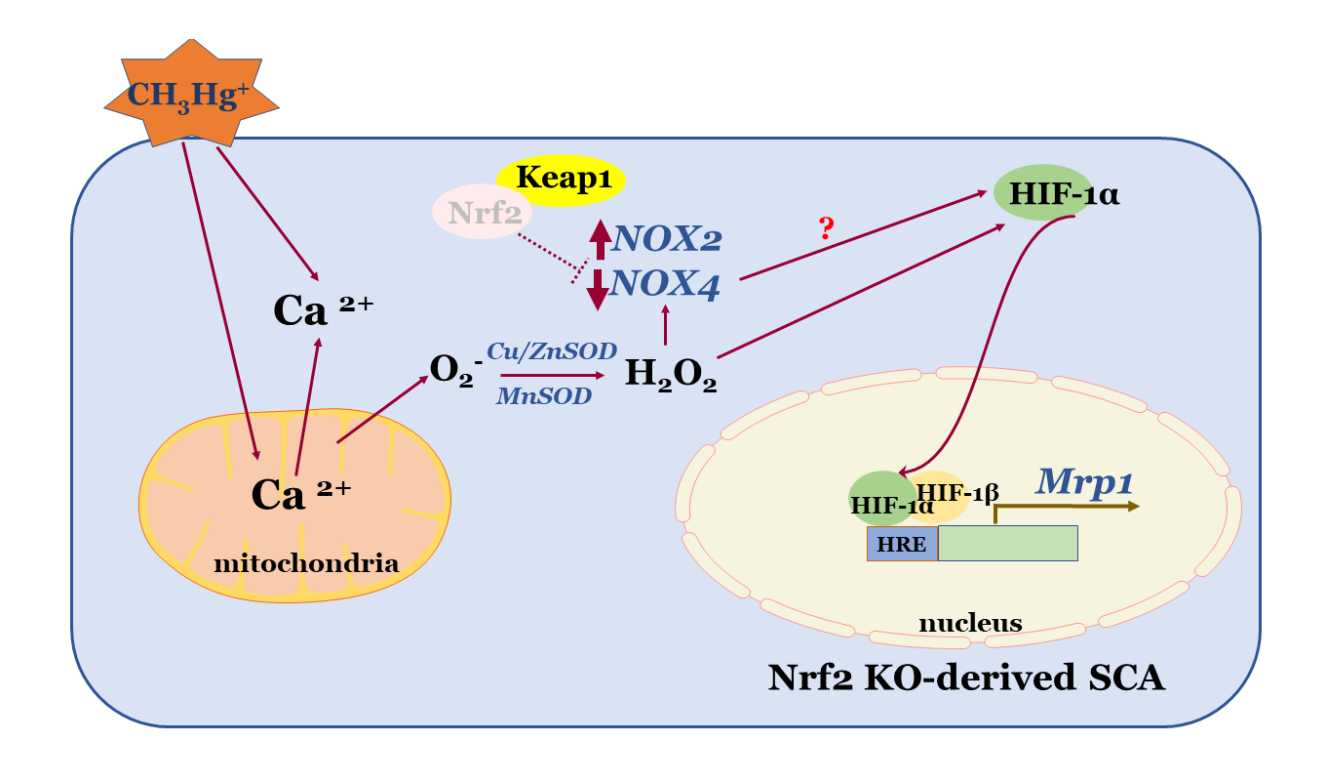


**Figure 3.17 Proposed mechanism of MeHg in the induction of** *Abcc1* **(Mrp1) expression in Nrf2 KO-derived SCAs.** The increase of Mrp1 transcript in Nrf2 KO derived SCAs following MeHg exposure could be due to the direct regulation of the hypoxia response element located in proximity of *Abcc1* (Mrp1) promotor region and /or indirectly through the production of NADPH oxidase2 (NOX2), which subsequently activate HIF-1α to regulate Mrp1 expression. The Nrf2 KO has been shown the increases of NOX2 but the reduction of NOX4 in organotypic hippocampal slice and neuronal-astrocytic cell culture (Kovac et al., 2015). However, whether NOX2 or NOX4 will be involved in regulating *Mrp1* expression in Nrf2 KO or WT derived SCAs remains in question.

Keap1 and Nrf2 mRNA are also regulated by Nrf2-ARE pathway (Hayes and Dinkova-Kostova, 2014), however, the mechanism by which the up-regulation of *Keap1* mRNA in Nrf2 KO derived SCAs is unclear. The up-regulation of *Keap1* mRNA relative to WT in Nrf2 KO derived SCAs with vehicle treatment (Figure 3.3) could be due to the hypomethylation of the *Keap1* genes as part of epigenetic regulation(Cheng et al., 2016) in Nrf2 KO mice. The microRNA (miRNA) also has a role in the regulation of Keap1 mRNA expression. The miR 141 (Shi, 2015) and miR200a (Eades et al., 2011; Yang et al., 2014) complimentarily bind to Keap1 mRNA and consequently cause translational silencing as part of the degradation process. In addition, Keap1 and Nrf2 protein levels are controlled by post-translational degradation processes. An autoregulatory loop between Keap1 and the ubiquitination related proteins Cul3 and Rbx1 controls Nrf2 cellular availability by which Nrf2 activation leads to the increase of the expression of Keap1, Cul3, and Rbx1, which in turn increases Nrf2 degradation (Yang and Jackson, 2019). On the other hand, Keapı level is controlled by the autophagy through the Cul3/p62 complex for maintenance of redox homeostasis (Taguchi et al., 2012). ROS induced the p62 up-regulation through the activation of Nrf2-ARE. Induced expression of p62 might facilitate the interaction between Keap1 and Clu3, thereby stimulating autophagy to accelerate protein degradation and clearance (Fan et al., 2010). Under conditional autophagy Atq7 gene deficiency in mice liver, the levels of Keap1 as well as p62 were increased compared to WT control (Komatsu et al., 2010; Taguchi et al., 2012). Interestingly, the absence of p62 in hepatocytes was also shown in the immunoblotting of hepatocyte from Nrf2 deficient mice but maintained the Keap1 protein level similar to WT control (Komatsu et al., 2010; Taguchi et al., 2012). Based on these lines of evidence, Keap1 at least in hepatocytes is degraded via autophagy in p62- dependent mechanism

(Taguchi et al., 2012). However, the *Keap1* mRNA level of Nrf2 deficient hepatocytes slightly decreased but was significantly different compared to WT control (Taguchi et al., 2012), whereas the *Keap1* mRNA level was elevated in Nrf2 KO SCAs (Figure 3.3). The differential expression of *Keap1* mRNA in Nrf2 deficient hepatocytes and SCAs was unknown, however, it could be due to cell type specific regulation of Keap1 transcription. The comparison of *Keap1* mRNA expression between these cell types in Nrf2 KO mice might explain the differential expression. The differential effect of MeHg to *Keap1* mRNA expression also displayed between WT and Nrf2 KO derived SCAs. The expression of *Keap1* mRNA was slightly affected by MeHg in WT derived SCAs, whereas the level of Keap1 mRNA was greatly reduced in Nrf2 KO derived SCAs. This suggests that the genetic background could influence the differential responses by SCAs during MeHg exposure.

The effect of MeHg in the increase of Vegf mRNA in WT SCAs might partially be due to 1. the induction of pro-inflammatory cytokine interleukin-1 (IL-1 $\beta$ ) and/or 2. The cross talk between hypoxia inducing factor -1 (HIF-1) pathway and the Nrf2 pathway (see **Figure 3.16**). In response to stimulation by the pro-inflammatory cytokine IL-1 $\beta$ , astrocytes generate and release VEGF that BBB permeability and promotes leukocyte extravasation (Sofroniew, 2015). Inactivation of astrocytic Vegfa expression reduced BBB breakdown, decreased lymphocyte infiltration and neuropathology in inflammatory and demyelinating lesions, and reduced paralysis in a mouse model of multiple sclerosis (Sofroniew, 2015). Disruption of BBB could elicit the effect of MeHg toxicity and pathology as a result of the entry of toxicants, inflammatory cytokines, and amino acids such as glutamate, which later exacerbate excitotoxicity. The *in vitro* treatment with inorganic mercuric chloride (1 $\mu$ M and 10  $\mu$ M HgCl<sub>2</sub>) increases IL-1 $\beta$  activity in

macrophage cell culture media and cell extracted supernatant (Zdolsek et al., 1994). The increase of IL-1\beta activity was time dependent beginning at 6h and greatly increasing following 24, 48 and 72h. The elevation of IL-1\beta activity was also detected in the mice exposed to HgCl2 (Zdolsek et al., 1994). However, MeHg exposure in cortical astrocytes and microglia cell culture did not allow the increase of IL-1β stimulated by PAM(3)CSK(4), a toll-like receptor (TLR) ligand that is used for induction of inflammatory cytokines (Bassett et al., 2012). The author suggested that the lack of IL-1\beta activity was due to the inability of the PAM(3)CSK(4) to induce these cytokines in astrocytes and microglia but was not due to MeHg (Bassett et al., 2012). An in vitro study in cortical astrocyte cultures showed that MeHg could be demethylated into inorganic Hg such as HgCl<sub>2</sub>. The demethylation of MeHg into Hg was mediated by ROS, particularly by mitochondrial ROS. In astrocytes, 5mM rotenone, an inhibitor of mitochondrial complex I, elicited demethylation of MeHg (1µM) but this was not observed with L-buthionine-S,R-sulfoximine (BSO), another ROS inducer (due to cellular GSH depletion) (Shapiro and Chan, 2008). The elevation of Vegf transcripts in WT SCAs could cause the biotransformation of MeHg into inorganic Hg in a mitochondrial ROS-mediated manner such that Hg<sup>2+</sup> later induces IL-1β activity. In fact, mitochondria are one of MeHg's target organelles and the impairment of mitochondrial membrane potential has been observed (Limke and Atchison, 2002) and is an early primary site of ROS generation (Limke and Atchison, 2002; Shanker et al., 2004b; Shanker et al., 2005b). ROS also serves as a signal indicating low levels of cellular oxygen (hypoxia). When cellular oxygen is low, mitochondrial complex III is unable to shuttle its electrons to cytochrome c properly, thereby causing a large increase of ROS, i.e., H<sub>2</sub>O<sub>2</sub> (Chandel et al., 2000), which activates

hypoxic signaling (Guzy and Schumacker, 2006; Waypa et al., 2016). Hypoxia initiates transcription of several gene products through hypoxia inducing factor-1 (HIF-1) pathway that helps sustain the supply of O2 to tissues and enhance cell survival during severe O2 deprivation. Gene products under the HIF-1 pathway, such as VEGF and erythropoietin1 (Epo1), give rise to angiogenesis and erythropoiesis, respectively, to augment O<sub>2</sub> supply to the tissues (Chandel et al., 2000; Mukandala et al., 2016). The elevation of Vegf mRNA in WT SCAs could be partly due to the activation of the HIF-1 pathway which directly promotes Vegf mRNA expression. It has been also demonstrated that there is cross talk between Nrf2 and HIF-1 pathways. Knock down of Nrf2 in cardiac micro-vascular endothelia cells (CMEC) significantly decreases heme oxygenase -1 (HO-1), an antioxidant gene product underlying Nrf2 regulation and VEGF as well as reducing vascular tube formation. Over expression of Nrf2 induces HO-1 expression and increases vascular tube formation (Kuang et al., 2013). Hypoxic environment induces the increase of Nrf2 expression in the nucleus of CMEC, suggesting hypoxia activates Nrf2 activity. However, knockdown of Nrf2 with siRNA diminishes nuclear Nrf2 expression in CMEC (Kuang et al., 2013). In addition, knockdown of Nrf2 under a hypoxic environment caused the reduction of HO-1, p-AKT and VEGF expression (Huang et al., 2018). When Keap1 was knocked down of in endothelial colony forming cells, angiogenesis was preserved in high ROS conditions (Gremmels et al., 2017). These data suggest that crosstalk between Nrf2 and HIF-1 pathways could regulate VEGF through the intermediate HO-1 and/ or PI3K-AKT pathway (see **Figure 3. 18**).

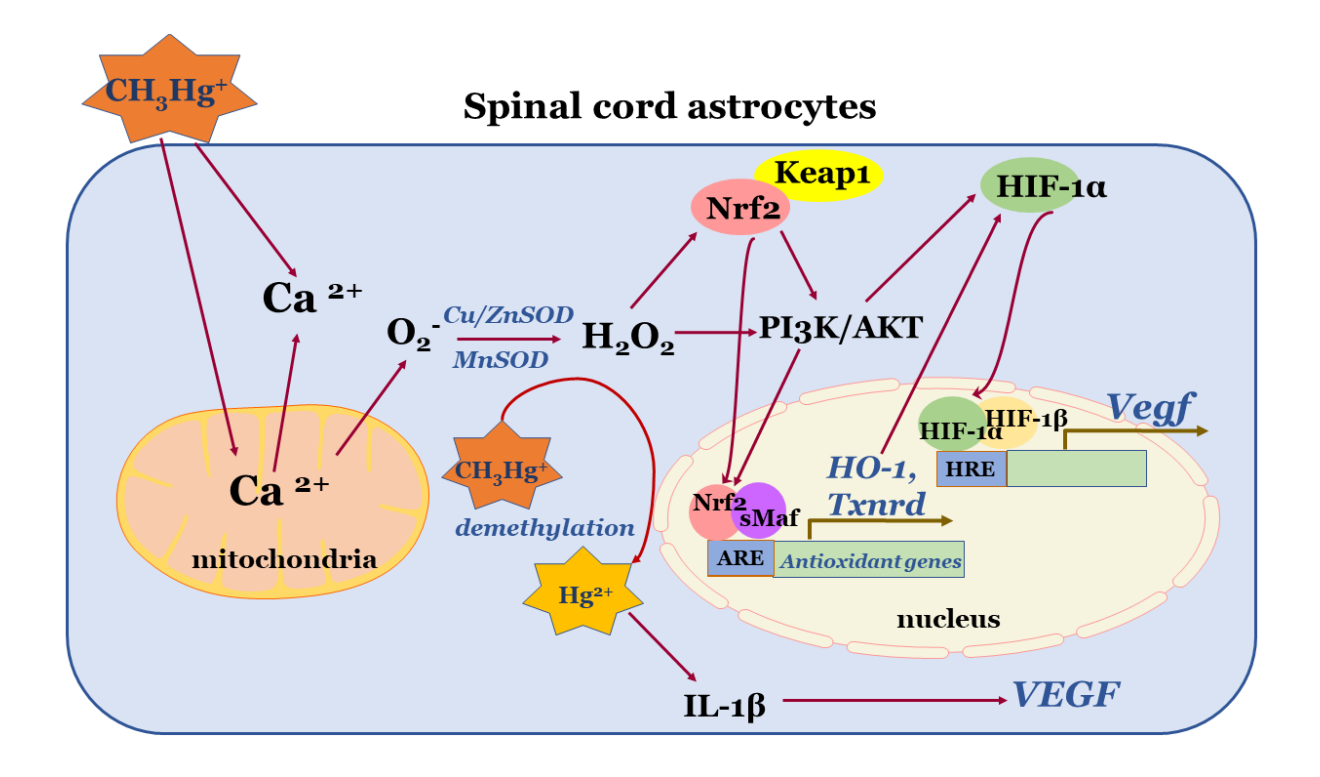


**Figure 3.18 Proposed mechanism of MeHg induced** *Vegf* mRNA expression in SCAs. The effect of MeHg in the increase of *Vegf* mRNA in WT SCAs might partially be due to 1. the induction of pro-inflammatory cytokine interleukin-1 (IL-1β) via the demethylation of MeHg into inorganic Hg (Hg<sup>2+</sup>) modulated by mitochondrial ROS (i.e.  $H_2O_2$ ) and/or 2. The cross-talk between HIF-1 and the Nrf2 pathways. Mitochondrial ROS activates Nrf2 to induce *HO-1* or *Txnrd* mRNA expression, which subsequently activates transcriptional factor HIF-1α to induce *Vegf* transcript expression.  $H_2O_2$  could also activate PI3K/AKT directly or via Nrf2 activity. PI3K/AKT later activates the HIF-1 pathway and induce *Vegf* expression. In addition, the  $Hg^{2+}$  has indicated it induced the IL-1β expression that positively regulates VEGF expression. The demethylation of MeHg to  $Hg^{2+}$  has been observed in rat cerebellar astrocytes cell culture (Shapiro and Chan, 2008).

The upregulation of *Vegf* mRNA in Nrf2 KO derived SCAs relative to WT derived SCAs could be a compensatory mechanism by HIF-1 pathway or other survival pathways. While MeHg induces *Vegf* elevation in WT SCAs, the reduction of *Vegf* expression following MeHg exposure in Nrf2 KO SCAs could be explained by the lack of the Nrf2 oxidative stress sensor pathway and thus only the HIF-1 pathway plays a prominent role in response to ROS. Therefore, the decrease of *Vegf* following MeHg exposure was observed in Nrf2 KO derived SCAs as opposed to the increase of *Vegf* as seen in WT SCAs as a result of synergistic response in WT to ROS generation by Nrf2 and HIF pathway. The increase of *Vegfa* mRNA rather than a decrease following 5uM MeHg exposure for 18h in WT SCAs might reflect the over production of ROS due to the chronic high concentration of MeHg exposure. The over production of ROS could activate both Nrf2 and HIF-1 pathway. The reduced expression of *Vegfa* mRNA in Nrf2 KO following MeHg exposure suggests that the genetic background plays a role in the regulation of protective gene expression.

Gene and environmental interaction may also play a role in disease pathogenesis in MeHg toxicity (Julvez and Grandjean, 2013). Similarly, VEGF secretion from astrocytes derived from transgenic SOD1 G93A mice appears to be lower than WT control (Van Den Bosch et al., 2004). MeHg-induced reduction of *Vegfa* in Nrf2 KO SCAs could contribute to the motor neuron degeneration through a mechanism by which AMPAR mediates Ca<sup>2+</sup> influx. VEGF has a protective role in the regulation of GluR2 subunit expression in motor neurons. Application of 20ng/ml VEGF to motor neurons in vitro induced the increase of GluR2 mRNA and reduced Ca<sup>2+</sup> influx (Bogaert et al., 2010). Moreover, 200ng/ml VEGF treatment for 1 week following excitotoxicity stimulation with 300µM kainic acid reduced motor neuron death to 30% (Bogaert et al., 2010). Astrocytes also play an essential role

in regulating the presence of GluR2 subunit in AMPAR required for Na<sup>+</sup> permeation following glutamate activation. AMPAR lacking GluR2 subunit allows Ca<sup>2+</sup> influx and subsequent Ca<sup>2+</sup>-mediated excitotoxicity in MNs (Laslo et al., 2001).

Besides its role in neuronal protection, VEGF may play a vital role in the BBB maintenance. The increase of VEGF could detrimentally increase the BBB permeability. Therefore, the increase of Vegf mRNA in WT SCAs could expose the CNS to a toxic environment. In rats, experimental exposure to 1.0mg/Kg body weight (low dose) MeHg caused the leakage of the toluidine blue-albumin dye into the nervous parenchyma as early as 12 h after the intoxication, indicating impairment and dysfunction of the BBB (Chang and Hartmann, 1972). Degenerative changes in the cerebellum and cerebrum occurred later in these rats. This also suggests that the impairment of BBB may precede the degeneration of the CNS (Shaw et al., 1975). Astrocytic-derived VEGF causes BBB disruption (Argaw et al., 2012). Inactivation of astrocytic Vegfa expression using specific deletion of Vegf with GFAP driven promotor (GfapCre:Vegfafl/fl ) reduced the BBB breakdown, decreased lymphocyte infiltration and neuropathology observed as inflammatory and demyelinating lesions, and reduced paralysis in a mouse model of multiple sclerosis (Argaw et al., 2012). One mechanism underlying this BBB permeability is that VEGF disrupts the endothelial transmembrane tight junction proteins claudin-5 (CLN-5) and occludin (OCLN) expression (Argaw et al., 2009). Claudins act as the primary determinant of tight junction properties, and OCLN is also a tight junction strand component and contributes to junction properties and regulates permeability (Argaw et al., 2009). The increase of Vegf mRNA expression following 5µM MeHg exposure to WT

SCAs for 18h suggests an alteration of the BBB is a possible mechanism by which MeHg induces CNS intoxication.

The increase of some antioxidant genes expression in Nrf2 KO derived SCAs could be a compensation of antioxidant. For example, in cancer cells, the metabolic pathways are highly active and result in a much higher basal ROS level than healthy cells. To circumvent the detrimental effects of oxidative stress, it is believed that the cancer cells must actively upregulate multiple antioxidant systems (Isaac et al., 2015). To handle high basal ROS production, the cancerous cells reprogram the glycolytic pathway to augment flux through the pentose phosphate pathway, a primary source of NADPH (Patra and Hay, 2014). The evolved mechanism ensures an adequate supply of NADPH, the proximal driver of the cellular antioxidant machinery to combat against ROS in cancerous cells rendering them to survive (Patra and Hay, 2014; Paul, 2015). Therefore, the Nrf2 KO possibly generated the alternative antioxidant pathways to compensate for the lack of a master antioxidant transcriptional factor Nrf2. Indeed, the Nrf2-ARE pathway was not the only pathway influenced by MeHg toxicity, but some other antioxidant pathways were also affected. Nrf2 is known to act by orchestrating an elaborate genetic program that enhances intrinsic cytoprotective functions, including drug-metabolizing, antioxidant, and antiinflammatory networks (Holmstrom et al., 2013). Therefore, lacking Nrf2 activity could exacerbate these cytoprotective functions. Furthermore, the differential expression of some of Nrf2 regulated genes were observed between WT and Nrf2 KO derived SCAs in this study and this contribute to the differential effect of MeHg to these genes' expression.

In conclusion, MeHg differentially affected antioxidant gene expression between WT and Nrf2 KO derived SCAs, demonstrating the role of the Nrf2 in MeHg induced toxicity. The

differential regulation of Keap1, Slc7a11, and Vegfa mRNA expression following MeHg exposure between these genotypes suggested that genetic predisposition also plays a role in differential susceptibility to MeHg. For example, the increase of Vegfa mRNA expression in WT derived SCAs, but a decrease in Nrf2 derived SCAs following MeHg exposure for 18h demonstrated that the genetic background plays a critical role in MeHg induced differential toxicity mechanism. There was cross-talk between signaling pathways in regulating the antioxidant genes: Abcc1 and Slc7a11 expression, regulated by Nrf2, in Nrf2 KO derived SCAs. Besides Nrf2, other redox-dependent transcription factors such as HIF might contribute to the differential response to MeHg exposure between these genotypes. The alteration of Glu transporter EAAT2/GLT-1 and system Xcexpression following MeHg exposure could contribute to MeHg induced excitotoxicity. Finally, the reduction of antioxidant genes involved in GSH synthesis and metabolism could affect the function of system Xc- and EAATs, contributing to MeHg-induced toxicity. These data lend support for an Nrf2-mediated mechanism of action whereby MeHg induces excitotoxicity and oxidative stress in SCAs that leads to neuronal degeneration.

#### **CHAPTER FOUR**

MECHANISMS UNDERLYING N-ACETYL CYSTEINE PROTECTION OF THE SPINAL CORD ASTROCYTE CELL CULTURE FROM METHYLMERCURY INDUCED TOXICITY

#### 4.1 Abstract

Neuronal toxicity of MeHg in SCAs includes dyregulation of the Keap1-Nrf2-ARE pathway and glutamate transporter expressions. MeHg also exacerbated SCAs derived from Nrf2 knockout degeneration compared to SCAs derived from wild type control. These previous data suggested that not only glutamate homeostasis and neuroprotective protein dysregulations but also the antioxidant system contributed to MeHg-induced toxicity in SCAs. The increase of cystine/glutamate transporter mRNA and reduction of their protein expressions in MeHg exposure also suggested that GSH and glutamate homeostasis were dysregulated. To test if activation of the Keap1-Nrf2-ARE pathway with a Nrf2 activator could ameliorate the toxicity of MeHg. Application of Nrf2 activators, including derivatives of synthetic triterpenoids such as bardoxolone methyl, the C-28 methyl ester of 2-cyano-3,12-dioxooleana-1,9-dien-28-oic acid (CDDO) known as CDDO-Me or RTA 402, or edaravone, did not protect against MeHg-induced SCAs degeneration. Nevertheless, the antioxidant N-acetyl-L-cysteine (NAC) had a protective effect against MeHg toxicity to SCAs. To determine further whether the concentration of NAC and treatment paradigms would affect NAC efficacy. Three different NAC treatment paradigms were tested its efficacy and mechanisms, with NAC 2 h pretreatment (NP), cotreatment (CO), and 3h post MeHg treatment (MP). All NAC treatments protected SCAs from MeHg in a concentration-dependent manner. NAC (0.1, 1.0, and 10mM) protected SCAs against 5µM MeHg induced degeneration over 24h. Meanwhile, 0.1mM NAC lost its potency around 30h compared to control; 1.0mM and 10mM retained their protective efficacy over 72h. With all NAC treatment paradigms, the optimum for NAC concentration was 1.0 mM since this concentration did not produce cell death, while 10mM NAC severely affected cell viability in NAC posttreatment. To get a better understanding of the protective mechanism by NAC, two hypotheses were tested. First, could NAC activate the Nrf2 pathway by increasing genes involved in GSH synthesis (Gclc) and activity (GPx1 and GPX4)? Second, did NAC directly react to MeHg as a chelating agent that subsequently reduced MeHg toxicity to SCAs? Nrf2 activity was determined by expression of antioxidant genes such as Gclc, GPx1, and GPX4 using qPCR. After 15h, 18h, and 20h of 1mM NAC treatment alone, respect to MP, CO, and NP paradigms, these time windows of NAC treatment did not increases Nrf2 or those antioxidant mRNA expressions in SCAs. The levels of these mRNA expression were relatively at the same level as the vehicle control. Application of NAC with MeHg treatments in all three paradigms also maintained expression of these mRNAs relatively to vehicle control levels, while 5µM MeHg for 18h treatment alone reduced the expression level of Keap1, Gclc, GPx1, GPx4, and Abcc1 mRNA significantly. NAC treatments alone, or NAC with MeHg treatments, maintained the expression level of glutamate transporter genes, including *Slc1a3*, *Slc1a2*, and *Slc7a11* mRNA to similar levels as vehicle treatments. To test the second hypothesis, if NAC directly reacted to MeHg and reduced its toxicity, SCAs were exposed to NAC for 2h then 5µM MeHg after NAC removal in culture media following by MeHg treatment. Following pretreatment of SCA with 1mM NAC for 2h with subsequent replaced with MeHg, SCAs viability was reduced considerably, starting at 1h MeHg exposure. This finding suggested that the protective mechanism by NAC was primarily due to its chelation of MeHg toxicity. The lack of intracellular NAC protection mechanism could be due to 1. poor membrane permeability of NAC, or 2. the short halflife of NAC in the cells if it was membrane permeable. Meanwhile, the rescue mechanism by NAC in the MP paradigm was unclear and has not yet been determined. It could be

possible that the chelating property of NAC could partly reduce the toxicity of MeHg in SCAs in MP treatment paradigm.

#### 4.2 Introduction

The mechanisms by which MeHg-induced SCAs degeneration involves dysregulation of the Keap1-Nrf2-ARE pathway by which it perturbs several genes underlying this redox sensing/antioxidant pathway. MeHg also dysregulated the expression of glial excitatory amino acid transporters (EAATs) Slc1a3 and Slc1a2 in SCAs. SCAs derived from a genetic knockout of Nrf2 mice (Nrf2 KO) were more susceptible to MeHg than those SCAs derived from wild type (WT). Some of the genes involving GSH synthesis and metabolism, such as Gclc, Gpx1, and Gpx4, were significantly decreased in both WT and Nrf2 KO following MeHg exposure (Chapter 3). The dysregulation of redox homeostasis intertwines with glutamate homeostasis that has also been implicated in MeHg-induced toxicity in SCAs. The study of the Keap1-Nrf2-ARE mRNA expression as a function of time during MeHg exposure in WT-derived SCAs exhibited the concomitant expressions cystine/glutamate antiporter (or system Xc-) Slc7a11 mRNA and excitatory amino acid transporter Slc1a3 and Slc1a2 mRNAs (Chapter 2). In addition, the increased basal level of Slc7a11 mRNA and Slc1a3, as well as Slc1a2 mRNAs in Nrf2 KO-derived SCAs were concurrent in vehicle-treated (control)(Chapter 3). The concomitant expression between these transporter mRNA in SCAs may support the finding that these transporters function cooperatively to regulate the homeostasis of cellular redox and glutamate homeostasis (Murphy et al., 1989; Murphy et al., 1990; Warr et al., 1999; Lewerenz et al., 2006).

To regulate the imbalance of intracellular redox homeostasis, the import of the cysteine, a rate-limiting substrate, is required for *de novo* GSH synthesis (Aoyama and Nakaki,

2013). L-cysteine is generally rapidly oxidized into L-cystine in normoxic or extracellular conditions (Yin et al., 2016). Therefore, extracellular L-cystine is a significant source of GSH precursor. L-cystine is later converted into L-cysteine intracellularly by the thioredoxin reductase enzyme (Txnrd1) (Yin et al., 2016). The intracellular cysteine is later utilized for de novo GSH synthesis. SystemXc- is one of the cystine transporters that imports one molecule of extracellular L-cystine in exchange for one molecule of intracellular glutamate (Warr et al., 1999; Conrad and Sato, 2012; Lewerenz et al., 2012). This exchange system depends upon the concentration gradient of L-cystine and extracellular glutamate (Warr et al., 1999). To reestablish the concentration gradient of these amino acids, the EAATs take up extracellular glutamate. These processes work in concert to protect against the dysregulation of redox and glutamate homeostasis (Warr et al., 1999; Lewerenz et al., 2006). HT22 mouse hippocampal neuronal cell line, which are resistant to a high concentration of glutamate (10-40mM), and hydrogen peroxide (H<sub>2</sub>O<sub>2</sub>), prominently expressed system Xc- mRNA (> 7- fold increase ) and significantly take up cystine (>7.5 fold) compared to sensitive HT22 cells. These oxidative glutamateresistant HT22 cells also expressed EAAT1, 2, and 3 mRNAs at higher levels than that in the sensitive HT22 cells (Lewerenz et al., 2006). Furthermore, co-overexpression of system Xc- together with EAATs protect HT22 cells against oxidative glutamate- toxicity more effectively than does overexpression of system Xc- or EAAT3 alone. Protection was concomitant with the increase of the intracellular GSH content (Lewerenz et al., 2006). Pharmacological inhibition of EAATs exacerbated oxidative glutamate toxicity by decreasing intracellular glutamate and GSH levels (Lewerenz et al., 2006). Mice with the genetic deletion of the Slc1a1 gene, coding for EAAT3/EAAC1, exhibited neuronal GSH reduction as well as memory and motor behavior decline with age (Aoyama et al., 2006).

The hippocampal slices of these mice were more susceptible to oxidative stress inducers such as  $H_2O_2$  and 3-morpholinosydnonimine (SIN-1), a nitric oxide generator than the wild-type (Aoyama et al., 2006). These effects were reversed by intraperitoneal injection (i.p.) of N-acetylcysteine (NAC) 4-6h before harvesting EAAC1 deleted mouse's brains. This impact of NAC on oxidant-scavenging capacity is due primarily to its role as a substrate for GSH synthesis (Aoyama et al., 2006). The neuroprotective effect of NAC was blocked with the coadministration of NAC and *de novo* GSH synthesis inhibitor buthionine sulphoximine (BSO) (Aoyama et al., 2006).

N-acetylcysteine (NAC), an FDA-approved drug, is a thiol-containing compound that has been used in clinical practice over decades. NAC was first used as an effective mucolytic for chronic obstructive pulmonary disease in the mid-1950s (Sheffner, 2008). Since the mid-1970s, NAC has been used as the first choice for the treatment of acetaminophen toxication (Prescott, 1983). NAC later has been widely used as a renal protectant in contrast-induced nephropathy and a therapeutic agent in HIV management (Berk et al., 2013; Rushworth and Megson, 2014). Recently, NAC has been demonstrated its clinical benefits for neurological diseases such as Alzheimer's, Parkinson's diseases and ALS (Arakawa and Ito, 2007; Tardiolo et al., 2018) and psychiatric disorders, including schizophrenia (Bulut et al., 2009; Rapado-Castro et al., 2017), depression and drug addiction (Dean et al., 2011; Berk et al., 2013; Minarini et al., 2017). Mechanisms by which NAC provides the clinical benefit involve its antioxidant property as well as being a precursor for GSH synthesis (Dringen and Hamprecht, 1999). The antioxidant property of NAC as its sulfhydryl moiety was well described in its disruption of disulfide bridges within the glycoprotein matrix of cystic fibrosis patients' mucus (Hurst et al., 1967;

Rushworth and Megson, 2014; Aldini et al., 2018). The antioxidant mechanism of NAC is also involved in its direct interaction with ROS and NOS as a free radical scavenger (Aldini et al., 2018). NAC, as a GSH synthesis precursor, has been demonstrated in both neurons and non-neurons. NAC incubation for 4h in rat neuronal cell culture exhibited an increase of intracellular GSH in NAC-concentration dependent manner (0.1, 1, 5mM) (Dringen and Hamprecht, 1999). Recently, the mechanism of NAC in neuroprotection was shown to be involved in the modulation of neurotransmitters in both humans and animal models (Dean et al., 2011; Berk et al., 2013). A single oral administration of 2400 mg NAC reduces glutamate levels in the anterior cingulate cortex of schizophrenia patients compared to placebo (McQueen et al., 2018). Prenatal stress-induced rat offsprings, which later showed dopamine reduction and learning and memory deficits, were prevented by NAC administration over the entire course of pregnancy (Bernhardt et al., 2018). Reverse of neurotransmitter homeostasis by NAC is involved in the regulation of system Xc- and the presynaptic metabotropic glutamate receptor mGluR2/3 (Kupchik et al., 2012; Berk et al., 2013; Chen et al., 2014). Another postulated mechanism of NAC is its involvment in the regulation of Keap1-Nrf2-Are pathway. The effects of 200μM H<sub>2</sub>O<sub>2</sub> induced an increase of Nrf2 and its downstream antioxidant gene heme oxygenase-1 (Ho-1) in osteoblast differentiation MC3T3-E1 cells were prevented by coadministrations of 2.5 and 5mM NAC (Lee et al., 2015). Several possible NAC mechanisms in neuronal protection and pathogenic mechanisms by MeHg induced toxicity in SCAs could involve maintaining redox and glutamate homeostasis. To characterize the mechanism of action of NAC on SCA would facilitate a better understanding of MeHg toxicity.

In this study, the different concentrations of NAC (0.1, 1.0, and 10mM) were based on the physiological values of intracellular GSH, which generally ranges from 0.5 to 10mM (Dringen, 2000; Shimizu et al., 2002) and previous studies in neuronal cell culture and cell lines (Dringen and Hamprecht, 1999; Shimizu et al., 2002; Lee et al., 2015) were used to test its efficacy in the protection and rescue of SCAs from MeHg exposure. The maximum MeHg concentration (5µM) in Chapter 2 was used to test the efficacy of NAC as a function of time. Three experimental treatment paradigms were employed for NAC: pretreatment (NP), cotreatment (CO), and posttreatment (MP), to differentiate a possible mechanism of NAC action against MeHg induced toxicity in SCAs. A mode of NAC's action in Keap1-Nrf2-ARE pathways, which were dysregulated in SCAs during MeHg exposure, was also examined with these experimental paradigms. To test if NAC acts as a chelating agent, SCAs viability was determined with pre-treatment of NAC for 2h, which was subsequently removed before administration of MeHg. The absence of NAC during the MeHg exposure paradigm could explain the mode of NAC's action as a thiolcontaining compound, in which it is reactive and chelates MeHg toxicity.

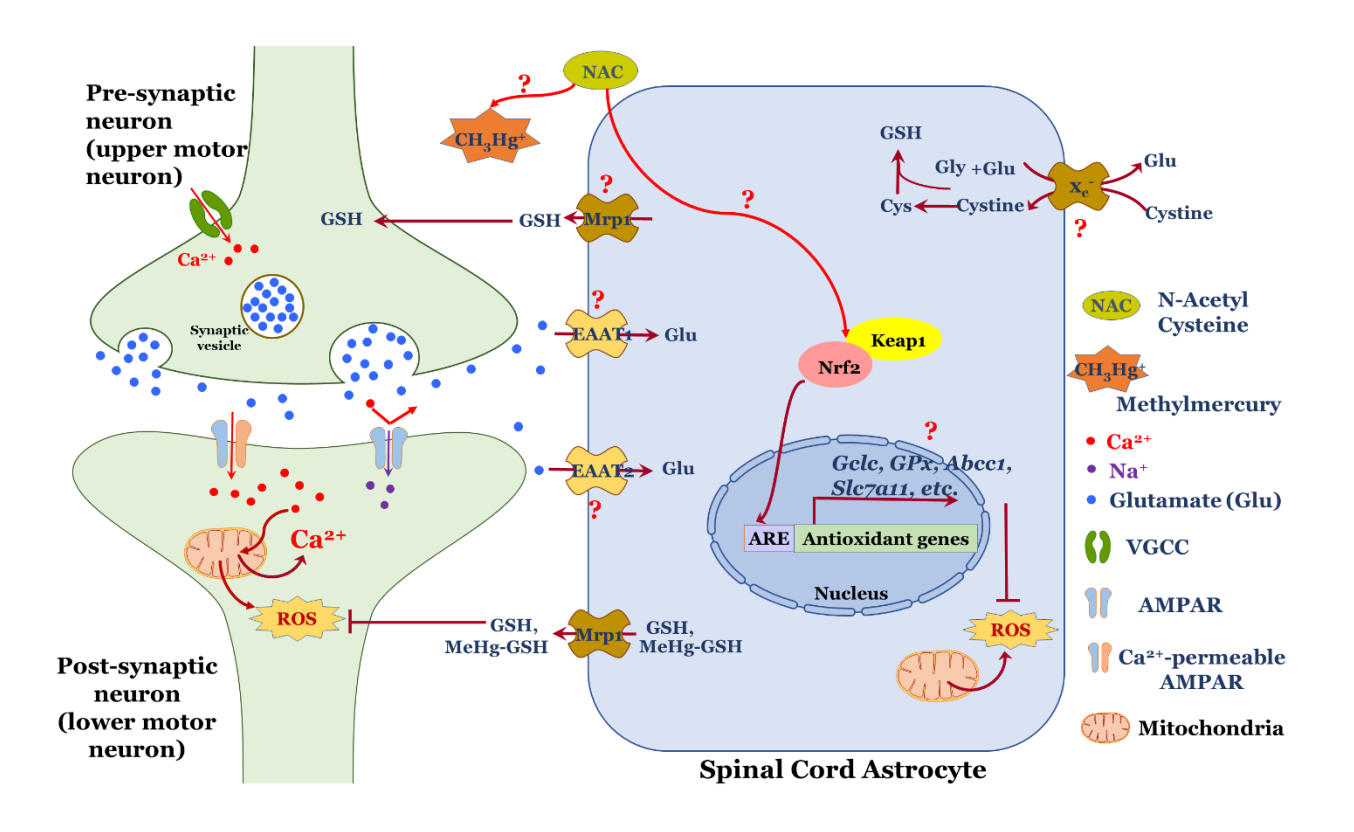


**Figure 4.1 Research aim 3: Working hypothesis of NAC actions in SCAs during MeHg exposure.** NAC would protect or rescue SCAs from MeHg-induced toxicity by maintaining cellular redox homeostasis either by 1). increase of Keap1-Nrf2-ARE pathway activity including increasing genes involving GSH synthesis or 2.) its thiol (-SH) reacting property, as antioxidant property to chelate MeHg.

#### 4.3 Materials and methods

#### 4.3.1 Chemicals

NAC and N-acetyl-L-cysteine amid (NACA) were obtained from Sigma (St.Louis, USA) (NAC; catalog number A7250-10G and NACA; catalog number A0737-5MG). Both NAC and NACA were dissolved in DMSO to obtain 1M stock concentration. They were aliquoted in amber tubes and kept at -20 °C until used for the experiments.

#### 4.3.2 MeHg exposure and NAC treatment regimens

To determine the efficacy of NAC concentration, SCAs DIV 28-30 were treated with 0.1, 1.0, and 10mM NAC with different treatment paradigms of 5µM MeHg exposure.

The NAC and MeHg treatment paradigm were as follows.

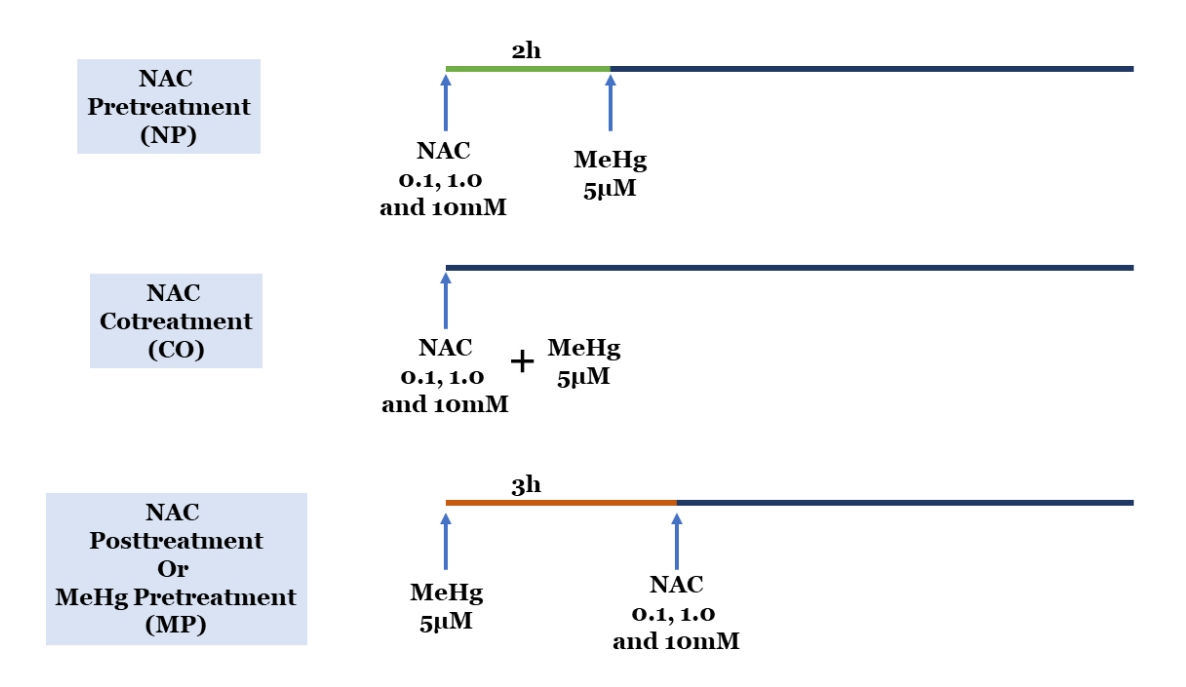


**Figure 4.2 MeHg exposure and NAC treatment regimens.** With NAC pretreatment (NP) regimen, different NAC concentrations were added in the SCAs 2h prior to MeHg exposure. NAC and MeHg were simultaneously administered to SCAs in cotreatment (CO). With NAC posttreatment or MeHg pretreatment (MP), NAC was added after SCAs were exposed to MeHg for 3h.

The Real-Time Glo<sup>™</sup> MT Cell Viability Assay (as described in chapter 2.3.6) was used to collect data from 1h following MeHg exposure, and every 3h thereafter, until the chemiluminescent signals were extinguished. For the gene expression assay with qPCR, SCAs were exposed to MeHg for 18h, which reduced more than 90% of SCAs viability as indicated in Chapter 2 and Figure 4.2, 4.3 and 4.4. The mRNAs from all treatments were harvested for RT-PCR and qPCR as described in Chapter 2.3.9.

#### 4.3.3 Cell viability assay with ethidium homodimer

The efficacy of NAC in SCAs protection from MeHg-induced toxicity was examined using ethidium homodimer-2 (Ethd-2). The SCAs cell cultures were treated with 1mM NAC for 2h. NAC was subsequently removed from cell culture media and replaced with 5µM MeHg. Cells were rinsed with cold PBS buffer and incubated with 0.1µM EthD-2 for 20min. Cells were then washed with PBS and fixed with Zamboni's fixative reagent (American MasterTech Scientific Laboratory Supplies, Inc., Lodi, CA, USA). The GFAP immunostaining and DAPI staining were followed by the standard immunocytochemistry procedure as described in Section 2.3, Chapter 2.

#### 4.4 Results

### 4.4.1 NAC protected SCAs from MeHg in a concentration-dependent fashion.

Several antioxidants have been reported to provide beneficial protection to neurons or cell lines against MeHg- induced toxicity (Shanker and Aschner, 2003a; Yamashita et al., 2004; Shanker et al., 2005b). This study was to test if antioxidants could protect SCAs from MeHg-toxicity. Nrf2 activators such as CDDO-IM (Liby, 2005), CDDO-ME (Stack et al., 2010), and edaravone were applied to test their efficacies for protection of SCAs against MeHg-induced toxicity. At concentrations ranging from 10uM to 10mM edaravone failed to protect SCAs against MeHg (See **Figure A.4 to A.7** in **Appendix**). The higher edaravone concentration caused a more significant cell death than did in MeHg treatment alone. A similar effect has shown with CDDO-IM and CDDO-ME treatment (See **Figure A.8 to A.11** in **Appendix**). However, different concentrations of NAC protected against the SCAs from MeHg induced cell death. Administration of NAC at 0.1, 1.0, and 10mM for 2h before applying 5µM MeHg into SCAs cell cultures caused a concentration-dependent protection (Figure 4.3). While SCAs exposed to MeHg exhibited a significant reduction of cell metabolic activity starting from 9h MeHg exposure, pretreatment with 0.1mM NAC 2h before MeHg exposure considerably extended a reduction of cell metabolic activity to 30h of MeHg exposure. When NAC concentration was increased to 1.0mM and 10mM NAC with the same pretreatment paradigm, NAC extended the further protection of SCAs from MeHg-induced toxicity across the experimental time course (over than 160 h) (Figure 4.3).

NAC perhaps interacted with MeHg directly due to its intrinsic thiol property and reduced MeHg toxicity to SCAs. Therefore, two additional NAC treatment paradigms, cotreatment of NAC and MeHg, and MeHg pretreatment followed by NAC application, were used to test its protective mechanisms. Coapplication of different NAC concentrations and 5μM MeHg showed a similar protective effect as that in the NAC pretreatment paradigms. Cotreatment of 1.0mM or 10mM NAC with MeHg protected SCAs from MeHg induced toxicity across the entire course of the examination (**Figure 4.4**). A significant reduction of SCAs metabolic activity still occurred at 30h MeHg exposure. On the other hand, 10 mM NAC treatment following 5μM MeHg exposure (MeHg pretreatment paradigm) did not protect SCAs from MeHg exposure, whereas 0.1 μM and 1.0 μM NAC did protect SCAs against MeHg. Treatment with 1.0 μM NAC after 3h of MeHg exposure in SCAs was more efficacious than that in the 0.1 μM NAC posttreatment (**Figure 4.5**).

All these NAC treatment paradigms suggested that 1.0mM NAC concentration provided the best efficacy among these NAC concentrations and caused no apparent effect in increase SCAs cytotoxicity.

## 4.4.2 Pretreatment, cotreatment, and posttreatment with 1.0mM NAC and 5µM MeHg maintained *Keap1* mRNA levels at similar levels to *Keap1* mRNA levels in vehicle treatment.

To understand if NAC protected SCAs against MeHg-induced toxicity through the Keap1-Nrf2-ARE pathway, expression of some species of mRNA under this pathway were examined in three NAC treatment paradigms, NP, CO and MP. Expression of the *Keap1* mRNA level was significantly reduced by about 0.3-fold following 18h of MeHg exposure compared to vehicle treatments. NAC alone with 1.0mM treatments neither reduced nor

enhanced *Keap1* mRNA expression in any NAC treatment paradigms compared to vehicle treatments. When treatment of NAC with MeHg, Keap1 mRNA levels were similar to vehicle or NAC alone in NP, CO, and MP treatment paradigms but was significantly higher than MeHg exposure alone (Figure 4.6). When determining the effect of NAC in Nrf2 mRNA expression in SCAs, NAC alone caused a significant increase of Nrf2 mRNA compared to MeHg alone in CO or MP but NP paradigm (indicated in \* in Figure 4.7). These differential expressions of Nrf2 could be due to a time-dependent efficacy of NAC. The periods of NAC treatments in SCAs among these experimental paradigms were different by which NP, CO, and MP were 20h, 18h, and 15h, respectively, when the mRNAs were collected after 18h of MeHg exposure regardless of the NAC treatment paradigms (Figure 4.7). At 18h of 5µM MeHg exposure, the SCAs viability was reduced by about 50% compared to control treatment (Chapter2); therefore, this MeHg exposure time was used to ensure that half of the SCAs cell culture population were affected by MeHg. A Two-Way ANOVA of all experimental paradigms did not suggest a significant reduction of Nrf2 mRNA relative to vehicle treatments when SCAs were exposed to MeHg for 18h. Statistical analysis also indicated the no effect cotreatment of NAC with MeHg on Nrf2 mRNA expression even though the levels of Nrf2 mRNA in these treatments were higher than those in the MeHg alone treatment (**Figure 4.7**). The results suggested that the protection of NAC against MeHg induced toxicity in SCAs could participate in the regulation of *Keap1* mRNA but maybe not the Nrf2 mRNA expression.

# 4.4.3 NAC protected and reversed the reduction of GSH metabolic pathways and transporters such as *Gclc*, *GPx1*, *GPx4*, *and Abcc1* mRNA levels in SCAs treated with MeHg.

NAC has its neuroprotective effects are reportedly in part due to its chemical property as a derivative of the amino acid L-cysteine (Clark et al., 2010). Cysteine is a rate-limiting substrate for *de novo* GSH synthesis, and intracellular GSH content increased in rat primary neuronal cell culture incubation with NAC (Dringen and Hamprecht, 1999). Since a MeHg exposure induced the reduction of expression of mRNAs involved in GSH metabolic pathways (results from Chapters 2 and 3), the effect of NAC in the protection of SCAs from MeHg induced toxicity could involve the maintenance of *Gclc*, *Gpx1*, and *Gpx4* mRNA expressions. To test if NAC would protect SCAs from MeHg toxicity through the maintenance of *Gclc*, *GPx1*, and *GPx4* mRNA expression, the gene expression assay using qPCR was used to determine the levels of these mRNA compared to vehicle, NAC alone and MeHg/NAC treatment regimen. The effects of NAC treatment with MeHg in NP, CO, and MP treatment paradigms resulted in levels of *Gclc*, *GPx1*, and *GPx4* mRNA similar to those of vehicle and NAC alone treatments and theses levels were significantly higher than the effect of MeHg treatment alone (**Figures 4.8, 4.9 and 4.10**).

Interestingly, when compared the effects of NAC treatment with MeHg in all NAC paradigms, the level of *Gclc* mRNA expression in NAC posttreatment after MeHg exposure for 3h (MP) in SCAs was significantly lower than that in the NAC pretreatment 2h following with MeHg (NP) and co-treatment (CO) (**indicated in & Figure 4.8**). These differentials of *Gclc* expressions could be explained by the toxic effect of MeHg in MP was progressed in SCAs for 3h, and NAC posttreatment for activation of *Gclc* could

have less efficacy than that in the NP and CO treatments where the beneficial effects of NAC provided the SCAs protection effects, not the rescue (reverse) MeHg-toxic effects. Nevertheless, the efficacy of NAC in reverse of MeHg-induced toxicity in SCAs was potent as well as its protective effects because the expressions of *Gclc* level were significantly higher than that in MeHg alone treatments. The results of *Gclc*, *Gpx1*, and *Gpx4* mRNA expressions in these experimental paradigms may explain the mechanism of NAC action in the protection of SCAs against MeHg-induced toxicity through which it maintained the redox homeostasis via upregulation of these GSH metabolic pathways.

Besides MeHg induced dysregulation of GSH metabolic pathway expression, SCAs GSH transport was also affected following MeHg exposure. Reductions of *Abcc1* mRNA encoding for multidrug-resistant associated protein (Mrp1) occurred after 5µM MeHg exposure for 18h in SCAs (Figure 4.11). All NAC experimental paradigms indicated the protection and reverse of *Abcc1* mRNA reduction from MeHg exposure (the asterisk (\*) indicated the difference from MeHg alone treatments, Figure 4.11). Interestingly, in the CO and MP experimental paradigms, *Abcc1* mRNA expression levels in NAC and MeHg exposure conditions were higher than those in the NP experimental paradigm (indicated with "&" in Figure 4.11). *Abcc1* expression level in NAC alone treatment was also significantly higher than the vehicle treatment in MP experimental paradigm (indicated with "#" in Figure 4.11). Upregulation of *Abcc1* mRNA in NAC treatment might suggest that NAC induced its protective effect through induction of Mpr1 transporter expression to increase the transport and export of GSH and toxic compounds from SCAs.

## 4.4.4 NAC protected and reversed the dysregulation of glutamate transport system in SCAs.

Glutamate-mediated excitotoxicity has been involved in MeHg induced neuronal and glial degeneration (Brookes, 1992a; Matyja and Albrecht, 1993; Qu, 2003). MeHg induced the dysregulation of vesicular glutamate release through synaptic transmission (Reynolds and Racz, 1987; Yuan and Atchison, 1995, 1997a). While non-vesicular glutamate release through the cystine/glutamate antiporter or system Xc- might be involved since MeHg at 0.5μM (Figure 2.9, Chapter 2) or 5μM (Figure 3.8 and 3.11 Chapter 3 and Figure 4.12) induced the increase of *Slc7a11* mRNA expression in SCAs. NAC is a substrate precursor for GSH synthesis, and usually, extracellular L-cysteine is rapidly oxidized into L-cystine in normoxic conditions in the extracellular space (Yin et al., 2016). Cystine could be transported into the cell through cystine/glutamate antiporter or system Xc-. To test whether NAC could affect dysregulation of *Scl7a11* expression during MeHg exposure and determine what the mode of NAC action would be in regulation of Scl7a11 expression. NP, CO, and MP of NAC treatment paradigms were compared to MeHg alone and vehicle treatments. The results of NAC with NP and CO did not differ from NAC treatment alone following exposure to 3h of MeHg. The levels of Scl7a11 expression in NAC treatment with MeHg in all NAC treatment paradigms were similar to vehicle treatments (Figure 4.11), which suggested 1mM NAC could protect and rescue the dysregulation of Scl7a11 expression during MeHg induced toxicity in SCAs.

MeHg not only dysregulated the expression of *Scl7a11*, but also that of glial glutamate transporters *Scl1a3* (**Figure 4.13**) and *Scl1a2* (**Figure 4.14**). MeHg reduced *Scl1a3* and *Scl1a2* expressions. NAC protected and reversed the effect of MeHg. Treatment with NAC

alone for 15h (1mM NAC in MP Figures 4.13 and 4.14) significantly increased *Scl1a3* and *Scl1a2* expressions compared to vehicle treatments (control) and NAC following MeHg treatments. These results suggested that NAC induced an increase of *Scl1a3* and *Scl1a2* expressions in SCAs. Those benefit maintenance of these mRNA expressions during MeHg exposure.

# 4.4.5 Pretreatment with NAC 2h and subsequently removal before exposure to MeHg was not protective.

NAC could protect and prevent dysregulation of Keap1-Nrf2-ARE pathway in SCAs during MeHg exposure in all three paradigms. NAC might boost this antioxidant pathway, thereby making SCAs more resistant to MeHg. Alternatively, NAC might act as a cysteine prodrug and substrate precursor for GSH synthesis. Thereby, it might increase the intracellular GSH level in SCAs, making them more resistant to MeHg-induced toxicity. To further characterize the mechanism by which NAC protected SCAs from MeHginduced cell death, SCAs were treated with 1mM or 10mM NAC for 2h. NAC was subsequently removed before administration of MeHg. The Real-Time Glo™ MT Cell Viability Assay was used to examine the cell metabolic activity of SCAs in different treatment conditions as a function of time. Neither 1mM nor 10mM NAC pretreatment prevented SCAs degeneration from MeHg induced toxicity. Results after 1mM or 10mM NAC pretreatment following 5µM MeHg were similar to those of MeHg treatment alone at every time point (Figure 4.15). In contrast, 1mM and 10mM NAC alone treatment exhibited the data in the same level of vehicle treatment in all data points (Figure 4.15). This experiment indicated that in the absence of NAC during MeHg exposure in SCAs, SCAs remained susceptible to MeHg induced toxicity regardless of whether the cells were pretreated with NAC. NAC did not increase intracellular GSH in SCAs or protect cytotoxicity from MeHg. This result was confirmed using the ethidium homodimer -2 (EthD-2), a cell- impermeant viability indicator that would emit the red fluorescence when it bound to dead cells' DNA. SCAs were co-stained with DAPI and GFAP to observe the SCAs structure and morphology. SCAs treated with MeHg for 18h showed the red fluorescent in the nucleus with few green fluorescence staining (Figure 4.16 Right Panel, Top). In contrast, vehicle alone (Figure 4.16 Left Panel, Top) and NAC alone (Figure 4.16 Left Panel, Bottom) treatments demonstrated emissions of blue fluorescence (DAPI) in the nucleus and very bright green fluorescence of GPAP along with SCAs structure and morphology. Pretreatment of NAC in SCAs for 2h prior to exposure to MeHg alone for 18h (NAC/MeHg) indicated a magenta color in nuclei and bright green fluorescence along with SCAs structure (Figure 4.16 Right Panel, Bottom). The degree of green fluorescence of GFAP staining in NAC/MeHg was much brighter and SCAs structure was maintained better than that in the MeHg treatment alone. The SCAs nuclei from NAC/MeHg treatment showed magenta, which indicated a combination of DAPI and EthD-2 colors. These data suggest that NAC provided some protection for SCAs structure during MeHg exposure; however, it did not protect SCAs from MeHg induced cytotoxicity.

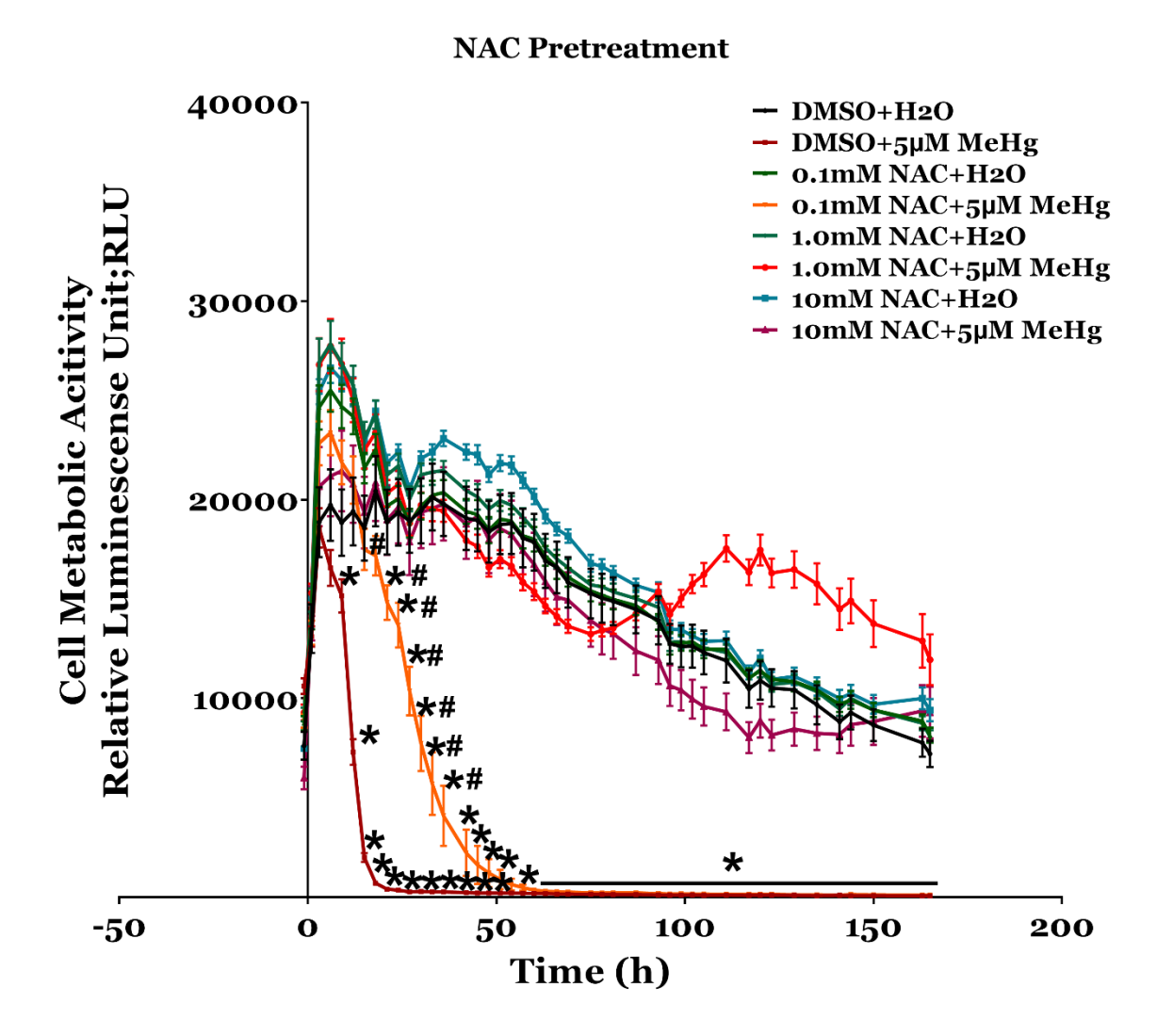
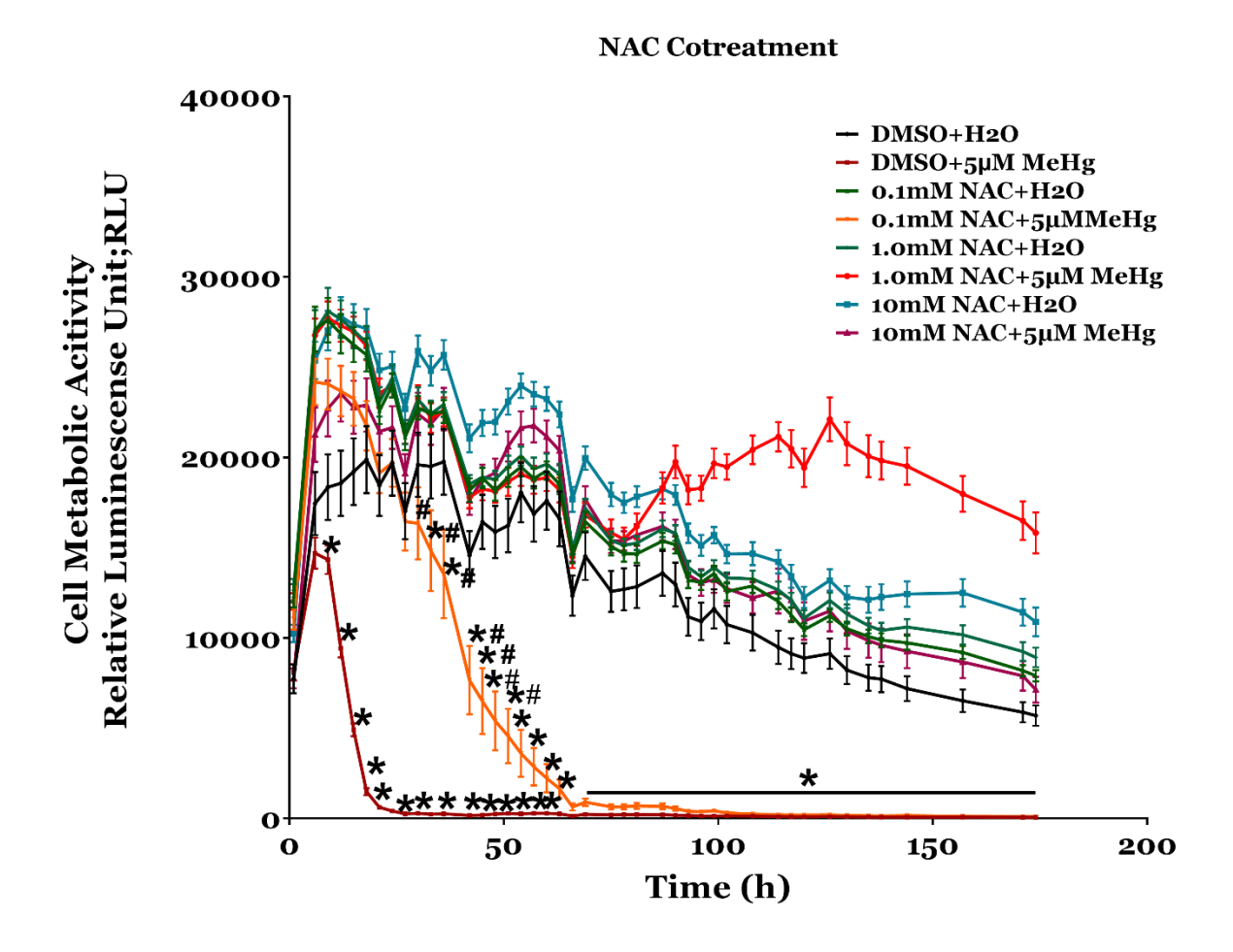


Figure 4.3 Cell metabolic activity as a function of time when SCAs were treated with 0.1, 1.0, or 10mM NAC for 2h prior to exposure with 5 $\mu$ M MeHg. Cell viability was determined during MeHg exposure from 1h after NAC treatment to 169h of MeHg exposure. NAC exhibited concentration-dependent protection against MeHg toxicity. While 0.1mM NAC pretreatment 2h prior to MeHg exposure showed a significant reduction of cell metabolic activity compared to vehivle control around 30h of MeHg exposure (\*). However, 0.1mM NAC concentration continued to protect some SCAs from MeHg-induced cell death until 42h of MeHg exposure (#) . With 1.0mM and 10mM NAC treatment 2h following with MeHg exposure protected SCAs from MeHg-induced toxicity across the all-time course of the examination. A Two-Way ANOVA with Tukey's multiple comparison *post hoc* was used for statistical analysis. The asterisk (\*) indicates a value statistically significant from DMSO+ $5\mu$ M MeHg. N=12 biological replications.



**Figure 4.4 Cell metabolic activity as a function of time when SCAs were cotreated with 0.1, 1.0, or 10mM NAC and 5μM MeHg or vehicle.** Cell viability was determined during MeHg exposure from 1h after NAC treatment to 174h of MeHg exposure. NAC exhibited concentration protection against MeHg induced toxicity. Cotreatment 0.1mM NAC with 5μM MeHg protected SCAs for 33h from MeHg exposure (\*). This 0.1mM NAC maintained its protection against MeHg toxicity for 60h since the cell metabolic activity was higher than that MeHg treatment alone (#). Cotreatment 1.0 or 10mM NAC with 5μM MeHg protected SCAs across timepoint observation. A Two-Way ANOVA with Tukey's multiple comparison *post hoc* was used for statistical analysis. The asterisk (\*) indicates a value statistically significant from DMSO+5μM MeHg. N=12 biological replications.

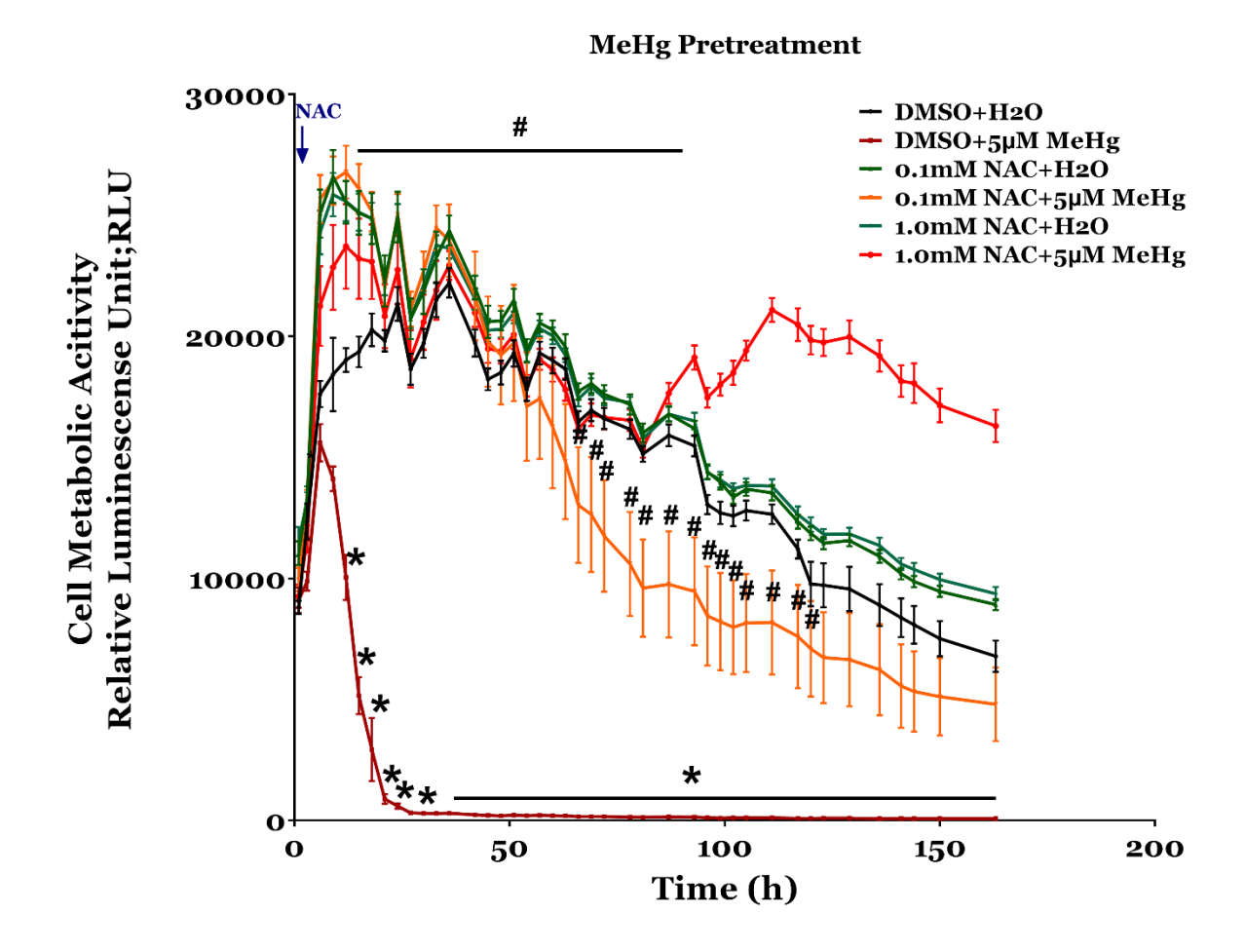
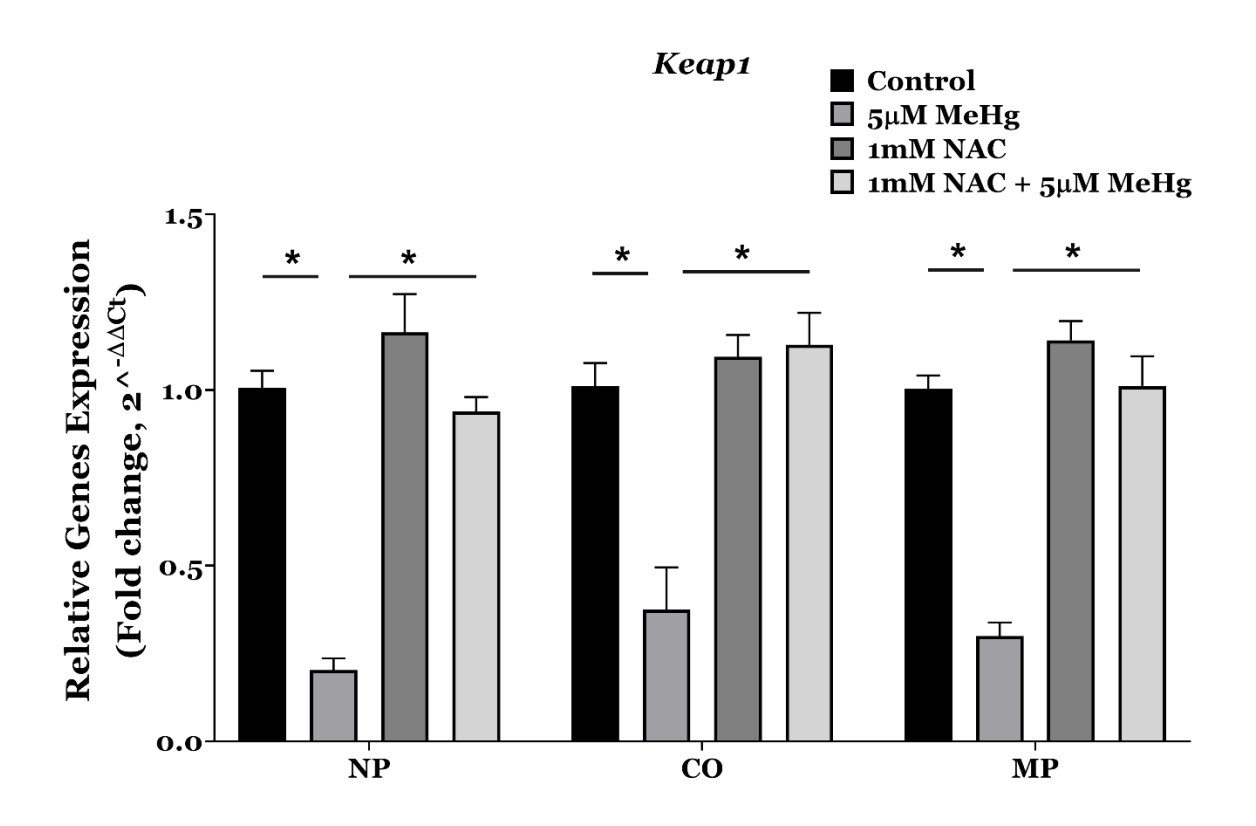


Figure 4.5 Cell metabolic activity as a function of time when SCAs were exposed to 5μM MeHg for 3h and 0.1 or 1.0 mM NAC was subsequently administered. Cell viability was determined during MeHg exposure from 1h after MeHg treatment to 163h of MeHg exposure. MeHg treatment caused the reduction of cell viability, starting from 9h of exposure. Both 0.1 and 1mM NAC efficiently rescued SCAs from MeHg-induced cell death. These concentrations remained its SCAs protection across all time points. The 1.0 mM NAC was more efficacious at recovering SCAs than was in 0.1mM NAC treatment. A Two-Way ANOVA with Tukey's multiple comparison *post hoc* was used for statistical analysis. The asterisk (\*) indicates a value statistically significant from DMSO+H<sub>2</sub>O. The number sign (#) indicates a value statistically significant from DMSO+5μM MeHg. N=12 biological replications.



**Figure 4.6 The effect of NAC on regulation of** *Keap1* **mRNA during MeHg exposure in SCAs.** NP, CO, and MP refer to NAC pretreatment 2h prior to MeHg exposure, NAC cotreatment with MeHg, and NAC treatment following 3h of MeHg, respectively. MeHg reduced *Keap1* mRNA expression, while all NAC treatment paradigms maintained *Keap1* mRNA expression at a similar level control treatment. A Two-Way ANOVA with Tukey's multiple comparison *post hoc* was used for statistical analysis. \* indicates statistically significant from MeHg treatment alone, N=6 biological replications

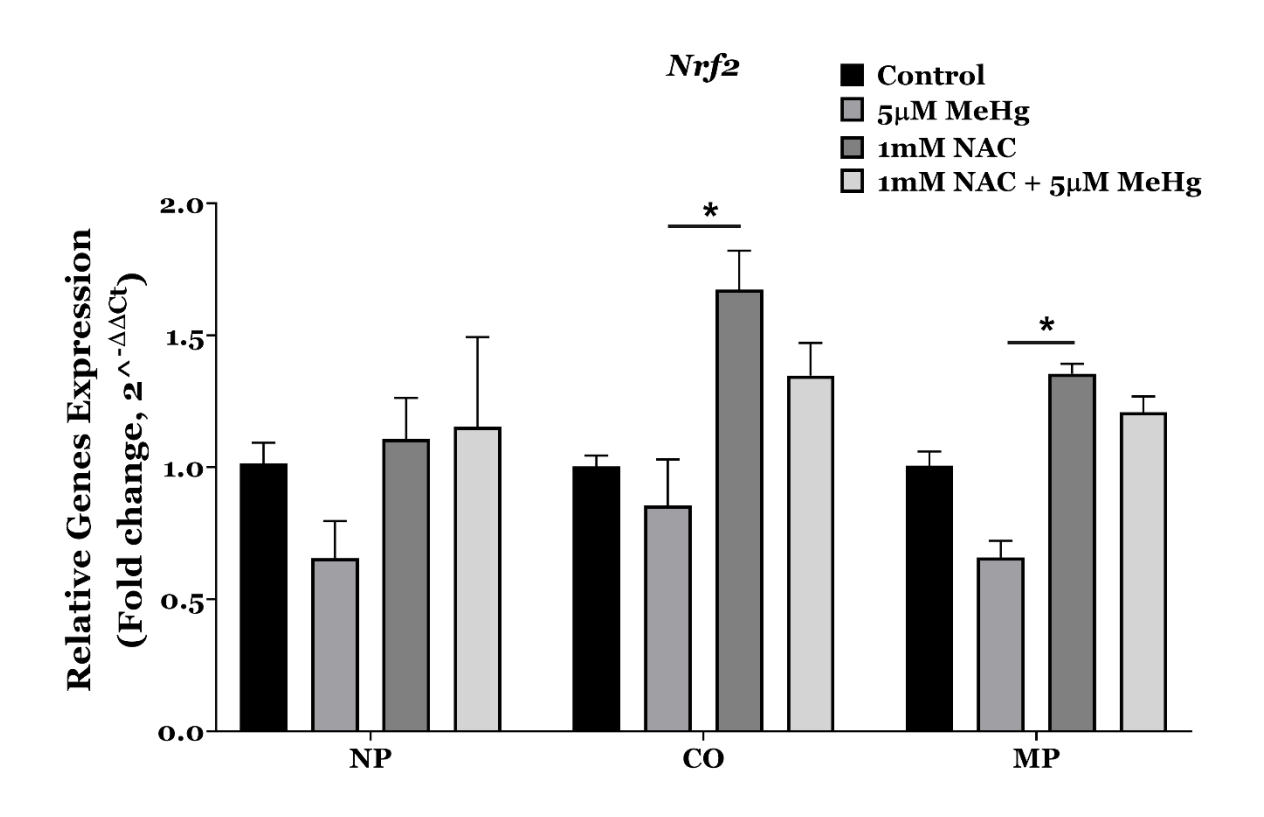
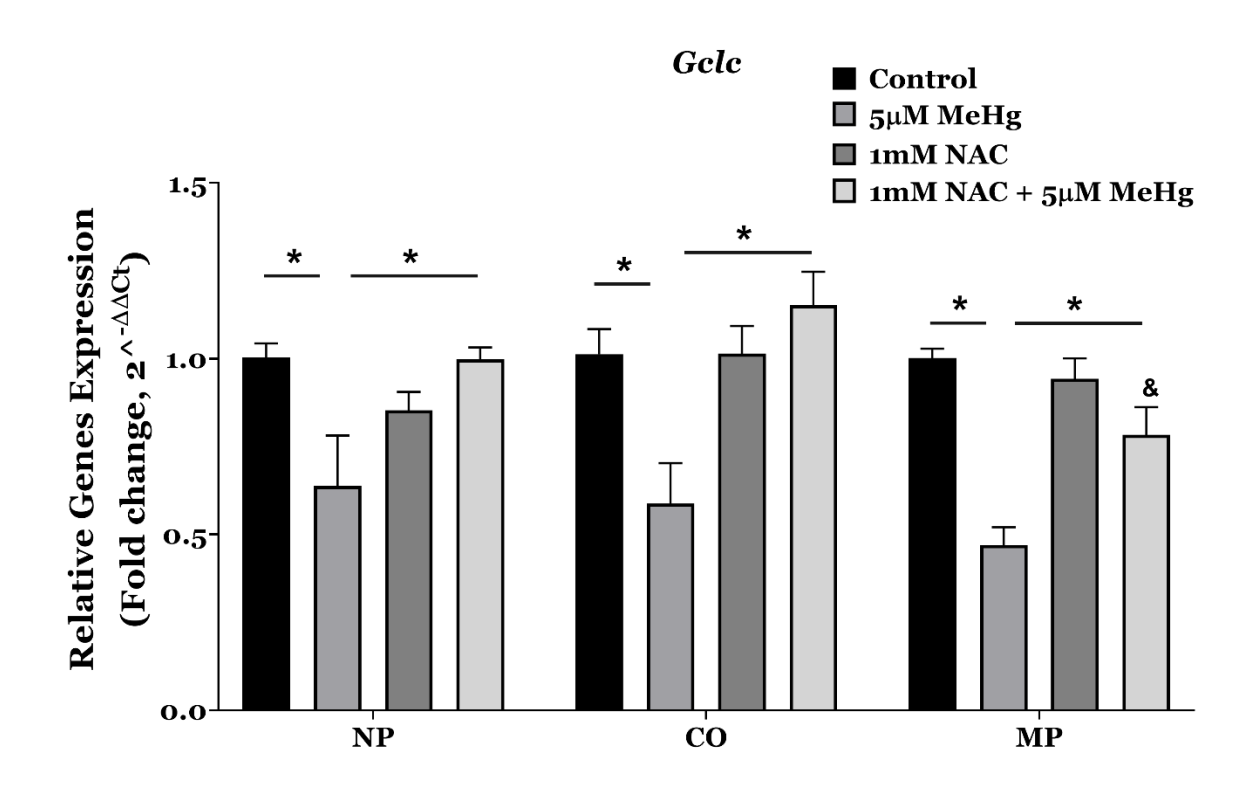
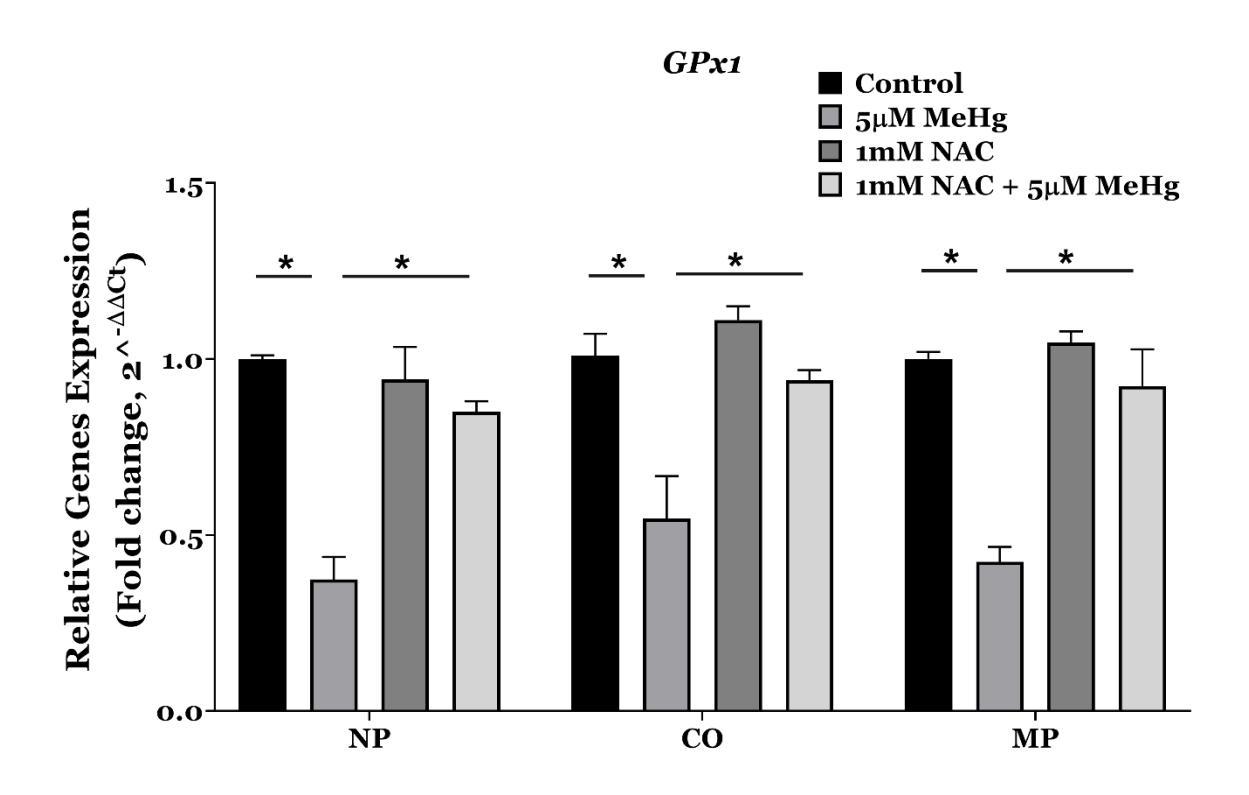


Figure 4.7 The effects of NAC on regulation of *Nrf2* mRNA during SCAs exposure to MeHg. NAC treatment paradigms are as described in Figure 4.5. MeHg appeared to reduce *Nrf2* mRNA expression; however, the reduction of Nrf2 in these treatments was not statistically significant. NAC treatment alone in CO and MP induced higher Nrf2 expression than MeHg treatment alone but not higher than vehicle control. NAC treatment with MeHg maintained Nrf2 expression level at a similar level of control. Two-Way ANOVA with Tukey's multiple comparison *post hoc* was used for statistical analysis. The asterisk (\*) indicates statistically significant from MeHg treatment alone, N=6 biological replications



**Figure 4.8 The effect of NAC on regulation of** *Gclc* mRNA during SCAs **exposure to MeHg.** MeHg reduced *Gclc* mRNA expression, while all NAC treatments, either alone or with MeHg, all experimental paradigms maintained *Gclc* mRNA expression at a similar level control treatments. A Two-Way ANOVA with Tukey's multiple comparison *post hoc* was used for statistical analysis. The asterisk (\*) indicates statistically significant from MeHg treatment alone. The ampersand (&) indicates MP different from NP and CO. N=6 biological replications,



**Figure 4.9** The effect of NAC on regulation of *GPx1* mRNA during SCAs exposure to MeHg. MeHg induced the reduction of *Gpx1* mRNA expression. All NAC treatments, either alone or with MeHg, all experimental paradigms maintained *Gpx1* mRNA expression at a similar level control treatments. Two-Way ANOVA with Tukey's multiple comparison *post hoc* was used for statistical analysis. The asterisk (\*) indicates statistically significant from MeHg treatment alone, N=6 biological replications

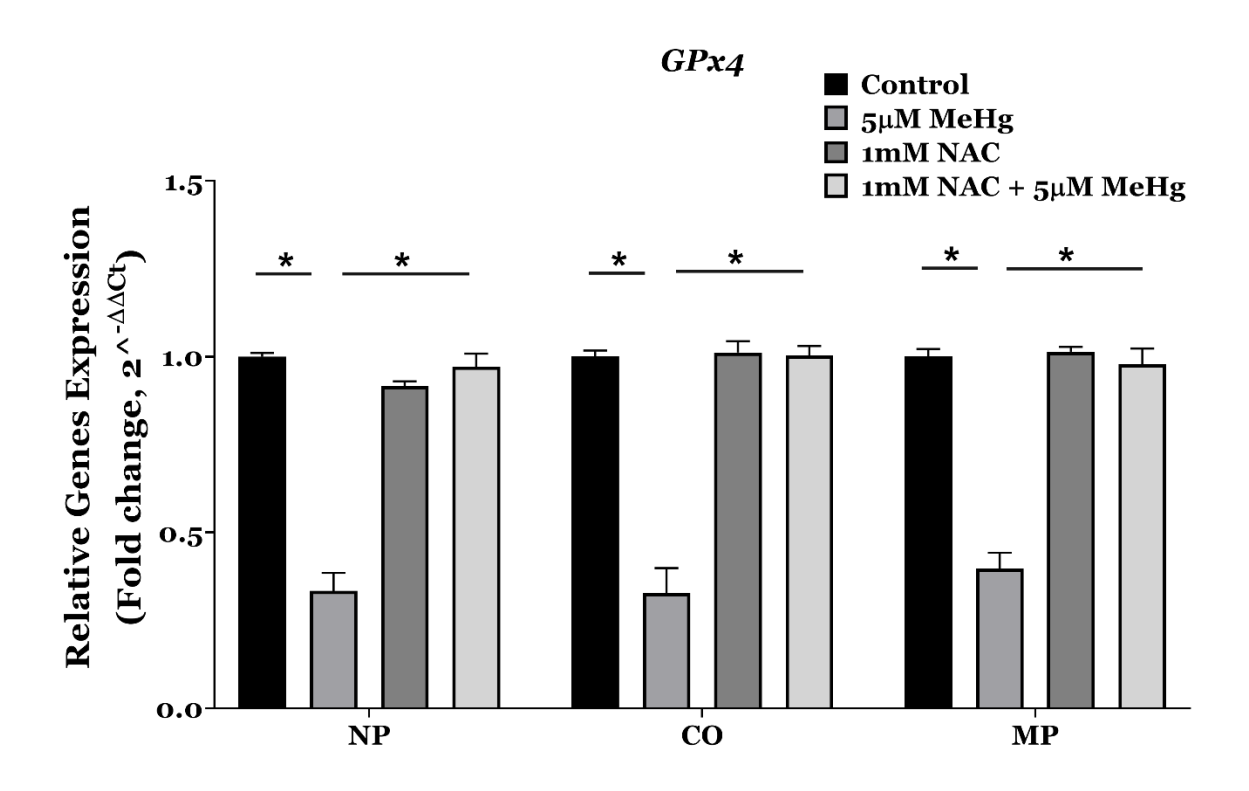


**Figure 4.10 The effect of NAC on regulation of** *GPx4* **mRNA during SCAs exposure to MeHg.** MeHg reduced *Gpx4* mRNA expression, while all NAC treatments, either alone or with MeHg, all experimental paradigms maintained *Gpx4* mRNA expression in a similar level of control treatments. A Two-Way ANOVA with Tukey's multiple comparison *post hoc* was used for statistical analysis. \* indicates statistically significant from MeHg treatment alone, N=6 biological replications

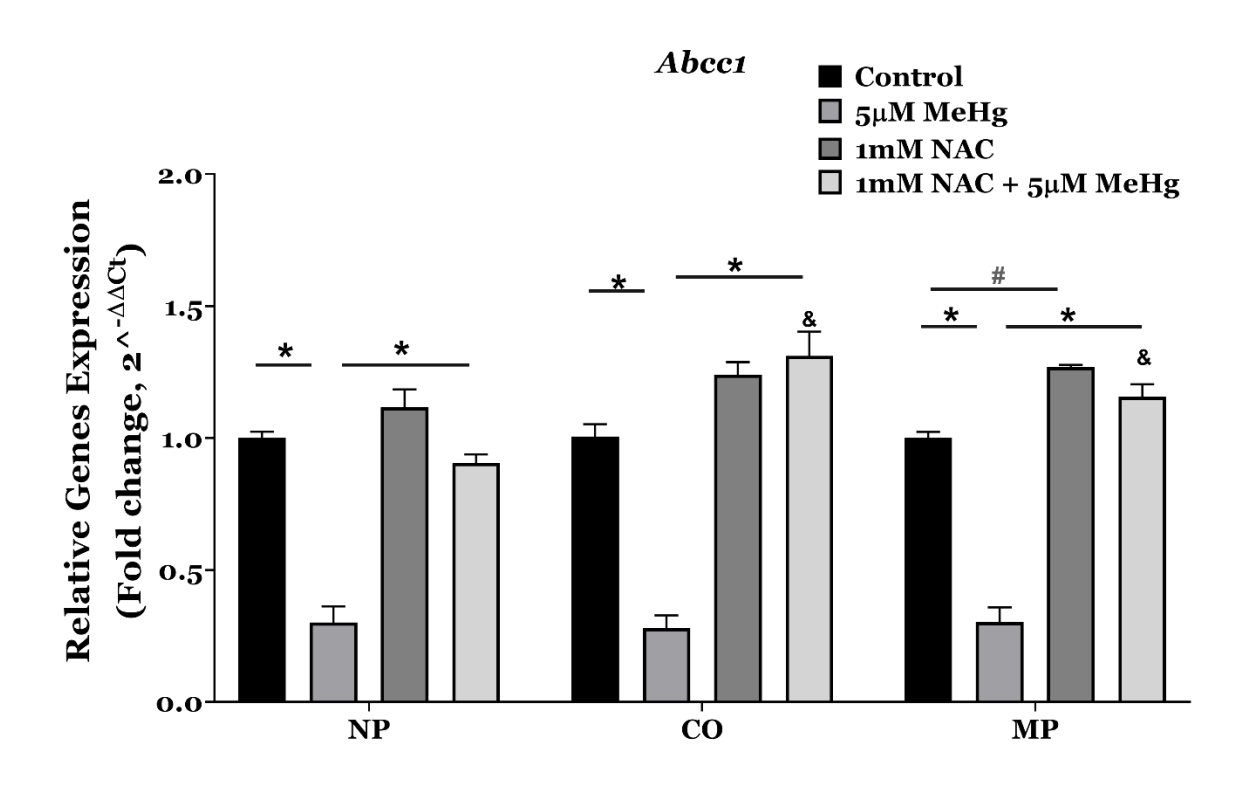


**Figure 4.11 The effect of NAC on regulation of** *Abcc1* **mRNA during SCAs exposure to MeHg.** MeHg reduced *Abcc1* mRNA expression, while all NAC treatments, alone and with MeHg all experimental paradigms, maintained *Abcc1* mRNA expression at a similar level control treatment. NAC alone treatment in MP (#) induced *Abcc1* expression higher than the vehicle treatment. NAC treatment with MeHg in CO and MP (&) induced *Abcc1* expression higher than that in NP. The Two-Way ANOVA with Tukey's multiple comparison *post hoc* was used for statistical analysis. The asterisk (\*) indicates a value statistically significant from MeHg treatment alone. The number sign (#) indicates a value statistically significant from control. The ampersand (&) indicates a value statistically significant from NAC pretreatment with MeHg, N=6 biological replications

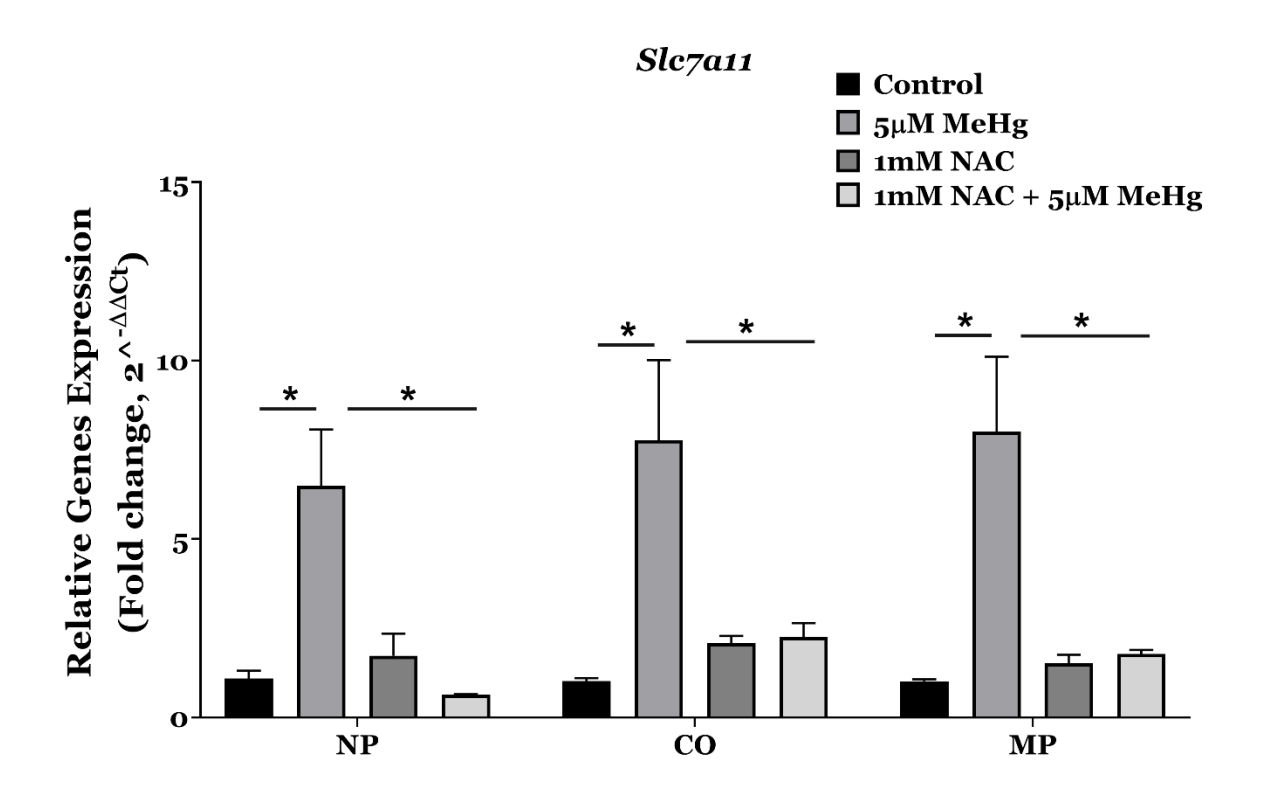


**Figure 4.12 The effect of NAC on regulation of** *Slc7a11* mRNA during SCAs **exposure to MeHg.** SCAs were incubated in NAC (1mM) either before (NP), during (CO) or following (MP) with 5μM MeHg treatments. MeHg induced the *Slc7a11* mRNA expression about 6-7- fold of increase. NAC treatments, either alone or with MeHg, maintained *Slc7a11* expression at a similar level control treatments in all experimental paradigms. The Two-Way ANOVA with Tukey's multiple comparison *post hoc* was used for statistical analysis. The asterisk (\*) indicates a value statistically significant from MeHg treatment alone, N=6 biological replications

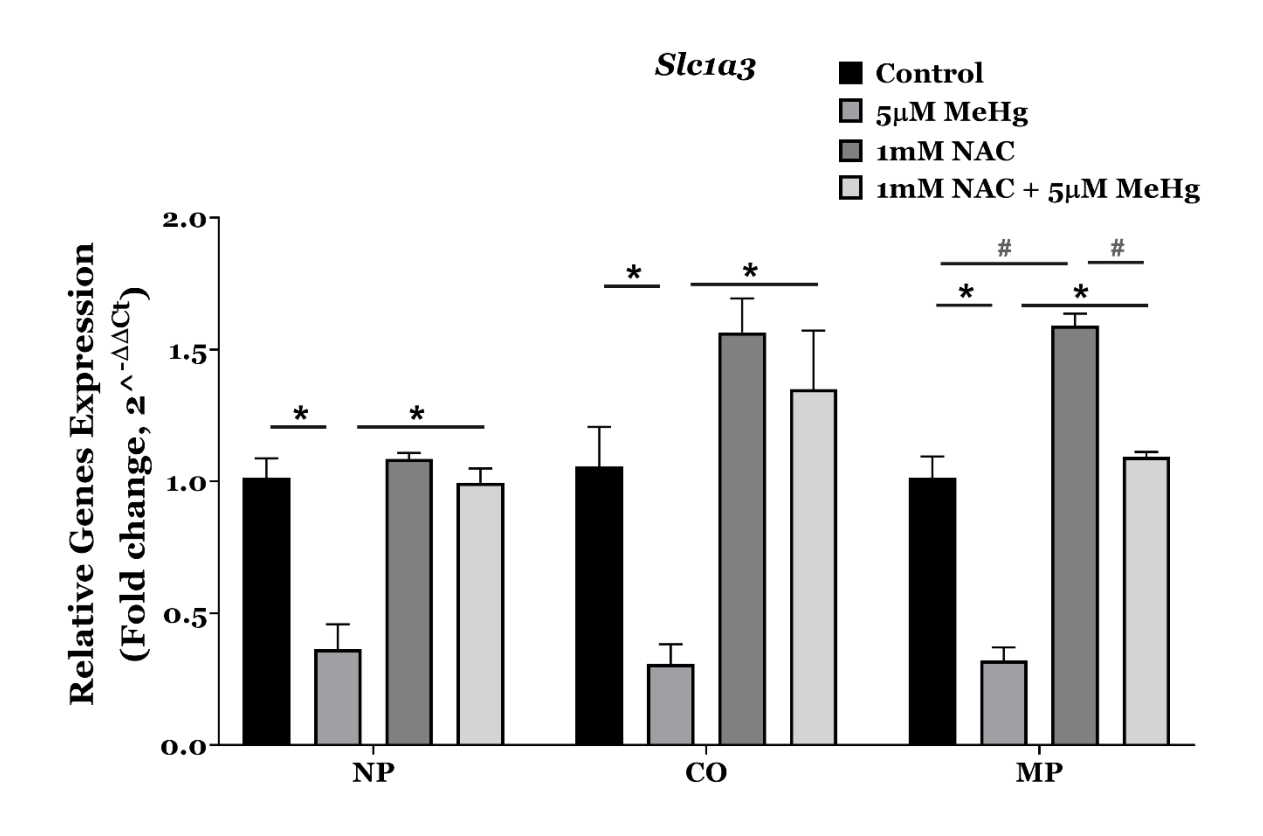


**Figure 4.13 The effect of NAC on regulation of** *Slc1a3* mRNA during SCAs **exposure to MeHg.** MeHg induced a reduction of *Slc1a3* mRNA expression. NAC treatments, either alone or with MeHg, maintained *Slc1a3* expression at a similar level control treatments in NP and CO paradigms. MP paradigm, NAC alone induced an increase of *Slc1a3* mRNA expression higher than that in control and NAC with MeHg (#). Two-Way ANOVA with Tukey's multiple comparison *post hoc* was used for statistical analysis. The asterisk (\*) indicates a value statistically significant from MeHg treatment alone. The number sign (#) indicates a value statistically significant from NAC alone in MP, N=6 biological replications

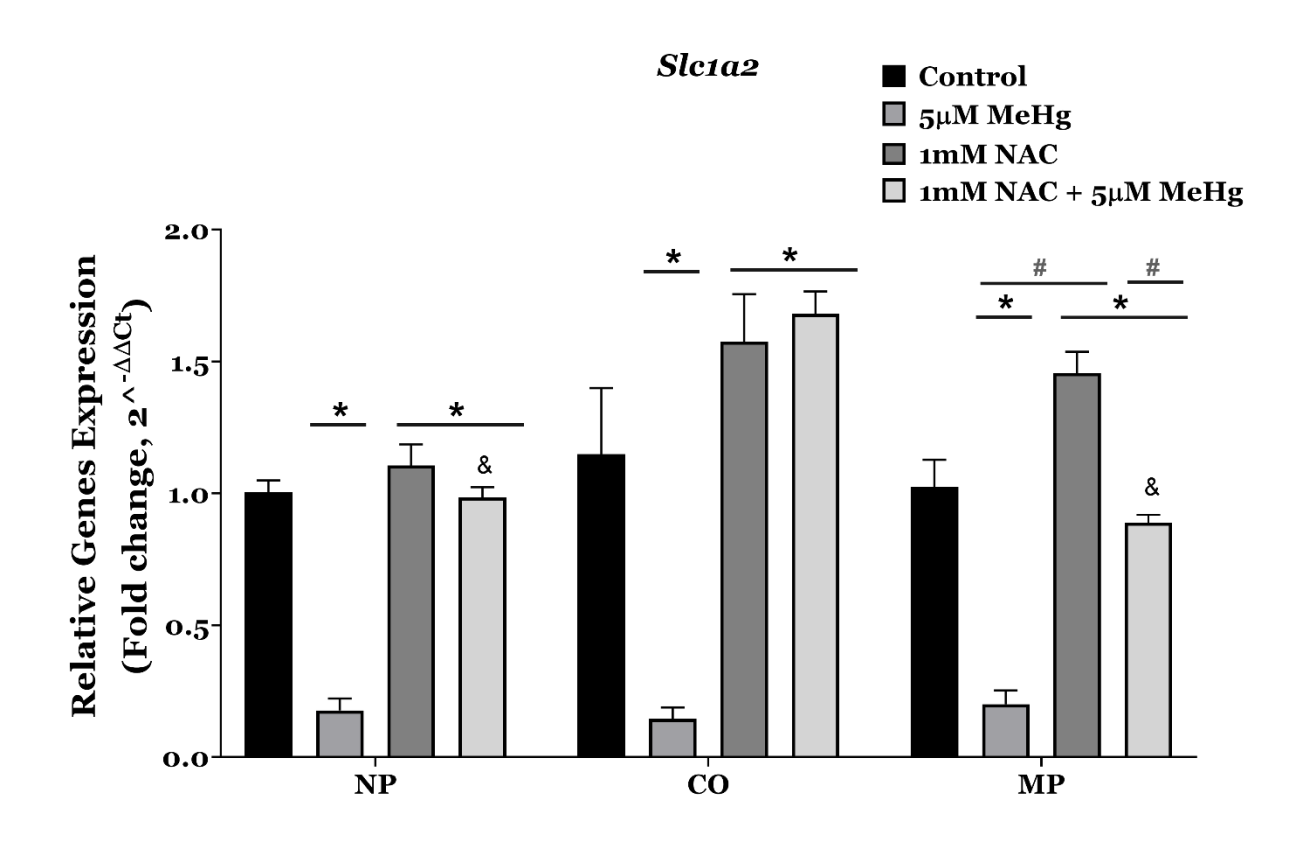


**Figure 4.14 The effect of NAC on regulation of** *Slc1a2* **mRNA during SCAs exposure to MeHg.** MeHg induced the reduction of *Slc1a2* mRNA expression. Conversely, all NAC treatment paradigms protected and rescued a reduction of *Slc1a2* mRNA expression from MeHg. The efficacy of NAC in maintaining *Slc1a2* expression was superior when it was coadministered with MeHg than that in NP and MP (&). With MP paradigm, NAC alone induced *Slc1a2* expression significantly higher than the control and NAC with MeHg (#). The Two-Way ANOVA with Tukey's multiple comparison *post hoc* was used for statistical analysis. The asterisk (\*) indicates a value statistically significant from MeHg treatment alone. The number sign (#) indicates a value statistically significant from NAC alone in MP. The ampersand (&) indicates a value statistically significant from NAC cotreatment with MeHg. N=6 biological replications

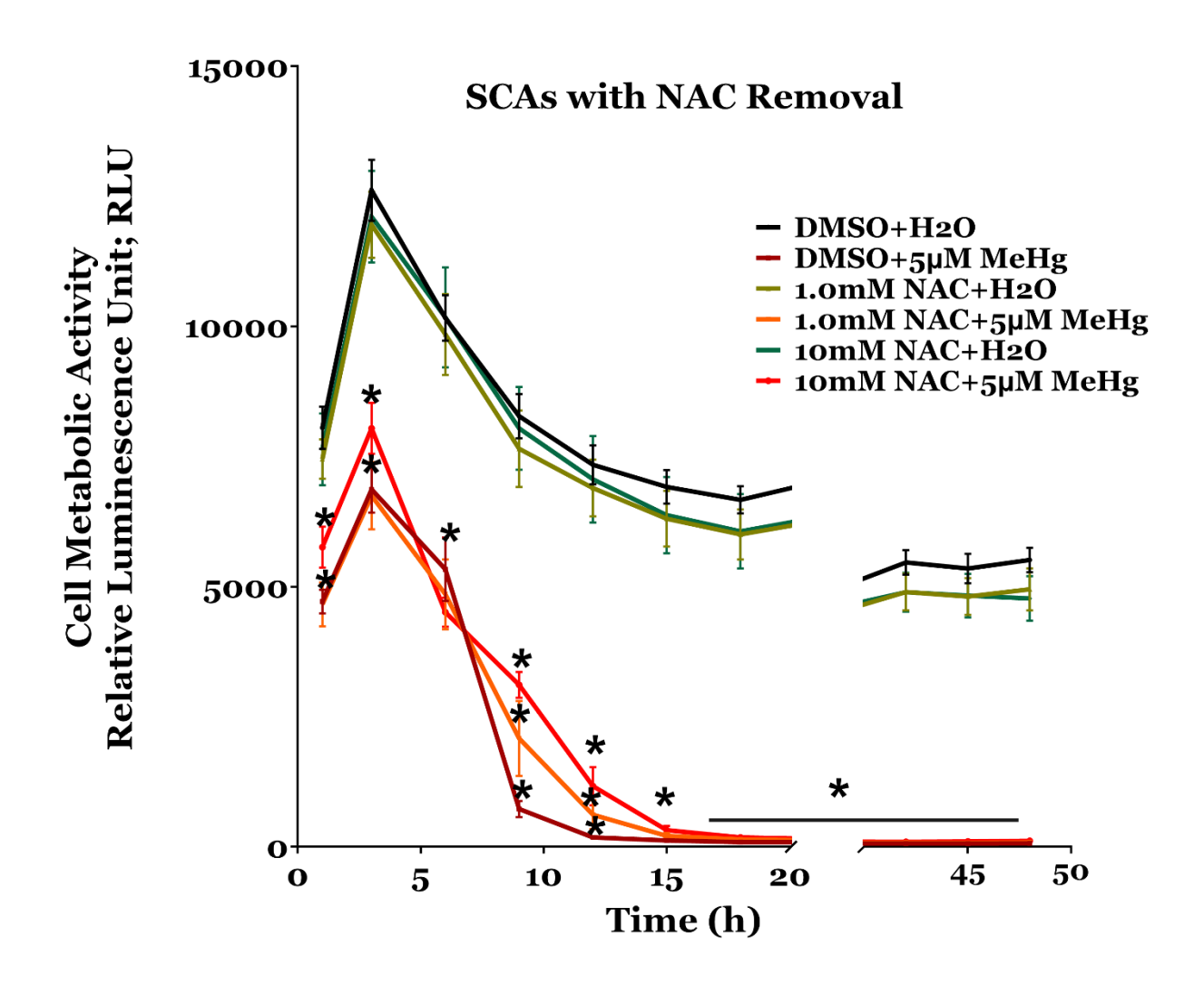
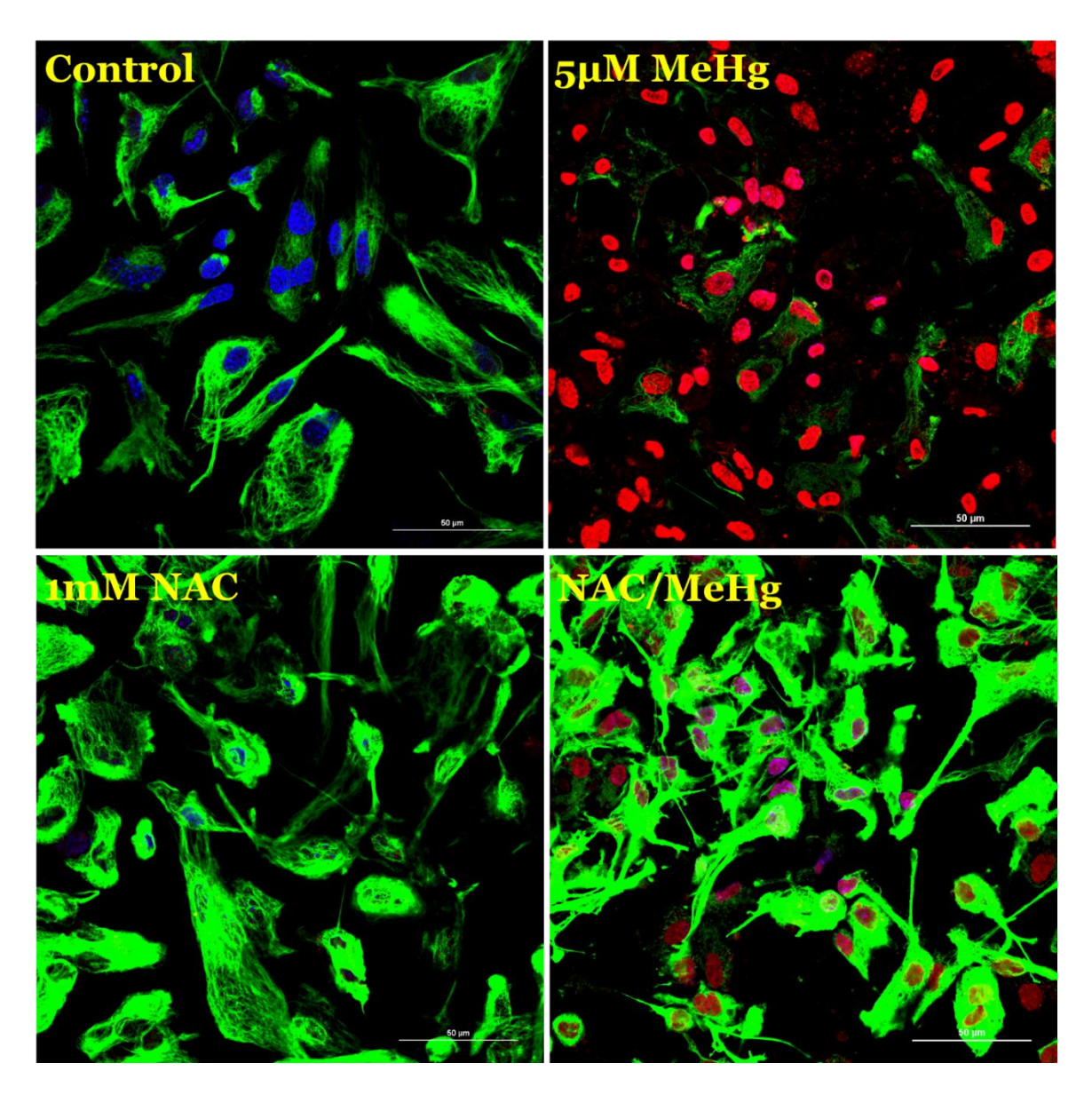


Figure 4.15 Cell metabolic activity as a function of time when SCAs were treated with 1.0 or 10mM NAC or vehicle (DMSO+H<sub>2</sub>O) for 2h, subsequently removed before administration of 5μM MeHg. All NAC concentrations did not protect SCAs from MeHg-induced toxicity. However, the reduction of cell viability appeared to be concentration-dependent protection of NAC. Reduction of cell metabolic activity was greater in lower NAC concentration than that in higher concentration. The Real-time glow cell viability assay was determined after 1h of MeHg exposure and every three hours thereafter. Two-Way ANOVA with Tukey's multiple comparison *post hoc* was used for statistical analysis. The asterisk (\*) indicates a value statistically significant from DMSO+H<sub>2</sub>O. N=6 biological replications



**Figure 4.16 Morphology of SCAs when treated with 1.0mM NAC or vehicle (DMSO) for 2h, subsequently removed before 5μM MeHg administration.** Cell viability assay was determined using EthD-2, a cell-impermeant viability indicator that permeates the compromised plasma membrane of dead cells or dying cells. When EthD-2 binds to nucleic acids, it emits red fluorescence as displayed in MeHg treatment (the top right panel). The bright red in MeHg treatment suggested cell death, and red and magenta nuclei in NAC/MeHg suggested cell dying. The nuclei of healthy cells were stained with DAPI as displayed in control and NAC treatments (left panels). SCAs cell structure was labeled with chicken IgY GPAP polyclonal (1:1,000; Invitrogen, Waltham, MA, USA). Alexa Fluor 488 (1:400; Invitrogen, Waltham, MA, USA) was used to determine the GFAP. Confocal Microscope Nikon C2 was employed to acquire all images with the same setting for each channel.

#### 4.5 Discussion

The investigation of the potential beneficial effect of NAC against MeHg induced SCAs toxicity was conducted with NP, CO, and MP. The application of different concentrations of NAC (0.1, 1.0, and 10mM) was based on the physiological values of intracellular GSH, which generally ranges from 0.5 to 10mM (Dringen, 2000; Shimizu et al., 2002) and previous studies in neurons and glial cells (Dringen and Hamprecht, 1999; Shimizu et al., 2002; Lee et al., 2015). The incubation of NAC in concentrations of 1.0 mM or 5.0 mM with other GSH substrates glutamate and glycine in the minimal medium for 4h in neuronal cell culture exhibited the intracellular GSH in about 171 and 230% of the control glutathione content (Dringen and Hamprecht, 1999). Pretreatment of NAC with concentrations of 1.0 mM or 10.0 mM but not 0.1mM for 18h protected human neuroblastoma SK-N-SH cells from 6-OHDA-induced cell death (Shimizu et al., 2002). Among other exogenous thiol-containing agents, NAC was more effective in protection against 6-OHDA-induced neuronal death than the exogenous GSH or L-cystine (Shimizu et al., 2002). These findings support the present study because NAC is the most effective antioxidant in combating MeHg induced toxicity in SCAs compared to other antioxidants, including triterpenoid derivatives. Neither Edaravone nor the semi-synthetic triterpenoids such as CDDO-ME (the C-28 methyl ester of 2-cyano-3,12-dioxoolean-1,9dien-28-oic acid, aka Bardoxolone methyl) and CDDO-Imidazolide (CDDO-IM) protected SCAs against MeHg induced toxicity (Wiwatratana and Atchison, 2018). Edaravone or Radicut® (3-methyl-1-phenyl-2-pyrazolin-5-one) is an antioxidant and a novel FDA-approved drug for amyotrophic lateral sclerosis (ALS). Edaravone has reported its efficacy in reducing toxicity from sodium nitroprusside, a nitric oxide donor, in rat astrocytes (Kawasaki et al., 2006; Kawasaki et al., 2007). CDDO-ME and CDDO-

IM have reported protecting motor neurons and slow disease progression in ALS G93A SOD1 mice (Neymotin et al., 2011). CDDO-ME and CDDO-IM are Nrf2 potent activators (Liby, 2005; Neymotin et al., 2011; Zhou et al., 2014). Despite NAC, concentrations of edaravone or CDDO-ME or CDDO-IM ranging from 0.1 to 1.0mM did not protect SCAs from MeHg-induced toxicity (Wiwatratana and Atchison, 2018). Therefore, the mechanisms by which NAC in protection against MeHg induced toxicity in SCAs was further elucidated.

Exposure SCAs to 5µM MeHg for 18h reduced metabolic activity of SCAs to about 90% of vehicle treatment (Chapter 2). In this study, a single NAC treatment protected against and rescued SCAs from MeHg-induced toxicity. The protection and rescue of NAC treatment depended upon NAC concentrations. NAC concentration with 0.1mM protected SCAs degeneration until 30h of MeHg exposure, while NAC concentrations with 1.0 and 10mM significantly defended SCAs degeneration more than 160 h of 5µM MeHg exposure in NP and CO experimental paradigms (Figure 4.3 and 4.4). The rescue effect of NAC in MP exhibited concentration-dependent (Figure 4.5), which differs from its protective effect against MeHg inducing SCAs degeneration in NP and CO (Figure 4.3 and 4.4). NAC concentration with 10mM did not rescue but exacerbated the effect of MeHg- induced SCAs degeneration (data are not shown). The adverse effect of high NAC concentration in the present study was supported by the cytotoxicity in U-87MG human astrocytoma, in which concentrations of NAC higher than 10mM are cytotoxic (Muniroh et al., 2015). In contrast, NAC concentrations with 0.1 and 1.0mM, which has no toxicity to U-87MG human astrocytoma (Muniroh et al., 2015), recovered SCAs from MeHg-induced toxicity over the time course (163h) of the MP experimental paradigm (Figure 4.4). Similary,

Muniroh et al. (2015) examined the efficacy of NAC in U-87MG human astrocytoma cells, using before (NP), simultaneously (CO), and after (MP) MeHg administration. Their results exhibit a concentration-dependent benefit of NAC against MeHg-induced proinflammatory cytokines induction (Muniroh et al., 2015). NAC with 5.0mM superior suppresses MeHg (4µM) induced the increase of interleukin (IL)-6 and monocyte chemoattractant protein (MCP)-1 in these cells than that in NAC with 0.5 μM (Muniroh et al., 2015). Similarly, in the present study, 1.0 mM NAC provided better protection and rescued SCAs from MeHg-toxicity than that with 0.1mM NAC concentration in all NP, CO, and MP treatment paradigms. Nevertheless, some differences in NAC treatment paradigms in Muniroh et al. (2015) were observed from the present study. 1.) NAC was removed and washed out before exposed to MeHg in Muniroh et al. study, whereas NAC was presented during MeHg exposure in the present study. 2.) Muniroh et al. incubated cells with NAC for 1h before MeHg exposure whereas NAC was pretreated for 2h the in present SCAs study. 3.) MeHg concentration was 4µM a slightly lower than the present study. 4.) The time of MeHg exposure was 6h in their study, whereas it was 18h in the present SCAs study. Therefore, the mechanism by which NAC protected SCAs in the present study was not due solely to intracellular NAC protection. The majority of studies have postulated that the primary mechanism of NAC in neuronal and non-neuronal protection is its prodrug substrate for de novo GSH synthesis (GSH-dependent mechanism)(Meister, 1988; Dringen and Hamprecht, 1999). Conversely, it has also reported the mechanism of NAC action is independent of GSH replenish (GSHindependent mechanisms). The difference of concentration-dependent efficacy of NAC in protection and recovery in MeHg- induced toxicity in SCAs could impact to the different mechanisms of NAC action.

Studies in rat neuronal primary cell culture revealed that NAC acts as a prodrug for cysteine for de novo GSH synthesis (Dringen and Hamprecht, 1999). With 1.0mM glutamate and glycine, NAC concentrations with 1.0 and 5.0 mM, not 0.1mM, increase the neuronal GSH levels at 4h of incubation (Dringen and Hamprecht, 1999). Both stereoisomers of NAC, N-acetyl-L-cysteine, and N-acetyl-D-cysteine promoted long-term survival as well as increased GSH levels of PC12 cell cultures from serum deprivation culture medium (Ferrari et al., 1995). The replenishment of intracellular GSH with NAC protected against cell degeneration from oxidative stress or glutamate-induced toxicity. Pretreatment of CGCs cell cultures with 1.0mM NAC for 3h and later exposure to 30 µM hydroxynonenal (HNE) could protect against the reduction of GCGs mitochondrial membrane potential and cell viability (Arakawa et al., 2006). Pretreatment with 1.0mM NAC alone appeared to increase the intracellular GSH level in this CGCs cell culture than in the vehicle treatment. This NAC pre-treatment also partially, but significantly, protected CGC from HNE-induced GSH depletion (Arakawa et al., 2006). When the neuronal N2a cell line was exposed with second hits of MG132 (Unnithan et al., 2012), paraquat (Unnithan et al., 2014), or hydrogen peroxide (H<sub>2</sub>O<sub>2</sub>) (Unnithan et al., 2014), NAC protected against neuronal N2a cells degeneration from these oxidative stress inducers. NAC entirely maintained GSH levels at the same level of vehicle treatment during these oxidative stress insults (Unnithan et al., 2012; Unnithan et al., 2014). Furthermore, coadministration of 3.0mM NAC with 1.0mM MG132 (Unnithan et al., 2012) or 125μM H<sub>2</sub>O<sub>2</sub> (Unnithan et al., 2014) protected the decrease of cell viability and GSH level in these N2a cell line with second hits of these oxidative stress-inducers (Unnithan et al., 2012; Unnithan et al., 2014). Cotreatment and posttreatment of NAC also increased intracellular GSH. Posttreatment of NAC in drinking water of pregnant Sprague Dawley rats previously exposing to lipopolysaccharide (LPS) for 4 h entirely prevented the reduction of hippocampal GSH content in offsprings (Lanté et al., 2008). Long-term potentiation (LTP) and spatial learning in these offsprings were completely preserved with 4h NAC posttreatment following the LPS challenge (Lanté et al., 2008). The Lanté et al. study also suggested that the efficacy of NAC depends upon the therapeutic window of NAC treatment. At the same time, the hippocampal GSH contents in offsprings were fully protected in both NAC administration to the mothers at the delivery and after two days of delivery. However, LTP of these offsprings with NAC administration to the mothers after two days of delivery was abolished (Lanté et al., 2008). Similary, the function of time with Real-Time viability assay in SCAs exhibited NAC treatment depending upon the time window of NAC application. The results of 0.1mM NAC in CO had better efficacy in SCAs protection against MeHg cytotoxicity than in the NP regimen. Compared to MeHg treatment alone, NAC lost its efficacy at 60h in CO and 42h in NP regimen (#, Figure 4.3 and 4.4). Surprisingly, 0.1mM NAC in MP (Figure 4.4) exhibited better efficacy than that in NP and CO because it lost potency in rescuing SCAs from MeHg at 129h (#, Figure 4.5). However, among 0.1, 1.0, and 10mM, 1.0mM NAC had better protection and rescued SCAs from MeHg induced cytotoxicity in all NAC regimens. The concentration and therapeutic window of NAC regimens in this SCAs study appeared to attribute to its efficacy.

NAC concentrations not only impact its efficacy but also its mode of action. A study of glutamate-induced cytotoxicity in C6 glial cells, which reduced cellular GSH content and cell viability, suggested that the protective mechanism of low NAC concentration was GSH-dependent antioxidant mechanism (Han et al., 1997). In contrast, high NAC

concentration was GSH-independent antioxidant mechanism (Han et al., 1997). Coadministration of glutamate (10 mM) with low NAC concentration (0.1mM) protected C6 glial cells against 10 mM glutamate-induced cell death, and this protection was failed when blocking GSH synthesis with L-buthionine-(S, R)-sulfoximine (BSO) (Han et al., 1997). In contrast, coadministration of 10mM glutamate with relatively high NAC concentrations (0.5, 1.0, and 2.0mM), C6 glial cell viability was completely preserved (>90%) in the presence of BSO (Han et al., 1997). Similarly, NAC maintained its protective efficacy in PC12 cell culture in serum-free medium with or without BSO (Yan et al., 1995). The 60mM NAC protected PC12 cell viability and increased more than 10-fold of intracellular GSH in PC12 cell culture in serum-free medium. The effect of 0.2mM BSO abolished only NAC impact on GSH level but not viability in PC12 cells (Yan et al., 1995). Therefore, 1mM and 10mM NAC protection against MeHg-indued SCAs death are possibly due mainly to its direct antioxidant effect, GSH-independent mechanism, whereas 0.1mM NAC in SCAs protection is primarily due to its GSH-dependent mechanism.

Since MeHg impaired the Keap1-Nrf2-ARE pathway in SCAs. NAC might impact this pathway. It remains unclear whether NAC activates or suppresses this pathway. The study of a mechanism by which a novel compound N-(4-(2-pyridyl)(1,3-thiazol-2-yl))-2-(2,4,6-trimethylphenoxy) acetamide (CPN-9) protected against H<sub>2</sub>O<sub>2</sub> -induced SH-SY5Y cells degeneration suggested that NAC suppressed CPN-9 activation of some genes underlying Keap1-Nrf2-ARE pathway (Kanno et al., 2012). CPN-9 appeared to cause the increase of *Nrf2*, *Ho-1*, *Nqo1*, *Gclm* mRNA, and protein expression but reduce *Keap1* mRNA and protein expression relative to the vehicle treatment (Kanno et al., 2012). The effects of

CPN-9 on activation of this pathway appeared to be more pronounced than Nrf2 activator, tert-butylhydroquinone (tBHQ), particularly the increase of Ho-1 (Kanno et al., 2012). The cotreatment of 2.5mM NAC with 40µM either tBHQ or CPN-9 in differentiated SH-SY5Y cells suppresses the increase of the majority of mRNA and proteins in Keap1-Nrf2-ARE pathway (Kanno et al., 2012). Cotreatment of 0.5mM or 1.0mM NAC with 40µM CPN-9 also reduced the protective effect of CPN-9 in these cells exposing to 60mM menadione, a ROS inducer, for 4h (Kanno et al., 2012). NAC treatment (5.0mM) also reduced the activation of Keap1-Nrf2-ARE pathway, including reduction of Ho-1, Gclm mRNA expression in shear stress-induced ROS-activation in human endothelial cells (Warabi et al., 2007). Similarly, MeHg induced the increase of *Slc7a11* mRNA expression, and NAC treatments (NP, CO, or MP) suppressed this mRNA expression in this SCAs study (Figure 4.11). Furthermore, MeHg caused the reduction of some of the mRNA expressions of the Keap1-Nrf2-ARE pathway, such as *Keap1*, *Gclc*, *Gpx1*, and *Gpx4*, and all NAC treatment paradigms increase these antioxidant genes expression at the same level as vehicle treatments (Figures 4.6, 4.8, 4.9, and 4.10). These results might suggest that the reduction of metabolic activity of SCAs exposed to 5µM MeHg for 18h could be partly to the impairment of the Keap1-Nrf2-ARE pathway, and 1.0 mM NAC provided the antioxidant effect to protect SCAs against MeHg-induced degeneration (Figures 4.3, 4.4, and 4.5). Some supporting evidence reported that the N-acetylcystien amide (NACA), a derivative of NAC, provided neuroprotection through the Keap1-Nrf2-ARE pathway in traumatic mouse brain injury (Zhou et al., 2018). The intraperitoneal injection (i.p.) of 100mg/kg NACA following 1h of traumatic brain injury (TBI) improve neurological status of TBI mice, reduce the number of apoptotic cells, and induce the increase of Ho-1, and Ngo-1 proteins, as well as increase the nuclear Nrf2 protein expression but not

cytoplasmic Nrf2 protein, compared to sham, TBI and TBI with vehicle groups (Zhou et al., 2018). The increase of cytoplasmic Nrf2 level suggested that NACA activated Nrf2 pathway and induced genes underlying the ARE promotor expression(Zhou et al., 2018). However, it remains uncertainty that the mechanism by NAC in protection or rescue SCAs from MeHg induced toxicity was underlying its activation of Keap1-Nrf2-ARE pathway. The study using Nrf2 KO mice could beter explain whether NAC protect the SCAs against MeHg induced toxicity through this pathway.

Besides, NAC has suggested its role in the modulation of brain glutamate homeostasis through glia activity, possibly through the activity of the system Xc-. The proton magnetic resonance spectroscopy results showed that the brain glutamate concentration of C57BL/6J mice i.p. injection with 150 mg/kg NAC showed a lower glutamate concentration than that in the saline-treated mice (Durieux et al., 2015). Since NAC is a cysteine derivative, it could be transported through a plasma membrane transporter, alanine-serine-cysteine (ASC) system, a neutral amino acid transporter (Bannai and Tateishi, 1986; Arakawa and Ito, 2007). However, cysteine is unstable in extracellular conditions and in the cell culture medium (Bannai, 1986). It is degraded into cystine and transport through the cystine/glutamate antiporter or system Xc- (Bannai and Tateishi, 1986; Banjac et al., 2008). The increase of systemXc- mRNA, Slc7a11 during MeHg exposure in SCAs (Figure 4.12) might suggest that the loss of redox homeostasis occurs through which MeHg activated Nrf2 and ARE subsequently increase *Slc7a11* expression. Similarly, The increase of *Slc7a11* expression is associated with an increase of Nrf2 activity and Nrf2 protein level in human breast cancer with exposure to H<sub>2</sub>O<sub>2</sub> (Habib et al., 2015). The increase of Slc7a11 and system Xc- also appeared to be associated with glutamate

release in these breast cancer cells (Habib et al., 2015). In SCAs, MeHg caused the reduction of *Slc1a3* and *Slc1a2* mRNA expression (Figure 4.13 and 4.14). The increase of *Scla7a11* and decrease of *Slc1a3* and *Slc1a2* mRNA expressions contributed to dysregulation of redox and glutamate homeostasis. All NAC treatments prevented and restored these transporter mRNA expressions could be partly to NAC maintained the intracellular cellular cysteine and GSH, which consequently reduced the non-vesicular glutamate release through the system Xc-. Nevertheless, the correlation between extracellular glutamate concentration and system Xc- expression level during MeHg exposure in SCAs might better explain an intertwined between these redox and glutamate and their dysfunction.

NAC has reported its increase in cysteine in the mice midbrain (Aoyama et al., 2007). Incubation of 5mM NAC in midbrain slice culture for 30min increased cysteine about two-fold control midbrain slice (Aoyama et al., 2007). Cysteine can be transported through EAATs. EAAC1/EAAT3 transports cysteine with a rate comparable to glutamate, with the affinity, 10-20-fold higher than that of GLAST/EAAT1 or GLT-1/EAAT2 (Zerangue and Kavanaugh, 1996a; Aoyama et al., 2006; Aoyama et al., 2007; Aoyama et al., 2012). Cotreatment of NAC with MPTP prevented MPTP-induced increase of plasma membrane EAAC1/EAAT3 expression and reduced nitrotyrosine, a biomarker of NOS in protein modification, in EAAC1 protein in the mice midbrain (Aoyama et al., 2007). NAC could potentially serve as a cysteine source for SCAs during MeHg exposure. Since in the present study, dysregulation of *Scl7a11* expression and *Slc1a3* and *Slc1a2* expression were prevented or restored at the same level of vehicle treatments by all NAC treatment paradigms. Further tailor for specific genes/pathway using systemXc- KO and or

EAAT1/EAAT2 mice would further explain the specificity of the NAC and MeHg mechanisms.

As discussed earlier, the millimolar range of NAC provided both protective and rescue effects in the present study, consistent with other studies in C6 glia cells (Han et al., 1997). A relatively high concentration of NAC (0.5 to 10 mM) could be a GSH-independent mechanism (Han et al., 1997). To elucidate the mechanism by NAC in SCAs, whether it provided the protective mechanism through its direct antioxidant property, GSHindependent mechanism, another experimental paradigm by which pretreatment of NAC for 2h and subsequently removed before treatment with a fresh medium containing only MeHg were tested. A Real-Time viability assay exhibited a considerable reduction of cell viability in NAC pretreatment, either 1.0mM or 10mM NAC, following the exposure of 5.0µM MeHg without NAC in fresh medium (Figure 4.14). This experimental paradigm was similar to studying the efficacy of NAC pretreatment in rat hippocampus neuronal culture by Falluel-Morel et al. (2012). When cotreatment of 300µM NAC with 3.0µM MeHg for 24h, NAC completely protected MeHg-induced hippocampal neuronal death (Falluel-Morel et al., 2012). However, when pretreatment of NAC either 4h or 24 h, and NAC was removed before exposure to MeHg, the cortical neurons underwent the apoptosis cell death pathway (Falluel-Morel et al., 2012). Therefore, these NAC concentrations exert protective effect in cortical neurons (Falluel-Morel et al., 2012) and SCAs through which its direct interaction with MeHg as a direct antioxidant to prevent MeHg toxicity.

Furthermore, the ethidium homodimer-2 (EthD-2) was applied to determine the SCAs dead cells with this NAC treatment paradigm to confirm these results. EthD-2 stained in

the nucleus of both MeHg treatment alone and NAC pretreatment 2h before exposed to MeHg (Figure 4.16). However, the GFAP staining remained intact in NAC pretreatment before MeHg exposure at a level similar to a vehicle and NAC alone treatments. This finding might suggest that the mechanism by which NAC protected SCAs against MeHginduced toxicity is mainly through its free radical scavenging agent property. NAC somewhat might act as a cysteine prodrug to increase intracellular GSH since some SCAs processes remained intact in NAC pretreatment. However, the therapeutic window and the concentration of NAC could play a role in its efficacy in this NAC treatment. Further experiments, including determination of GSH level in NAC treatment with MeHg and using the BSO, an inhibitor of GSH synthesis, could better explain its role in a GSH precursor. Moreover, the membrane permeability of NAC could contribute to its role in SCAs protection. Some studies suggested that NAC is membrane-impermeable while its derivative NACA posses membrane-permeable and greater bioavailability, including in the CNS (Penugonda and Ercal, 2011). According to the pretreatment of NAC and removal, before MeHg exposure, the considerable reduction of SCAs viability suggested that NAC reduced MeHg-toxicity through direct interaction, mainly extracellularly. The main extracellular effect could imply that NAC posses weak membrane permeability, particularly in SCAs. Some studies suggested that NAC potentiates the toxicity of MeHg through its enhanced MeHg uptake into the cells, including the CNS (Hirayama, 1985) through the cysteine-MeHg and or GSH-MeHg complex transport system (Aschner and Clarkson, 1988; Kerper et al., 1992; Mokrzan et al., 1995). This issue appeared not to be the case in SCAs. Since coadministration of NAC and MeHg did not exacerbate the toxicity but rather protect SCAs degeneration for a more extended period during MeHg exposure (Figure 4.4). NAC is negatively charged at physiological pH, which limits its ability to cross any biological membranes (Sunitha et al., 2013; Tobwala et al., 2015). Thus, NAC is potentially used for therapeutic benefit in MeHg intoxication mainly through it direct antioxidant property that directly interacts to MeHg to reducing toxicity.

NAC has shown its therapeutic benefit for the treatment of Hg- and MeHg-intoxication (Falluel-Morel et al., 2012). An accidental Hg exposure to a healthy 15-year-old male who later developed muscle pain, tremor, ataxia, and new onset of hypertension ineffectively recovered from 21 days of chelation with 2,3-dimercaptosuccinic acid (DMSA) (Spiller et al., 2017), a sulfhydryl-containing, water-soluble, non-toxic, metal chelator (Miller, 1998). However, by three days after he started treatment with selenium (Se) and NAC, his clinical symptoms showed noticeable improvement. By ten days, delusion and abnormal pain were resolved (Spiller et al., 2017). His blood Hg dramatically reduced by five days after treatment. After three months with continued Se and NAC supplement, his tremor, tachycardia, and insomnia had resolved, and by five months, he returned to active, athletic activity, and hypertension had resolved (Spiller et al., 2017). In animal studies showed that oral administration of NAC with HgCl<sub>2</sub> or MeHg in male mice for 2 weeks or 4 weeks effectively protected plasma lipid peroxidation increase in these mice (Chen et al., 2006). Mice received 10mg/ml NAC in drinking water for the first 48h after i.p. injection with 25µmol/kg body weight of MeHg excreted Hg through the urine by about 50% compared to about 10% Hg excretion in control MeHg treatment mice (Ballatori et al., 1998). The distribution of Hg in whole blood, kidney, liver, and brain were significantly lower in this NAC treatment in both male and female C57BL/6J mice as compared to MeHg treatment alone (Ballatori et al., 1998). The mechanism by NAC in enhancing excretion of MeHg was suggested by its ability to readily bind to MeHg,

resulting in forming MeHg-NAC complex, which exports from the body. The *in vitro* and *in vivo* studies suggested that MeHg-NAC complexes might be transported from the circulation into renal tubular epithelial cells through organic anion transporter-1 (Oat1) (Koh, 2002; Zalups and Ahmad, 2005) and subsequently were excreted into the tubular fluid through multidrug resistance-associated protein-2 (Mrp2/Abcc2) (Madejczyk et al., 2007). MeHg induced the reduction of Mrp1 protein and *Abcc1* mRNA expression in SCAs (chapter 3), and NAC could prevent the reduction of *Abcc1* (Figure 4.11). The reduction of these transporters could heighten the cellular toxicity of MeHg, and NAC ameliorated these reductions in SCAs mainly through its direct interaction with MeHg resulting in the reduction of MeHg cellular toxicity.

The mechanistic rescue effect by NAC after SCAs exposed to MeHg has yet been elucidated. Indeed, its direct interaction with MeHg resulting in the reduction of MeHg cellular toxicity is possible the primary mechanism. NAC has reported its suppressed the expression of the inflammatory cytokines in U-87MG human astrocytoma cells (Muniroh et al., 2015) and murine RAW264.7 macrophages cell line (David et al., 2017). The non-cytotoxic concentrations of MeHg (2uM) in the macrophage cell line induced the increase of murine macrophage inflammation protein-2 (MIP-2) within 3h of exposure. Among NAC treatment paradigms, NAC posttreatment was more effective than NAC pretreatment and cotreatment (David et al., 2017). Likewise, in this SCAs study, NAC in MP regimen provided better results in maintaining cell metabolic activity against MeHg induced cytotoxicity last longer than in the CO and NP regimen. According to statistical analysis compared to MeHg alone treatments (# in Figure 4.3, 4.4, and 4.5), 0.1mM NAC maintained cell metabolic activity in MP, CO, and NP for 129h, 60h, and 42 h,

respectively. The difference between the SCAs and the RAW264.7 macrophage cell line study was that MeHg was removed before adding NAC into treatment media in the RAW264.7 cells (David et al., 2017), whereas, MeHg remained in the treatment media when adding NAC in SCAs cells. Therefore, a mode of NAC action in RAW264.7 cells suggests the role of intracellular protective mechanisms of NAC (David et al., 2017). In contrast, a mode of NAC action in this SCAs study could be extracellular and intracellular protective mechanisms. Some further experiments, such as the removal of MeHg before administration of NAC, could eliminate the direct interaction of MeHg. Besides, an evaluation of intracellular GSH level in SCAs during MeHg exposure with and without NAC could explain the intracellular mechanism by NAC to restore the cellular activity in SCAs after MeHg exposure.

The results from the present study suggested that the protective mechanism by NAC was primarily due to its direct antioxidant property by which it directly binds to MeHg, resulting in attenuation of the MeHg cytotoxicity. The protective mechanism by NAC depends upon NAC concentration. The millimolar NAC range was mainly due to its GSH-independent mechanism, while the submillimolar rage was GSH-dependent mechanisms, which was supported by the results from C6 glia cells (Han et al., 1997). NAC lacking intracellular protective mechanisms in SCAs was possibly due to its poor membrane permeability. This poor SCAs membrane permeability property of NAC provides a benefit for NAC to be an effective treatment in MeHg intoxication and prevent the distribution of MeHg to the CNS.

## CHAPTER FIVE CONCLUSION AND DISCUSSION

The results from this study have suggested and explained several gaps in MeHg induced neurotoxicity, particularly in SCAs.

5.1 The comparative concentration-response curves and function of time of susceptibility between the early developmental stage (DIV14) and the fully developmental stage (DIV30) of SCAs exhibited age-related susceptibility. SCAs (DIV30) viability was compromised with the 0.1 µM (0.0216ppm) MeHg exposure for 9h, while this concentration did not affect SCAs DIV14 (Figure 2.2). The onset of metabolic reduction (cell viability) of the SCAs DIV114 occurred sooner than that in SCAs DIV30 (see **Figure 2.3** for the comparative summary), yet the IC50 in SCAs DIV14 were higher than that in SCAs DIV 30 in a more extended time of MeHg exposure starting from 9h to 24h. The earlier appearance of the cell viability reduction with higher IC50 in DIV14 could be explained by their ability to recover from MeHg insult that the recoverability of DIV14 is better than the DIV30 (aged cells). The resilience of SCAs DIV 14 to MeHg might be due to their antioxidant pathways are more active and well-regulated than the aged SCAs DIV30. Oxidative stress and chronic inflammation are hallmarks of aging. The oxidative damage of macromolecules, including proteins and nucleic acids, increases with age, leading to a decline in cell and tissue functions (Frazzini et al., 2006). The impairment of antioxidant mechanisms in aged cells could impede the aged SCAs against any mild toxic insults as such non-toxic MeHg concentration. The decline in transcriptional activity of Nrf2 in aged rats (24-28 months old) contributed to the reduction of total GSH and GCL levels in the liver when compared to younger rats (2-5) months old) (Suh et al., 2004). Moreover, the aged mice (13 months old) exhibited a

significant reduction of Nrf2 protein in the lumbar spinal cord as well as its antioxidants

NQO-1 and HO-1 compared to the one-month-old mice (Suh et al., 2004). These antioxidant proteins were also significantly reduced in SCAs (DIV 60) compared to SCAs DIV 14 (Duan et al., 2009). In SCAs DIV 30, compared to SCAs DIV 14, the expression of HO-1 was significantly reduced (Duan et al., 2009). Furthermore, the reduction of mitochondrial membrane potential (ΔΨm) was pronounced in SCAs DIV60 compared to SCAs DIV 14 (Duan et al., 2009). The decline in the Nrf2-ARE pathway and loss of ΔΨm in aged SCAs could contribute to the susceptibility of MeHg in this study. Further study has shown that MeHg perturbed this pathway in SCAs DIV 30 (Chapter 2). Nevertheless, the comparative Nrf2 and ARE gene and protein expressions between SCAs DIV 14 and SCAs DIV 30 would better explain the susceptibility of MeHg in aged SCAs (DIV 30) compared to SCAs DIV14. The additional experiments of the Keap1-Nrf2-ARE pathway expressed in SCAs DIV 14 and ΔΨm would further explain this question.

# 5.2 The primary antioxidant pathway Keap1-Nrf2-ARE pathways were dysregulated during MeHg exposure in SCAs.

The fluctuations of antioxidant gene expressions were seen in SCAs assessed under a function of time of 0.5µM MeHg, the lowest concentration exhibiting toxicity to both SCAs DIV 14 and DIV 30. The expressions of *Keap1*, *Nrf2*, *Gclc*, *Abcc1* mRNAs significantly increased at 6h of MeHg exposure and declined at 15h of MeHg exposure (Chapter 2). Two critical genes for the GSH synthesis pathway, *Gclc*, a rate-limiting enzyme for GSH synthesis, and *Abcc1* (Mrp1), a GSH transporter, exhibited a biphasic increase of these gene expressions. The biphasic induction could be explained by the nature of MeHg property and Nrf2 activity. The highly reactive MeHg perhaps exerted

the first phase to the sulfhydryl group of Keap1. MeHg has been shown its binding to recombinant Keap1 protein with SDS-PAGE assay (Toyama et al., 2007). MeHg would potentially interrupt the sulfhydryl bonding between Keap1 and Nrf2, which later induced the up-regulation of the gene underlying ARE expression. Following the increase of these mRNA expressions, the reduction of mRNA expressions occurred after 9 h of MeHg exposure. The reduction of these mRNA expressions could be due to the reduction of Nrf2 activity. The half-life of Nrf2 is about 20 min under a basal condition, which it is rapidly degraded under ubiquitin-proteasome degradation (Ma, 2013). Nrf2 activity is also induced by other metal such as Zn<sup>2+</sup>(Silbajoris et al., 2014; Wages et al., 2014). Elevation of Zn<sup>2+</sup> is involved in the cellular mechanism by which MeHg induced toxicity in the synaptosome (Denny and Atchison, 1994b), neuronal cell line (Denny and Atchison, 1994b), cerebellar neurons(Limke, 2004; Edwards et al., 2005), and brainstem (Johnson et al., 2011). The elevation of Zn<sup>2+</sup> in MeHg exposure might induce the increase of Nrf2 activity, as seen in the up-regulation of *Gclc* and *Abcc1* in the second phase. The peak of the second phase was lower than the first phase could be multiple factors, for example, the cell survival stage, lower affinity to thiol of Zn<sup>2+</sup> than MeHg (Kensler et al., 2007).

#### 5.3 The regulation of redox and glutamate homeostasis are intertwined in SCAs.

The concomitant expression of system Xc- (*Scl7a11*a) and EAAT1/2 (*Slc1a3/Slc1a2*) mRNAs exhibited in a function of time studies in MeHg exposure in Chapter 2 might suggest the molecular mechanisms between the redox and glutamate homeostasis in SCAs are intertwined. During MeHg exposure in SCAs, the increases of the 1<sup>st</sup> peak at 30 min of *Slc7a11* mRNA expression (**Figure 2.9**) was followed by the increase of *Slc1a3* and

Slc1a2 mRNA expression at 3h of MeHg exposure (Figure 2.10 2.11, and 2.12). The concomitant increase of basal Slc7a11, and Slc1a3 and Slc1a2 expression levels also exhibited in Nrf2-KO derived SCAs compared to WT-derived SCAs (Figure 3.8, 3.9 and **3.10 in vehicle treatments).** Both Slc1a3 and Slc1a2 expression levels in Nrf2-KO SCAs significantly increased compared to WT SCAs (Figure 3.9 and 3.10, **respectively)** and corresponded to the increase of *Slc7a11* mRNA expression in Nrf2-KO SCAs (Figure 3.8). These concomitant expressions might support the cooperative function between system Xc- and EAAT1/2 activity to regulate redox and glutamate homeostasis (Lewerenz et al., 2006). The evidence supporting the cooperative expression/function of EAAT2 and the antioxidant pathway is the study in aged mice that exhibited the reduction of Nrf2 and antioxidant proteins concomitant with the reduction of EAAT2 (Duan et al., 2009). The aged animals shared remarkable similarity to Nrf2 KO mice (Duan et al., 2009; Zhang et al., 2015; Li et al., 2018; Schmidlin et al., 2019), and the significant reductions of EAAT2 expressions were exhibited in both aged SCAs and spinal cord aged mice (Duan et al., 2009). This finding might imply that in aged animals whose oxidative stress is more prevalent than the antioxidant system posses the dysregulation of glutamate homeostasis. Functionally, the system Xc- exchanges extracellular cystine with intracellular glutamate with 1:1 ratio (Warr et al., 1999) for de novo GSH synthesis (Murphy et al., 1989). This exchange would consequently cause an increase of extracellular glutamate via a non-vesicular glutamate release mechanism (Massie et al., 2015). The earliest induction of Slc7a11 mRNA expression might suggest the response of SCAs to MeHg exposure, which activated Nrf2 activity to combat MeHg-insults by inducing the expression of Slc7a11. The increase of Slc7a11 could also suggest the imbalance of intracellular GSH during MeHg exposure, as seen in

triphasic *Slc7a11* expression (**Figure 2.9**). The elevation of EAAT1/2 following system Xc- elevation suggested the defending mechanism in the early phase of MeHg exposure by which SCAs attempted to balance the redox and glutamate homeostasis. Since the activity of system Xc- depends upon the concentration gradience not only of the extracellular cystine but also the extracellular glutamate. When extracellular glutamate concentration is relatively higher than the intracellular glutamate concentration, the exchange for extracellular cystine with intracellular glutamate would be limited. Ultimately, the vicious cycle of the loss of the intracellular GSH to combat against the elevation of ROS following with the excitotoxicity would occur which could also occur in SCAs during MeHg intoxication. The functional study of system Xc- and EAAT1/2 should be further determined to confirm their cooperative function. The early phase of MeHg exposure for 30min to 3 h will also decipher the initial cellular mechasnims by which MeHg-induced toxicity in SCAs whether or not the excitotoxicity and antioxidant are intertwined and when they involve in the toxicity.

5.4 The biphasic elevation of *Vegfa* mRNA expression during MeHg exposure in SCAs would contribute to the blood spinal cord barrier (BSCB) permeability.

The increase of *Vegfa* mRNA expression in this SCAs during MeHg exposure (**Figure 2.13**) was similar to the results in the human brain microvascular endothelial cells and pericytes cell cultures exposed to MeHg for 12h and 18h (Hirooka et al., 2013). The expression of *Vegfa* and VEGF-A elevated in human pericytes cell culture, and the expressions of VEGF receptor- 1 and -2 also increased in endothelial cells (Hirooka et al.,

2013). The increases of Vegfa mRNA and VEGF-A expressions in human pericytes were not associated with the increase of the HIF pathway but rather through the paracrine fashion (Hirooka et al., 2013). This finding might suggest the secretion of VEGF-A from neighboring cells, including astrocytes, might play a role in the regulation of Vegfa expression in pericytes. The elevation of VEGF is not only associated with vascular plasticity related to angiogenesis in developing CNS but is also associated with BBB permeability in mature CNS (Argaw et al., 2009). The increase of VEGF following MeHg exposure could increase the microvascular tissue permeability and cause an edematous change around this tissue (Hirooka et al., 2013). The edematous changes in white matter were suggested as the cause of the localization lesion (Hirooka et al., 2013). While the global CNS damages were observed in fetus and infant cases, the local CNS damages were observed in chronic MeHg exposure in adult Minamata cases (Korogi et al., 1998; Eto et al., 2010). The predominant local damages were selectively expressed in the calcarine region, the precentral and postcentral gyri, and the temporal transverse gyrus (Hunter and Russell, 1954; Eto, 1997) where were most advanced in the depths of the sulci (Eto, 1997). Perhaps, a selective CNS damage in adult MeHg exposure may involve the brain edemas as a result of abnormal accumulation of the perivascular tissue caused by the increase of BBB permeability. The elevation of astrocytic VEGF might take part in BBB permeability in MeHg toxicity since the permeability barrier formed by cerebral endothelial cells is supported by trophic factors secreted by other cells in the BBB, particularly astrocytes (Demeuse et al., 2002). The increase of Vegfa expression in SCAs may involve in the mechanism by which specificity of MeHg susceptibility in the CNS including the gracile fasciculus in the spinal cord as well as in calcarine sulcus and gyrus in cerebrum and cerebellum (Eto, 1997) as a resulting from blood-spinal cord barrier

(BSCB) and BBB disruption. The cellular mechanism involved in MeHg induced the elevation of BSCB, and BBB will further determine whether or not the HIF pathway involved in this BSCB/BBB permeability during MeHg exposure. If so, whether the elevation of *Vegfa* and VEGFA contributes to BSCB/BBB permeability. **Determination** of the spinal cord slice exposure to 1ppm MeHg for 30 min to 3 h whether the changes of the expression of VEGFA protein using enzyme-linked immune assay (ELISA) and VEGF A receptor, VEGFR2/flk-1, expression using immunohistochemistry (Argaw et al., 2006) would explain the mechanism by which astrocytic VEGF in the regulation of BSCB permeability. The inflammatory cytokine such as IL-1\beta and hypoxia inducing factor (HIF) pathway will further clarify the specific signaling pathway in the regulation of the BSCB during MeHg exposure in the spinal cord. Alternatively, the SCAs coculture with the endothelial cells (Demeuse et al., 2002) would be employed to determine these IL-1β and HIF-VEGF pathways and the interaction between these two cells in MeHg- induced BSCB permeability mechanisms.

# 5.5 Genetic disruption of Nrf2, a master regulator of the Keap1-Nrf2-ARE pathway, rendered SCAs are more susceptible to MeHg.

The real-time viabilities of the Nrf2 KO-derived SCAs showed a more susceptible to MeHg compared to WT-derived SCAs. A one-hour exposure of 5  $\mu$ M MeHg significantly reduced cell viability of Nrf2 KO SCAs by 60% compared to WT SCAs, which did not affect by this MeHg concentration and time of exposure (**Figure 3.1**). Consistently, the cell viability of the primary hepatocytes derived from Nrf2 KO mice reduced considerably by about 70% when exposed to 5 $\mu$ M MeHg for 24h while the WT derived hepatocytic viability was

spared (Toyama et al., 2007). The greater susceptibility of Nrf2 KO derived cells, including SCAs and hepatocytes, might be explained by the loss of redox homeostasis in the Nrf2 KO mice. The loss of major regulator of antioxidant pathways in Nrf2 KO significantly contributes to SCAs are more susceptible to MeHg due to the overproduction of ROS. The comparison of basal ROS level in glial-cortical neuronal coculture derived from WT, Nrf2 KO, and Keap1 KD found that the level of ROS was significantly higher in Nrf2 KO derived glial-cortical neuronal coculture compare to WT derived coculture, whereas the basal ROS level from Keap1 KD was similar to WT coculture (Kovac et al., 2015). In addition, the Nrf2 KO-derived primary cortical astrocyte cell culture increased in their susceptibility when increased H<sub>2</sub>O<sub>2</sub> concentration (Bell et al., 2015). Conversely, the WT-derived astrocytes were not severely affected as the concentration of H<sub>2</sub>O<sub>2</sub> increase (Bell et al., 2015). Nrf2 KO-derived neurons in a mixed 10% glial culture system were significantly sensitive to MPP+ and rotenone compared with WT-derived neurons (Lee et al., 2003a). The loss of Nrf2 in the regulation of the Keap1-Nrf2-ARE pathway would compromise cells to non-adverse concentrations of toxicants and neurotoxin such as MeHg. The genetic predisposition, therefore, involves the susceptibility to MeHg, such as in SCAs. The exposure to non-toxic levels of MeHg might trigger the onset of motor neuron diseases such as ALS or PD in vulnerable people or exacerbating an existing condition. The comparative susceptibility between WT and ALS mice models, such as SOD1 mutants, would warrant and decipher the susceptibility among individuals with ALS. The study in human transgenics SOD1 G93A mice model by Johnson et al. (2012) demonstrated that the non-toxic levels of MeHg hasten the disease onset and the progression in this ALS mice model (Johnson et al., 2011). The cellular toxicity mechanisms of MeHg has involved the dysregulation of intracellular Ca<sup>2+</sup> and Zn<sup>2+</sup> as well as the glutamate receptors, mainly AMPAR functions in motor neurons in the brainstem (Johnson et al., 2011). The disease progression of ALS has been proposed as the dysfunction of astrocytes, and intracellular Zn<sup>2+</sup> is also involved in oxidative stress (Wages et al., 2014) and Nrf2 activation (Silbajoris et al., 2014). The cellular mechanisms, including intracellular Ca<sup>2+</sup> and Zn<sup>2+</sup>, involving MeHg induced the ALS symptom progression in cerebral astrocytes, and SCAs derived from human TgSOD1 G93A will further explain the susceptibility and disease progression in this mice model.

## 5.6 The loss of Nrf2 in Nrf2 KO derived SCAs contributed to the significant reduction of GSH synthesis and metabolism pathways.

The Nrf2 KO derived SCAs was more susceptible to MeHg compared to WT derived SCAs, mainly the significant loss of genes involving the GSH synthesis and metabolism. The noticeable reductions of *Gclc*, *GPx1*, and *GPx4* mRNAs in Nrf2 KO derived SCAs, were significant contributors to susceptibility in Nrf2 KO derived SCAs compared to WT derived SCAs (**Figures 3.4, 3.5 and 3.6**). These mRNA expressions further decreased when exposed 5µM MeHg in both WT, and Nrf2 KO derived SCAs for 18h. The reductions of *GPx1* and *GPx4* mRNAs also greatly exhibited in Nrf2 KO derived SCAs compare to WT SCAs. Similarly to SCAs results, the expression of *GPx1* mRNA expression was reduced in both male and female cerebrum but not cerebellum from C57BL/6J mice that exposure to 5ppm MeHg through drinking water from the early gestational period until postnatal day 21 (Ruszkiewicz et al., 2016). The GPx1 and GPx4 activities significantly reduced in Swiss adult male mice exposed to 40ppm MeHg in drinking water for 21 days compared to untreated mice (Zemolin et al., 2012). The determination of gene expression

underlying Nrf2 with microarray data confirmed the reductions of known ARE-containing genes in Nrf2 KO derived cortical astrocytes such as *Sod1*, *Gclc*, and *Gclm* (Lee et al., 2003b). Noteworthy, the *Gclm* expression level was not affected by the absence of Nrf2 in cortical neurons (Lee et al., 2003a) but did so in cortical astrocytes (Lee et al., 2003b). The differential effects of lacking Nrf2 in the regulation of *Glcm* mRNA expression between cortical neurons and astrocytes are of interest and might further explain the differential susceptibility of these CNS cells to MeHg. Despite this, the reduction of *Gclc* mRNA expression in SCAs derived from Nrf2 KO was consistent with results from Bell et al. (2015) in cortical astrocytes derived from Nrf2 KO (Bell et al., 2015).

## 5.7 Other signaling pathways involved in the regulation of some of the genes underlying the Nrf2 and ARE pathway.

Although Nrf2 mediates several antioxidant genes underlying ARE region, loss of Nrf2 in Nrf2 KO derived SCAs exhibited unexpected antioxidant genes expressions. Nrf2 regulates transporter gene expressions underlying ARE such as *Abcc1* encoding for Mrp1 (Hayashi et al., 2003), and *Slc7a11* mRNA encoding for the cystine/glutamate transporter (system Xc-) (Bridges et al., 2012b). The basal level of *Abcc1* and *Slc7a11* expressions in Nrf2 KO derived SCAs relative to WT derived SCAs unexpectedly increased (**Figure 3.7** and 3.8). Not only does Nrf2 significantly regulate *Abcc1* and *Slc7a11* expression, but other signaling pathways also regulate these gene expressions. Nrf2 KO mice possing a high basal ROS level would induce a higher level of pro-inflammatory cytokines relative to WT mice. For example, the pro-inflammatory cytokine IL-1β, which specifically upregulated system Xc- in astrocytes but not in neurons or microglia (Jackman et al., 2010)

might elicit the increase of Slc7a11 expression in Nrf2 KO derived SCAs. The IL-1β might exert on system Xc- expression through the activation of NF-kB (Yang et al., 2005; He et al., 2015) and AP1 (Yang et al., 2005) pathways. Recently, the regulation of system Xcunderlying regulation of IL-1β, and NF-kB was confirmed in cortical astrocytes (Shi et al., 2016), which suggested that hypoxic injury occurs (Jackman et al., 2010). Under hypoxia, some antioxidant genes such as Abcc1 mRNA (Lv et al., 2015) are regulated by the activation of hypoxia inducing factor-1α (HIF-1α) pathway. Some pieces of evidence in colon cancer cells reported that a hypoxia response element (HRE) loci were in the proximal promoter of the *Abcc1* gene, where the HIF-1α can directly bind and regulate Mrp1 expression (Lv et al., 2015). Consistently, when suppression of HIF -1α with siRNA occurred in these colon cancer cells, the expression of Mrp1 mRNA was significantly reduced (Lv et al., 2015). The expressions of HIF-1 and Mrp1 were significantly correlated in several cancer tissues such as colorectal, gastric, and bladder tissues (Toth and Warfel, 2017). In addition, the induction of ROS generation with menadione in the breast cancer cell line without Nrf2 exhibited the elevation of HIF-  $1\alpha$  mRNA expression (Lacher et al., 2018) that suggested the alternative signaling pathway in *Mrp1* induction, despite Nrf2. ROS or a pro-oxidant NOX, may act as an intermediate molecule between Nrf2 and HIF-1 pathway. NOX involves in the regulation of HIF activities through multiple pathways such as Ca<sup>2+</sup>/calmodulin kinase (CaMK) dependent pathway, PI<sub>3</sub>K-mTOR pathway, and ROS- evoke stabilized HIF-1α pathway (Yuan et al., 2008). The intermittent hypoxia stimulated NOx2 activation in the ROS-dependent elevation of [Ca2+]in, which later stimulated the activation of the HIF-1 pathway in PC12 cells (Nanduri et al., 2015). The regulation of Nox expression by Nrf2 appeared to be cell type-specific. For example, Nrf2 negatively regulates Nox4 expression in endothelial cells. Conversely, Nrf2 possitively

regulate Nox4 elevation in the mouse and human lung endothelium in response to hyperoxia (Kovac et al., 2015). In cortical neuron-astrocyte coculture and mouse embryonic fibroblasts showed that *Nox2* mRNA was dramatically increase while *Nox4* mRNA was decrease in Nrf2 KO compared to WT (Kovac et al., 2015). Perhaps, the elevation of Mrp1 transcripts in Nrf2 KO derived SCAs may be regulated by a cross-talk between Nrf2 and HIF pathway by which NOX2 acts as an intermediate mediator in the regulation of *Abcc1* elevation through the activation of HIF-1 pathway as a compensatory antioxidant mechanism (see Figure 3.17). Additionally, STAT3/STAT5, growth factors, neuronal activity, and amino acid starvation could regulate the promoter region of *Slc7a11* gene (Massie et al., 2015) (see Figure 3.16). The activation of the ATF4 through PI3K and GSK3β also elicited the expression of system Xc in glioblastoma (Lewerenz et al., 2014). Thus, these pathways could play a critical role in the compensation of the induction of *Slc7a11* and *Abcc1* in Nrf2 KO derived SCAs.

## 5.8 Genetic predisposition exhibited differential mechanisms by which MeHg induced neurotoxicity in SCAs.

Although the majority of genes underlying Nrf2 regulation were affected by MeHg in Nrf2 KO derived SCAs similar to WT derived SCAs, few genes were affected by MeHg differently among these genotypes. For example, while MeHg induced the increase of *Slc7a11* expression about 5.3-fold increase in WT SCAs, MeHg appeared to diminish the *Slc7a11* expression about 0.54-fold decrease in Nrf2 KO SCAs (Figure 3.8). Besides, MeHg induced the increase of *Vegfa* expression in WT SCAs (about 2.5-fold increase), whereas it pronouncedly diminished the *Vegfa* expression in Nrf2 KO derived SCAs (about 11.75-fold decrease) (Figure 3.15). Also, MeHg slightly but insignificantly

induced the reduction of *Slc1a*3 expression in WT SCAs, but it did so considerably in Nrf2 KO derived SCAs (Figure 3.9). Meanwhile, MeHg affected the reduction of Slc1a2 in both WT and Nrf2 KO SCAs, which pronouncedly diminished in Nrf2 KO SCAs (Figure **3.10)**. MeHg significantly reduced *Keap1* mRNA (0.26-fold decrease) in Nrf2 KO derived SCAs compared to its genotype treated vehicle. In contrast, Keap1 mRNA was not significantly affected by MeHg exposure in WT derived SCAs (Figure 3.3). Although immunocytochemistry showed significant reductions of both system Xc- and EAAT2 in both WT and Nrf2 KO SCAs following MeHg exposure (Figures 3.13 and 3.14), it is possible that the differential molecular mechanisms contributed to the reduction of these transporter expressions. These findings suggested that the molecular pathways involved in MeHg induced the dysregulation of Keap1, system Xc-, EAAT1/2, and Vegfa expressions in WT differed from Nrf2 KO. Further elucidation of these differential mechanisms will tailor the signature pathway(s) involving the differential susceptibility of SCAs to MeHg. All in all, genetic predisposition plays a critical role in MeHg induced differential toxicity mechanisms with both transcriptional and translational levels.

## 5.9 The antioxidant NAC could protect and rescue SCAs from MeHg induced degeneration in a concentration-dependent manner.

NAC concentrations ranging from 0.1, 1.0, and 10mM protect SCAs against 5µM MeHg induced degeneration over 24h. Meanwhile, 0.1mM NAC lost its potency around 30h compared to control; 1.0mM and 10mM remained their protective efficacy over 72h in both NP and CO NAC treatments (**Figures 4.3 and 4.4**). MeHg induced a significant SCAs degeneration starting from 9h of 5µM MeHg exposure, whereas pretreatment of

0.1mM NAC 2h before MeHg exposure considerably extended a reduction of cell metabolic activity to 30h of MeHg exposure. When increases NAC concentration to 1.0mM and 10mM NAC with the same NAC pretreatment paradigm, these NAC concentrations extend the protection of SCAs from MeHg-induced toxicity across the time course of the examination (over than 160 h) (Figure 4.3). Similarly, the co-application of these NAC concentrations and 5µM MeHg exhibited prolong protective effects (Figure **4.4)**, as exhibited in the NAC pretreatment paradigms. While 10mM NAC was effectively protected SCAs from MeHg in both NP and CO treatment paradigms, 10mM NAC treatment following 5µM MeHg exposure for 3h (MP) did not protect SCAs from MeHg induced toxicity. Nevertheless, 0.1 µM and 1.0 µM NAC rescued SCAs from MeHginduced toxicity in the MP treatment paradigm (Figure 4.5). Overall, the optimum NAC concentration in all treatment paradigms was 1.0mM, which extended SCAs degeneration in NP, CO, and MP. These results were supported by the finding in U-87MG human astrocytoma that the 10mM NAC was toxic to these cells, whereas 0.1 and 1.0mM NAC were not affected cell viability (Muniroh et al., 2015). The applications of 0.5 and 5mM NAC in NP, CO, and MP exposed to 4µM MeHg U-87MG human astrocytoma for 6h could suppress MeHg toxicity in these cells (Muniroh et al., 2015). The magnitudes or ratios of NAC to MeHg in the U-87MG human astrocytoma study were equal to 125-fold and 1,250fold in 0.5mM and 5mM NAC with 4µM MeHg, respectively (Muniroh et al., 2015), which relatively higher than this SCAs study, 20-fold and 200- fold in 0.1 and 1mM NAC with 5μM MeHg, respectively. Given that, the 0.1mM NAC would sufficiently protect and suppress MeHg induced toxicity in SCAs, and 1mM NAC was the optimum NAC concentration for prolonged MeHg exposure. Furthermore, different NAC concentrations exert different mechanisms of NAC actions. The study in the C6 glial cells suggested that

the high NAC concentration (1mM) was GSH-independent, whereas the low NAC concentration (0.1mM) was GSH-dependent antioxidant mechanism (Han et al., 1997). The application of BSO to inhibit the *de novo* GSH synthesis in PC12 cells revealed that with high NAC concentration (60mM) could maintain PC 12 cell viability despite GSH level reduction (Yan et al., 1995). This BSO application suggested that high NAC concentration exerts its protective mechanism through the GSH-independent antioxidant mechanism in PC12 cells (Yan et al., 1995). However, the therapeutic NAC window and cell types also play a critical role in NAC action. The mechanism of NAC after MeHg exposure (MP) remained unclear whether 0.1mM NAC exerts its action through the GSH-dependent antioxidant mechanism in SCAs or not. More detailed studies using GSH assay and application of BSO to inhibit intracellular GSH synthesis will better explain this question.

5.10 The primary NAC mechanism in protecting SCAs during MeHg exposure in the NAC pretreatment paradigm was its direct antioxidant property or GSH-independent antioxidant mechanism.

The NAC pretreatment paradigm (**Figure 4.3**) showed the protective effect of all NAC concentrations, and indeed, different NAC concentrations play different modes of protective mechanism. Another experimental paradigm with 1.0mM or 10mM NAC pretreatment later removal before exposure to 5µM MeHg revealed that the real-time SCAs viabilities were significantly reduced to the same rate as MeHg treatment alone (**Figure 4.15**). These results were confirmed with cell viability assay with the EthD-2, a cell-impermeant dye permeating only plasma membrane compromised cells, which showed similar results of the red nuclei staining in MeHg exposure similar to NAC

treatment before MeHg exposure in SCAs (Figure 4.16). Similarly, pretreatments of NAC either 4h or 24 h later removed and exposed to MeHg (a 100-fold NAC to MeHg ratio) the cortical neurons underwent the apoptosis cell death pathway (Falluel-Morel et al., 2012). These data support NAC's protective role through which its direct interaction with MeHg as a direct antioxidant to prevent MeHg toxicity. Despite the morphologies of SCAs in MeHg treatment alone were more severely affected and loss of GFAP staining than vehicle treatment, the NAC treatment before MeHg exposure showed the morphologies less impaired and remained GFAP staining at a level similar to a vehicle and NAC alone treatments (Figure 4.16). NAC somewhat might act as a cysteine prodrug for increasing intracellular GSH. Pretreatment of NACA, a derivative of NAC following traumatic brain injury in mice, significantly reduced apoptotic cell death through the activation of Nrf2 and its antioxidant Ho-1 and Nqo-1 (Zhou et al., 2018). However, the intracellular protective mechanism by NAC in SCAs remains unclear. The study using Nrf2 KO mice could better explain whether NAC protects the SCAs against MeHg induced toxicity through this pathway. Furthermore, the membrane permeability, particularly the BBB permeability of NAC, remains controversial. It has been concerned that NAC will facilitate MeHg entering the CNS through its molecular mimicry of the methionine transport system in the form of the cysteine-MeHg, and or GSH-MeHg complex (Aschner and Clarkson, 1988; Kerper et al., 1992; Mokrzan et al., 1995). This issue appeared not to be the case in SCAs. Since cotreatment of NAC and MeHg did not exacerbate the toxicity but rather protect SCAs degeneration for a more extended period of MeHg exposure (Figure 4.4). NAC is negatively charged at physiological pH, limiting its ability to cross any biological membranes (Sunitha et al., 2013; Tobwala et al., 2015). On the other hand, in MP

treatment paradigm, following MeHg exposure for 3h, 0.1mM, and 1.0mM NAC could suppress MeHg induced SCAs degeneration for over 16oh exposure (Figure 4.5). Therapeutic efficacy of NAC demonstrated in a man who accidentally exposed to mercury, and NAC treatment with selenium reversed his neurological symptoms considerably to normal physiological conditions (Spiller et al., 2017). NAC is, therefore, potentially used for therapeutic benefit in MeHg intoxication mainly through its direct antioxidant property that directly interacts with MeHg to reducing toxicity (Hunter and Russell, 1954).

#### **APPENDIX**

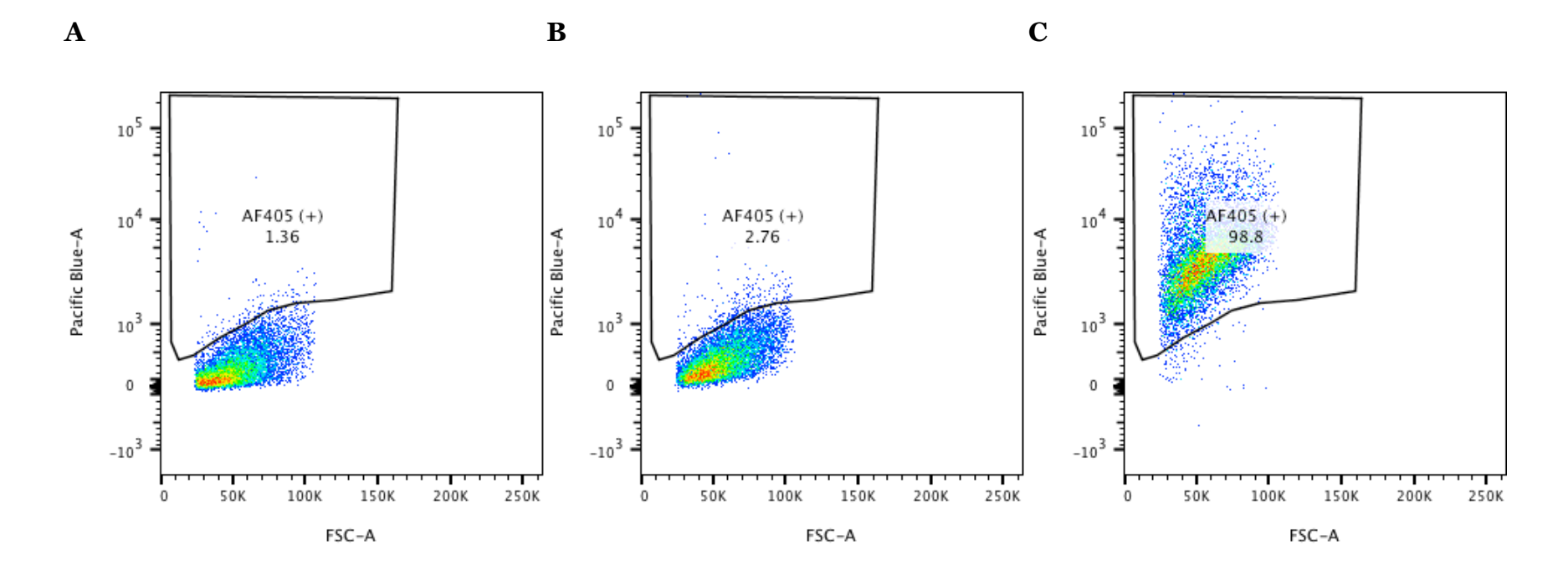


Figure A.1 Representative diagram of immunological positive to GFAP in SCA DIV30. SCAs were isolated and culture from B57BL/6Jmice spinal cord. Spinal cord astrocytes were purified using Anti-GLAST (ACSA-1) antibody from Miltenyi Biotec following magnetic bead isolation by immunopanning technique. SCA DIV30 were stained with anti-rabbit GFAP polyclonal antibody to determine the population of GFAP+ cell from this cell culture technique. The anti-GFAP was determined using goat-anti-rabbit AF405. Percent of GFAP+ were analyzed using Fluorescence-Activated Cell Sorter (FAC) (BD Biosciences, Franklin Lakes, NJ, USA). Data were analyzed using FlowJo software (FlowJO, LLC). A. Non- staining cells, B. Only AF405 staining cells using as a gate for determination AF405+ (in this case, it is GFAP+ cells) and C. Both anti-GFAP and AF405 staining cells. The value presented in the gate is indicated a percent cell that expressed immunogen (rabbit anti-GFAP) and reacted to anti-rabbit AF405.

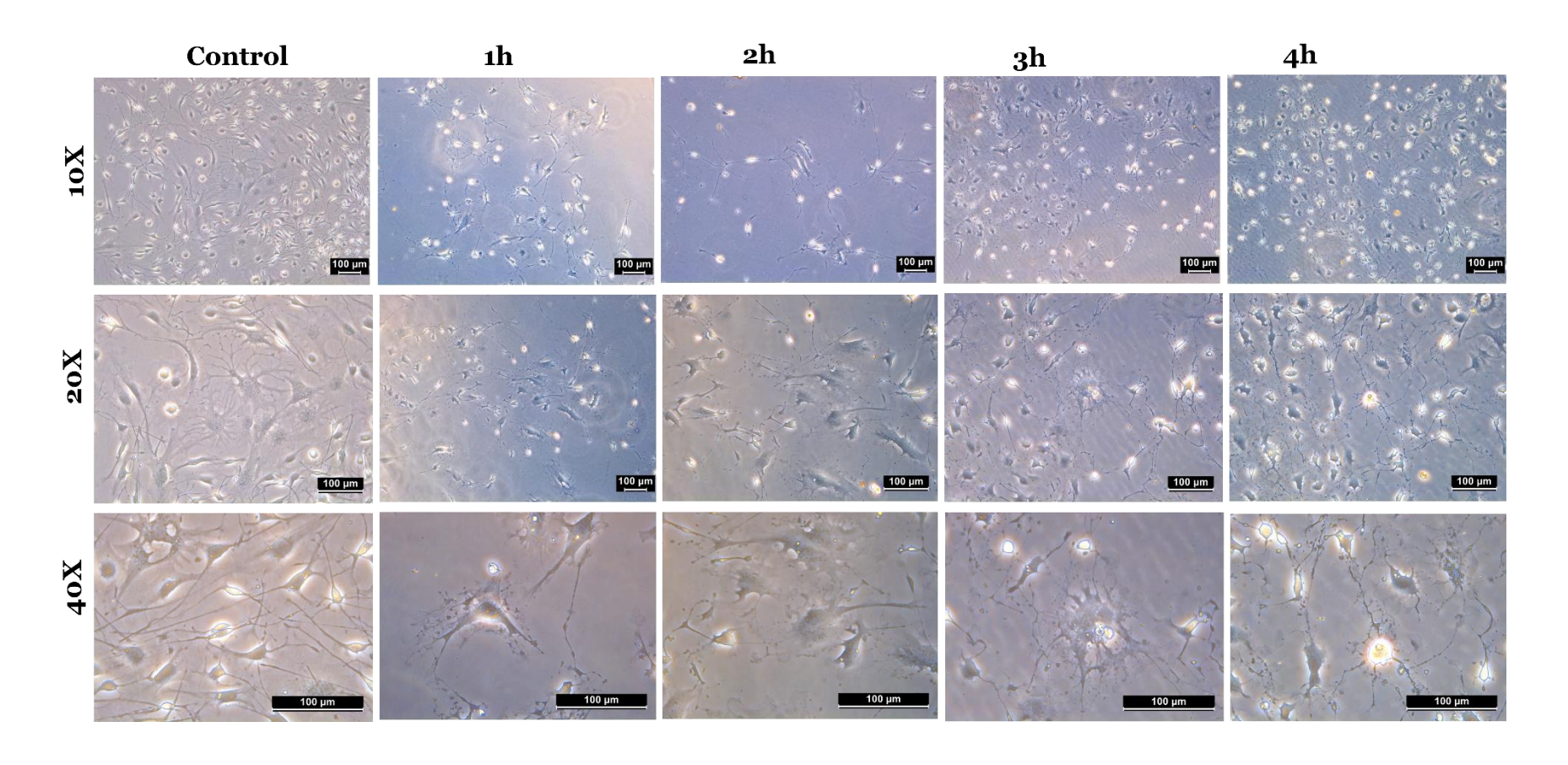


Figure A.2 Pathological and morphological features of SCAs DIV14 as a function of time of 0.5  $\mu M$  MeHg exposure, from 1h to 4h.

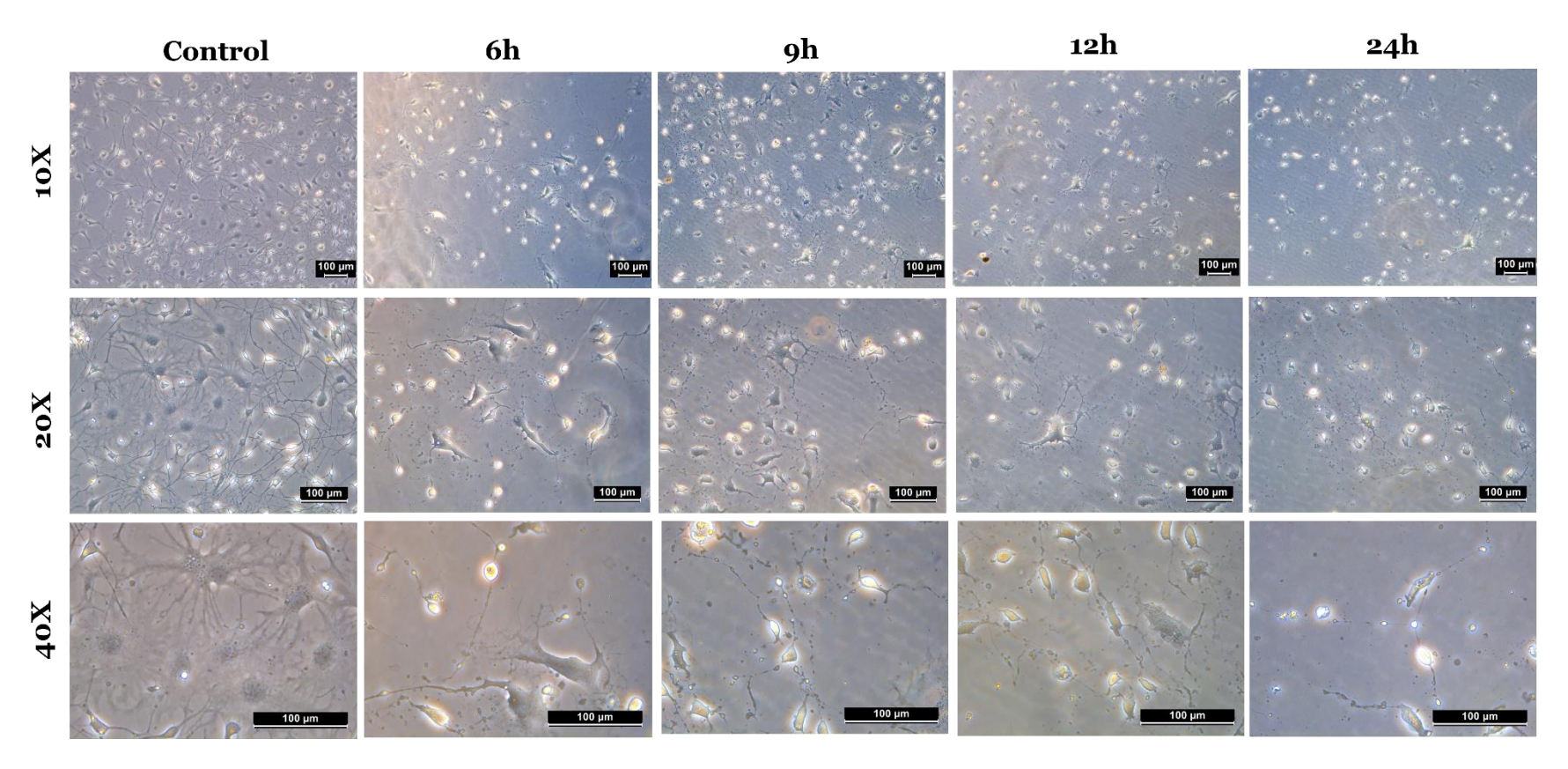


Figure A.3 Pathological and morphological features of SCAs DIV14 as a function of time of 0.5  $\mu M$  MeHg exposure, from 6h to 24h.

Table A1 Primers lists for this research.

Targeted mRNA	Primer's ID	Amplicon length		
EAAT1 (GLAST-1) solute carrier family 1 (glial high affinity glutamate transporter), member 3; <i>Slc1a3</i> gene)	olute carrier family 1 (glial high affinity glutamate Mm00600697			
EAAT2 (GLT-1) (solute carrier family 1 (glial high affinity glutamate transporter), member 2;Slc1a2 gene)	Mm01275814 m1	135		
Gclc (Glutamate-cysteine ligase catalytic subunit is one of two units of Glutamate-cysteine ligase (a rate limiting enzyme for GSH synthesis)	Mm0080265 5 m1	98		
Gpx1 glutathione peroxidase 1	Mm0065676 7_g1	134		
Gpx4 glutathione peroxidase 4	Mm00515041 m1	103		
Mrp1 (ATP-binding cassette, sub-family C (CFTR/MRP), member 1; Abcc1 gene)	Mm00456156 _m1	67		
Vegf (vascular endothelial growth factor A; Vegfa gene)	Mm00437306 _m1	61		
xCT (system xc <sup>-</sup> ) (solute carrier family 7 (anionic amino acid transporter light chain, system xc <sup>-</sup> ), member 11; <i>Sclc7a11</i> gene)	Mm0044253 0 m1	66		
The mouse glyceraldehyde-3-phosphate dehydrogenase (Gapdh) endogenous control VIC $^{\rm TM}$ /MGB probe with primer limited	Catalog number: 4352339E	107		

All primers were obtained from TaqMan gene expression assay (Applied BioSystems, Foster City, USA)

Table A2 Primary antibodies used in this research

Target Proteins	antibody	Catalog number	Company	ratio	Lot number
ALDH1L1	Mouse IgG2a	MO22143	NEUROMICS	1:1,000	401914
EAAT3	Rabbit Polyclonal SLC1A1 antibody	12686-1- AP	Proteintech	1:100	ND
GFAP	Chicken IgY GFAP Polyclonal antibody	PA1- 10004	Invitrogen, Thermo Fisher	1:1,000	TG2600202
GFAP (for FAC)	Rabbit anti-GFAP Polyclonal28400	840001	BioLegend	1:1,000	B209356
GLT-1	Guinea pig Glutamate transporter polyclonal antibody	AB1783	MilliPore Sigma	1:1,000	2945625
Keap1	Mouse IgG1 Keap1 monoclonal antibody (1F10B6)	MA5- 17106	Invitrogen, Thermo Fisher	1:50	TJ2652135
Mrp1	Mouse IgG1 Mrp1 monoclonal antibody (IU5C1)	MA5- 16112	Invitrogen, Thermo Fisher	1:150	TG2598821
Nrf2	Rabbit IgG Nrf2 Polyclonal antibody	PA5- 27882	Invitrogen, Thermo Fisher	1:400	ND
Xc- (SLC7A11)	Rabbit IgG SLC7A11 Polyclonal Antibody	PA1- 16893	Invitrogen, Thermo Fisher	1:500	TG2598823A

ND=non-determined

Table A3 Secondary antibodies used in this research

Target species	antibody	ratio	Catalog number	Lot number	Company
Chicken	Goat anti-Chicken IgY, Alexa Fluor 488	1:200	A-11039	1937504	Invitrogen, Thermo Fisher
Guinea pig	Goat anti-Guinea pig IgG secondary antibody, Alexa Fluor 594	1:200	A-11076	1848493	Invitrogen, Thermo Fisher
Mouse	Goat anti-Mouse IgG (H+L) Highly cross absorbed secondary antibody, Alexa Flour 488	1:200	A-11029	1874804	Invitrogen, Thermo Fisher
Mouse	Goat anti-Mouse IgG1 cross absorbed secondary antibody, Alexa Flour 647	1:200	A-21240	1977346	Invitrogen, Thermo Fisher
Rabbit	Goat anti-Rabbit IgG (H+L) Highly cross absorbed secondary antibody, Alexa Fluor 488	1:200	A-11034	1851447	Invitrogen, Thermo Fisher

Note: All secondary antibodies raised against goat were employed to determine target proteins

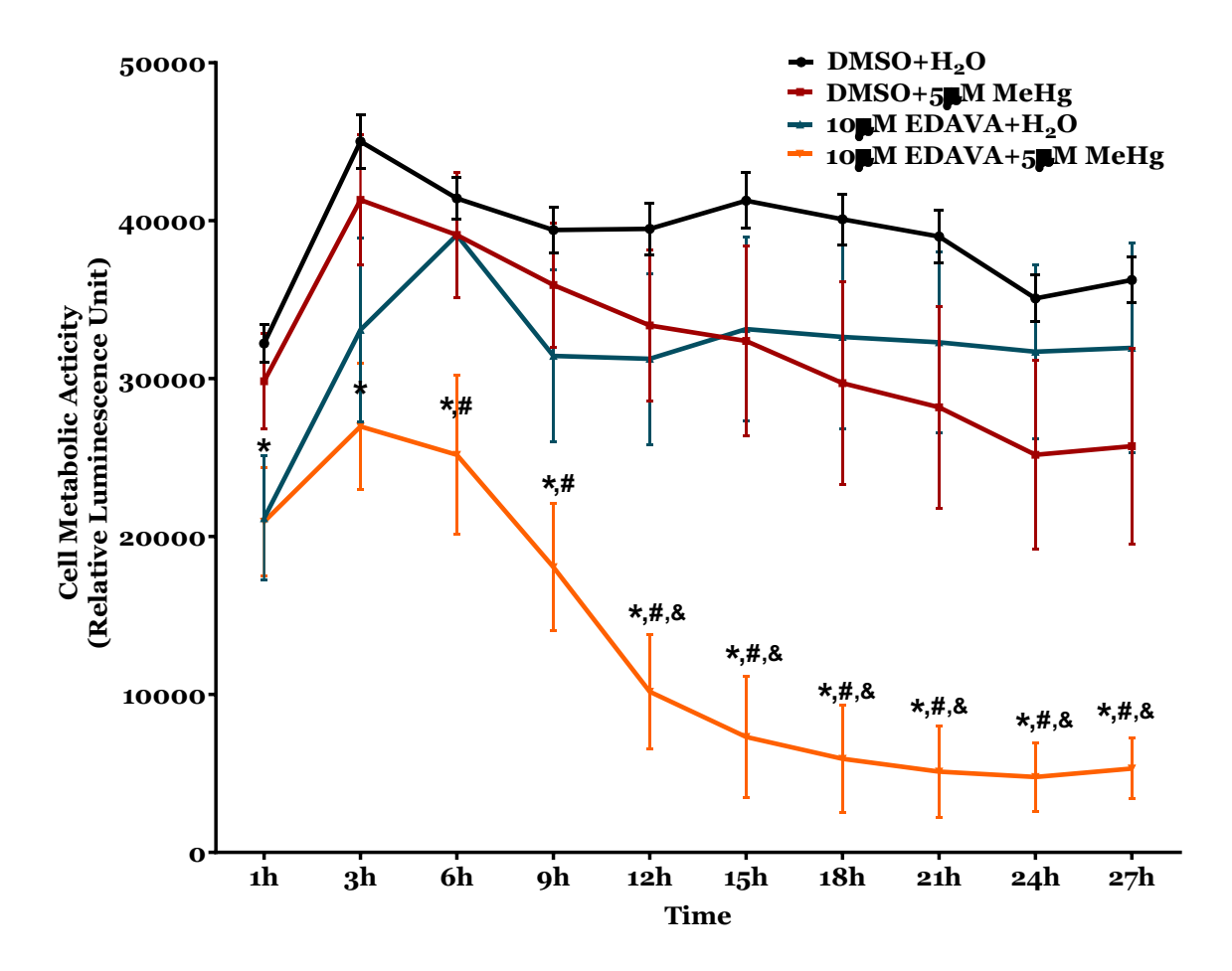


Figure A.4 SCAs were treated with 10 $\mu$ M Edaravone (EDAVA) 1h prior to exposure with 5 $\mu$ M MeHg. Cell viability was determined during MeHg exposure from 1h to 27h. \* indicates p< 0.05 when compared to DMSO+ $H_2O$ ; # indicates p< 0.05 when compared to DMSO+ $\mu$ M MeHg; & indicates p< 0.05 when compared to EDAVA+ $\mu$ D. Every experiment was performed with N=7.

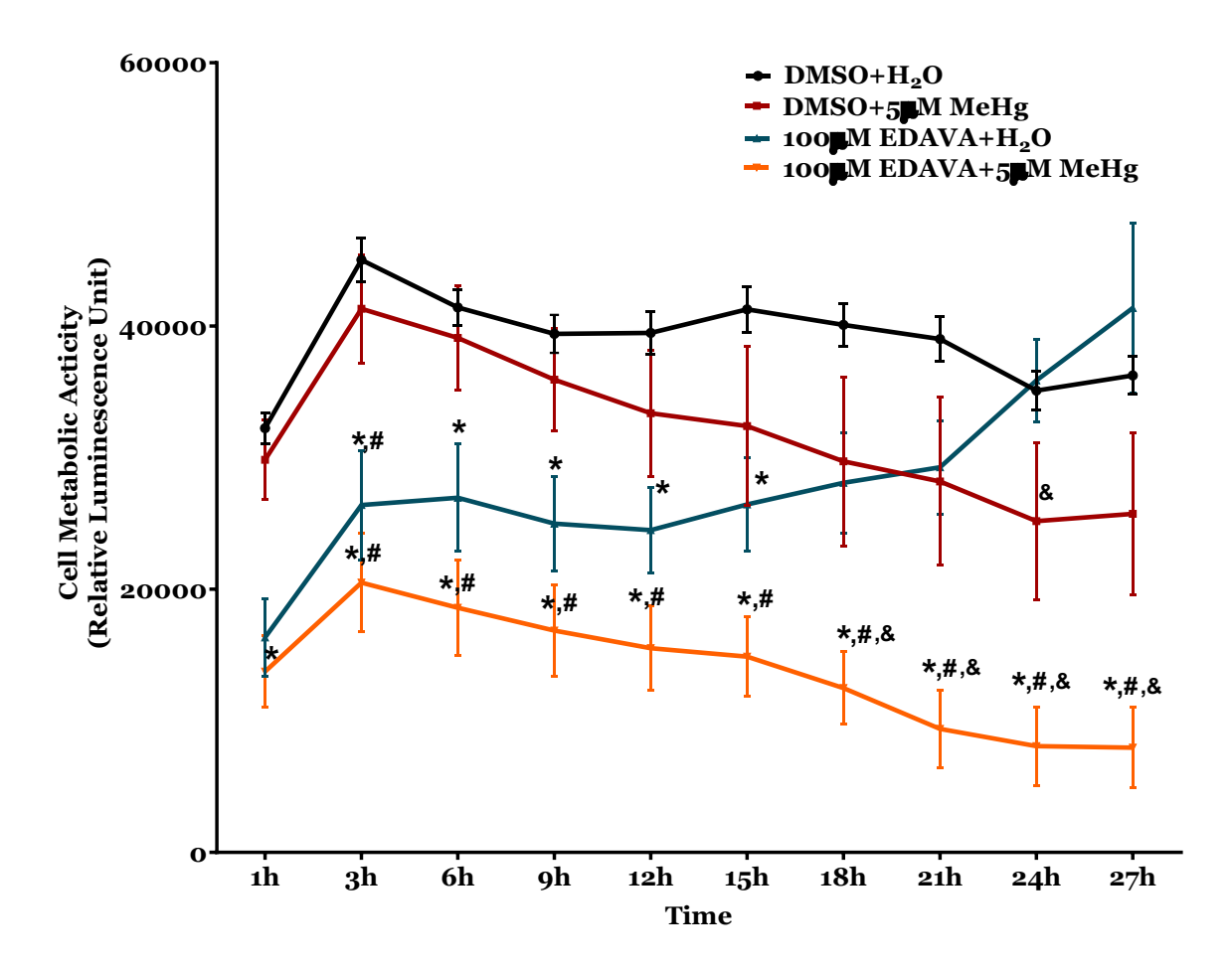
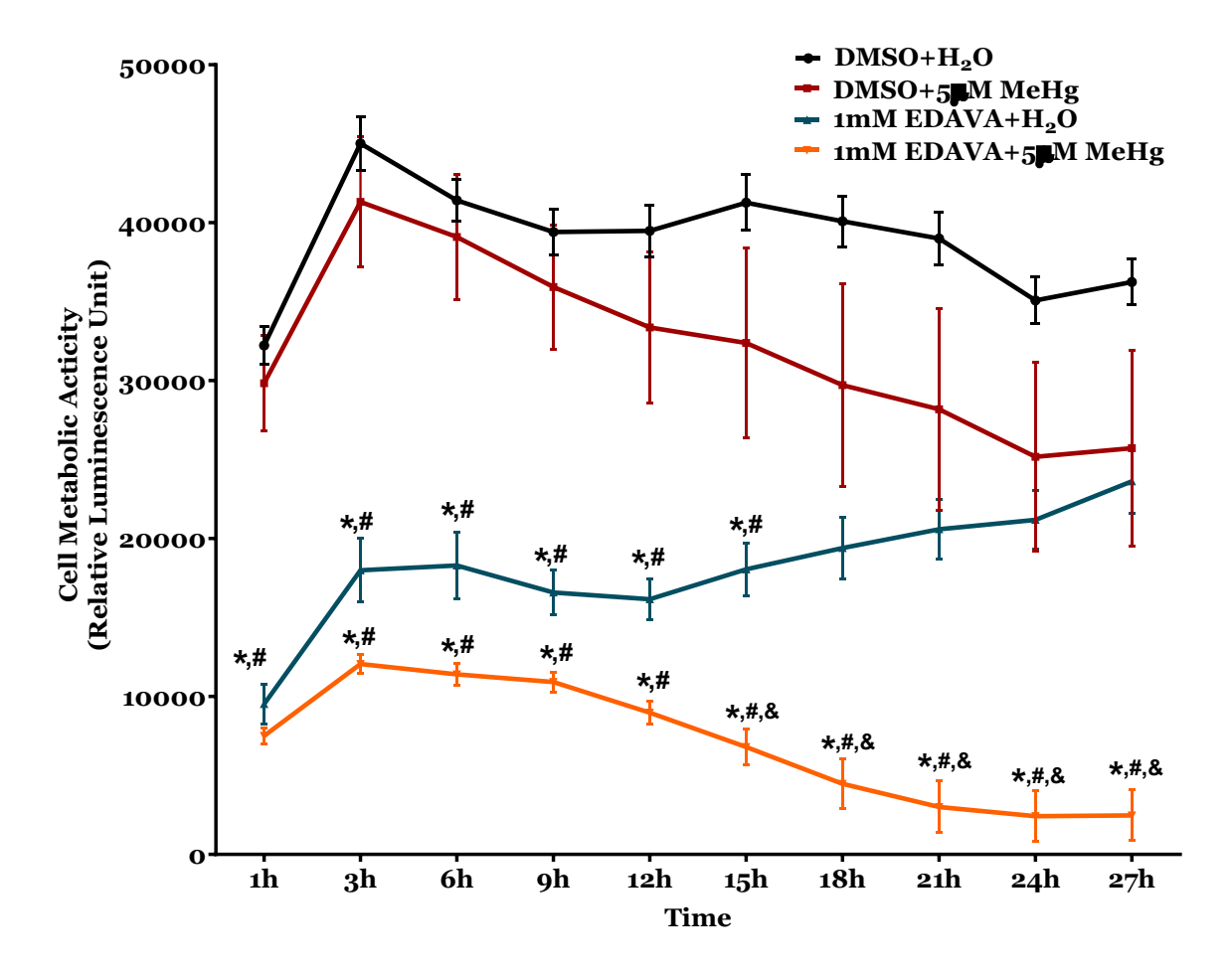


Figure A.5 SCAs were treated with 100 $\mu$ M Edaravone (EDAVA) 1h prior to exposure with 5 $\mu$ M MeHg. Cell viability was determined during MeHg exposure from 1h to 27h. \* indicates p< 0.05 when compared to DMSO+ $H_2O$ ; # indicates p< 0.05 when compared to DMSO+ $\mu$ M MeHg; & indicates p< 0.05 when compared to EDAVA+ $\mu$ D. Every experiment was performed with N=7.



**Figure A.6 SCAs were treated with 1mM Edaravone (EDAVA) 1h prior to exposure with 5μM MeHg.** Cell viability was determined during MeHg exposure from 1h to 27h. \* indicates p< 0.05 when compared to DMSO+H<sub>2</sub>O; # indicates p< 0.05 when compared to DMSO+5μM MeHg; & indicates p< 0.05 when compared to EDAVA+H<sub>2</sub>O. Every experiment was performed with N=7.

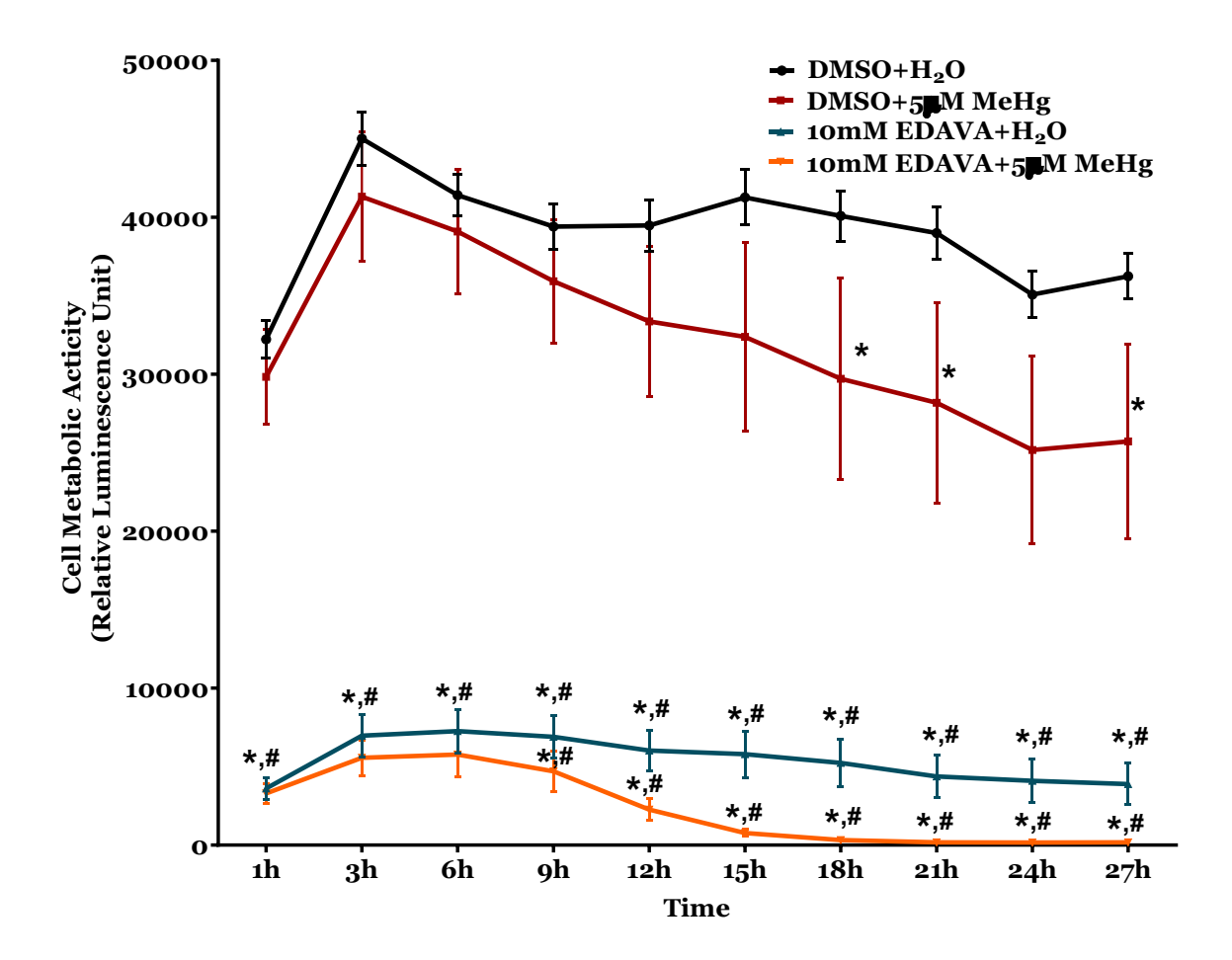
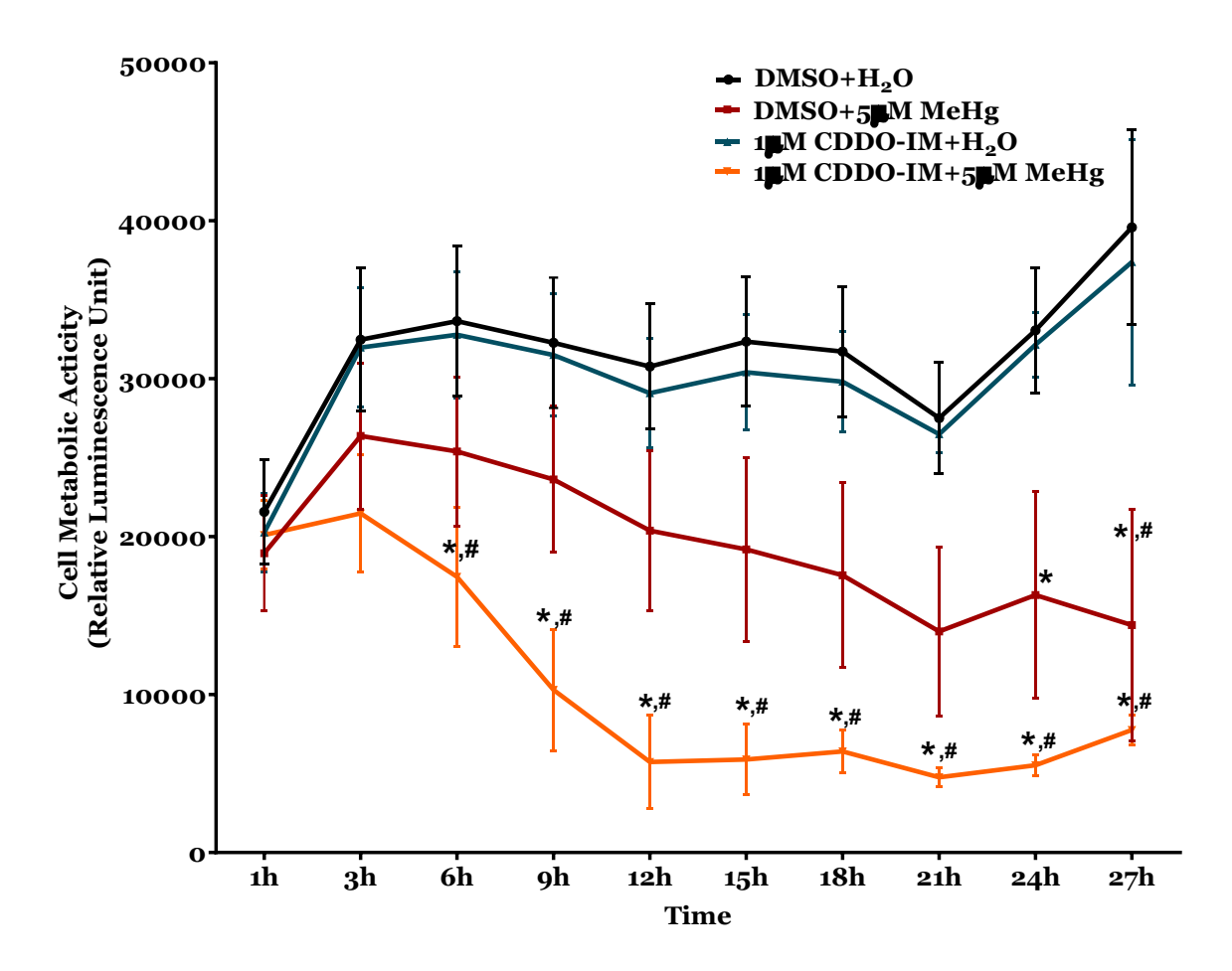
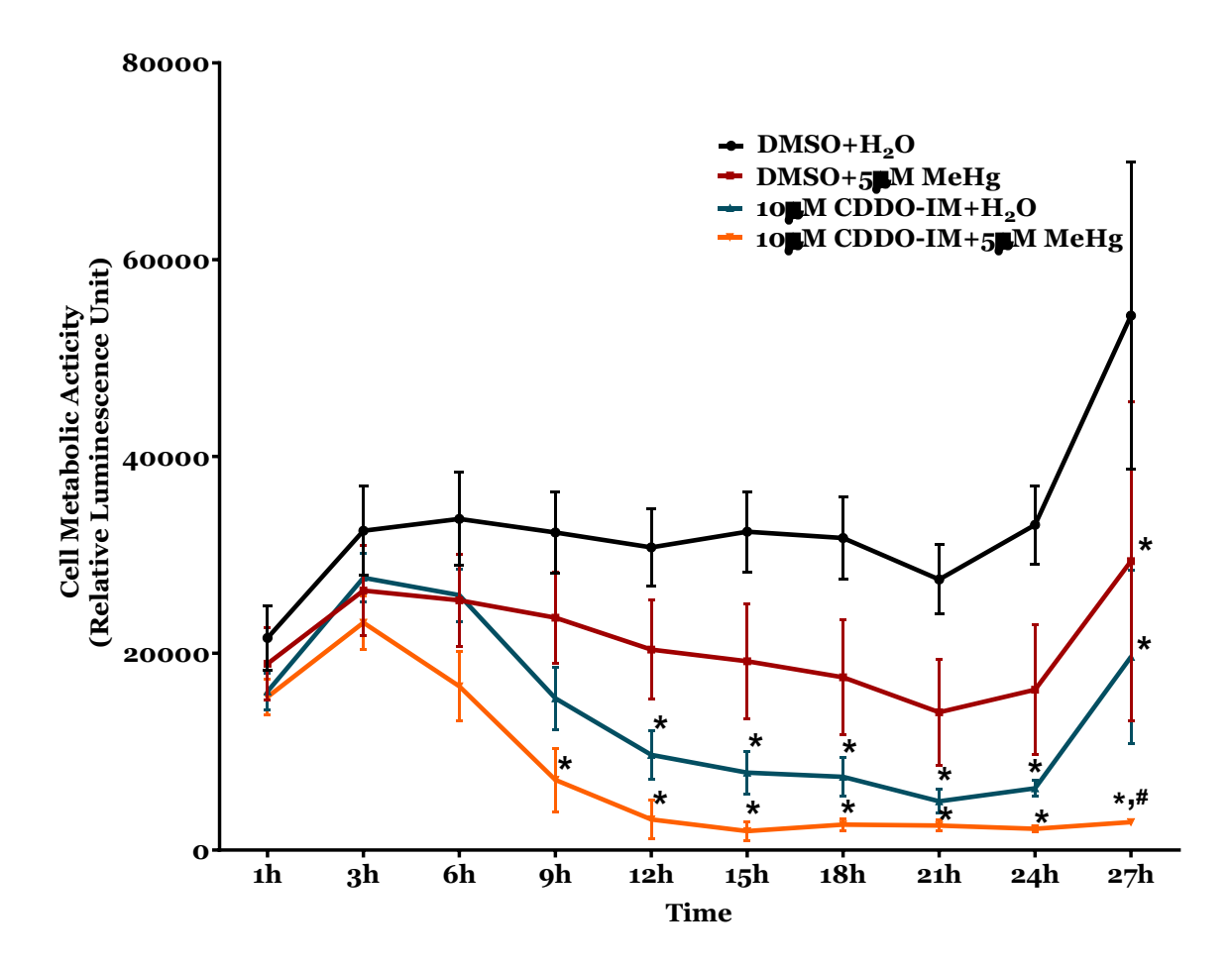


Figure A.7 SCAs were treated with 10mM Edaravone (EDAVA) 1h prior to exposure with  $5\mu$ M MeHg. Cell viability was determined during MeHg exposure from 1h to 27h. \* indicates p< 0.05 when compared to DMSO+ $H_2O$ ; # indicates p< 0.05 when compared to DMSO+ $\mu$ M MeHg; & indicates p< 0.05 when compared to EDAVA+ $\mu$ C. Every experiment was performed with N=7.



**Figure A.8 SCAs were treated with 1μM CDDO-IM for 1h prior to exposure with 5μM MeHg.** Cell viability was determined during MeHg exposure from 1h to 27h. \* indicates statistically significant from DMSO+H<sub>2</sub>O, # indicates statistically significant from CDDO-IM+H<sub>2</sub>O, and & indicates statically significant from DMSO+MeHg. N=7 Biological replications using Two-Way ANOVA with Tukey's post hoc.



**Figure A.9 SCAs were treated with 10μM CDDO-IM for 1h prior to exposure with 5μM MeHg.** Cell viability was determined during MeHg exposure from 1h to 27h. \* indicates statistically significant from DMSO+H<sub>2</sub>O, # indicates statistically significant from CDDO-IM+H<sub>2</sub>O, and & indicates statically significant from DMSO+MeHg. N=7 Biological replications using Two-Way ANOVA with Tukey's post hoc.

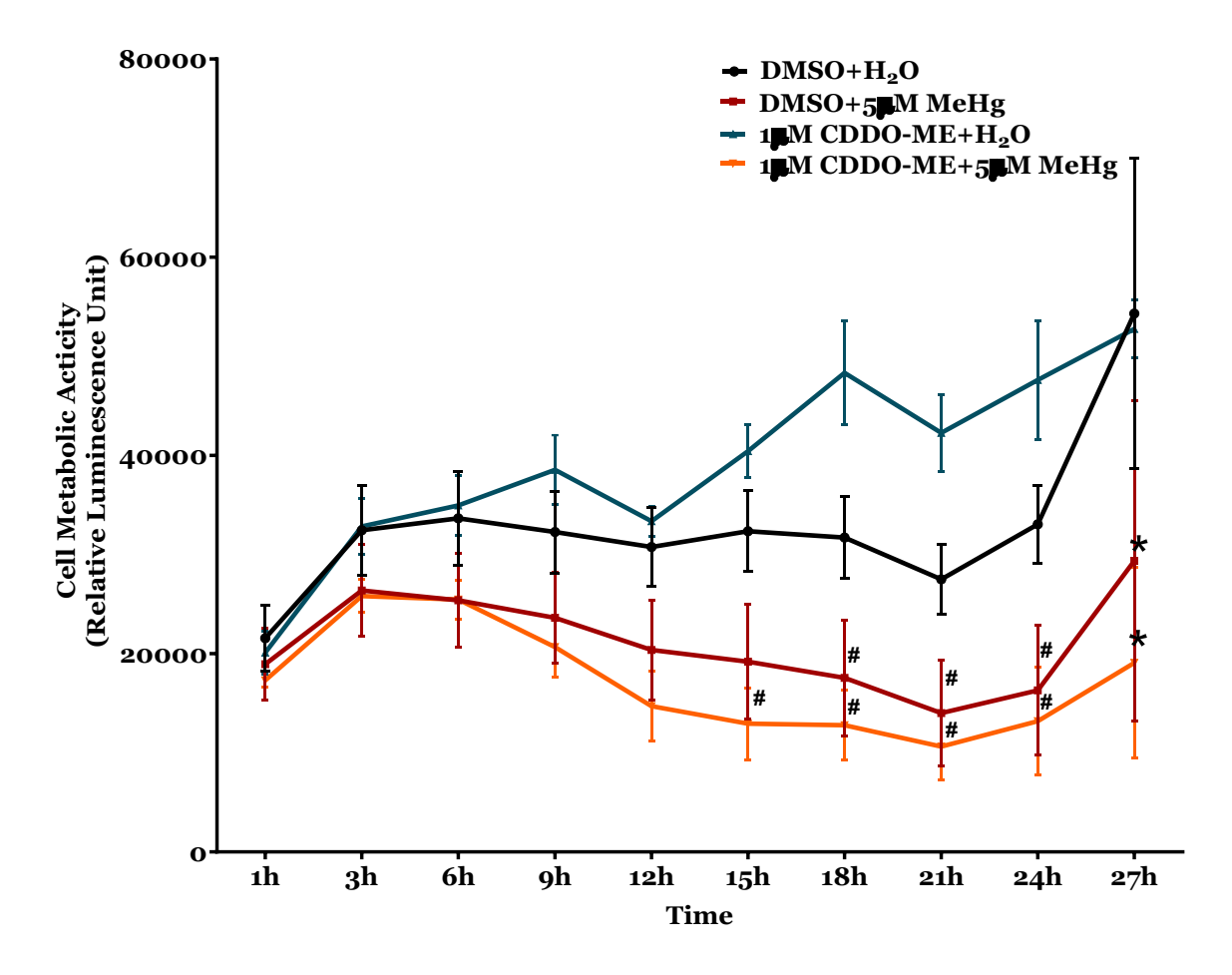


**Figure A.10 SCAs were treated with 1μM CDDO-ME for 1h prior to exposure with 5μM MeHg.** Cell viability was determined during MeHg exposure from 1h to 27h. \* indicates statistically significant from DMSO+H<sub>2</sub>O, # indicates statistically significant from CDDO-ME+H<sub>2</sub>O, and & indicates statically significant from DMSO+MeHg. N=7 Biological replications using Two-Way ANOVA with Tukey's post hoc.

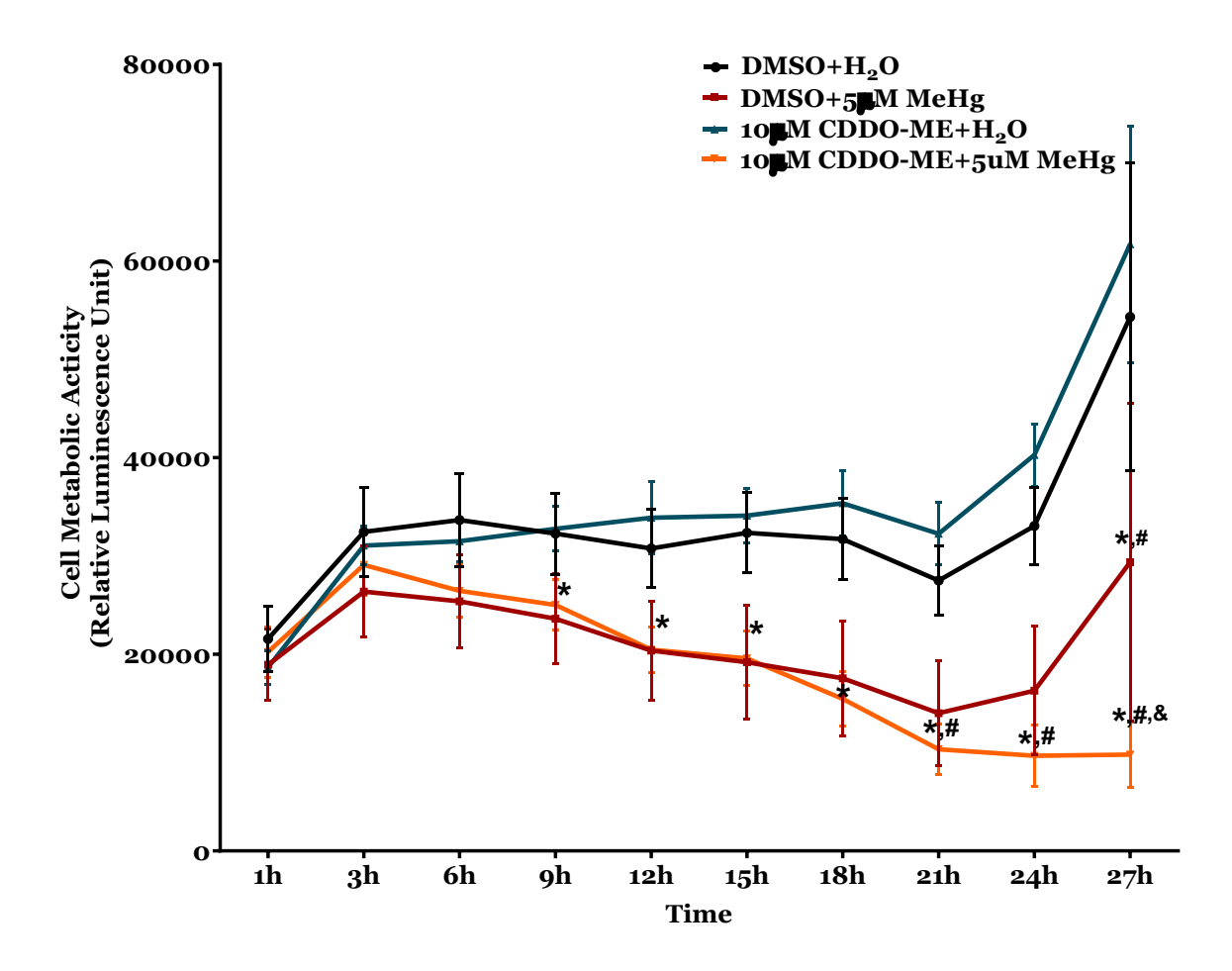


**Figure A.11 SCAs were treated with 10μM CDDO-ME for 1h prior to exposure with 5μM MeHg.** Cell viability was determined during MeHg exposure from 1h to 27h. \* indicates statistically significant from DMSO+H<sub>2</sub>O, # indicates statistically significant from CDDO-ME+H<sub>2</sub>O, and & indicates statically significant from DMSO+MeHg. N=7 Biological replications using Two-Way ANOVA with Tukey's post hoc.

#### **REFERENCES**

#### REFERENCES

- Agocs MM, Etzel RA, Parrish RG, Paschal DC, Campagna PR, Cohen DS, Kilbourne EM, Hesse JL (1990) Mercury Exposure from Interior Latex Paint. New England Journal of Medicine 323:1096-1101.
- Ahlgren-Beckendorf JA, Reising AM, Schander MA, Herdler JW, Johnson JA (1999) Coordinate regulation of NAD(P)H:Quinone oxidoreductase and glutathione-Stransferases in primary cultures of rat neurons and glia: Role of the antioxidant/electrophile responsive element. Glia 25:131-142.
- Albrecht J, Talbot M, Kimelberg HK, Aschner M (1993) The role of sulfhydryl groups and calcium in the mercuric chloride-induced inhibition of glutamate uptake in rat primary astrocyte cultures. Brain Research 607:249-254.
- Aldini G, Altomare A, Baron G, Vistoli G, Carini M, Borsani L, Sergio F (2018) N-Acetylcysteine as an antioxidant and disulphide breaking agent: the reasons why. Free Radical Research 52:751-762.
- Allaman I, Bélanger M, Magistretti PJ (2011) Astrocyte—neuron metabolic relationships: for better and for worse. Trends in Neurosciences 34:76-87.
- Allen JW, Shanker G, Aschner M (2001a) Methylmercury inhibits the in vitro uptake of the glutathione precursor, cystine, in astrocytes, but not in neurons. 894:131-140.
- Allen JW, Shanker G, Aschner M (2001b) Methylmercury inhibits the in vitro uptake of the glutathione precursor, cystine, in astrocytes, but not in neurons. Brain Research 894:131-140.
- Allen JW, Mutkus LA, Aschner M (2001c) Methylmercury-mediated inhibition of 3H-d-aspartate transport in cultured astrocytes is reversed by the antioxidant catalase. Brain Research 902:92-100.
- Amonpatumrat S, Sakurai H, Wiriyasermkul P, Khunweeraphong N, Nagamori S, Tanaka H, Piyachaturawat P, Kanai Y (2008) L-Glutamate Enhances Methylmercury Toxicity by Synergistically Increasing Oxidative Stress. Journal of Pharmacological Sciences 108:280-289.

- Andrew AS, Chen CY, Caller TA, Tandan R, Henegan PL, Jackson BP, Hall BP, Bradley WG, Stommel EW (2018) Toenail mercury Levels are associated with amyotrophic lateral sclerosis risk. Muscle & Nerve.
- Aoyama K, Nakaki T (2013) Impaired Glutathione Synthesis in Neurodegeneration. International Journal of Molecular Sciences 14:21021-21044.
- Aoyama K, Nakaki T (2015) Glutathione in Cellular Redox Homeostasis: Association with the Excitatory Amino Acid Carrier 1 (EAAC1). Molecules 20:8742-8758.
- Aoyama K, Watabe M, Nakaki T (2008) Regulation of Neuronal Glutathione Synthesis. Journal of Pharmacological Sciences 108:227-238.
- Aoyama K, Watabe M, Nakaki T (2012) Modulation of neuronal glutathione synthesis by EAAC1 and its interacting protein GTRAP3-18. Amino Acids 42:163-169.
- Aoyama K, Matsumura N, Watabe M, Nakaki T (2007) Oxidative stress on EAAC1 is involved in MPTP-induced glutathione depletion and motor dysfunction. European Journal of Neuroscience 27:20-30.
- Aoyama K, Suh SW, Hamby AM, Liu J, Chan WY, Chen Y, Swanson RA (2006) Neuronal glutathione deficiency and age-dependent neurodegeneration in the EAAC1 deficient mouse. Nature Neuroscience 9:119-126.
- Arakawa M, Ito Y (2007) N-acetylcysteine and neurodegenerative diseases: Basic and clinical pharmacology. The Cerebellum 6:308-314.
- Arakawa M, Ushimaru N, Osada N, Oda T, Ishige K, Ito Y (2006) N-acetylcysteine selectively protects cerebellar granule cells from 4-hydroxynonenal-induced cell death. Neuroscience Research 55:255-263.
- Argaw AT, Gurfein BT, Zhang Y, Zameer A, John GR (2009) VEGF-mediated disruption of endothelial CLN-5 promotes blood-brain barrier breakdown. 106:1977-1982.
- Argaw AT, Zhang Y, Snyder BJ, Zhao ML, Kopp N, Lee SC, Raine CS, Brosnan CF, John GR (2006) IL-1 Regulates Blood-Brain Barrier Permeability via Reactivation of the Hypoxia-Angiogenesis Program. 177:5574-5584.

- Argaw AT, Asp L, Zhang J, Navrazhina K, Pham T, Mariani JN, Mahase S, Dutta DJ, Seto J, Kramer EG, Ferrara N, Sofroniew MV, John GR (2012) Astrocyte-derived VEGF-A drives blood-brain barrier disruption in CNS inflammatory disease. 122:2454-2468.
- Aschner M, Clarkson TW (1988) Uptake of methylmercury in the rat brain: effects of amino acids. Brain Research 462:31-39.
- Aschner M, Aschner JL (1990) Mercury neurotoxicity: Mechanisms of blood-brain barrier transport. Neuroscience & Biobehavioral Reviews 14:169-176.
- Atchison WD (2005) Is chemical neurotransmission altered specifically during methylmercury-induced cerebellar dysfunction? Trends Pharmacol Sci 26:549-557.
- Atchison WD, Narahashi T (1982) Methylmercury-induced depression of neuromuscular transmission in the rat. Neurotoxicology 3:37-50.
- ATSDR AfTSaDR (1999) Toxicological profile for Mercury. In: (U.S. Department of Health and Human Services PHS, ed). Atlanta, GA.
- Augustine GJ, Santamaria F, Tanaka K (2003) Local Calcium Signaling in Neurons. Neuron 40:331-346.
- Bailey JM, Colón-Rodríguez A, Atchison WD (2017) Evaluating a Gene-Environment Interaction in Amyotrophic Lateral Sclerosis: Methylmercury Exposure and Mutated SOD1. Current Environmental Health Reports.
- Bakir F (1973) Methylmercury poisoning in Iraq. Science (American Association for the Advancement of Science) 181:230-241.
- Ballatori N, Boyer JL (1986) Slow biliary elimination of methyl mercury in the marine elasmobranchs, Raja erinacea and Squalus acanthias. 85:407-415.
- Ballatori N, Lieberman MW, Wang W (1998) N-acetylcysteine as an antidote in methylmercury poisoning. Environmental health perspectives 106:267-271.
- Banjac A, Perisic T, Sato H, Seiler A, Bannai S, Weiss N, Kölle P, Tschoep K, Issels RD, Daniel PT, Conrad M, Bornkamm GW (2008) The cystine/cysteine cycle: a redox

- cycle regulating susceptibility versus resistance to cell death. Oncogene 27:1618-1628.
- Bannai S (1986) Exchange of cystine and glutamate across plasma membrane of human fibroblasts. The Journal of biological chemistry 261:2256-2263.
- Bannai S, Tateishi N (1986) Role of membrane transport in metabolism and function of glutathione in mammals. The Journal of Membrane Biology 89:1-8.
- Barber SC, Shaw PJ (2010) Oxidative stress in ALS: Key role in motor neuron injury and therapeutic target. 48:629-641.
- Barber TE (1978) Inorganic mercury intoxication reminiscent of amyotrophic lateral sclerosis. Journal of occupational medicine: official publication of the Industrial Medical Association 20:667-669.
- Barres B, Chun L, Corey D (1989) Calcium current in cortical astrocytes: induction by cAMP and neurotransmitters and permissive effect of serum factors. The Journal of Neuroscience 9:3169-3175.
- Bartolome J, Whitmore WL, Seidler FJ, Slotkin TA (1984) Exposure to methylmercury un utero: Effects on biochemical development of catecholamine neurotransmitter systems. Life Sciences 35:657-670.
- Bassett T, Bach P, Chan HM (2012) Effects of methylmercury on the secretion of proinflammatory cytokines from primary microglial cells and astrocytes. NeuroToxicology 33:229-234.
- Baxter PS, Hardingham GE (2016) Adaptive regulation of the brain's antioxidant defences by neurons and astrocytes. Free Radical Biology and Medicine 100:147-152.
- Beal MF (1992) Mechanisms of excitotoxicity in neurologic diseases. The FASEB Journal 6:3338-3344.
- Bélanger M, Allaman I, Pierre (2011) Brain Energy Metabolism: Focus on Astrocyte-Neuron Metabolic Cooperation. Cell Metabolism 14:724-738.
- Bell KFS, Al-Mubarak B, Martel M-A, McKay S, Wheelan N, Hasel P, Márkus NM, Baxter P, Deighton RF, Serio A, Bilican B, Chowdhry S, Meakin PJ, Ashford MLJ, Wyllie

- DJA, Scannevin RH, Chandran S, Hayes JD, Hardingham GE (2015) Neuronal development is promoted by weakened intrinsic antioxidant defences due to epigenetic repression of Nrf2. Nature Communication 6:7066.
- Bellinger FP, Bellinger MT, Seale LA, Takemoto AS, Raman AV, Miki T, Manning-Boğ AB, Berry MJ, White LR, Ross G (2011) Glutathione Peroxidase 4 is associated with Neuromelanin in Substantia Nigra and Dystrophic Axons in Putamen of Parkinson's brain. 6:8.
- Bergman O, Ben-Shachar D (2016) Mitochondrial Oxidative Phosphorylation System (OXPHOS) Deficits in Schizophrenia: Possible Interactions with Cellular Processes. 61:457-469.
- Bergson P, Lipkind G, Lee SP, Duban M-E, Hanck DA (2011) Verapamil Block of T-Type Calcium Channels. Molecular Pharmacology 79:411-419.
- Berk M, Malhi GS, Gray LJ, Dean OM (2013) The promise of N-acetylcysteine in neuropsychiatry. Trends in Pharmacological Sciences 34:167-177.
- Bernhardt LK, Bairy KL, Madhyastha S (2018) Neuroprotective Role of N-acetylcysteine against Learning Deficits and Altered Brain Neurotransmitters in Rat Pups Subjected to Prenatal Stress. Brain sciences 8.
- Berridge MJ (1998) Neuronal Calcium Signaling. Neuron 21:13-26.
- Bjørn-Yoshimoto WE, Underhill SM (2016) The importance of the excitatory amino acid transporter 3 (EAAT3). Neurochemistry international 98:4-18.
- Blackburn D, Sargsyan S, Monk PN, Shaw PJ (2009) Astrocyte function and role in motor neuron disease: A future therapeutic target? Glia 57:1251-1264.
- Bogaert E, Van Damme P, Poesen K, Dhondt J, Hersmus N, Kiraly D, Scheveneels W, Robberecht W, Van Den Bosch L (2010) VEGF protects motor neurons against excitotoxicity by upregulation of GluR2. Neurobiology of Aging 31:2185-2191.
- Bolaños JP (2016) Bioenergetics and redox adaptations of astrocytes to neuronal activity. Journal of Neurochemistry 139:115-125.

- Bradford AB, Mancini JD, Atchison WD (2015) Methylmercury-Dependent Increases in Fluo4 Fluorescence in Neonatal Rat Cerebellar Slices Depend on Granule Cell Migrational Stage and GABAA Receptor Modulation. 356:2-12.
- Branco V, Godinho-Santos A, Gonçalves J, Lu J, Holmgren A, Carvalho C (2014) Mitochondrial thioredoxin reductase inhibition, selenium status, and Nrf-2 activation are determinant factors modulating the toxicity of mercury compounds. Free Radical Biology and Medicine 73:95-105.
- Bridges CC, Joshee L, Zalups RK (2011) MRP2 and the handling of mercuric ions in rats exposed acutely to inorganic and organic species of mercury. Toxicol Appl Pharmacol 251:50-58.
- Bridges CC, Joshee L, Zalups RK (2012a) Placental and fetal disposition of mercuric ions in rats exposed to methylmercury: role of Mrp2. Reprod Toxicol 34:628-634.
- Bridges RJ, Natale NR, Patel SA (2012b) System xc- cystine/glutamate antiporter: an update on molecular pharmacology and roles within the CNS. British Journal of Pharmacology 165:20-34.
- Brookes N (1988) Specificity and Reversibility of the Inhibition by HgCl2of Glutamate Transport in Astrocyte Cultures. Journal of Neurochemistry 50:1117-1122.
- Brookes N, Kristt DA (1989) Inhibition of Amino Acid Transport and Protein Synthesis by HgCl2and Methylmercury in Astrocytes: Selectivity and Reversibility. Journal of Neurochemistry 53:1228-1237.
- Bryan HK, Olayanju A, Goldring CE, Park BK (2013) The Nrf2 cell defence pathway: Keap1-dependent and -independent mechanisms of regulation. Biochemical Pharmacology 85:705-717.
- Bulut M, Savas HA, Altindag A, Virit O, Dalkilic A (2009) Beneficial effects of Nacetylcysteine in treatment resistant schizophrenia. The World Journal of Biological Psychiatry 10:626-628.
- Callaghan B (2011) The Association of Exposure to Lead, Mercury, and Selenium and the Development of Amyotrophic Lateral Sclerosis and the Epigenetic Implications. Neuro-degenerative diseases 8:1-8.

- Camacho A, Massieu L (2006) Role of Glutamate Transporters in the Clearance and Release of Glutamate during Ischemia and its Relation to Neuronal Death. Archives of Medical Research 37:11-18.
- Cardoso BR, Hare DJ, Bush AI, Roberts BR (2017) Glutathione peroxidase 4: a new player in neurodegeneration? Molecular Psychiatry 22:328-335.
- Carocci A, Rovito N, Sinicropi MS, Genchi G (2014) Mercury Toxicity and Neurodegenerative Effects. In, pp 1-18: Springer International Publishing.
- Castoldi AF, Blandini F, Randine G, Samuele A, Manzo L, Coccini T (2006) Brain monoaminergic neurotransmission parameters in weanling rats after perinatal exposure to methylmercury and 2,2',4,4',5,5'-hexachlorobiphenyl (PCB153). Brain Res 1112:91-98.
- Castoldi AF, Johansson C, Onishchenko N, Coccini T, Roda E, Vahter M, Ceccatelli S, Manzo L (2008) Human developmental neurotoxicity of methylmercury: Impact of variables and risk modifiers. Regulatory Toxicology and Pharmacology 51:201-214.
- Chaboub LS, Deneen B (2012) Developmental Origins of Astrocyte Heterogeneity: The Final Frontier of CNS Development. 34:379-388.
- Chan K, Lu R, Chang JC, Kan YW (1996) NRF2, a member of the NFE2 family of transcription factors, is not essential for murine erythropoiesis, growth, and development. 93:13943-13948.
- Chandel NS, McClintock DS, Feliciano CE, Wood TM, Melendez JA, Rodriguez AM, Schumacker PT (2000) Reactive Oxygen Species Generated at Mitochondrial Complex III Stabilize Hypoxia-inducible Factor-1α during Hypoxia. Journal of Biological Chemistry 275:25130-25138.
- Chang LW (1972) Ultrastructural studies of the nervous system after mercury intoxication II. Pathological changes in the nerve fibers. Acta neuropathologica 20:316-334.
- Chang LW, Hartmann HA (1972) Blood-brain barrier dysfunction in experimental mercury intoxication. 21:179-184.

- Charleston JS, Body RL, Mottet NK, Vahter ME, Burbacher TM (1995a) Autometallographic Determination of Inorganic Mercury Distribution in the Cortex of the Calcarine Sulcus of the Monkey Macaca fascicularis Following Long-Term Subclinical Exposure to Methylmercury and Mercuric Chloride. Toxicology and Applied Pharmacology 132:325-333.
- Charleston JS, Bolender RP, Mottet NK, Body RL, Vahter ME, Burbacher TM (1994) Increases in the Number of Reactive Glia in the Visual Cortex of Macaca fascicularis Following Subclinical Long-Term Methyl Mercury Exposure. Toxicology and Applied Pharmacology 129:196-206.
- Charleston JS, Body RL, Bolender RP, Mottet NK, Vahter ME, Burbacher TM (1995b) Changes in the number of astrocytes and microglia in the thalamus of the monkey Macaca fascicularis following long-term subclinical methylmercury exposure. NeuroToxicology 17:127-138.
- Chen L, Hambright WS, Na R, Ran Q (2015) Ablation of the Ferroptosis Inhibitor Glutathione Peroxidase 4 in Neurons Results in Rapid Motor Neuron Degeneration and Paralysis. Journal of Biological Chemistry 290:28097-28106.
- Chen Y-W, Lin H-C, Ng M-C, Hsiao Y-H, Wang C-C, Gean P-W, Chen PS (2014) Activation of mGluR2/3 underlies the effects of N-acetylcystein on amygdala-associated autism-like phenotypes in a valproate-induced rat model of autism. Frontiers in Behavioral Neuroscience 8.
- Chen Y, Swanson RA (2003) The glutamate transporters EAAT2 and EAAT3 mediate cysteine uptake in cortical neuron cultures. Journal of Neurochemistry 84:1332-1339.
- Chen YW, Huang CF, Tsai KS, Yang RS, Yen CC, Yang CY, Lin-Shiau SY, Liu SH (2006) The Role of Phosphoinositide 3-Kinase/Akt Signaling in Low-Dose Mercury-Induced Mouse Pancreatic -Cell Dysfunction In Vitro and In Vivo. Diabetes 55:1614-1624.
- Cheng D, Wu R, Guo Y, Kong A-NT (2016) Regulation of Keap1–Nrf2 signaling: The role of epigenetics. Current Opinion in Toxicology 1:134-138.
- Cheng X, Siow RCM, Mann GE (2011) Impaired Redox Signaling and Antioxidant Gene Expression in Endothelial Cells in Diabetes: A Role for Mitochondria and the Nuclear Factor-E2-Related Factor 2-Kelch-Like ECH-Associated Protein 1 Defense Pathway. Antioxidants & Redox Signaling 14:469-487.

- Chepelev NL, Zhang H, Liu H, McBride S, Seal AJ, Morgan TE, Finch CE, Willmore WG, Davies KJA, Forman HJ (2013) Competition of nuclear factor-erythroid 2 factors related transcription factor isoforms, Nrf1 and Nrf2, in antioxidant enzyme induction. Redox Biology 1:183-189.
- Cho Y, Bannai S (1990) Uptake of Glutamate and Cystine in C-6 Glioma Cells and in Cultured Astrocytes. Journal of Neurochemistry 55:2091-2097.
- Choi BH, Yee S, Robles M (1996) The Effects of Glutathione Glycoside in Methyl Mercury Poisoning. Toxicology and Applied Pharmacology 141:357-364.
- Clark J, Clore EL, Zheng K, Adame A, Masliah E, Simon DK (2010) Oral N-Acetyl-Cysteine Attenuates Loss of Dopaminergic Terminals in α-Synuclein Overexpressing Mice. PloS One 5:e12333.
- Clarkson TW (1972) The Pharmacology of Mercury Compounds. 12:375-406.
- Clarkson TW (1993) Mercury: major issues in environmental health. Environmental Health Perspectives 100:31-38.
- Clarkson TW, Magos L (2006) The Toxicology of Mercury and Its Chemical Compounds. Critical Reviews in Toxicology 36:609-662.
- Clarkson TW, Vyas JB, Ballatori N (2007) Mechanisms of mercury disposition in the body. American Journal of Industrial Medicine 50:757-764.
- Clement AM, Nguyen MD, Roberts EA, Garcia ML, Boillée S, Rule M, McMahon AP, Doucette W, Siwek D, Ferrante RJ, Brown RH, Julien J-P, Goldstein LSB, Cleveland DW (2003) Wild-Type Nonneuronal Cells Extend Survival of SOD1 Mutant Motor Neurons in ALS Mice. Science 302:113-117.
- Clifton JC, 2nd (2007) Mercury exposure and public health. Pediatr Clin North Am 54:237-269, viii.
- Coccini T, Randine G, Candura SM, Nappi RE, Prockop LD, Manzo L (1999) Low-Level Exposure to Methylmercury Modifies Muscarinic Cholinergic Receptor Binding Characteristics in Rat Brain and Lymphocytes: Physiologic Implications and New Opportunities in Biologic Monitoring. 108:29-33.

- Coccini T, Roda E, Castoldi AF, Goldoni M, Poli D, Bernocchi G, Manzo L (2007) Perinatal co-exposure to methylmercury and PCB153 or PCB126 in rats alters the cerebral cholinergic muscarinic receptors at weaning and puberty. Toxicology 238:34-48.
- Cole SPC (2006) Transport of glutathione and glutathione conjugates by MRP1. Trends in pharmacological sciences (Regular ed) 27:438-446.
- Cole SPC (2014a) Multidrug Resistance Protein 1 (MRP1, ABCC1), a "Multitasking" ATP-binding Cassette (ABC) Transporter. Journal of Biological Chemistry 289:30880-30888.
- Cole SPC (2014b) Targeting Multidrug Resistance Protein 1 (MRP1,ABCC1): Past, Present, and Future. Annual Review of Pharmacology and Toxicology 54:95-117.
- Colón-Rodríguez A, Hannon HE, Atchison WD (2017) Effects of methylmercury on spinal cord afferents and efferents—A review. NeuroToxicology 60:308-320.
- Compeau GC, Bartha R (1985) Sulfate-reducing bacteria: principal methylators of mercury in anoxic estuarine sediment. Applied and environmental microbiology 50:498-502.
- Compeau GC, Bartha R (1987) Effect of salinity on mercury-methylating activity of sulfate-reducing bacteria in estuarine sediments. Applied and environmental microbiology 53:261-265.
- Conrad M, Sato H (2012) The oxidative stress-inducible cystine/glutamate antiporter, system x c : cystine supplier and beyond. Amino Acids 42:231-246.
- Corona JC, Tapia R (2007) Ca2+-permeable AMPA receptors and intracellular Ca2+ determine motoneuron vulnerability in rat spinal cord in vivo. 52:1219-1228.
- Costa LG (2017) Chapter 12 Developmental Exposure to Metals and its Contribution to Age-Related Neurodegeneration. In: Biometals in Neurodegenerative Diseases (White AR, Aschner M, Costa LG, Bush AI, eds), pp 217-229: Academic Press.
- Counsil NR (2000) Toxicological effects of methylmercury: National Academies Press.
- Culbreth M, Aschner M (2018) GSK-3β, a double-edged sword in Nrf2 regulation: Implications for neurological dysfunction and disease. F1000Research 7:1043.

- Culbreth M, Zhang Z, Aschner M (2017) Methylmercury augments Nrf2 activity by downregulation of the Src family kinase Fyn. NeuroToxicology 62:200-206.
- Dalton TP, Dieter MZ, Yang Y, Shertzer HG, Nebert DW (2000) Knockout of the Mouse Glutamate Cysteine Ligase Catalytic Subunit (Gclc) Gene: Embryonic Lethal When Homozygous, and Proposed Model for Moderate Glutathione Deficiency When Heterozygous. Biochemical and Biophysical Research Communications 279:324-329.
- Danbolt NC (2001) Glutamate uptake. Progress in Neurobiology 65:1-105.
- Danbolt NC, Furness DN, Zhou Y (2016) Neuronal vs glial glutamate uptake: Resolving the conundrum. Neurochemistry international 98:29-45.
- Daré E, Fetissov S, Hökfelt T, Hall H, Ögren SO, Ceccatelli S (2003) Effects of prenatal exposure to methylmercury on dopamine-mediated locomotor activity and dopamine D2 receptor binding. 367:500-508.
- David J, Nandakumar A, Muniroh M, Akiba S, Yamamoto M, Koriyama C (2017) Suppression of methylmercury-induced MIP-2 expression by N-acetyl-l-cysteine in murine RAW264.7 macrophage cell line. European Journal of Medical Research 22:45.
- Davidson PW, Palumbo D, Myers GJ, Cox C, Shamlaye CF, Sloane-Reeves J, Cernichiari E, Wilding GE, Clarkson TW (2000) Neurodevelopmental Outcomes of Seychellois Children from the Pilot Cohort at 108 Months Following Prenatal Exposure to Methylmercury from a Maternal Fish Diet. Environmental Research 84:1-11.
- Davidson PW, Jean Sloane R, Myers GJ, Hansen ON, Huang L-S, Georger LA, Cox C, Thurston SW, Shamlaye CF, Clarkson TW (2008) Association between prenatal exposure to methylmercury and visuospatial ability at 10.7 years in the seychelles child development study. 29:453-459.
- Davidson PW, Cory-Slechta DA, Thurston SW, Huang L-S, Shamlaye CF, Gunzler D, Watson G, Van Wijngaarden E, Zareba G, Klein JD, Clarkson TW, Strain JJ, Myers GJ (2011) Fish consumption and prenatal methylmercury exposure: Cognitive and behavioral outcomes in the main cohort at 17 years from the Seychelles child development study. NeuroToxicology 32:711-717.

- De Haan JB, Bladier C, Griffiths P, Kelner M, O'Shea RD, Cheung NS, Bronson RT, Silvestro MJ, Wild S, Zheng SS, Beart PM, Hertzog PJ, Kola I (1998) Mice with a Homozygous Null Mutation for the Most Abundant Glutathione Peroxidase, Gpx1, Show Increased Susceptibility to the Oxidative Stress-inducing Agents Paraquat and Hydrogen Peroxide. Journal of Biological Chemistry 273:22528-22536.
- Dean O, Giorlando F, Berk M (2011) N-acetylcysteine in psychiatry: current therapeutic evidence and potential mechanisms of action. Journal of Psychiatry & Neuroscience 36:78-86.
- Demeuse P, Kerkhofs A, Struys-Ponsar C, Knoops B, Remacle C, Van Den Bosch De Aguilar P (2002) Compartmentalized coculture of rat brain endothelial cells and astrocytes: a syngenic model to study the blood-brain barrier. Journal of neuroscience methods 121:21-31.
- Denny MF, Atchison WD (1994a) Methylmercury-Induced Elevations in Intrasynaptosomal Zinc Concentrations: An 19F-NMR Study. Journal of Neurochemistry 63:383-386.
- Denny MF, Atchison WD (1994b) Methylmercury-induced elevations in intrasynaptosomal zinc concentrations: an 19F-NMR study. J Neurochem 63:383-386.
- Desagher S, Glowinski J, Premont J (1996) Astrocytes protect neurons from hydrogen peroxide toxicity. The Journal of Neuroscience 16:2553-2562.
- Dhakshinamoorthy S, Jain AK, Bloom DA, Jaiswal AK (2005) Bach1 Competes with Nrf2 Leading to Negative Regulation of the Antioxidant Response Element (ARE)-mediated NAD(P)H:Quinone Oxidoreductase 1 Gene Expression and Induction in Response to Antioxidants. Journal of Biological Chemistry 280:16891-16900.
- Di Giorgio FP, Carrasco MA, Siao MC, Maniatis T, Eggan K (2007) Non-cell autonomous effect of glia on motor neurons in an embryonic stem cell-based ALS model. Nature Neuroscience 10:608-614.
- Díez S (2009) Human health effects of methylmercury exposure. Rev Environ Contam Toxicol 198:111-132.
- Dinkova-Kostova AT, Holtzclaw WD, Cole RN, Itoh K, Wakabayashi N, Katoh Y, Yamamoto M, Talalay P (2002) Direct evidence that sulfhydryl groups of Keap1

- are the sensors regulating induction of phase 2 enzymes that protect against carcinogens and oxidants. Proceedings of the National Academy of Sciences 99:11908-11913.
- Divito CB, Borowski JE, Glasgow NG, Gonzalez-Suarez AD, Torres-Salazar D, Johnson JW, Amara SG (2017) Glial and Neuronal Glutamate Transporters Differ in the Na+ Requirements for Activation of the Substrate-Independent Anion Conductance. Frontiers in Molecular Neuroscience 10.
- Dreiem A, Seegal RF (2007) Methylmercury-induced changes in mitochondrial function in striatal synaptosomes are calcium-dependent and ROS-independent. NeuroToxicology 28:720-726.
- Dreiem A, Gertz CC, Seegal RF (2005) The Effects of Methylmercury on Mitochondrial Function and Reactive Oxygen Species Formation in Rat Striatal Synaptosomes Are Age-Dependent. Toxicological Sciences 87:156-162.
- Dringen R (2000) Metabolism and functions of glutathione in brain. Progress in Neurobiology 62:649-671.
- Dringen R, Hamprecht B (1999) N-Acetylcysteine, but not methionine or 2-oxothiazolidine-4-carboxylate, serves as cysteine donor for the synthesis of glutathione in cultured neurons derived from embryonal rat brain. Neuroscience Letters 259:79-82.
- Dringen R, Hirrlinger J (2003) Glutathione pathways in the brain. Biol Chem 384:505-516.
- Dringen R, Pfeiffer B, Hamprecht B (1999) Synthesis of the Antioxidant Glutathione in Neurons: Supply by Astrocytes of CysGly as Precursor for Neuronal Glutathione. The Journal of Neuroscience 19:562-569.
- Dringen R, Gutterer JM, Hirrlinger J (2000) Glutathione metabolism in brain. European Journal of Biochemistry 267:4912-4916.
- Drukarch B, Schepens E, Jongenelen CAM, Stoof JC, Langeveld CH (1997) Astrocyte-mediated enhancement of neuronal survival is abolished by glutathione deficiency. Brain research 770:123-130.

- Drukarch B, Schepens E, Stoof JC, Langeveld CH, Van Muiswinkel FL (1998) Astrocyteenhanced neuronal survival is mediated by scavenging of extracellular reactive oxygen species. Free Radical Biology and Medicine 25:217-220.
- Duan W, Zhang R, Guo Y, Jiang Y, Huang Y, Jiang H, Li C (2009) Nrf2 activity is lost in the spinal cord and its astrocytes of aged mice. In Vitro Cellular & Developmental Biology Animal 45:388-397.
- Duellman SJ, Zhou W, Meisenheimer P, Vidugiris G, Cali JJ, Gautam P, Wennerberg K, Vidugiriene J (2015) Bioluminescent, Nonlytic, Real-Time Cell Viability Assay and Use in Inhibitor Screening. Assay and drug development technologies 13:456-465.
- Durieux AMS, Fernandes C, Murphy D, Labouesse MA, Giovanoli S, Meyer U, Li Q, So P-W, McAlonan G (2015) Targeting Glia with N-Acetylcysteine Modulates Brain Glutamate and Behaviors Relevant to Neurodevelopmental Disorders in C57BL/6J Mice. Frontiers in Behavioral Neuroscience 9.
- Eades G, Yang M, Yao Y, Zhang Y, Zhou Q (2011) miR-200a Regulates Nrf2 Activation by Targeting Keap1 mRNA in Breast Cancer Cells. 286:40725-40733.
- Edwards JR, Marty MS, Atchison WD (2005) Comparative sensitivity of rat cerebellar neurons to dysregulation of divalent cation homeostasis and cytotoxicity caused by methylmercury. Toxicol Appl Pharmacol 208:222-232.
- Emerit J, Edeas M, Bricaire F (2004) Neurodegenerative diseases and oxidative stress. Biomedicine & Pharmacotherapy 58:39-46.
- EPA U (2001) Resources for Mercury Science and Research. In: (Agency USEP, ed).
- Escartin C, Joon Won S, Malgorn C, Auregan G, Berman AE, Chen PC, Deglon N, Johnson JA, Won Suh S, Swanson RA (2011a) Nuclear Factor Erythroid 2-Related Factor 2 Facilitates Neuronal Glutathione Synthesis by Upregulating Neuronal Excitatory Amino Acid Transporter 3 Expression. The Journal of neuroscience: the official journal of the Society for Neuroscience 31:7392-7401.
- Escartin C, Joon Won S, Malgorn C, Auregan G, Berman AE, Chen P-C, Déglon N, Johnson JA, Won Suh S, Swanson RA (2011b) Nuclear factor erythroid 2-related factor 2 facilitates neuronal glutathione synthesis by upregulating neuronal excitatory amino acid transporter 3 expression. The Journal of Neuroscience 31:7392-7401.

- Eto K (1997) Review Article: Pathology of Minamata Disease. Toxicologic Pathology 25:614-623.
- Eto K, Marumoto M, Takeya M (2010) The pathology of methylmercury poisoning (Minamata disease). Neuropathology:471-479.
- Falluel-Morel A, Lin L, Sokolowski K, McCandlish E, Buckley B, DiCicco-Bloom E (2012) N-acetyl cysteine treatment reduces mercury-induced neurotoxicity in the developing rat hippocampus. Journal of neuroscience research 90:743-750.
- Fan W, Tang Z, Chen D, Moughon D, Ding X, Chen S, Zhu M, Zhong Q (2010) Keap1 facilitates p62-mediated ubiquitin aggregate clearance via autophagy. Autophagy 6:614-621.
- Farina M (2003) Methylmercury Increases Glutamate Release from Brain Synaptosomes and Glutamate Uptake by Cortical Slices from Suckling Rat Pups: Modulatory Effect of Ebselen. Toxicological Sciences 73:135-140.
- Faro LRF, Do Nascimento JLM, Alfonso M, Durán R (2002) Mechanism of action of methylmercury on in vivo striatal dopamine release. 40:455-465.
- Feng S, Xu Z, Wang F, Yang T, Liu W, Deng Y, Xu B (2017) Sulforaphane Prevents Methylmercury-Induced Oxidative Damage and Excitotoxicity Through Activation of the Nrf2-ARE Pathway. Molecular Neurobiology 54:375-391.
- Fernandez-Fernandez S, Almeida A, Bolaños Juan P (2012) Antioxidant and bioenergetic coupling between neurons and astrocytes. Biochemical Journal 443:3-11.
- Ferrari G, Yan C, Greene L (1995) N-acetylcysteine (D- and L-stereoisomers) prevents apoptotic death of neuronal cells. The Journal of Neuroscience 15:2857-2866.
- Fok-Seang J, Miller RH (1992) Astrocyte precursors in neonatal rat spinal cord cultures. J Neurosci 12:2751-2764.
- Fonfría E, Daré E, Benelli M, Suñol C, Ceccatelli S (2002) Translocation of apoptosisinducing factor in cerebellar granule cells exposed to neurotoxic agents inducing oxidative stress. European Journal of Neuroscience 16:2013-2016.

- Frazzini V, Rockabrand E, Mocchegiani E, Sensi SL (2006) Oxidative stress and brain aging: is zinc the link? Biogerontology 7:307-314.
- Friberg L, Mottet NK (1989) Accumulation of methylmercury and inorganic mercury in the brain. Biological trace element research 21:201-206.
- Fuentes-Antrás J, Osorio-Martínez E, Ramírez-Torres M, Colmena I, Fernández-Morales JC, Hernández-Guijo JM (2013) Methylmercury decreases cellular excitability by a direct blockade of sodium and calcium channels in bovine chromaffin cells: an integrative study. 465:1727-1740.
- Fujimura M, Usuki F (2014) Low in situ expression of antioxidative enzymes in rat cerebellar granular cells susceptible to methylmercury. Archives of toxicology 88:109-113.
- Fukai T, Ushio-Fukai M (2011) Superoxide Dismutases: Role in Redox Signaling, Vascular Function, and Diseases. 15:1583-1606.
- Furuta A, Rothstein JD, Martin LJ (1997) Glutamate Transporter Protein Subtypes Are Expressed Differentially during Rat CNS Development. The Journal of Neuroscience 17:8363-8375.
- Gage JC (1975) Mechanisms for the biodegradation of organic mercury compounds: The actions of ascorbate and of soluble proteins. Toxicology and Applied Pharmacology 32:225-238.
- Gardaneh M, Gholami M, Maghsoudi N (2011) Synergy Between Glutathione Peroxidase-1 and Astrocytic Growth Factors Suppresses Free Radical Generation and Protects Dopaminergic Neurons against 6-Hydroxydopamine. 14:195-204.
- Gegelashvili G, Schousboe A (1997) High Affinity Glutamate Transporters: Regulation of Expression and Activity. Molecular Pharmacology 52:6-15.
- Gegg ME, Clark JB, Heales SJR (2005) Co-culture of neurones with glutathione deficient astrocytes leads to increased neuronal susceptibility to nitric oxide and increased glutamate-cysteine ligase activity. Brain Research 1036:1-6.
- Gilbert SG, Grant-Webster KS (1995) Neurobehavioral effects of developmental methylmercury exposure. Environmental health perspectives 103 Suppl 6:135-142.

- Giménez-Llort L, Ahlbom E, Daré E, Vahter M, Ögren SO, Ceccatelli S (2001) Prenatal exposure to methylmercury changes dopamine-modulated motor activity during early ontogeny: age and gender-dependent effects. Environmental Toxicology and Pharmacology 9:61-70.
- Goyer RA, Aposhian V, Arab L, Bellinger D, Burbacher T, Burke T, Jacobson J, Knobeloch L, Stern A, Ryan L (2000) Toxicological effects of methylmercury. Washington, DC: National Research Council.
- Grandjean P, Satoh H, Murata K, Eto K (2010) Adverse Effects of Methylmercury: Environmental Health Research Implications. 118:1137-1145.
- Gremmels H, De Jong OG, Hazenbrink DH, Fledderus JO, Verhaar MC (2017) The Transcription Factor Nrf2 Protects Angiogenic Capacity of Endothelial Colony-Forming Cells in High-Oxygen Radical Stress Conditions. Stem Cells International 2017:1-11.
- Gundacker C, Gencik M, Hengstschläger M (2010) The relevance of the individual genetic background for the toxicokinetics of two significant neurodevelopmental toxicants: Mercury and lead. Mutation Research/Reviews in Mutation Research 705:130-140.
- Guttenplan KA, Weigel MK, Adler DI, Couthouis J, Liddelow SA, Gitler AD, Barres BA (2020) Knockout of reactive astrocyte activating factors slows disease progression in an ALS mouse model. Nature Communications 11.
- Guzy RD, Schumacker PT (2006) Oxygen sensing by mitochondria at complex III: the paradox of increased reactive oxygen species during hypoxia. Experimental Physiology 91:807-819.
- Habib E, Linher-Melville K, Lin H-X, Singh G (2015) Expression of xCT and activity of system xc- are regulated by NRF2 in human breast cancer cells in response to oxidative stress. Redox Biology 5:33-42.
- Hampe CS, Mitoma H, Manto M (2018) GABA and Glutamate: Their Transmitter Role in the CNS and Pancreatic Islets. In: New Developments In Neurotransmission Research (Samardzic J, ed): InTech.

- Han D, Sen CK, Roy S, Kobayashi MS, Tritschler HJ, Packer L (1997) Protection against glutamate-induced cytotoxicity in C6 glial cells by thiol antioxidants. The American journal of physiology 273:R1771-1778.
- Harada M (1995) Minamata disease: methylmercury poisoning in Japan caused by environmental pollution. Critical reviews in toxicology 25:1-24.
- Hare MF, Atchison WD (1992) Comparative action of methylmercury and divalent inorganic mercury on nerve terminal and intraterminal mitochondrial membrane potentials. The Journal of pharmacology and experimental therapeutics 261:166-172.
- Hare MF, McGinnis KM, Atchison WD (1993) Methylmercury increases intracellular concentrations of Ca++ and heavy metals in NG108-15 cells. The Journal of pharmacology and experimental therapeutics 266:1626-1635.
- Haugeto Ø, Ullensvang K, Levy LM, Chaudhry FA, Honoré T, Nielsen M, Lehre KP, Danbolt NC (1996) Brain Glutamate Transporter Proteins Form Homomultimers. Journal of Biological Chemistry 271:27715-27722.
- Hayashi A, Suzuki H, Itoh K, Yamamoto M, Sugiyama Y (2003) Transcription factor Nrf2 is required for the constitutive and inducible expression of multidrug resistance-associated protein1 in mouse embryo fibroblasts. Biochemical and Biophysical Research Communications 310:824-829.
- Hayes JD (2016) Regulation of the CNC-bZIP transcription factor Nrf2 by Keap1 and the axis between GSK-3 and  $\beta$ -TrCP. Current opinion in toxicology 1:92-103.
- Hayes JD, Dinkova-Kostova AT (2014) The Nrf2 regulatory network provides an interface between redox and intermediary metabolism. Trends in Biochemical Sciences 39:199-218.
- He L, Vasiliou K, Nebert DW (2009) Analysis and update of the human solute carrier (SLC) gene superfamily. Human Genomics 3:195.
- He Y, Jackman NA, Thorn TL, Vought VE, Hewett SJ (2015) Interleukin-1β protects astrocytes against oxidant-induced injury via an NF-κB-dependent upregulation of glutathione synthesis. Glia 63:1568-1580.

- Herden CJ, Pardo NE, Hajela RK, Yuan Y, Atchison WD (2008) Differential effects of methylmercury on gamma-aminobutyric acid type A receptor currents in rat cerebellar granule and cerebral cortical neurons in culture. The Journal of pharmacology and experimental therapeutics 324:517-528.
- Hertz L, Peng L, Lai JC (1998) Functional studies in cultured astrocytes. Methods 16:293-310.
- Hewett JA (2009) Determinants of regional and local diversity within the astroglial lineage of the normal central nervous system. 110:1717-1736.
- Hidalgo C, Arias-Cavieres A (2016) Calcium, Reactive Oxygen Species, and Synaptic Plasticity. Physiology 31:201-215.
- Himi T, Ikeda M, Yasuhara T, Nishida M, Morita I (2003) Role of neuronal glutamate transporter in the cysteine uptake and intracellular glutathione levels in cultured cortical neurons. 110:1337-1348.
- Hirayama K (1985) Effects of combined administration of thiol compounds and methylmercury chloride on mercury distribution in rats. Biochemical Pharmacology 34:2030-2032.
- Hirooka T, Yamamoto C, Yasutake A, Eto K, Kaji T (2013) Expression of VEGF-related proteins in cultured human brain microvascular endothelial cells and pericytes after exposure to methylmercury. 38:837-845.
- Hirrlinger J, Dringen R (2005) Multidrug Resistance Protein 1-Mediated Export of Glutathione and Glutathione Disulfide from Brain Astrocytes. In: Methods in Enzymology, pp 395-409: Academic Press.
- Ho S-C, Liu J-H, Wu R-Y (2003) Establishment of the mimetic aging effect in mice caused by D-galactose. Biogerontology 4:15-18.
- Hogstad S, Svenneby G, Torgner IA, Kvamme E, Hertz L, Schousboe A (1988) Glutaminase in neurons and astrocytes cultured from mouse brain: Kinetic properties and effects of phosphate, glutamate, and ammonia. Neurochemical research 13:383-388.

- Holmstrom KM, Baird L, Zhang Y, Hargreaves I, Chalasani A, Land JM, Stanyer L, Yamamoto M, Dinkova-Kostova AT, Abramov AY (2013) Nrf2 impacts cellular bioenergetics by controlling substrate availability for mitochondrial respiration. Biology Open 2:761-770.
- Hösli E, Hösli L (1995) Autoradiographic studies on the uptake of 3H-noradrenaline and 3H-serotonin by neurones and astrocytes in explant and primary cultures of rat CNS: Effects of antidepressants. International Journal of Developmental Neuroscience 13:897-908.
- Hsi H-C, Hsu Y-W, Chang T-C, Chien L-C (2016) Methylmercury Concentration in Fish and Risk-Benefit Assessment of Fish Intake among Pregnant versus Infertile Women in Taiwan. PLOS ONE 11:e0155704.
- Huang Y, Mao Y, Li H, Shen G, Nan G (2018) Knockdown of Nrf2 inhibits angiogenesis by downregulating VEGF expression through PI3K/Akt signaling pathway in cerebral microvascular endothelial cells under hypoxic conditions. Biochemistry and Cell Biology 96:475-482.
- Hughes WL (1957) A PHYSICOCHEMICAL RATIONALE FOR THE BIOLOGICAL ACTIVITY OF MERCURY AND ITS COMPOUNDS. Annals of the New York Academy of Sciences 65:454-460.
- Hunter D, Russell DS (1954) Focal cerebral and cerebellar atrophy in a human subject due to organic mercury compounds. Journal of Neurology, Neurosurgery & Psychiatry 17:235-241.
- Hurst GA, Shaw PB, LeMaistre CA (1967) Laboratory and Clinical Evaluation of the Mucolytic Properties of Acetylcysteine. American Review of Respiratory Disease 96:962-970.
- Igata A (1993) Epidemiological and clinical features of Minamata disease. Environmental Research 63:157-169.
- Isaac et al. (2015) Glutathione and Thioredoxin Antioxidant Pathways Synergize to Drive Cancer Initiation and Progression. Cancer Cell 27:211-222.
- J.E. B (1985) Growth and Differentiation of Neural Cells in Defined Media. In: Cell Culture in the Neurosciences (J.E. B, G. S, eds): Springer, Boston, MA.

- Jackman NA, Uliasz TF, Hewett JA, Hewett SJ (2010) Regulation of System xc–Activity and Expression in Astrocytes by Interleukin-1β. 58:1806-1815.
- Jain AK, Jaiswal AK (2007) GSK-3β Acts Upstream of Fyn Kinase in Regulation of Nuclear Export and Degradation of NF-E2 Related Factor 2. Journal of Biological Chemistry 282:16502-16510.
- Ji SG, Weiss JH (2018) Zn(2+)-induced disruption of neuronal mitochondrial function: Synergism with Ca(2+), critical dependence upon cytosolic Zn(2+) buffering, and contributions to neuronal injury. Exp Neurol 302:181-195.
- Jiang J, Amara SG (2011) New views of glutamate transporter structure and function: Advances and challenges. Neuropharmacology 60:172-181.
- Johnson FO, Yuan Y, Hajela RK, Chitrakar A, Parsell DM, Atchison WD (2011) Exposure to an Environmental Neurotoxicant Hastens the Onset of Amyotrophic Lateral Sclerosis-Like Phenotype in Human Cu2+/Zn2+ Superoxide Dismutase 1 G93A Mice: Glutamate-Mediated Excitotoxicity. NeuroToxicology 338:518-527.
- Johnson JA, Johnson DA, Kraft AD, Calkins MJ, Jakel RJ, Vargas MR, Chen P-C (2008) The Nrf2-ARE Pathway: An Indicator and Modulator of Oxidative Stress in Neurodegeneration. Annals of the New York Academy of Sciences 1147:61-69.
- Joselow MM, Louria DB, Browder AA (1972) Mercurialism: Environmental and Occupational Aspects. Annals of internal medicine 76:119-130.
- Juang MS, Yonemura K (1975a) Increased spontaneous transmitter release from presynaptic nerve terminal by methylmercuric chloride. 256:211-213.
- Juang MS, Yonemura K (1975b) Increased spontaneous transmitter release from presynaptic nerve terminal by methylmercuric chloride. Nature 256:211-213.
- Juárez BI, Martí Nez ML, Montante M, Dufour L, Garcí A E, Jiménez-Capdeville ME (2002) Methylmercury increases glutamate extracellular levels in frontal cortex of awake rats. 24:767-771.
- Julvez J, Grandjean P (2013) Genetic susceptibility to methylmercury developmental neurotoxicity matters. 4.

- Kalisch BE, Racz WJ (1996) The effects of methylmercury on endogenous dopamine efflux from mouse striatal slices. Toxicology Letters 89:43-49.
- Kallman AM (2003) ADAR2 A->I editing: site selectivity and editing efficiency are separate events. Nucleic Acids Research 31:4874-4881.
- Kanno T, Tanaka K, Yanagisawa Y, Yasutake K, Hadano S, Yoshii F, Hirayama N, Ikeda J-E (2012) A novel small molecule, N-(4-(2-pyridyl)(1,3-thiazol-2-yl))-2-(2,4,6-trimethylphenoxy) acetamide, selectively protects against oxidative stress-induced cell death by activating the Nrf2–ARE pathway: Therapeutic implications for ALS. Free Radical Biology and Medicine 53:2028-2042.
- Kansanen E, Kuosmanen SM, Leinonen H, Levonen A-L (2013) The Keap1-Nrf2 pathway: Mechanisms of activation and dysregulation in cancer. Redox Biology 1:45-49.
- Kaur P, Aschner M, Syversen T (2006) Glutathione modulation influences methyl mercury induced neurotoxicity in primary cell cultures of neurons and astrocytes. NeuroToxicology 27:492-500.
- Kaur P, Aschner M, Syversen T (2007) Role of glutathione in determining the differential sensitivity between the cortical and cerebellar regions towards mercury-induced oxidative stress. Toxicology 230:164-177.
- Kawasaki T, Ishihara K, Ago Y, Baba A, Matsuda T (2007) Edaravone (3-Methyl-1-phenyl-2-pyrazolin-5-one), a Radical Scavenger, Prevents 1-Methyl-4-phenyl-1,2,3,6-tetrahydropyridine-Induced Neurotoxicity in the Substantia Nigra but Not the Striatum. Journal of Pharmacology and Experimental Therapeutics 322:274-281.
- Kawasaki T, Ishihara K, Ago Y, Nakamura S, Itoh S, Baba A, Matsuda T (2006) Protective effect of the radical scavenger edaravone against methamphetamine-induced dopaminergic neurotoxicity in mouse striatum. 542:92-99.
- Ke T, Gonçalves FM, Gonçalves CL, Dos Santos AA, Rocha JBT, Farina M, Skalny A, Tsatsakis A, Bowman AB, Aschner M (2019) Post-translational modifications in MeHg-induced neurotoxicity. Biochimica et Biophysica Acta (BBA) Molecular Basis of Disease 1865:2068-2081.
- Kensler TW, Wakabayashi N, Biswal S (2007) Cell Survival Responses to Environmental Stresses Via the Keap1-Nrf2-ARE Pathway. Annual Review of Pharmacology and Toxicology 47:89-116.

- Kerper LE, Ballatori N, Clarkson TW (1992) Methylmercury transport across the bloodbrain barrier by an amino acid carrier. American Journal of Physiology -Regulatory, Integrative and Comparative Physiology 262:R761-R765.
- Kerstetter AE, Miller RH (2012) Isolation and culture of spinal cord astrocytes. Methods in molecular biology (Clifton, NJ) 814:93-104.
- Kim P, Choi BH (1995) Selective inhibition of glutamate uptake by mercury in cultured mouse astrocytes. Yonsei Medical Journal 36:299.
- Kimelberg HK, Goderie SK, Conley PA, Higman S, Goldschmidt R, Amundson RH (1992) Uptake of [3H]serotonin and [3H]glutamate by primary astrocyte cultures. I. Effects of different sera and time in culture. Glia 6:1-8.
- King JK, Kostka JE, Frischer ME, Saunders FM (2000) Sulfate-reducing bacteria methylate mercury at variable rates in pure culture and in marine sediments. Applied and environmental microbiology 66:2430-2437.
- Kinoshita PF, Leite JA, Orellana AMM, Vasconcelos AR, Quintas LEM, Kawamoto EM, Scavone C (2016) The Influence of Na+, K+-ATPase on Glutamate Signaling in Neurodegenerative Diseases and Senescence. 7.
- Kobayashi H, Yuyama A, Matsusaka N, Takeno K, Yanagiya I (1981) Neuropharmacological effect of methylmercury in mice with special reference to the central cholinergic system. The Japanese Journal of Pharmacology 31:711-718.
- Koh AS (2002) Identification of a Mechanism by Which the Methylmercury Antidotes N-Acetylcysteine and Dimercaptopropanesulfonate Enhance Urinary Metal Excretion: Transport by the Renal Organic Anion Transporter-1. Molecular Pharmacology 62:921-926.
- Komatsu M, Kurokawa H, Waguri S, Taguchi K, Kobayashi A, Ichimura Y, Sou Y-S, Ueno I, Sakamoto A, Tong KI, Kim M, Nishito Y, Iemura S-I, Natsume T, Ueno T, Kominami E, Motohashi H, Tanaka K, Yamamoto M (2010) The selective autophagy substrate p62 activates the stress responsive transcription factor Nrf2 through inactivation of Keap1. Nature Cell Biology 12:213-223.
- Komuro H, Rakic P (1996) Intracellular Ca2+ Fluctuations Modulate the Rate of Neuronal Migration. 17:275-285.

- Korogi Y, Takahashi M, Okajima T, Eto K (1998) Invited. MR findings of Minamata disease Organic mercury poisoning. Journal of Magnetic Resonance Imaging 8:308-316.
- Kovac S, Angelova PR, Holmström KM, Zhang Y, Dinkova-Kostova AT, Abramov AY (2015) Nrf2 regulates ROS production by mitochondria and NADPH oxidase. Biochimica et Biophysica Acta (BBA) General Subjects 1850:794-801.
- Kozakiewicz M, Kornatowski M, Krzywińska O, Kędziora-Kornatowska K (2019) Changes in the blood antioxidant defense of advanced age people. Clinical interventions in aging 14:763-771.
- Kraft AD (2004) Nuclear Factor E2-Related Factor 2-Dependent Antioxidant Response Element Activation by tert-Butylhydroquinone and Sulforaphane Occurring Preferentially in Astrocytes Conditions Neurons against Oxidative Insult. 24:1101-1112.
- Kranich O, Dringen R, Sandberg M, Hamprecht B (1998) Utilization of cysteine and cysteine precursors for the synthesis of glutathione in astroglial cultures: Preference for cystine. Glia 22:11-18.
- Kuang L, Feng J, He G, Jing T (2013) Knockdown of Nrf2 inhibits the angiogenesis of rat cardiac micro-vascular endothelial cells under hypoxic conditions. Int J Biol Sci 9:656-665.
- Kulshreshtha D, Vijayalakshmi K, Alladi PA, Sathyaprabha TN, Nalini A, Raju TR (2011) Vascular Endothelial Growth Factor Attenuates Neurodegenerative Changes in the NSC-34 Motor Neuron Cell Line Induced by Cerebrospinal Fluid of Sporadic Amyotrophic Lateral Sclerosis Patients. Neurodegenerative Diseases 8:322-330.
- Kumagai Y, Kanda H, Shinkai Y, Toyama T (2013) The Role of the Keap1/Nrf2 Pathway in the Cellular Response to Methylmercury. 2013:1-8.
- Kupchik YM, Moussawi K, Tang X-C, Wang X, Kalivas BC, Kolokithas R, Ogburn KB, Kalivas PW (2012) The Effect of N-Acetylcysteine in the Nucleus Accumbens on Neurotransmission and Relapse to Cocaine. 71:978-986.
- Kwak M-K, Itoh K, Yamamoto M, Kensler TW (2002) Enhanced Expression of the Transcription Factor Nrf2 by Cancer Chemopreventive Agents: Role of Antioxidant

- Response Element-Like Sequences in the nrf2 Promoter. Molecular and Cellular Biology 22:2883-2892.
- L. H (1990) Dibutyryl Cyclic AMP Treatment of Astrocytes in Primary Cultures as a Substitute for Normal Morphogenic and 'Functiogenic' Transmitter Signals. In: Molecular Aspects of Development and Aging of the Nervous System (J.M. L, A. P, E. G, P.S. T, A. V, eds), pp 227-244. Boston, MA: Springer.
- Lacher SE, Levings DC, Freeman S, Slattery M (2018) Identification of a functional antioxidant response element at the HIF1A locus. Redox Biology 19:401-411.
- Lambrechts D, Storkebaum E, Carmeliet P (2004) VEGF: necessary to prevent motoneuron degeneration, sufficient to treat ALS? 10:275-282.
- Lambrechts D et al. (2003) VEGF is a modifier of amyotrophic lateral sclerosis in mice and humans and protects motoneurons against ischemic death. Nature Genetics 34:383-394.
- Lange SC, Bak LK, Waagepetersen HS, Schousboe A, Norenberg MD (2012) Primary Cultures of Astrocytes: Their Value in Understanding Astrocytes in Health and Disease. Neurochemical research 37:2569-2588.
- Lanté F, Meunier J, Guiramand J, De Jesus Ferreira M-C, Cambonie G, Aimar R, Cohen-Solal C, Maurice T, Vignes M, Barbanel G (2008) LateN-acetylcysteine treatment prevents the deficits induced in the offspring of dams exposed to an immune stress during gestation. Hippocampus 18:602-609.
- Laslo P, Lipski J, Nicholson LFB, Miles GB, Funk GD (2001) GluR2 AMPA Receptor Subunit Expression in Motoneurons at Low and High Risk for Degeneration in Amyotrophic Lateral Sclerosis. Experimental Neurology 169:461-471.
- Lavoie RA, Jardine TD, Chumchal MM, Kidd KA, Campbell LM (2013) Biomagnification of Mercury in Aquatic Food Webs: A Worldwide Meta-Analysis. Environmental Science & Technology 47:13385-13394.
- Lebel CP, Ali SF, McKee M, Bondy SC (1990) Organometal-induced increases in oxygen reactive species: The potential of 2',7'-dichlorofluorescin diacetate as an index of neurotoxic damage. 104:17-24.

- Lee D, Kook SH, Ji H, Lee SA, Choi KC, Lee KY, Lee JC (2015) N-acetyl cysteine inhibits H2O2-mediated reduction in the mineralization of MC3T3-E1 cells by down-regulating Nrf2/HO-1 pathway. BMB Reports 48:636-641.
- Lee J-M, Shih AY, Murphy TH, Johnson JA (2003a) NF-E2-related Factor-2 Mediates Neuroprotection against Mitochondrial Complex I Inhibitors and Increased Concentrations of Intracellular Calcium in Primary Cortical Neurons. Journal of Biological Chemistry 278:37948-37956.
- Lee J-M, Calkins MJ, Chan K, Kan YW, Johnson JA (2003b) Identification of the NF-E2-related Factor-2-dependent Genes Conferring Protection against Oxidative Stress in Primary Cortical Astrocytes Using Oligonucleotide Microarray Analysis. Journal of Biological Chemistry 278:12029-12038.
- Lee JM, Calkins MJ, Chan K, Kan YW, Johnson JA (2003c) Identification of the NF-E2-related Factor-2-dependent Genes Conferring Protection against Oxidative Stress in Primary Cortical Astrocytes Using Oligonucleotide Microarray Analysis. 278:12029-12038.
- Lehnherr I (2014) Methylmercury biogeochemistry: a review with special reference to Arctic aquatic ecosystems. Environmental Reviews 22:229-243.
- Leier I, Jedlitschky G, Buchholz U, Center M, Cole SPC, Deeley RG, Keppler D (1996) ATP-dependent glutathione disulphide transport mediated by the MRP geneencoded conjugate export pump. Biochemical Journal 314:433-437.
- Leonhardt R, Haas H, Büsselberg D (1996) Methyl mercury reduces voltage-activated currents of rat dorsal root ganglion neurons. Naunyn Schmiedebergs Arch Pharmacol 354:532-538.
- Levy LM, Warr O, Attwell D (1998) Stoichiometry of the Glial Glutamate Transporter GLT-1 Expressed Inducibly in a Chinese Hamster Ovary Cell Line Selected for Low Endogenous Na+-Dependent Glutamate Uptake. The Journal of Neuroscience 18:9620-9628.
- Lewerenz J, Klein M, Methner A (2006) Cooperative action of glutamate transporters and cystine/glutamate antiporter system Xc- protects from oxidative glutamate toxicity. Journal of Neurochemistry 98:916-925.

- Lewerenz J, Maher P, Methner A (2012) Regulation of xCT expression and system xcfunction in neuronal cells. Amino Acids 42:171-179.
- Lewerenz J, Albrecht P, Tien M-LT, Henke N, Karumbayaram S, Kornblum HI, Wiedau-Pazos M, Schubert D, Maher P, Methner A (2009) Induction of Nrf2 and xCT are involved in the action of the neuroprotective antibiotic ceftriaxone in vitro. Journal of Neurochemistry 111:332-343.
- Lewerenz J, Baxter P, Kassubek R, Albrecht P, Van Liefferinge J, Westhoff M-A, Halatsch M-E, Karpel-Massler G, Meakin PJ, Hayes JD, Aronica E, Smolders I, Ludolph AC, Methner A, Conrad M, Massie A, Hardingham GE, Maher P (2014) Phosphoinositide 3-Kinases Upregulate System xc- via Eukaryotic Initiation Factor 2α and Activating Transcription Factor 4 A Pathway Active in Glioblastomas and Epilepsy. Antioxidants & Redox Signaling 20:2907-2922.
- Leyshon-Sørland K, Jasani B, Morgan AJ (1994) The localization of mercury and metallothionein in the cerebellum of rats experimentally exposed to methylmercury. The Histochemical Journal 26:161-169.
- Li J, Zhang L, Chu Y, Namaka M, Deng B, Kong J, Bi X (2016) Astrocytes in Oligodendrocyte Lineage Development and White Matter Pathology. Front Cell Neurosci 10:119.
- Li Y, Zhao X, Hu Y, Sun H, He Z, Yuan J, Cai H, Sun Y, Huang X, Kong W, Kong W (2018) Age-associated decline in Nrf2 signaling and associated mtDNA damage may be involved in the degeneration of the auditory cortex: Implications for central presbycusis. International Journal of Molecular Medicine.
- Liby K (2005) The Synthetic Triterpenoids, CDDO and CDDO-Imidazolide, Are Potent Inducers of Heme Oxygenase-1 and Nrf2/ARE Signaling. Cancer Research 65:4789-4798.
- Liddell JR (2017) Are Astrocytes the Predominant Cell Type for Activation of Nrf2 in Aging and Neurodegeneration? Antioxidants (Basel) 6.
- Limke TL (2004) Acute Exposure to Methylmercury Causes Ca2+ Dysregulation and Neuronal Death in Rat Cerebellar Granule Cells through an M3 Muscarinic Receptor-Linked Pathway. Toxicological Sciences 80:60-68.

- Limke TL, Atchison WD (2002) Acute Exposure to Methylmercury Opens the Mitochondrial Permeability Transition Pore in Rat Cerebellar Granule Cells. 178:52-61.
- Limke TL, Otero-Montanez JK, Atchison WD (2003) Evidence for Interactions between Intracellular Calcium Stores during Methylmercury-Induced Intracellular Calcium Dysregulation in Rat Cerebellar Granule Neurons. 304:949-958.
- Limke TL, Heidemann SR, Atchison WD (2004a) Disruption of intraneuronal divalent cation regulation by methylmercury: are specific targets involved in altered neuronal development and cytotoxicity in methylmercury poisoning? Neurotoxicology 25:741-760.
- Limke TL, Bearss JJ, Atchison WD (2004b) Acute Exposure to Methylmercury Causes Ca2+ Dysregulation and Neuronal Death in Rat Cerebellar Granule Cells through an M3 Muscarinic Receptor-Linked Pathway. Toxicological Sciences 80:60-68.
- Liu W, Xu Z, Deng Y, Xu B, Yang H, Wei Y, Feng S (2014) Excitotoxicity and oxidative damages induced by methylmercury in rat cerebral cortex and the protective effects of tea polyphenols. Environmental Toxicology 29:269-283.
- Livak KJ, Schmittgen TD (2001) Analysis of relative gene expression data using real-time quantitative PCR and the 2(-Delta Delta C(T)) Method. Methods 25:402-408.
- Lu SC (2013) Glutathione synthesis. Biochimica et Biophysica Acta (BBA) General Subjects 1830:3143-3153.
- Lubos E, Loscalzo J, Handy DE (2011) Glutathione Peroxidase-1 in Health and Disease: From Molecular Mechanisms to Therapeutic Opportunities. 15:1957-1997.
- Ludwin SK, Kosek JC, Eng LF (1976) The topographical distribution of S-100 and GFA proteins in the adult rat brain: An immunohistochemical study using horseradish peroxidase-labelled antibodies. The Journal of Comparative Neurology 165:197-207.
- Lunn JS, Sakowski SA, Kim B, Rosenberg AA, Feldman EL (2009) Vascular endothelial growth factor prevents G93A-SOD1-induced motor neuron degeneration. Dev Neurobiol 69:871-884.

- Lv Y, Zhao S, Han J, Zheng L, Yang Z, Zhao L (2015) Hypoxia-inducible factor-1α induces multidrug resistance protein in colon cancer.1941.
- Ma Q (2013) Role of Nrf2 in Oxidative Stress and Toxicity. Annual Review of Pharmacology and Toxicology 53:401-426.
- Madejczyk MS, Aremu DA, Simmons-Willis TA, Clarkson TW, Ballatori N (2007) Accelerated Urinary Excretion of Methylmercury following Administration of Its Antidote N-Acetylcysteine Requires Mrp2/Abcc2, the Apical Multidrug Resistance-Associated Protein. Journal of Pharmacology and Experimental Therapeutics 322:378-384.
- Mahaffey KR (1999) Methylmercury: a new look at the risks. Public Health Rep 114:396-413.
- Maher JM, Dieter MZ, Aleksunes LM, Slitt AL, Guo G, Tanaka Y, Scheffer GL, Chan JY, Manautou JE, Chen Y, Dalton TP, Yamamoto M, Klaassen CD (2007) Oxidative and electrophilic stress induces multidrug resistance-associated protein transporters via the nuclear factor-E2-related factor-2 transcriptional pathway. 46:1597-1610.
- Mahmoud S, Gharagozloo M, Simard C, Gris D (2019) Astrocytes Maintain Glutamate Homeostasis in the CNS by Controlling the Balance between Glutamate Uptake and Release. Cells 8:184.
- Malm O (1998) Gold Mining as a Source of Mercury Exposure in the Brazilian Amazon. Environmental Research 77:73-78.
- Mangelsdorf I, Walach H, Mutter J (2017) Healing of Amyotrophic Lateral Sclerosis: A Case Report. Complementary Medicine Research 24:175-181.
- Marty M, Atchison W (1997a) Pathways Mediating CaEntry in Rat Cerebellar Granule Cells FollowingExposure to Methyl Mercury. 147:319-330.
- Marty MS, Atchison WD (1997b) Pathways mediating Ca2+ entry in rat cerebellar granule cells following in vitro exposure to methyl mercury. Toxicol Appl Pharmacol 147:319-330.

- Marty MS, Atchison WD (1998a) Elevations of Intracellular Ca2+as a Probable Contributor to Decreased Viability in Cerebellar Granule Cells Following Acute Exposure to Methylmercury. Toxicology and Applied Pharmacology 150:98-105.
- Marty MS, Atchison WD (1998b) Elevations of intracellular Ca2+ as a probable contributor to decreased viability in cerebellar granule cells following acute exposure to methylmercury. Toxicology and Applied Pharmacology 150:98-105.
- Massaad CA, Klann E (2011) Reactive Oxygen Species in the Regulation of Synaptic Plasticity and Memory. Antioxidants & Redox Signaling 14:2013-2054.
- Massie A, Boillée S, Hewett S, Knackstedt L, Lewerenz J (2015) Main path and byways: non-vesicular glutamate release by system x c as an important modifier of glutamatergic neurotransmission. Journal of neurochemistry 135:1062-1079.
- Mattson MP (2007) Calcium and neurodegeneration. Aging Cell 6:337-350.
- Matyja E, Albrecht J (1993) Ultrastructural evidence that mercuric chloride lowers the threshold for glutamate neurotoxicity in an organotypic culture of rat cerebellum. Neuroscience Letters 158:155-158.
- McBean GJ (2002) Cerebral cystine uptake: a tale of two transporters. Trends in Pharmacological Sciences 23:299-302.
- McConnachie LA, Mohar I, Hudson FN, Ware CB, Ladiges WC, Fernandez C, Chatterton-Kirchmeier S, White CC, Pierce RH, Kavanagh TJ (2007) Glutamate Cysteine Ligase Modifier Subunit Deficiency and Gender as Determinants of Acetaminophen-Induced Hepatotoxicity in Mice. 99:628-636.
- McQueen G, Lally J, Collier T, Zelaya F, Lythgoe DJ, Barker GJ, Stone JM, McGuire P, Maccabe JH, Egerton A (2018) Effects of N-acetylcysteine on brain glutamate levels and resting perfusion in schizophrenia. Psychopharmacology.
- Meakin PJ, Chowdhry S, Sharma RS, Ashford FB, Walsh SV, McCrimmon RJ, Dinkova-Kostova AT, Dillon JF, Hayes JD, Ashford MLJ (2014) Susceptibility of Nrf2-Null Mice to Steatohepatitis and Cirrhosis upon Consumption of a High-Fat Diet Is Associated with Oxidative Stress, Perturbation of the Unfolded Protein Response, and Disturbance in the Expression of Metabolic Enzymes but Not with Insulin Resistance. 34:3305-3320.

- Meister A (1988) Glutathione metabolism and its selective modification. Journal of Biological Chemistry 263:17205-17208.
- Mennini T, Bigini P, Ravizza T, Vezzani A, Calvaresi N, Tortarolo M, Bendotti C (2002) Expression of glutamate receptor subtypes in the spinal cord of control andmnd mice, a model of motor neuron disorder. Journal of neuroscience research 70:553-560.
- Meszlényi V, Patai R, Polgár TF, Nógrádi B, Körmöczy L, Kristóf R, Spisák K, Tripolszki K, Széll M, Obál I, Engelhardt JI, Siklós L (2020) Passive Transfer of Sera from ALS Patients with Identified Mutations Evokes an Increased Synaptic Vesicle Number and Elevation of Calcium Levels in Motor Axon Terminals, Similar to Sera from Sporadic Patients. International Journal of Molecular Sciences 21:5566.
- Meyer K, Ferraiuolo L, Miranda CJ, Likhite S, McElroy S, Renusch S, Ditsworth D, Lagier-Tourenne C, Smith RA, Ravits J, Burghes AH, Shaw PJ, Cleveland DW, Kolb SJ, Kaspar BK (2014) Direct conversion of patient fibroblasts demonstrates non-cell autonomous toxicity of astrocytes to motor neurons in familial and sporadic ALS. Proceedings of the National Academy of Sciences 111:829-832.
- Miller AL (1998) Dimercaptosuccinic acid (DMSA), a non-toxic, water-soluble treatment for heavy metal toxicity. Altern Med Rev 3:199-207.
- Miller RH, Raff MC (1984) Fibrous and protoplasmic astrocytes are biochemically and developmentally distinct. The Journal of neuroscience: the official journal of the Society for Neuroscience 4:585-592.
- Miller RH, Zhang H, Fok-Seang J (1994) Glial cell heterogeneity in the mammalian spinal cord. Perspectives on developmental neurobiology 2:225-231.
- Minagar A, Alexander JS (2003) Blood-brain barrier disruption in multiple sclerosis. Multiple Sclerosis Journal 9:540-549.
- Minarini A, Ferrari S, Galletti M, Giambalvo N, Perrone D, Rioli G, Galeazzi GM (2017) N-acetylcysteine in the treatment of psychiatric disorders: current status and future prospects. Expert Opin Drug Metab Toxicol 13:279-292.
- Minich T, Riemer J, Schulz JB, Wielinga P, Wijnholds J, Dringen R (2006) The multidrug resistance protein 1 (Mrp1), but not Mrp5, mediates export of glutathione and

- glutathione disulfide from brain astrocytes. Journal of Neurochemistry 97:373-384.
- Miura K, Clarkson TW (1993) Reduced Methylmercury Accumulation in a Methylmercury-Resistant Rat Pheochromocytoma PC12 Cell Line. Toxicology and applied pharmacology 118:39-45.
- Miura K, Clarkson TW, Ikeda K, Naganuma A, Imura N (1994) Establishment and Characterization of Methylmercury-Resistant PC12 Cell Line. Environmental Health Perspectives 102:313-315.
- Mochizuki Y, Furukawa K (1987) Application of Coomassie brilliant blue staining to cultured hepatocytes. Cell Biology International Reports 11:367-371.
- Mokrzan EM, Kerper LE, Ballatori N, Clarkson TW (1995) Methylmercury-thiol uptake into cultured brain capillary endothelial cells on amino acid system L. Journal of Pharmacology and Experimental Therapeutics 272:1277-1284.
- Møller-Madsen B (1990) Localization of mercury in CNS of the rat: II. Intraperitoneal injection of methylmercuric chloride (CH3HgCl) and mercuric chloride (HgCl2). Toxicology and Applied Pharmacology 103:303-323.
- Møller-Madsen B (1991) Localization of Mercury in CNS of the Rat III. Oral Administration of Methylmercuric Chloride (CH3HgCl). Toxicological Sciences 16:172-187.
- Motohashi H, Yamamoto M (2004) Nrf2-Keap1 defines a physiologically important stress response mechanism. Trends in molecular medicine 10:549-557.
- Mukandala G, Tynan R, Lanigan S, O'Connor J (2016) The Effects of Hypoxia and Inflammation on Synaptic Signaling in the CNS. 6:6.
- Mundy WR, Freudenrich TM (2000) Sensitivity of immature neurons in culture to metalinduced changes in reactive oxygen species and intracellular free calcium. Neurotoxicology 21:1135-1144.
- Muniroh M, Khan N, Koriyama C, Akiba S, Vogel CFA, Yamamoto M (2015) Suppression of methylmercury-induced IL-6 and MCP-1 expressions by N-acetylcysteine in U-87MG human astrocytoma cells. Life Sciences 134:16-21.

- Muramatsu H, Katsuoka F, Toide K, Shimizu Y, Furusako S, Yamamoto M (2013) Nrf2 deficiency leads to behavioral, neurochemical and transcriptional changes in mice. Genes to Cells:n/a-n/a.
- Murphy TH, Schnaar RL, Coyle JT (1990) Immature cortical neurons are uniquely sensitive to glutamate toxicity by inhibition of cystine uptake. The FASEB journal 4:1624-1633.
- Murphy TH, Miyamoto M, Sastre A, Schnaar RL, Coyle JT (1989) Glutamate toxicity in a neuronal cell line involves inhibition of cystine transport leading to oxidative stress. Neuron 2:1547-1558.
- Murphy TH, Yu J, Ng R, Johnson DA, Shen H, Honey CR, Johnson JA (2001) Preferential expression of antioxidant response element mediated gene expression in astrocytes. 76:1670-1678.
- Mutkus L, Aschner JL, Syversen T, Aschner M (2005) Methylmercury Alters the In Vitro Uptake of Glutamate in GLAST- and GLT-1-Transfected Mutant CHO-K1 Cells. Biological trace element research 107:231-246.
- Myers GJ, Davidson PW (2000) Does methylmercury have a role in causing developmental disabilities in children? Environmental Health Perspectives 108:413-420.
- Myers GJ, Davidson PW, Cox C, Shamlaye C, Cernichiari E, Clarkson TW (2000) Twenty-Seven Years Studying the Human Neurotoxicity of Methylmercury Exposure. Environmental Research 83:275-285.
- Nafia I, Re DB, Masmejean F, Melon C, Kachidian P, Kerkerian-Le Goff L, Nieoullon A, Had-Aissouni L (2008) Preferential vulnerability of mesencephalic dopamine neurons to glutamate transporter dysfunction. 105:484-496.
- Nagai M, Re DB, Nagata T, Chalazonitis A, Jessell TM, Wichterle H, Przedborski S (2007) Astrocytes expressing ALS-linked mutated SOD1 release factors selectively toxic to motor neurons. Nature Neuroscience 10:615-622.
- Naganuma A, Miura K, Tanaka-Kagawa T, Kitahara J, Seko Y, Toyoda H, Imura N (1998) Overexpression of manganese-superoxide dismutase prevents methylmercury tox1city in hela cells. Life Sciences 62:PL157-PL161.

- Nanduri J, Vaddi DR, Khan SA, Wang N, Makarenko V, Semenza GL, Prabhakar NR (2015) HIF-1a Activation by Intermittent Hypoxia Requires NADPH Oxidase Stimulation by Xanthine Oxidase. PLOS ONE 10:e0119762.
- Narahashi T, Arakawa O, Nakahiro M (1991) Role of Neuronal Ion Channels in Mercury Intoxication. In: Advances in Mercury Toxicology (Suzuki T, Imura N, Clarkson TW, eds), pp 191-207. Boston, MA: Springer US.
- Neymotin A, Calingasan NY, Wille E, Naseri N, Petri S, Damiano M, Liby KT, Risingsong R, Sporn M, Beal MF, Kiaei M (2011) Neuroprotective effect of Nrf2/ARE activators, CDDO ethylamide and CDDO trifluoroethylamide, in a mouse model of amyotrophic lateral sclerosis. Free Radical Biology and Medicine 51:88-96.
- Ni M, Li X, Yin Z, Jiang H, Sidoryk-Wegrzynowicz M, Milatovic D, Cai J, Aschner M (2010a) Methylmercury induces acute oxidative stress, altering Nrf2 protein level in primary microglial cells. toxicological sciences 116:590-603.
- Ni M, Li X, Yin Z, Jiang H, Sidoryk-Wegrzynowicz M, Milatovic D, Cai J, Aschner M (2010b) Methylmercury Induces Acute Oxidative Stress, Altering Nrf2 Protein Level in Primary Microglial Cells. Toxicology Science 116:590-603.
- Ni M, Li X, Yin Z, Sidoryk-Węgrzynowicz M, Jiang H, Farina M, Rocha JBT, Syversen T, Aschner M (2011) Comparative study on the response of rat primary astrocytes and microglia to methylmercury toxicity. Glia 59:810-820.
- Nieoullon A, Canolle B, Masmejean F, Guillet B, Pisano P, Lortet S (2006) The neuronal excitatory amino acid transporter EAAC1/EAAT3: does it represent a major actor at the brain excitatory synapse? Journal of Neurochemistry 98:1007-1018.
- Nierenberg DW, Nordgren RE, Chang MB, Siegler RW, Blayney MB, Hochberg F, Toribara TY, Cernichiari E, Clarkson T (1998) Delayed cerebellar disease and death after accidental exposure to dimethylmercury. The New England journal of medicine 338:1672-1676.
- Niture SK, Khatri R, Jaiswal AK (2014) Regulation of Nrf2—an update. Free Radical Biology and Medicine 66:36-44.
- Niture SK, Kaspar JW, Shen J, Jaiswal AK (2010) Nrf2 signaling and cell survival. Toxicology and Applied Pharmacology 244:37-42.

- Norenberg MD, Martinez-Hernandez A (1979) Fine structural localization of glutamine synthetase in astrocytes of rat brain. 161:303-310.
- Norton W, Farooq M (1989) Astrocytes cultured from mature brain derive from glial precursor cells. The Journal of Neuroscience 9:769-775.
- Norton WT, Farooq M, Chiu F-C, Bottenstein JE (1988) Pure astrocyte cultures derived from cells isolated from mature brain. Glia 1:403-414.
- NRC NRC (2000) Toxicological Effects of Methylmercury. In: Toxicological effects of methylmercury (Goyer RA, Aposhian V, Arab L, Bellinger D, Burbacher T, Burke T, Jacobson J, Knobeloch L, Stern A, Ryan L, eds). Washington (DC): National Academies Press (US).
- O'Donovan SM, Sullivan CR, McCullumsmith RE (2017) The role of glutamate transporters in the pathophysiology of neuropsychiatric disorders. npj Schizophrenia 3.
- Obrist D, Agnan Y, Jiskra M, Olson CL, Colegrove DP, Hueber J, Moore CW, Sonke JE, Helmig D (2017) Tundra uptake of atmospheric elemental mercury drives Arctic mercury pollution. Nature 547:201-204.
- Ohkubo M, Miyamoto A, Shiraishi M (2016) Heavy metal chelator TPEN attenuates fura-2 fluorescence changes induced by cadmium, mercury and methylmercury.
- Ohtsuji M, Katsuoka F, Kobayashi A, Aburatani H, Hayes JD, Yamamoto M (2008) Nrf1 and Nrf2 Play Distinct Roles in Activation of Antioxidant Response Element-dependent Genes. Journal of Biological Chemistry 283:33554-33562.
- Okajima T, Mishima I, Tokuomi H (1976) Minamata disease with a long-term follow-up. Int J Neurol 11:62-72.
- Otis TS, Dodson PD (2009) Transporter Proteins in Neurons and Glia. In: Encyclopedia of Neuroscience (Squire LR, ed), pp 1159-1166. Oxford: Academic Press.
- Pabinger S, Rödiger S, Kriegner A, Vierlinger K, Weinhäusel A (2014) A survey of tools for the analysis of quantitative PCR (qPCR) data. Biomolecular Detection and Quantification 1:23-33.

- Pace N, Weerapana E (2014) Zinc-Binding Cysteines: Diverse Functions and Structural Motifs. Biomolecules 4:419-434.
- Pachernegg S, Mã<sup>1</sup>/<sub>4</sub>Nster Y, Muth-Kã¶Hne E, Fuhrmann G, Hollmann M (2015) GluA2 is rapidly edited at the Q/R site during neural differentiation in vitro. Frontiers in Cellular Neuroscience 9.
- Paco S, Hummel M, Plá V, Sumoy L, Aguado F (2016) Cyclic AMP signaling restricts activation and promotes maturation and antioxidant defenses in astrocytes. 17.
- Pacyna EG, Pacyna JM, Sundseth K, Munthe J, Kindbom K, Wilson S, Steenhuisen F, Maxson P (2010) Global emission of mercury to the atmosphere from anthropogenic sources in 2005 and projections to 2020. Atmospheric Environment 44:2487-2499.
- Pajarillo E, Rizor A, Lee J, Aschner M, Lee E (2019) The role of astrocytic glutamate transporters GLT-1 and GLAST in neurological disorders: potential targets for neurotherapeutics. Neuropharmacology.
- Pamphlett R, Waley P (1996) Motor neuron uptake of low dose inorganic mercury. Journal of the Neurological Sciences 135:63-67.
- Pamphlett R, Slater M, Thomas S (1998) Oxidative damage to nucleic acids in motor neurons containing mercury. Journal of the Neurological Sciences 159:121-126.
- Parkin Kullmann JA, Pamphlett R (2018) A Comparison of Mercury Exposure from Seafood Consumption and Dental Amalgam Fillings in People with and without Amyotrophic Lateral Sclerosis (ALS): An International Online Case-Control Study. International journal of environmental research and public health 15:2874.
- Patra KC, Hay N (2014) The pentose phosphate pathway and cancer. Trends in Biochemical Sciences 39:347-354.
- Paul (2015) Reactive Oxygen Species in Cancer: A Dance with the Devil. Cancer Cell 27:156-157.
- Pekny M, Pekna M (2014) Astrocyte Reactivity and Reactive Astrogliosis: Costs and Benefits. Physiological Reviews 94:1077-1098.

- Penugonda S, Ercal N (2011) Comparative evaluation of N-acetylcysteine (NAC) and N-acetylcysteine amide (NACA) on glutamate and lead-induced toxicity in CD-1 mice. Toxicology Letters 201:1-7.
- Philbert MA, Beiswanger CM, Waters DK, Reuhl KR, Lowndes HE (1991) Cellular and regional distribution of reduced glutathione in the nervous system of the rat: Histochemical localization by mercury orange and o-phthaldialdehyde-induced histofluorescence. 107:215-227.
- Pletz J, Sanchez-Bayo F, Tennekes HA (2016) Dose-response analysis indicating time-dependent neurotoxicity caused by organic and inorganic mercury-Implications for toxic effects in the developing brain. Toxicology 347-349:1-5.
- Portaro S, Naro A, Giorgianni R, Mazzon E, Calabrò RS (2019) Heavy metal intoxication and amyotrophic lateral sclerosis: causal or casual relationship? Aging Clinical and Experimental Research.
- Prescott LF (1983) Paracetamol Overdosage. Drugs 25:290-314.
- Qu H (2003) Effect of methylmercury on glutamate metabolism in cerebellar astrocytes in culture. Neurochemistry international 43:411-416.
- Rabenstein DL, Fairhurst MT (1975) Nuclear magnetic resonance studies of the solution chemistry of metal complexes. XI. Binding of methylmercury by sulfhydryl-containing amino acids and by glutathione. Journal of the American Chemical Society 97:2086-2092.
- Raff M, Abney E, Cohen J, Lindsay R, Noble M (1983) Two types of astrocytes in cultures of developing rat white matter: differences in morphology, surface gangliosides, and growth characteristics. The Journal of Neuroscience 3:1289-1300.
- Ramanathan G, Atchison WD (2011) Ca2+ entry pathways in mouse spinal motor neurons in culture following in vitro exposure to methylmercury. NeuroToxicology 32:742-750.
- Rapado-Castro M, Dodd S, Bush AI, Malhi GS, Skvarc DR, On ZX, Berk M, Dean OM (2017) Cognitive effects of adjunctive N-acetyl cysteine in psychosis. Psychological Medicine 47:866-876.

- Ray S, Corenblum MJ, Anandhan A, Reed A, Ortiz FO, Zhang DD, Barnes CA, Madhavan L (2018) A Role for Nrf2 Expression in Defining the Aging of Hippocampal Neural Stem Cells. Cell Transplantation 27:589-606.
- Reichard JF, Motz GT, Puga A (2007) Heme oxygenase-1 induction by NRF2 requires inactivation of the transcriptional repressor BACH1. Nucleic Acids Research 35:7074-7086.
- Reynolds JN, Racz WJ (1987) Effects of methylmercury on the spontaneous and potassium-evoked release of endogenous amino acids from mouse cerebellar slices. Canadian Journal of Physiology and Pharmacology 65:791-798.
- Rezania K, Roos RP (2013) Spinal cord: motor neuron diseases. Neurologic clinics 31:219-239.
- Rice DC (1996) Evidence for delayed neurotoxicity produced by methylmercury. Neurotoxicology 17:583-596.
- Rice ME, Russo-Menna I (1997) Differential compartmentalization of brain ascorbate and glutathione between neurons and glia. Neuroscience 82:1213-1223.
- Rivera-Caraballo KA, Wiwatratana D, Atchison WD (2017) Expression of Excitatory Amino Acid Transporter mRNA During Methylmercury Exposure in Mouse Spinal Cord Astrocytes and Neuroblastoma Spinal Cord NSC-34. In: Society of Toxicology. San Antonio, Texas, USA.
- Robitaille S, Mailloux RJ, Chan HM (2016) Methylmercury alters glutathione homeostasis by inhibiting glutaredoxin 1 and enhancing glutathione biosynthesis in cultured human astrocytoma cells. Toxicology Letters 256:1-10.
- Rooney JPK (2007) The role of thiols, dithiols, nutritional factors and interacting ligands in the toxicology of mercury. Toxicology 234:145-156.
- Roos D, Seeger R, Puntel R, Vargas Barbosa N (2012) Role of Calcium and Mitochondria in MeHg-Mediated Cytotoxicity. Journal of Biomedicine and Biotechnology 2012:1-15.
- Rosenstein J (2004) New roles for VEGF in nervous tissue?beyond blood vessels. Experimental Neurology 187:246-253.

- Rosenstein JM, Krum JM, Ruhrberg C (2010) VEGF in the nervous system. Organogenesis 6:107-114.
- Rothstein JD, Martin L, Levey AI, Dykes-Hoberg M, Jin L, Wu D, Nash N, Kuncl RW (1994) Localization of neuronal and glial glutamate transporters. 13:713-725.
- Rothstein JD, Dykes-Hoberg M, Pardo CA, Bristol LA, Jin L, Kuncl RW, Kanai Y, Hediger MA, Wang Y, Schielke JP, Welty DF (1996) Knockout of Glutamate Transporters Reveals a Major Role for Astroglial Transport in Excitotoxicity and Clearance of Glutamate. Neuron 16:675-686.
- Roybon L, Nuno, Garcia-Diaz A, Eun, Sattler R, Jackson-Lewis V, Yoon, C, Jeffrey, Przedborski S, Wichterle H, Christopher (2013) Human Stem Cell-Derived Spinal Cord Astrocytes with Defined Mature or Reactive Phenotypes. Cell Reports 4:1035-1048.
- Rushworth GF, Megson IL (2014) Existing and potential therapeutic uses for N-acetylcysteine: The need for conversion to intracellular glutathione for antioxidant benefits. Pharmacology & Therapeutics 141:150-159.
- Ruszkiewicz JA, Bowman AB, Farina M, Rocha JBT, Aschner M (2016) Sex- and structure-specific differences in antioxidant responses to methylmercury during early development. NeuroToxicology 56:118-126.
- Rybka J, Kupczyk D, Kędziora-Kornatowska K, Pawluk H, Czuczejko J, Szewczyk-Golec K, Kozakiewicz M, Antonioli M, Carvalho LA, Kędziora J (2011) Age-related changes in an antioxidant defense system in elderly patients with essential hypertension compared with healthy controls. Rodox Report 16:71-77.
- Sakai K, Okabe M, Eto K, Takeuchi T (1975) histochemical demonstration of mercury in human tissue cells of minamata disease by use of autoradiographic procedure. Acta Histochemica et Cytochemica 8:257-264.
- Sakamoto M, Tatsuta N, Chan HM, Domingo JL, Murata K, Nakai K (2018) Brain methylmercury uptake in fetal, neonate, weanling, and adult rats. Environ Res 167:15-20.
- Salim S (2016) Oxidative Stress and the Central Nervous System. Journal of Pharmacology and Experimental Therapeutics 360:201-205.

- Sanfeliu C, Sebastià J, Kim SU (2001) Methylmercury neurotoxicity in cultures of human neurons, astrocytes, neuroblastoma Cells. NeuroToxicology 22:317-327.
- Santana LNdS, Bittencourt LO, Nascimento PC, Fernandes RM, Teixeira FB, Fernandes LMP, Freitas Silva MC, Nogueira LS, Amado LL, Crespo-Lopez ME, Maia CdSF, Lima RR (2019) Low doses of methylmercury exposure during adulthood in rats display oxidative stress, neurodegeneration in the motor cortex and lead to impairment of motor skills. Journal of Trace Elements in Medicine and Biology 51:19-27.
- Sceniak MP, Spitsbergen JB, Sabo SL, Yuan Y, Atchison WD (2020) Acute neurotoxicant exposure induces hyperexcitability in mouse lumbar spinal motor neurons. J Neurophysiol 123:1448-1459.
- Schieber M, Navdeep (2014) ROS Function in Redox Signaling and Oxidative Stress. Current Biology 24:R453-R462.
- Schiønning JD, Eide R, Møller-Madsen B, Ernst E (1993) Detection of Mercury in Rat Spinal Cord and Dorsal Root Ganglia after Exposure to Mercury Vapor. Experimental and Molecular Pathology 58:215-228.
- Schiønning JDk, Møller-Madsen B, Danscher G (1991) Mercury in the dorsal root ganglia of rats treated with inorganic or organic mercury. Environmental Research 56:48-56.
- Schmidlin CJ, Dodson MB, Madhavan L, Zhang DD (2019) Redox regulation by NRF2 in aging and disease. Free Radical Biology and Medicine.
- Schroeter (2001) Astrocytes induce manganese superoxide dismutase in brain capillary endothelial cells. Neuroreport 12.
- Semenza GL (2007) Hypoxia-Inducible Factor 1 (HIF-1) Pathway. Science's STKE 2007:cm8-cm8.
- Sensi SL, Yin HZ, Weiss JH (2000) AMPA/kainate receptor-triggered Zn2+entry into cortical neurons induces mitochondrial Zn2+uptake and persistent mitochondrial dysfunction. European Journal of Neuroscience 12:3813-3818.

- Sensi SL, Yin HZ, Carriedo SG, Rao SS, Weiss JH (1999) Preferential Zn2+ influx through Ca2+-permeable AMPA/kainate channels triggers prolonged mitochondrial superoxide production. Proceedings of the National Academy of Sciences 96:2414-2419.
- Shah SZA, Zhao D, Hussain T, Sabir N, Mangi MH, Yang L (2018) p62-Keap1-NRF2-ARE Pathway: A Contentious Player for Selective Targeting of Autophagy, Oxidative Stress and Mitochondrial Dysfunction in Prion Diseases. Frontiers in Molecular Neuroscience 11.
- Shanker G, Aschner M (2001) Identification and characterization of uptake systems for cystine and cysteine in cultured astrocytes and neurons: Evidence for methylmercury-targeted disruption of astrocyte transport. Journal of neuroscience research 66:998-1002.
- Shanker G, Aschner M (2003a) Methylmercury-induced reactive oxygen species formation in neonatal cerebral astrocytic cultures is attenuated by antioxidants. Molecular Brain Research 110:85-91.
- Shanker G, Aschner M (2003b) Methylmercury-induced reactive oxygen species formation in neonatal cerebral astrocytic cultures is attenuated by antioxidants. Brain research Molecular brain research 110:85-91.
- Shanker G, Allen JW, Mutkus LA, Aschner M (2001a) Methylmercury inhibits cysteine uptake in cultured primary astrocytes, but not in neurons. Brain Research 914:159-165.
- Shanker G, Allen JW, Mutkus LA, Aschner M (2001b) Methylmercury inhibits cysteine uptake in cultured primary astrocytes, but not in neurons. Brain Research 914:159-165.
- Shanker G, Aschner JL, Syversen T, Aschner M (2004a) Free radical formation in cerebral cortical astrocytes in culture induced by methylmercury. Molecular Brain Research 128:48-57.
- Shanker G, Aschner JL, Syversen T, Aschner M (2004b) Free radical formation in cerebral cortical astrocytes in culture induced by methylmercury. 128:48-57.

- Shanker G, Syversen T, Aschner JL, Aschner M (2005a) Modulatory effect of glutathione status and antioxidants on methylmercury-induced free radical formation in primary cultures of cerebral astrocytes. 137:11-22.
- Shanker G, Syversen T, Aschner JL, Aschner M (2005b) Modulatory effect of glutathione status and antioxidants on methylmercury-induced free radical formation in primary cultures of cerebral astrocytes. Molecular Brain Research 137:11-22.
- Shapiro AM, Chan HM (2008) Characterization of demethylation of methylmercury in cultured astrocytes. Chemosphere 74:112-118.
- Shaw CM, Mottet NK, Body RL, Luschei ES (1975) Variability of neuropathologic lesions in experimental methylmercurial encephalopathy in primates. The American journal of pathology 80:451-470.
- Sheffner AL (2008) The reduction in vitro in viscosity of mucoprotein solutions by a new mucolytic agent, N-acetyl-L-cysteine. 106:298-310.
- Shi J, He Y, Hewett SJ, Hewett JA (2016) Interleukin 1β Regulation of the System x c Substrate-specific Subunit, xCT, in Primary Mouse Astrocytes Involves the RNA-binding Protein HuR. 291:1643-1651.
- Shi L (2015) MiR-141 Activates Nrf2-Dependent Antioxidant Pathway via Down-Regulating the Expression of Keap1 Conferring the Resistance of Hepatocellular Carcinoma Cells to 5-Fluorouracil. Cellular physiology and biochemistry 35:2333-2348.
- Shibata T, Yamada K, Watanabe M, Ikenaka K, Wada K, Tanaka K, Inoue Y (1997) Glutamate Transporter GLAST Is Expressed in the Radial Glia—Astrocyte Lineage of Developing Mouse Spinal Cord. The Journal of Neuroscience 17:9212-9219.
- Shih AY, Erb H, Sun X, Toda S, Kalivas PW, Murphy TH (2006) Cystine/Glutamate Exchange Modulates Glutathione Supply for Neuroprotection from Oxidative Stress and Cell Proliferation. 26:10514-10523.
- Shih AY, Johnson DA, Wong G, Kraft AD, Jiang L, Erb H, Johnson JA, Murphy TH (2003) Coordinate regulation of glutathione biosynthesis and release by Nrf2-expressing glia potently protects neurons from oxidative stress. The Journal of Neuroscience 23:3394-3406.

- Shimizu E, Hashimoto K, Komatsu N, Iyo M (2002) Roles of endogenous glutathione levels on 6-hydroxydopamine-induced apoptotic neuronal cell death in human neuroblastoma SK-N-SH cells. Neuropharmacology 43:434-443.
- Shinyashiki M, Kumagai Y, Homma-Takeda S, Nagafune J, Takasawa N, Suzuki J, Matsuzaki I, Satoh S, Sagai M, Shimojo N (1996) Selective inhibition of the mouse brain Mn-SOD by methylmercury. Environ Toxicol Pharmacol 2:359-366.
- Sienko DG (1990) Amyotrophic Lateral Sclerosis. Archives of neurology 47:38.
- Silbajoris R, Dailey L, Wages P, Speen A, Simmons S, Bromberg P, Samet J (2014) The Ubiquitous Pm Component Zinc Induces Ho-1 Expression Through Multiple Targets In The Nrf2/keap1 Signaling Pathway. American journal of respiratory and critical care medicine 189.
- Simmons-Willis TA, Koh AS, Clarkson TW, Ballatori N (2002) Transport of a neurotoxicant by molecular mimicry: the methylmercury—l-cysteine complex is a substrate for human L-type large neutral amino acid transporter (LAT) 1 and LAT2. Biochemical Journal 367:239-246.
- Simpson RB (1961) Association Constants of Methylmercury with Sulfhydryl and Other Bases. Journal of the American Chemical Society 83:4711-4717.
- Sirois JE, Atchison WD (2000) Methylmercury affects multiple subtypes of calcium channels in rat cerebellar granule cells. Toxicol Appl Pharmacol 167:1-11.
- Skerfving SB, Copplestone JF (1976) Poisoning caused by the consumption of organomercury-dressed seed in Iraq. Bull World Health Organ 54:101-112.
- Sofroniew MV (2015) Astrocyte barriers to neurotoxic inflammation. 16:249-263.
- Sommer B, Köhler M, Sprengel R, Seeburg PH (1991) RNA editing in brain controls a determinant of ion flow in glutamate-gated channels. Cell 67:11-19.
- Sonnewald U, Rae C (2010) Pyruvate Carboxylation in Different Model Systems Studied by 13C MRS. Neurochemical research 35:1916-1921.

- Spiller HA, Hays HL, Burns G, Casavant MJ (2017) Severe elemental mercury poisoning managed with selenium and N-acetylcysteine administration. Toxicology Communications 1:24-28.
- Stack C, Ho D, Wille E, Calingasan NY, Williams C, Liby K, Sporn M, Dumont M, Beal MF (2010) Triterpenoids CDDO-ethyl amide and CDDO-trifluoroethyl amide improve the behavioral phenotype and brain pathology in a transgenic mouse model of Huntington's disease. Free Radical and Medicine 49:147-158.
- Stanimirovic DB, Ball R, Small DL, Muruganandam A (1999) Developmental regulation of glutamate transporters and glutamine synthetase activity in astrocyte cultures differentiated in vitro. International Journal of Developmental Neuroscience 17:173-184.
- Su M, Wakabayashi K, Kakita A, Ikuta F, Hitoshi T (1998) Selective involvement of large motor neurons in the spinal cord of rats treated with methylmercury. Journal of the Neurological Sciences 156:12-17.
- Su ZZ, Leszczyniecka M, Kang DC, Sarkar D, Chao W, Volsky DJ, Fisher PB (2003) Insights into glutamate transport regulation in human astrocytes: Cloning of the promoter for excitatory amino acid transporter 2 (EAAT2). 100:1955-1960.
- Suchak SK, Baloyianni NV, Perkinton MS, Williams RJ, Meldrum BS, Rattray M (2003) The 'glial' glutamate transporter, EAAT2 (Glt-1) accounts for high affinity glutamate uptake into adult rodent nerve endings. Journal of Neurochemistry 84:522-532.
- Suda I, Hirayama K (1992) Degradation of methyl and ethyl mercury into inorganic mercury by hydroxyl radical produced from rat liver microsomes. Arch Toxicol 66:398-402.
- Suda I, Totoki S, Takahashi H (1991) Degradation of methyl and ethyl mercury into inorganic mercury by oxygen free radical-producing systems: Involvement of hydroxyl radical. 65:129-134.
- Suh JH, Shenvi SV, Dixon BM, Liu H, Jaiswal AK, Liu RM, Hagen TM (2004) Decline in transcriptional activity of Nrf2 causes age-related loss of glutathione synthesis, which is reversible with lipoic acid. Proceedings of the National Academy of Sciences 101:3381-3386.

- Sun X, Hu X, Wang D, Yuan Y, Qin S, Tan Z, Gu Y, Huang X, He C, Su Z (2017) Establishment and characterization of primary astrocyte culture from adult mouse brain. Brain Research Bulletin 132:10-19.
- Sunitha K, Hemshekhar M, Thushara RM, Santhosh MS, Yariswamy M, Kemparaju K, Girish KS (2013) N-Acetylcysteine amide: a derivative to fulfill the promises of N-Acetylcysteine. Free Radical Research 47:357-367.
- Susin SA, Lorenzo HK, Zamzami N, Marzo I, Snow BE, Brothers GM, Mangion J, Jacotot E, Costantini P, Loeffler M, Larochette N, Goodlett DR, Aebersold R, Siderovski DP, Penninger JM, Kroemer G (1999) Molecular characterization of mitochondrial apoptosis-inducing factor. Nature 397:441-446.
- Sutherland M, Delaney T, Noebels J (1996) Glutamate transporter mRNA expression in proliferative zones of the developing and adult murine CNS. The Journal of Neuroscience 16:2191-2207.
- Swanson RA, Liu J, Miller JW, Rothstein JD, Farrell K, A. Stein B, Longuemare MC (1997) Neuronal Regulation of Glutamate Transporter Subtype Expression in Astrocytes. The Journal of Neuroscience 17:932-940.
- Sykiotis GP, Bohmann D (2010) Stress-Activated Cap'n'collar Transcription Factors in Aging and Human Disease. Science Signaling 3:re3-re3.
- Syversen T, Kaur P (2012) The toxicology of mercury and its compounds. Journal of Trace Elements in Medicine and Biology 26:215-226.
- Syversen TLM (1974) Biotransformation of Hg-203 Labelled Methyl Mercuric Chloride in Rat Brain Measured by Specific Determination of Hg2+. Acta Pharmacologica et Toxicologica 35:277-283.
- Tabata H (2015) Diverse subtypes of astrocytes and their development during corticogenesis. Frontiers in Neuroscience 9.
- Taguchi K, Fujikawa N, Komatsu M, Ishii T, Unno M, Akaike T, Motohashi H, Yamamoto M (2012) Keap1 degradation by autophagy for the maintenance of redox homeostasis. Proceedings of the National Academy of Sciences 109:13561-13566.

- Takeda A (2011) Insight into Glutamate Excitotoxicity from Synaptic Zinc Homeostasis. International Journal of Alzheimer's Disease 2011:1-8.
- Tardiolo G, Bramanti P, Mazzon E (2018) Overview on the Effects of N-Acetylcysteine in Neurodegenerative Diseases. Molecules 23:3305.
- Tardy M (1981) Effect of prostaglandins and dibutyryl cyclic AMP on the morphology of cells in primary astroglial cultures and on metabolic enzymes of GABA and glutamate metabolism. Experientia 37:19-21.
- Tiernan CT, Edwin EA, Goudreau JL, Atchison WD, Lookingland KJ (2013) The Role of De Novo Catecholamine Synthesis in Mediating Methylmercury-Induced Vesicular Dopamine Release From Rat Pheochromocytoma (PC12) Cells. 133:125-132.
- Tiernan CT, Edwin EA, Hawong H-Y, Ríos-Cabanillas M, Goudreau JL, Atchison WD, Lookingland KJ (2015) Methylmercury Impairs Canonical Dopamine Metabolism in Rat Undifferentiated Pheochromocytoma (PC12) Cells by Indirect Inhibition of Aldehyde Dehydrogenase. Toxicological Sciences 144:347-356.
- Tobwala S, Khayyat A, Fan W, Ercal N (2015) Comparative evaluation of N-acetylcysteine and N-acetylcysteineamide in acetaminophen-induced hepatotoxicity in human hepatoma HepaRG cells. Experimental Biology and Medicine 240:261-272.
- Tokuomi H, Okajima T, Kanai J, Tsunoda M, Ichiyasu Y, Misumi H, Shimomura K, Takaba M (1961) Minamata disease. World Neurol 2:536-545.
- Tollefson L, Cordle F (1986) Methylmercury in fish: a review of residue levels, fish consumption and regulatory action in the United States. Environmental health perspectives 68:203-208.
- Tonelli C, Chio IIC, Tuveson DA (2018) Transcriptional Regulation by Nrf2. Antioxidants & Redox Signaling 29:1727-1745.
- Torp R, Danbolt NC, Babaie E, Bjørås M, Seeberg E, Storm-Mathisen J, Ottersen OP (1994) Differential Expression of Two Glial Glutamate Transporters in the Rat Brain: an In Situ Hybridization Study. 6:936-942.
- Toth R, Warfel N (2017) Strange Bedfellows: Nuclear Factor, Erythroid 2-Like 2 (Nrf2) and Hypoxia-Inducible Factor 1 (HIF-1) in Tumor Hypoxia. Antioxidants 6:27.

- Toyama T, Shinkai Y, Yasutake A, Uchida K, Yamamoto M, Kumagai Y (2011) Isothiocyanates Reduce Mercury Accumulation via an Nrf2-Dependent Mechanism during Exposure of Mice to Methylmercury. Environmental Health Perspectives 119:1117-1122.
- Toyama T, Sumi D, Shinkai Y, Yasutake A, Taguchi K, Tong KI, Yamamoto M, Kumagai Y (2007) Cytoprotective role of Nrf2/Keap1 system in methylmercury toxicity. Biochemical and Biophysical Research Communications 363:645-650.
- Travnikov O (2005) Contribution of the intercontinental atmospheric transport to mercury pollution in the Northern Hemisphere. Atmospheric Environment 39:7541-7548.
- Trotti D, Danbolt NC, Volterra A (1998) Glutamate transporters are oxidant-vulnerable: a molecular link between oxidative and excitotoxic neurodegeneration? 19:328-334.
- Trotti D, Rizzini BL, Rossi D, Haugeto O, Racagni G, Danbolt NC, Volterra A (1997) Neuronal and Glial Glutamate Transporters Possess an SH-based Redox Regulatory Mechanism. European Journal of Neuroscience 9:1236-1243.
- Tsujita T, Peirce V, Baird L, Matsuyama Y, Takaku M, Walsh SV, Griffin JL, Uruno A, Yamamoto M, Hayes JD (2014) Transcription Factor Nrf1 Negatively Regulates the Cystine/Glutamate Transporter and Lipid-Metabolizing Enzymes. Molecular and Cellular Biology 34:3800-3816.
- Ullensvang K, Lehre KP, Storm-Mathisen J, Danbolt NC (1997) Differential Developmental Expression of the Two Rat Brain Glutamate Transporter Proteins GLAST and GLT. 9:1646-1655.
- UNEP UNEP (2013) Global Mercury Assessment 2013: Sources, emissions, releases, and environmental transport. In. Geneva, Switzerland.
- Unnithan AS, Choi HJH, Titler AM, Posimo JM, Leak RK (2012) Rescue from a two hit, high-throughput model of neurodegeneration with N-acetyl cysteine. 61:356-368.
- Unnithan AS, Jiang Y, Rumble JL, Pulugulla SH, Posimo JM, Gleixner AM, Leak RK (2014) N-Acetyl cysteine prevents synergistic, severe toxicity from two hits of oxidative stress. 560:71-76.

- Unoki T, Abiko Y, Toyama T, Uehara T, Tsuboi K, Nishida M, Kaji T, Kumagai Y (2016) Methylmercury, an environmental electrophile capable of activation and disruption of the Akt/CREB/Bcl-2 signal transduction pathway in SH-SY5Y cells. Scientific Reports 6:28944.
- Vahter M, Mottet NK, Friberg L, Lind B, Shen DD, Burbacher T (1994) Speciation of mercury in the primate blood and brain following long-term exposure to methyl mercury. Toxicology and Applied Pharmacology 124:221-229.
- Vahter ME, Mottet NK, Friberg LT, Lind SB, Charleston JS, Burbacher TM (1995)
  Demethylation of Methyl Mercury in Different Brain Sites of Macaca-fascicularis
  Monkeys during Long-Term Subclinical Methyl Mercury Exposure. Toxicology
  and Applied Pharmacology 134:273-284.
- Van Damme P, Van Den Bosch L, Van Houtte E, Callewaert G, Robberecht W (2002) GluR2-Dependent Properties of AMPA Receptors Determine the Selective Vulnerability of Motor Neurons to Excitotoxicity. Journal of Neurophysiology 88:1279-1287.
- Van Damme P, Bogaert E, Dewil M, Hersmus N, Kiraly D, Scheveneels W, Bockx I, Braeken D, Verpoorten N, Verhoeven K, Timmerman V, Herijgers P, Callewaert G, Carmeliet P, Van Den Bosch L, Robberecht W (2007) Astrocytes regulate GluR2 expression in motor neurons and their vulnerability to excitotoxicity. Proceedings of the National Academy of Sciences 104:14825-14830.
- Van Den Bosch L, Storkebaum E, Vleminckx V, Moons L, Vanopdenbosch L, Scheveneels W, Carmeliet P, Robberecht W (2004) Effects of vascular endothelial growth factor (VEGF) on motor neuron degeneration. Neurobiology of Disease 17:21-28.
- Vandenberghe W, Robberecht W, Brorson JR (2000) AMPA Receptor Calcium Permeability, GluR2 Expression, and Selective Motoneuron Vulnerability. The Journal of Neuroscience 20:123-132.
- Vanduyn N, Nass R (2014) The putative multidrug resistance protein MRP-7 inhibits methylmercury-associated animal toxicity and dopaminergic neurodegeneration in Caenorhabditis elegans. 128:962-974.
- Vanduyn N, Settivari R, Wong G, Nass R (2010) SKN-1/Nrf2 Inhibits Dopamine Neuron Degeneration in a Caenorhabditis elegans Model of Methylmercury Toxicity. Toxicological Sciences 118:613-624.

- Vanselow BK, Keller BU (2000) Calcium dynamics and buffering in oculomotor neurones from mouse that are particularly resistant during amyotrophic lateral sclerosis (ALS)-related motoneurone disease. The Journal of physiology 525:433-445.
- Vargas MR, Johnson DA, Sirkis DW, Messing A, Johnson JA (2008) Nrf2 Activation in Astrocytes Protects against Neurodegeneration in Mouse Models of Familial Amyotrophic Lateral Sclerosis. The Journal of neuroscience: the official journal of the Society for Neuroscience 28:13574-13581.
- Vargas MR, Burton NC, Gan L, Johnson DA, Schäfer M, Werner S, Johnson JA (2013) Absence of Nrf2 or Its Selective Overexpression in Neurons and Muscle Does Not Affect Survival in ALS-Linked Mutant hSOD1 Mouse Models. 8:e56625.
- Vaughn JE, Pease DC (1967) Electron microscopy of classically stained astrocytes. 131:143-153.
- Vollrath V, Ana, Iruretagoyena M, Chianale J (2006) Role of Nrf2 in the regulation of the Mrp2 (ABCC2) gene. 395:599-609.
- Von Burg R, Northington FK, Shamoo A (1980) Methylmercury inhibition of rat brain muscarinic receptors. Toxicology and Applied Pharmacology 53:285-292.
- Waagepetersen HS, Qu H, Schousboe A, Sonnewald U (2001) Elucidation of the quantitative significance of pyruvate carboxylation in cultured cerebellar neurons and astrocytes. Journal of neuroscience research 66:763-770.
- Wages PA, Silbajoris R, Speen A, Brighton L, Henriquez A, Tong H, Bromberg PA, Simmons SO, Samet JM (2014) Role of H2O2 in the oxidative effects of zinc exposure in human airway epithelial cells. 3:47-55.
- Wallace DC (2005) A Mitochondrial Paradigm of Metabolic and Degenerative Diseases, Aging, and Cancer: A Dawn for Evolutionary Medicine. Annual Review of Genetics 39:359-407.
- Wang (2010) Selective neuronal vulnerability to oxidative stress in the brain. Frontiers in Aging Neuroscience.
- Wang L, Jiang H, Yin Z, Aschner M, Cai J (2008) Methylmercury Toxicity and Nrf2-dependent Detoxification in Astrocytes. 107:135-143.

- Wang L, Jiang H, Yin Z, Aschner M, Cai J (2009a) Methylmercury Toxicity and Nrf2-dependent Detoxification in Astrocytes. Toxicological Sciences 107:135-143.
- Wang X, Pal R, Chen X-w, Limpeanchob N, Kumar KN, Michaelis EK (2005) High intrinsic oxidative stress may underlie selective vulnerability of the hippocampal CA1 region. Molecular Brain Research 140:120-126.
- Wang X, Pal R, Chen X-W, Kumar KN, Kim O-J, Michaelis EK (2007) Genome-wide transcriptome profiling of region-specific vulnerability to oxidative stress in the hippocampus. Genomics 90:201-212.
- Wang X, Zaidi A, Pal R, Garrett AS, Braceras R, Chen X-W, Michaelis ML, Michaelis EK (2009b) Genomic and biochemical approaches in the discovery of mechanisms for selective neuronal vulnerability to oxidative stress. BMC Neuroscience 10:12.
- Warabi E, Takabe W, Minami T, Inoue K, Itoh K, Yamamoto M, Ishii T, Kodama T, Noguchi N (2007) Shear stress stabilizes NF-E2-related factor 2 and induces antioxidant genes in endothelial cells: Role of reactive oxygen/nitrogen species. 42:260-269.
- Warr O, Takahashi M, Attwell D (1999) Modulation of extracellular glutamate concentration in rat brain slices by cystine-glutamate exchange. Journal of Physiology 514:783-793.
- Watts SD, Torres-Salazar D, Divito CB, Amara SG (2014) Cysteine Transport through Excitatory Amino Acid Transporter 3 (EAAT3). PLoS ONE 9:e109245.
- Waypa GB, Smith KA, Schumacker PT (2016) O2 sensing, mitochondria and ROS signaling: The fog is lifting. 47-48:76-89.
- Weiss B, Clarkson TW, Simon W (2002a) Silent Latency Periods in Methylmercury Poisoning and in Neurodegenerative Disease. Environmental Health Perspectives 110:851-854.
- Weiss B, Clarkson TW, Simon W (2002b) Silent latency periods in methylmercury poisoning and in neurodegenerative disease. Environmental Health Perspectives 110:851-854.

- Wersinger E, Schwab Y, Sahel J-A, Rendon A, Pow DV, Picaud S, Roux MJ (2006) The glutamate transporter EAAT5 works as a presynaptic receptor in mouse rod bipolar cells. 577:221-234.
- WHO WHOIPoCS (1990) Environmental health criteria 101 Methylmercury / published under the joint sponsorship of the United Nations Environment Programme. In: (the International Labour Organisation atWHO, ed). Geneva, Switzerland: World Health Organization.
- Wiwatratana D, Atchison WD (2018) Assessment of antioxidant compounds in the protection of spinal cord astrocytes from methylmercury toxicity. In: 45th Pharmacology Research Colloquium. East Lansing, Michigan.
- Wobeser G, Nielsen NO, Schiefer B (1976) Mercury and Mink. II. Experimental methyl mercury intoxication. Can J Comp Med 40:34-45.
- Wright A, Vissel B (2012) The essential role of AMPA receptor GluR2 subunit RNA editing in the normal and diseased brain. Frontiers in Molecular Neuroscience 5.
- Xu B, Xu Z-F, Deng Y, Liu W, Yang H-B, Wei Y-G (2012a) Protective effects of MK-801 on methylmercury-induced neuronal injury in rat cerebral cortex: Involvement of oxidative stress and glutamate metabolism dysfunction. Toxicology 300:112-120.
- Xu B, Xu ZF, Deng Y, Liu W, Yang HB, Wei YG (2012b) Protective effects of MK-801 on methylmercury-induced neuronal injury in rat cerebral cortex: involvement of oxidative stress and glutamate metabolism dysfunction. Toxicology 300:112-120.
- Yamashita T, Ando Y, Nakamura M, Obayashi K, Terazaki H, Haraoka K, Guo SX, Ueda M, Uchino M (2004) Inhibitory effect of α-tocopherol on methylmercury-induced oxidative steress. Environ Health Prev Med 9:111-117.
- Yan CYI, Ferrari G, Greene LA (1995) N-Acetylcysteine-promoted Survival of PC12 Cells Is Glutathione-independent but Transcription-dependent. Journal of Biological Chemistry 270:26827-26832.
- Yan Z, Spaulding HR (2020) Extracellular superoxide dismutase, a molecular transducer of health benefits of exercise. Redox Biology 32:101508.

- Yang H, Magilnick N, Lee C, Kalmaz D, Ou X, Chan JY, Lu SC (2005) Nrf1 and Nrf2 Regulate Rat Glutamate-Cysteine Ligase Catalytic Subunit Transcription Indirectly via NF- B and AP-1. Molecular and Cellular Biology 25:5933-5946.
- Yang J-J, Tao H, Hu W, Liu L-P, Shi K-H, Deng Z-Y, Li J (2014) MicroRNA-200a controls Nrf2 activation by target Keap1 in hepatic stellate cell proliferation and fibrosis. 26:2381-2389.
- Yang Y, Jackson R (2019) Astrocyte identity: evolutionary perspectives on astrocyte functions and heterogeneity. Current Opinion in Neurobiology 56:40-46.
- Yee S, Choi BH (1996) Oxidative stress in neurotoxic effects of methylmercury poisoning. Neurotoxicology 17:17-26.
- Yin J, Ren W, Yang G, Duan J, Huang X, Fang R, Li C, Li T, Yin Y, Hou Y, Kim SW, Wu G (2016) l-Cysteine metabolism and its nutritional implications. Molecular Nutrition & Food Research 60:134-146.
- Yin Z, Milatovic D, Aschner JL, Syversen T, Rocha JBT, Souza DO, Sidoryk M, Albrecht J, Aschner M (2007a) Methylmercury induces oxidative injury, alterations in permeability and glutamine transport in cultured astrocytes. Brain Research 1131:1-10.
- Yin Z, Milatovic D, Aschner JL, Syversen T, Rocha JBT, Souza DO, Sidoryk M, Albrecht J, Aschner M (2007b) Methylmercury induces oxidative injury, alterations in permeability and glutamine transport in cultured astrocytes. 1131:1-10.
- Yin Z, Lee E, Ni M, Jiang H, Milatovic D, Rongzhu L, Farina M, Rocha JBT, Aschner M (2011) Methylmercury-induced alterations in astrocyte functions are attenuated by ebselen. Neurotoxicology 32:291-299.
- Yoshida E, Abiko Y, Kumagai Y (2014) Glutathione Adduct of Methylmercury Activates the Keap1-Nrf2 Pathway in SH-SY5Y Cells. Chemical Research in Toxicology 27:1780-1786.
- Yu ACH, Drejer J, Hertz L, Schousboe A (1983) Pyruvate Carboxylase Activity in Primary Cultures of Astrocytes and Neurons. 41:1484-1487.

- Yuan G, Nanduri J, Khan S, Semenza GL, Prabhakar NR (2008) Induction of HIF-1α expression by intermittent hypoxia: Involvement of NADPH oxidase, Ca 2+ signaling, prolyl hydroxylases, and mTOR. Journal of cellular physiology 217:674-685.
- Yuan Y, Atchison WD (1993a) Disruption by methylmercury of membrane excitability and synaptic transmission of CA1 neurons in hippocampal slices of the rat. Toxicol Appl Pharmacol 120:203-215.
- Yuan Y, Atchison WD (1995) Methylmercury acts at multiple sites to block hippocampal synaptic transmission. The Journal of pharmacology and experimental therapeutics 275:1308-1316.
- Yuan Y, Atchison WD (1997a) Action of methylmercury on GABA(A) receptor-mediated inhibitory synaptic transmission is primarily responsible for its early stimulatory effects on hippocampal CA1 excitatory synaptic transmission. The Journal of pharmacology and experimental therapeutics 282:64-73.
- Yuan Y, Atchison WD (1997b) Action of Methylmercury on GABA<sub>A</sub>Receptor-Mediated Inhibitory Synaptic Transmission Is Primarily Responsible for Its Early Stimulatory Effects on Hippocampal CA1 Excitatory Synaptic Transmission. Journal of Pharmacology and Experimental Therapeutics 282:64-73.
- Yuan Y, Atchison WD (1999) Comparative effects of methylmercury on parallel-fiber and climbing-fiber responses of rat cerebellar slices. The Journal of pharmacology and experimental therapeutics 288:1015-1025.
- Yuan Y, Atchison WD (2003) Methylmercury Differentially Affects GABAAReceptor-Mediated Spontaneous IPSCs in Purkinje and Granule Cells of Rat Cerebellar Slices. The Journal of physiology 550:191-204.
- Yuan Y, Atchison WD (2005) Methylmercury Induces a Spontaneous, Transient Slow Inward Chloride Current in Purkinje Cells of Rat Cerebellar Slices. Journal of Pharmacology and Experimental Therapeutics 313:751-764.
- Yuan Y, Atchison WD (2007a) Methylmercury-Induced Increase of Intracellular Ca2+ Increases Spontaneous Synaptic Current Frequency in Rat Cerebellar Slices. Molecular Pharmacology 71:1109-1121.

- Yuan Y, Atchison WD (2007b) Methylmercury-Induced Increase of Intracellular Ca2+ Increases Spontaneous Synaptic Current Frequency in Rat Cerebellar Slices. Mol Pharmacol 71:1109-1121.
- Yuan Y, Otero-Montanez JK, Yao A, Herden CJ, Sirois JE, Atchison WD (2005) Inwardly rectifying and voltage-gated outward potassium channels exhibit low sensitivity to methylmercury. Neurotoxicology 26:439-454.
- Yuan YK, Atchison WD (1993b) Disruption by Methylmercury of Membrane Excitability and Synaptic Transmission of CA1 Neurons in Hippocampal Slices of the Rat. Toxicology and Applied Pharmacology 120:203-215.
- Zalups RK, Ahmad S (2005) Transport of N-acetylcysteine s-conjugates of methylmercury in Madin-Darby canine kidney cells stably transfected with human isoform of organic anion transporter 1. The Journal of pharmacology and experimental therapeutics 314:1158-1168.
- Zängerle L, Cuénod M, Winterhalter KH, Do KQ (1992) Screening of Thiol Compounds: Depolarization-Induced Release of Glutathione and Cysteine from Rat Brain Slices. Journal of Neurochemistry 59:181-189.
- Zdolsek JM, Söder O, Hultman P (1994) Mercury induces in vivo and in vitro secretion of interleukin-1 in mice. Immunopharmacology 28:201-208.
- Zeevalk GD, Razmpour R, Bernard LP (2008) Glutathione and Parkinson's disease: Is this the elephant in the room? Biomedicine & Pharmacotherapy 62:236-249.
- Zemolin APP, Meinerz DF, de Paula MT, Mariano DOC, Rocha JBT, Pereira AB, Posser T, Franco JL (2012) Evidences for a role of glutathione peroxidase 4 (GPx4) in methylmercury induced neurotoxicity in vivo. Toxicology 302:60-67.
- Zerangue N, Kavanaugh MP (1996a) Flux coupling in a neuronal glutamate transporter. Nature 383:634-637.
- Zerangue N, Kavanaugh MP (1996b) Interaction of L-cysteine with a human excitatory amino acid transporter. The Journal of Physiology 493:419-423.
- Zhang H, Davies KJA, Forman HJ (2015) Oxidative stress response and Nrf2 signaling in aging. Free Radical Biology and Medicine 88:314-336.

- Zhou S-F, Wang Y-Y, Zhe H, Yang Y, He Z (2014) Bardoxolone methyl (CDDO-Me) as a therapeutic agent: an update on its pharmacokinetic and pharmacodynamic properties. Drug Design, Development and Therapy:2075.
- Zhou Y, Wang H-D, Zhou X-M, Fang J, Zhu L, Ding K (2018) N-acetylcysteine amide provides neuroprotection via Nrf2-ARE pathway in a mouse model of traumatic brain injury. Drug Design, Development and Therapy Volume 12:4117-4127.
- Zhu M, Fahl WE (2001) Functional Characterization of Transcription Regulators That Interact with the Electrophile Response Element. Biochemical and Biophysical Research Communications 289:212-219.